New Polymeric Receptors:

Microgels and RAFT copolymers, their synthesis and supramolecular binding to low-molecular-weight compounds and proteins

Alan F. Tominey BSc (Hons) AMRSC

In Fulfilment of the Requirements for the Degree

Doctor of Philosophy

A Thesis Presented to Chemistry, School of Engineering and Physical Sciences, Heriot Watt University

March 2009

The copyright in this thesis is owned by the author. Any quotation from the thesis or use of any of the information contained in it must acknowledge this thesis as the source of the quotation or information.

The aim of this thesis is to explore the use of microgels and linear copolymers as supramolecular receptors for low molecular weight compounds and proteins. It was postulated that the long-range interactions made possible by repeating units within a polymer would be advantageous in creating high affinity supramolecular hosts in a competitive aqueous environment.

Tetrazoles frequently replace carboxylic acids in pharmaceutical drugs, their binding to amidines was investigated as a model system to determine their exact mode of interaction with an arginine analogue, where there has been some ambiguity in the literature regarding the preferred binding sites for tetrazolates. ^{1}H NMR studies and crystal structures of model complexes were used to investigate their interactions. A preference for protonated amines over guanidine-like amidines was observed, it was postulated that this would infer a degree of selectivity to microgels and linear copolymers incorporating the tetrazolate functional group.

Microgels and linear copolymers were synthesised and investigated using ^{1}H NMR, UV-Vis and ITC titrations to determine their affinity for selected ligands, such as the biologically significant polyamine spermine and proteins such as haemoglobin and cytochrome C.

A living free radical polymerisation (RAFT) process was used to create linear copolymers with defined molecular weights and low polydisperisties.

Evidence for the microgels and linear copolymers binding to the target molecules will be discussed. Evidence for the structural manipulation of the polymers, via dynamic combinatorial chemistry, to create highly specific hosts will be presented and discussed.

For my family and friends,
whose support and friendship has not gone unnoticed

I would like to gratefully acknowledge my supervisor Dr. Arno Kraft for his support and encouragement throughout this research project, his limitless patience was put to the test on numerous occasions, a lesser man would have cracked under the pressure.

My gratitude is also extended to Dr. Valeria Arrighi, Dr. Alan Boyd, Christine Graham, Dr. Georgina Rosair and Dr. Roderick Ferguson, all of these people have offered valuable advice and knowledge throughout my research and their contributions have all been gratefully received. I would like to also thank, Dr. Sijbren Otto and his group for allowing me to work at Cambridge University; in particular, Fred Ludlow and Zaida Rodriguez-Docampo, Dr. Thomas Schrader and Sun Wei from Duisburg-Essen and Dr. Steven Rimmer at Sheffield Universtiy.

I would also like to thank Mary Pratt and John MacConnachie for ensuring that there is never a dull moment and that the flow of non-chemistry related knowledge within the department is kept at a high level.

I believe a special mention for Ian Scullion is in order, Ian was often a sounding board for various extravagant ideas that would never have worked and was always far to willing to digress wildly of subject, he is greatly missed.

This list would not be complete without mentioning my friends and co-workers in the Bat-cave, this would have been a long and arduous affair without their company, and also my fellow post-graduate students (both past and present) in various other groups I wish them all the luck in the world with their own projects.

I believe it goes without saying that I am deeply appreciative of the love and support of my family and friends who have made all of this possible and have all contributed in their own way (but I shall say it anyway).

Finally I would like to thank the EPSRC and Heriot Watt University for funding and the opportunity to complete my studies.

ACADEMIC REGISTRY
Research Thesis Submission

Name*:*	Alan Frazer Tominey		
School/PGI:	Engineering and Physical Sciences		
Version: *(i.e. First, Resubmission, Final)*	First	Degree Sought:	PhD

Declaration

In accordance with the appropriate regulations I hereby submit my thesis and I declare that:

1) the thesis embodies the results of my own work and has been composed by myself
2) where appropriate, I have made acknowledgement of the work of others and have made reference to work carried out in collaboration with other persons
3) the thesis is the correct version of the thesis for submission*.
4) my thesis for the award referred to, deposited in the Heriot-Watt University Library, should be made available for loan or photocopying, subject to such conditions as the Librarian may require
5) I understand that as a student of the University I am required to abide by the Regulations of the University and to conform to its discipline.

* *Please note that it is the responsibility of the candidate to ensure that the correct version of the thesis is submitted.*

Signature of Candidate*:*		Date:	

Submission

Submitted By *(name in capitals):*	
Signature of Individual Submitting:	
Date Submitted:	

For Completion in Academic Registry

Received in the Academic Registry by *(name in capitals):*			
Method of Submission *(Handed in to Academic Registry; posted through internal/external mail):*			
Signature:		Date:	

Table of contents

List of abbreviations

Arg’	arginine
ATRP	Atom transfer radical polymerisation
BAC	*N,N’*-cystaminebisacrylamide
Boc	*N*-butoxycarbonyl protecting group
BP	bisphosphonate monomer **1**
CTA	Chain transfer agent
cytC	cytochrome C
DCC	Dynamic Combinatorial Chemistry
DCL	Dynamic combinatorial Library
DCPL	Dynamic combinatorial polymer library
DMSO	dimethyl sulfoxide
HMGN	haemoglobin
ITC	Isothermal Titration Calorimetry
K_a	Association constant
K_d	Disassociation constant
LCST	Lower critical solubility temperature
M_w	Weight average molecular weight
M_n	Number average molecular weight
M_{peak}	Peak molecular weight
MAA	methacrylic acid
MBA	*N,N’*-methylene-bisacrylamide
MIPs	Molecularly imprinted polymers
NIPAAM	*N*-isopropylacrylamide
NMP	nitroxide-mediated polymerisation
pNIPAAM	poly(*N*-isopropylacrylamide)
RAFT	Reversible addition-fragmentation chain transfer
SAMs	Self assembled monolayers
SDS	sodium dodecylsulfate
SMA	sodium methacrylate
TET	sodium (5-methacrylamido)tetrazolate
TRIS	tris(hydroxymethyl)aminomethane hydrochloride buffer
Tyr’	tryosine

Table of Figures

List of tables

1 Introduction

1.1 Preface

In Nature, interactions between proteins and proteins, protein receptors and ligands, and enzymes and substrates are commonly thought of as being driven by shape. In essence, the lock and key analogy is a valid illustration of many important key recognition mechanisms in Nature. Complimentary interactions of binding site and substrate (Fig 1.1) serve to create highly selective binding sites even at low concentrations. In 1958, this idea was modified by Daniel Koshland [1] who put forward the induced fit model. It stipulates that, due to the flexible structures of enzymes, the active site is continually reshaped by interactions with the substrate as the substrate interacts with the enzyme.

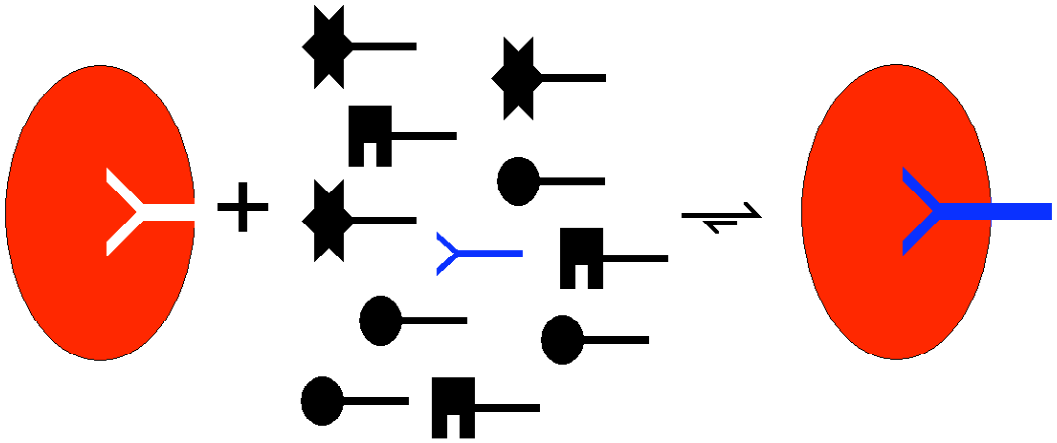

Figure 1.1. An illustration of the lock and key analogy, first postulated by Emil Fischer in 1894.

Enzymes deliver a wide variety of biochemical reactions with very high efficiency and selectivity, even at very low concentrations. The key to this behaviour seems to be the creation of a favourable environment for the substrate, where electrostatic interactions and hydrophobic/hydrophilic interactions between the enzyme-substrate complex are complimentary to each other, thus stabilising the complex. This is, in reality, the "shape" factor mentioned above.

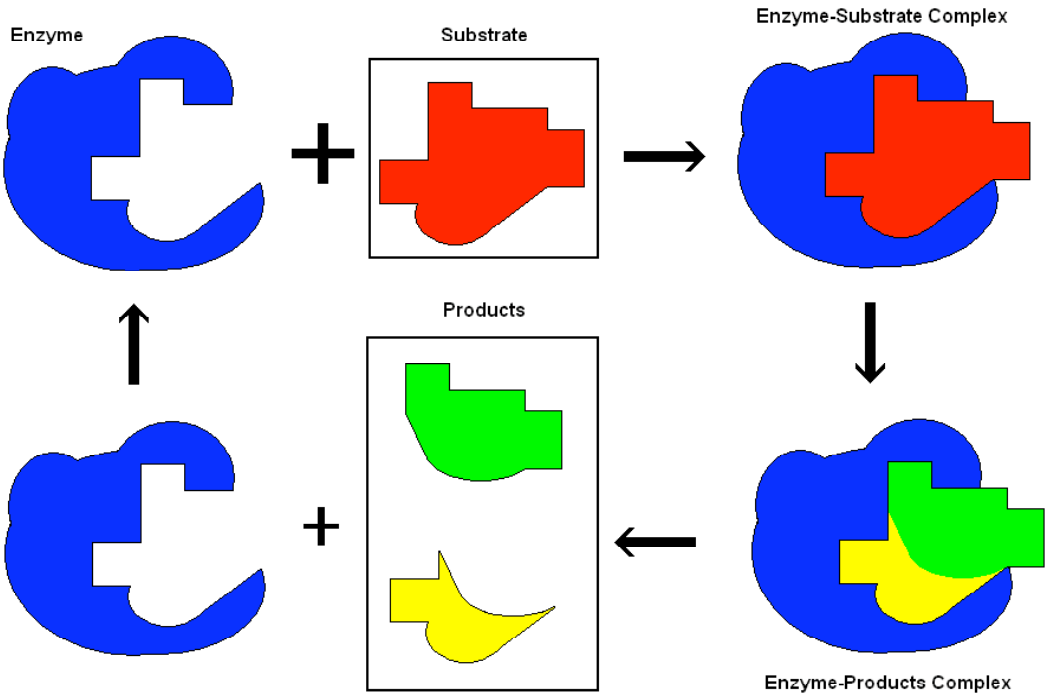

Figure 1.2 The creation of a favourable active site within the protein molecule allows for a strong interaction between an enzyme and its substrate. This is instrumental in the catalytic activity of the enzyme.

The building blocks of all proteins are amino acids. What makes proteins special, however, with respect to their diversity, is that all proteins are comprised of only 20 amino acids. The old adage that "the whole is greater than the sum of its parts" applies in a very succinct way to the area of proteins. The complex interactions between the amino acid monomer units impart a whole array of secondary, tertiary and even quaternary structures to the protein itself. So, with growing complexity, the final function of the protein becomes even more specialised. This gives rise to incredibly specific "lock and key" interactions, which are the cornerstone of the complexity of biological systems (Fig 1.2).

This only comes about due to the unique, almost mechanical, methods that Nature has to construct these macromolecules. The current cutting edge of polymer chemistry is still in no way able to reproduce such molecular architectures, on an efficient and reproducible scale.

One of the goals of supramolecular chemistry is to use the same motifs illustrated above to create man-made hosts that mimic natural proteins such as enzymes for catalysis and the adaptability of immunoglobins shown in the immune system. The processes and understanding involved in designing synthetic macromolecules with the specificity that rivals proteins is a long way off, but today the onus falls on determining the plausibility of novel synthetic routes towards introducing functional groups and binding sites into simple polymeric systems with a view to one day applying these methods to make more complex, enzyme-like synthetic polymers.

1.2 Polymers in supramolecular chemistry

1.2.1 Linear polymers and target-specific binding

Polymers can be linear, branched or crosslinked. In efforts to develop strong supramolecular receptors, linear polymers have shown a great deal of promise when interacting with selected ligands. In protein recognition, the ability of the long polymer chain to make multiple contacts to a protein surface serves to increase the binding affinity to a point where it can even be competitive in solutions of physiological ionic strength.

The surface interactions of proteins have been studied in great detail recently. [2, 3, 4] High numbers of arginine residues have been identified as integral in protein-protein interactions. [5] In addition to this, the complimentary interaction of hydrophobic "patches" on the surface of the proteins must not be underestimated. These areas of low hydrophilicity are usually surrounded by charged residues, which again serve to highlight the complex balance between electrostatic and hydrophobic interactions.

Schrader et al. have shown that incorporation of a weak, but selective, arginine-binding bisphosphonate into a linear polymer creates a powerful polymeric receptor that shows a bias towards arginine-rich proteins such as histone H1 and lysozyme. [6] This implies a direct connection between the microscopic contribution of the arginine specific

monomer **1** and the macroscopic interactions of the linear polymers (Fig 1.3). It would seem that the long-range interactions that serve to enhance the binding strength do not detract from the polymers specificity.

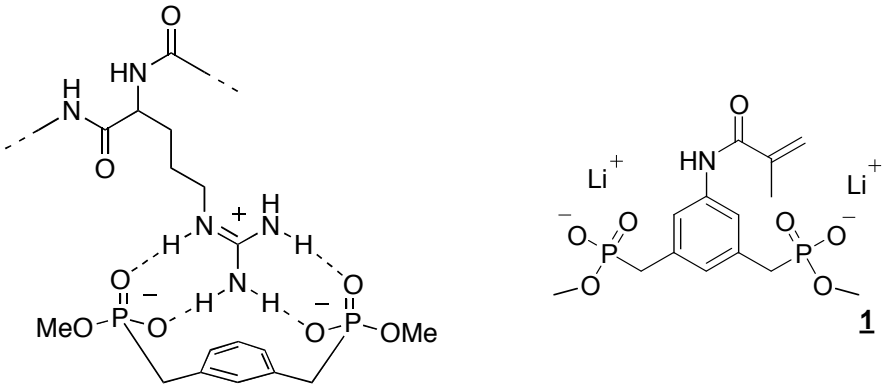

Figure 1.3 A schematic representation of a bisphosphonate dianion-arginine complex with K_a = 86 000 M^{-1} in DMSO and methacrylamide monomer 1.

This work followed on from an elegant procedure first reported by Hamilton et al. that created well-defined surface recognition moieties by mounting aspartate-rich and glutamate-rich cyclopeptides onto calixarene and porphyrin scaffolds (Fig 1.5 & 1.6). [7, 8 , 9] Sub-micro-molar and nano-molar binding was observed, giving both a powerful inhibitor for chymotrypsin and strong complexing agent for equine cytochrome C (Fig 1.4). It was postulated that the large surface area creates kinetically favoured surface binding with the protein by mounting the cyclopeptide loops onto the calixarene.

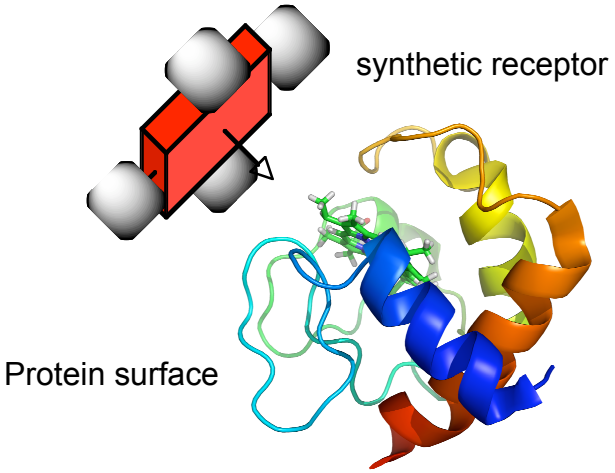

Figure 1.4 A number of different hydrophobic groups, shown as a red cuboid, and charged groups, displayed as grey spheres, were used to iterate a strong synthetic receptor for cytochrome C using this general arrangement.

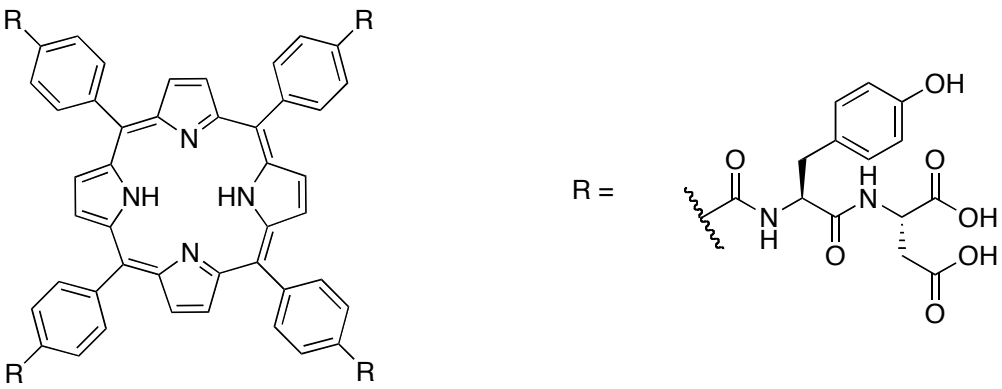

Figure 1.5 Structure of the artificial cytochrome C receptor displayed above (Fig 1.4). The tetraphenylporphyrin is represented by the red cuboid, amino acid derivatives are represented by the grey spheres.

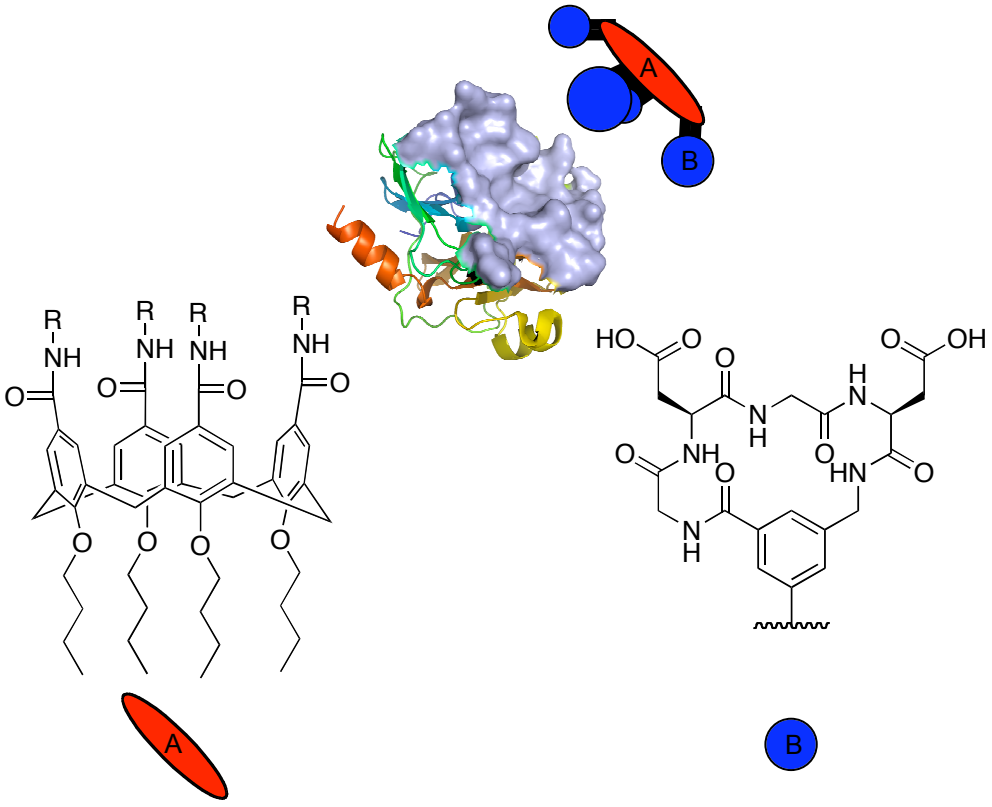

Figure 1.6 α-Chymotrypsin inhibitor based on a calix[4]arene core and peptide loop branches synthesised by Hamilton [7]. Calix[4]arene unit is represented in red and the peptide unit in blue. Protein surface is displayed above as a grey surface. The synthetic receptor binds strongly to the active site of the protease, shown by the surface in the protein diagram.

From this work it is clear that, when reinforced by multiple interactions, even weak binding motifs can be recognised as good systems for supramolecular binding.

Hamilton and Schrader's work has highlighted the co-operative nature of supramolecular chemistry with respect to natural systems, like proteins. Focusing on specificity, rather than outright binding strength paid off when these highly *specific* systems are repeated, allowing the strength of the interaction to be increased.

Polymers offer such an opportunity; where enough complimentary binding groups create a strong affinity and a linear polymer would still maintain a relatively high degree of solubility. A notable drawback, however, from using a high concentration of charged groups on linear polymers is the polyelectrolyte behaviour, which can result in highly viscous solutions even at low concentrations of polymers such as Schrader's poly (bisphosphonate). This effect can prove to be a thorn in the side of the polymer chemist looking to take advantage of these highly soluble, highly charged polymers.

1.2.2 Macroscopic gels

Macroscopic gels do not have such a strong need for enhanced solubility. For chromatographic purposes, many macroscopic gels have been synthesised in which the final polymer is ground into small pieces and then suspended in a medium. Such crosslinked polymers may rely on the high concentration of charged groups, or more specialised functionality, to create favourable binding sites. The extensive crosslinking creates cavities with high affinities, while the solubility of the overall polymer decreases. [10]

Molecularly imprinted polymers are typical examples of this. This process, developed by Wulff over 35 years ago [11], is predominantly used for the chromatographic separation of low-molecular-weight compounds and catalysis.[12] This highly adaptable technique has met with a wide array of success over the years when dealing with low molecular weight compounds. There is, however, a distinct lack of examples in the literature of molecularly imprinted polymers for proteins. This is perhaps an indicator of the limitations of the scalability of the traditional molecular imprinting techniques. [13]

Molecular imprinting or templating will be discussed later.

1.2.3 Colloids and microgels

1.2.3.1 Definitions and discovery

In the search for more efficient and diverse molecular architectures, colloids and microgels lend themselves as capable molecular scaffolds.

Since 1999 Rotello has been working on polymer-coated nanoparticles as Self Assembled Monolayers (or SAMs) with the idea of using them as multivalent receptors. [14, 15] The functionalised surface of metal nanoparticles was initially used to recognise and weakly bind flavin molecules via hydrogen bonding in solvents such as chloroform. These highly versatile molecular structures were quickly developed for protein binding as well; cytochrome C [16] (cyt C) and chymotrypsin [17] have shown high levels of binding (down to the nM range in the case of cyt C).

These monolayer-protected clusters form an attractive family of artificial receptors, as they offer highly versatile ways of creating well-defined organic entities in the size range of bio-macromolecules such as proteins. These highly soluble polymeric supports do not have the drawbacks of viscosity that linear polymers have and they maintain high solubility, unlike macroscopic gels, however aggregation can be a significant problem. Another method of creating polymeric colloidal particles is by creating sub-microscopic gel particles or microgels.

A microgel can be defined as a semi-rigid mass of lyophilic sol dispersed in a medium that, in turn, is fully absorbed by the sol particle. Meaning that the colloidal suspension of particles has a strong affinity for the liquid in which it is dispersed and in. [18] Microgels, as defined by Funke et al., are discrete and highly crosslinked polymeric particles that swell in a good environment and have a size in the submicrometer range (*ca.* 0.01 to several μm). [19] They were initially discovered in the early part of the last century. Thought of as mere precursors to macroscopic networks, [20] they were initially seen as a problem in the process of solution polymerisation. Further research

into their properties has led them to be regarded as highly useful commodities in fields as diverse as surface coatings [21] and biomedical science. [22]

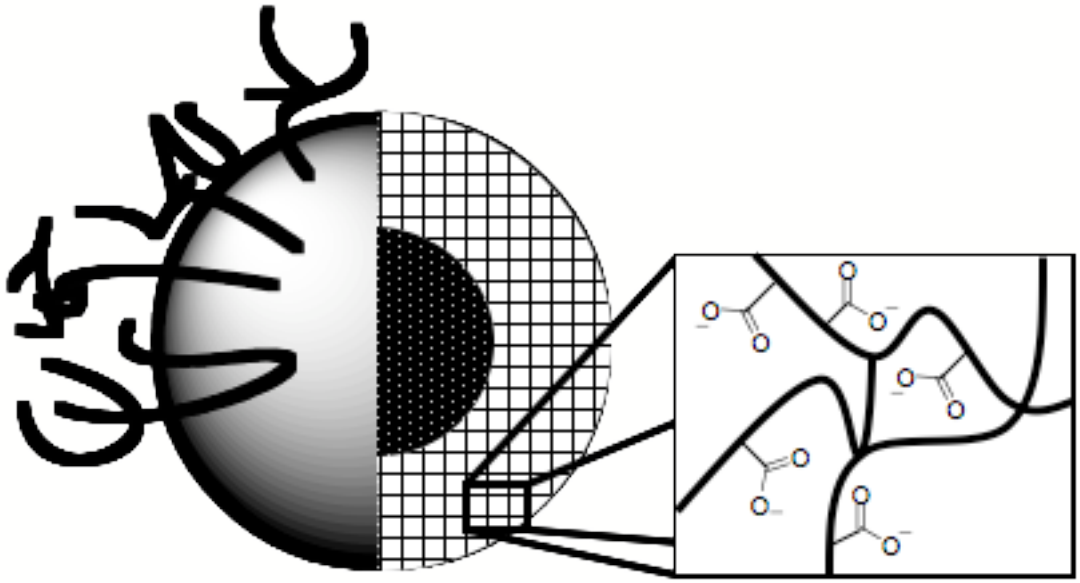

Figure 1.7 A schematic representation of a microgel particle. A densely packed core surrounded by a crosslinked shell. Anionic groups can be incorporated into the microgel by using different monomers. These charged groups are assumed to be evenly distributed around the microgel.

Microgels have been ordained with the prefix micro- due to their small size in relation to other known gel systems, which places them on the border of being considered as true solutes when incorporated into a medium. Occasionally referred to as latexes or latex particles, they have a tendency to form colloidal solutions. This is due in part to their hydrophobic nature and small overall charge. Their dimensions and behaviour in solution also relies heavily on their environmental conditions. [23, 24] Microgels have been studied with a view to applying them to areas such as catalysis, molecular recognition and as chemical sensors. The robustness of these man-made polymers is postulated to have great advantages when dealing with issues of chemical stability and inertness. The stability of these polymers to extremes in temperature, pH and harsh solvents far outstrips that of similar structures that are biological in origin.

Microgels are usually prepared by dilute precipitation polymerisation with a high crosslinker-to-monomer ratio; this gives rise to a spongy spherical polymer with an inhomogeneous internal structure. [25] (Fig 1.7).

Much work has been done to try and determine the structure of microgels. Whilst it is true that the precipitation polymerisation process in the presence of sodium lauryl sulphate (SDS) gives spherical microgels, the actual internal structure was initially less well understood. The general consensus at the present time suggests a densely packed core surrounded by a less dense shell. Wu and Pelton postulated that the higher reactivity of the methylene-bisacrylamide crosslinker commonly used in the synthesis of polyacrylamide microgels would lead to a core-shell arrangement (Fig 1.7), [26] which has been further backed up by other studies. [27, 28, 29]

1.2.3.2 Applications and advantages

Although the earliest uses for microgels were dominated by industrial applications such as surface coatings, [30] more recent investigations have focused on "smart materials" or environmentally sensitive materials.

The discovery that poly(*N*-isopropylacrylamide), or pNIPAAM (Fig 1.8), has a lower critical solubility temperature (LCST) i.e undergoes a reversible coil-to-globule transition at *ca*. 32 ^{o}C gave rise to a new class of environmentally sensitive polymers which have the advantage of being susceptible to external influence.

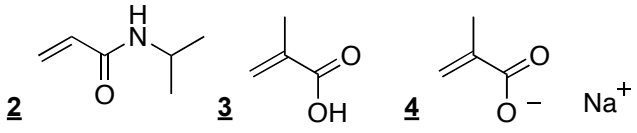

2 **3** **4**

Figure 1.8 The structure of some commonly used monomers that yield environmentally sensitive materials: 2, *N*-isopropylacrylamide, 3, methacrylic acid and 4, sodium methacrylate.

The homopolymer of **2** shows such a transition as a result of a change in temperature, whereas poly(methacrylic acid) and poly(sodium methacrylate), from monomers **3** and

4 respectively, do so following a change in pH. Application of this concept to microgels [31] gave rise to systems with a very fast swelling response time, when compared to macroscopic slab gels, and a surprisingly monodisperse size range.[32] Stimuli-responsive microgels almost instantaneously sparked off the development of many ideas for their application in advanced drug delivery. [33, 34, 35]

In 1998, Kiser et al. accomplished the loading of the anti-cancer drug doxorubicin (Fig 1.9) onto a microgel and the subsequent targeted release was described as an artificial secretory granule. [22] In this case, the mechanism behind the controlled drug release was due to ion exchange where the doxorubicin was loaded onto a polyanionic polymer network, which was coated with a lipid bilayer. Particle swelling and ion exchange were then used to release the doxorubicin; this is an example of how an environmentally responsive polymer and pharmaceutical drugs can be used to develop highly efficient therapeutical treatments. Since then, more studies have focused on the encapsulation of hydrophobic drugs in polymeric nanoparticles. [36]

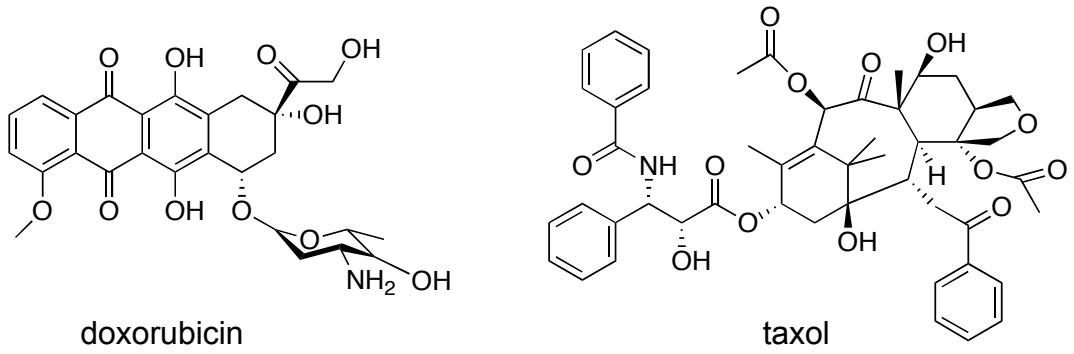

Figure 1.9 Structures of doxorubicin and taxol. These hydrophobic drugs are current front-runners in the fight against cancer.

Another possible methodology for the delivery of drugs that are highly lipophilic would be to exploit a hydrophobic environment within the microgels. In 2002, Bromberg et al. incorporated polyether chains onto a lightly crosslinked polyanionic microgel [37] resulting in aggregation of the polyether chains within the microgel structure; this allowed the loading of hydrophobic drugs such as taxol and mitoxantrone. There has also been some evidence to suggest that microgel particles can be employed as new vectors to significantly increase the intracellular uptake of therapeutic agents such as

DNA and RNA. [38] An added advantage of using microgels is that they should be more robust and not denature as easily, unlike a protein once it has been taken outside its native temperature and pH range. Proteins typically lose their secondary, tertiary and/ or quaternary structure when exposed to extremes of heat or pH. A microgel would be far more capable of withstanding a more hostile environment, with the added advantage that the swelling response can be well predicted and in some cases controlled. [39, 40, 41]

To date, the most widely used co-monomer for the production of a polyanionic microgel has been methacrylic acid (MAA) and its sodium salt (SMA), (Fig 1.3) which produces negatively charged functional groups within the microgels and allows for both the binding of the drugs and control of the swelling via pH or ion concentration. The disadvantage of this approach arises from the difference in reactivity ratios when comparing NIPAAM with MAA or even SMA. [42, 43]

In summary, when combined, the relative ease of synthesis, high solubility and the low viscosity intrinsic to microgels, these sub-microscopic particles lend themselves very easily as fertile ground for the development of new supramolecular receptors.

1.3 Molecular recognition

1.3.1 Templating

The modern templating process essentially serves to secure complementary functional groups, hydrogen bond donors and acceptors, hydrophobic or Van der Waals interactions, all in a conformation that is conducive to that of a favourable binding environment to a template (Fig 1.10). There is a wealth of literature regarding templating processes and "molecular imprinting", including numerous reviews and monographs. [12, 44 , 45] The most common method of imprinting makes use of covalent or non-covalent binding of a polymerisable unit to a substrate, which is then polymerised by radical initiation in the presence of high amounts of crosslinker and small amounts of porogen (solvent).

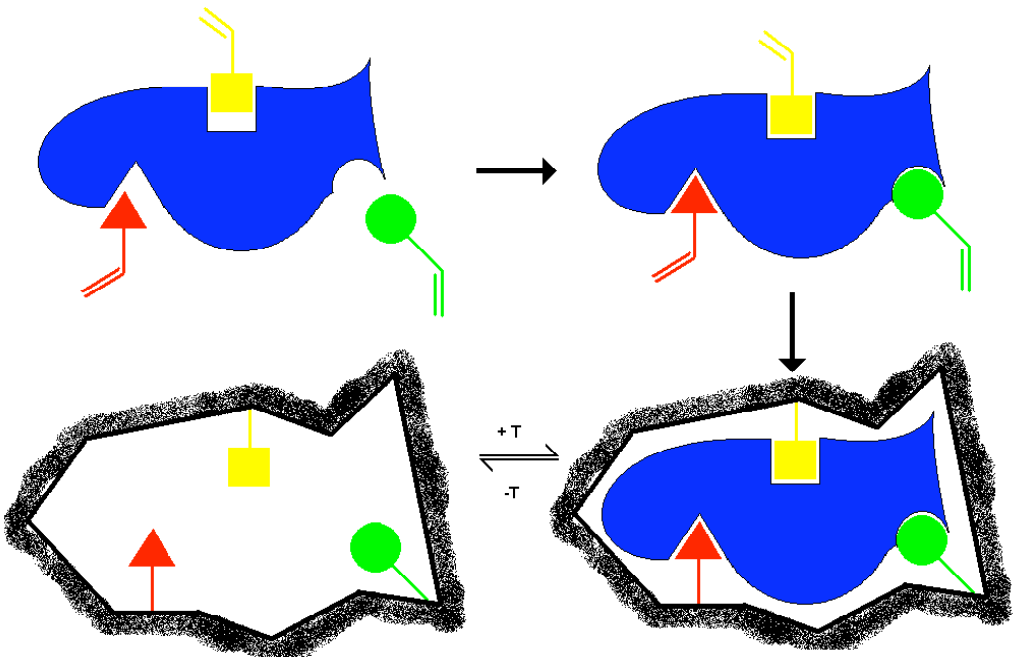

Figure 1.10 Representation of a typical imprinting process. The crosslinked polymer is synthesised in the presence of a suitable template. After polymerisation, the template is removed to reveal a binding cavity, which is configured specifically for the template (adapted from reference 12).

Another method, which has proven to be valuable, employs structurally related compounds in the templating process (Fig 1.12). In this case, the template is usually destroyed once polymerisation is complete. This process has been used to introduce

selective binding sites for dopamine by creating bidentate receptor sites with a good degree of selectivity.[46] The poor uptake of homovanillic acid, a structurally similar compound, (Fig 1.11) is thought to be due to the negative charge of the carboxylic acid and the steric bulk of the methylester groups. Indeed, binding of catechol and tyramine were also observed to be weaker in comparison to dopamine (Fig 1.12). This result suggests the cooperativity of the two functional groups with in the binding cavity and suggests a definite selective cavity is present. However, the conditions of the re-binding experiments suggest that this interaction is not solely due to supramolecular interactions the formation of a cyclic boronate ester clearly has a large role in the affinity.

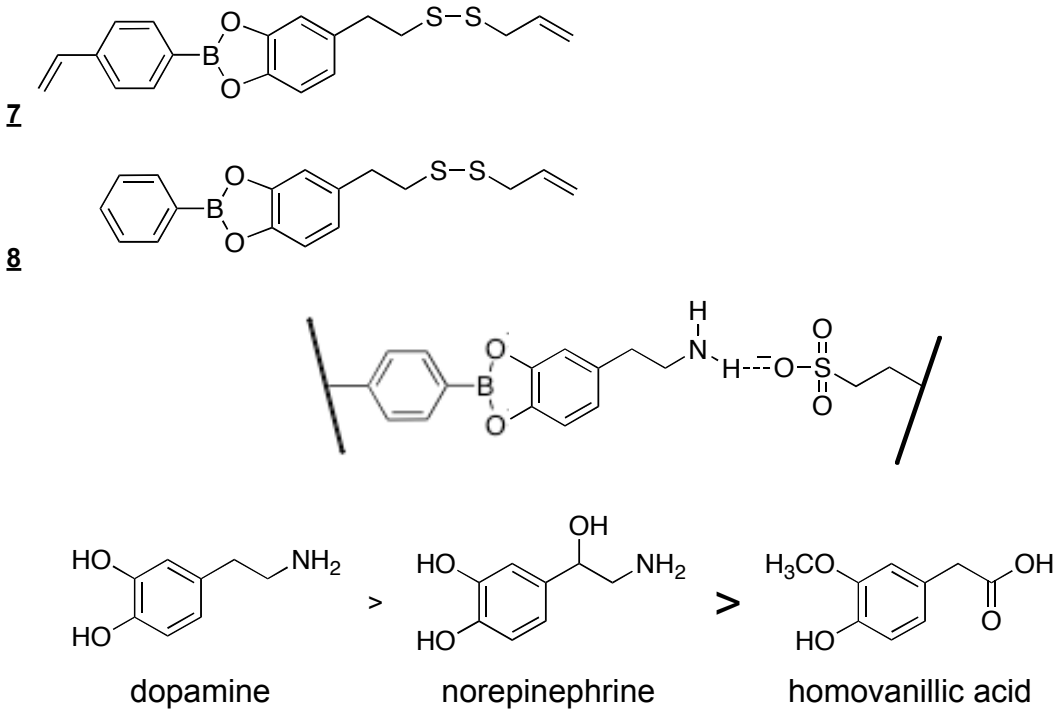

Figure 1.11 After incorporating monomers 7 or 8 into a polymer the template is removed through oxidation to leave a cavity that is selective towards dopamine and some related compounds at pH 11.

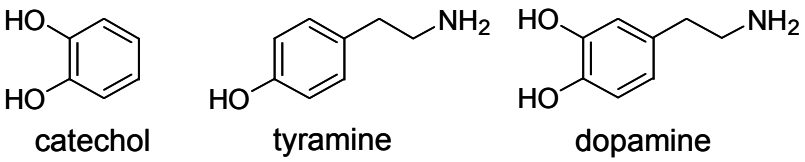

Figure 1.12 Catechol, tryamine, and structurally similar dopamine. Both tyramine and catechol share different moieties with dopamine. Their difference in binding strengths hints at the cooperativity of the polymer functional groups.

Monomer **7** created binding sites that were less selective (but stronger), [46] than those created with monomer **8**, with its unpolymerisable boronic acid group. The boronic acid functionality, whilst increasing the strength of the interaction throught the formation of a cyclic diester, is also broadening the range of compounds that feel "comfortable" binding inside the cavity. The sulfonic acid alone is not strong enough to attract the wide range of structurally related compounds and therefore a degree of selectivity is observed. This was evident when polymers from template **8** bind dopamine and the structurally similar tyramine but show relatively little affinity to anything else studied. This could also indicate that the size and shape of the binding cavity are important as well as the complimentary interactions, this example seems to indicate that higher complexity can lead to greater selectivity.

Molecularly imprinted polymers are generally obtained in the form of highly crosslinked, macroscopic polymer networks which are then ground to produce an insoluble powder. The degree of crosslinking has a significant effect on the efficiency of the polymer as a host. This has a direct effect on the solubility of the final polymer and therefore a great deal of research has focused on using highly soluble polymers with a lower degree of crosslinking. [12]

1.3.2 Applications in catalysis

The templating process is predominantly used in imprinted catalysts to create active sites within which a substrate can be accommodated or can even stabilise a transition state, in much the same way as enzymes do. [47] An imprinting process was used to determine whether the imprinted polymers behave as catalysts in hydrolysing the target carbonate faster. (Fig 1.13)

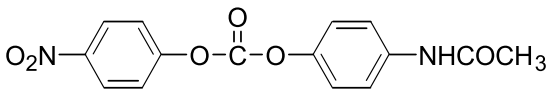

Figure 1.13 A targeted carbonate, which bears a structural similarity to the template used in Pasetto's work. (Fig 1.14) [47]

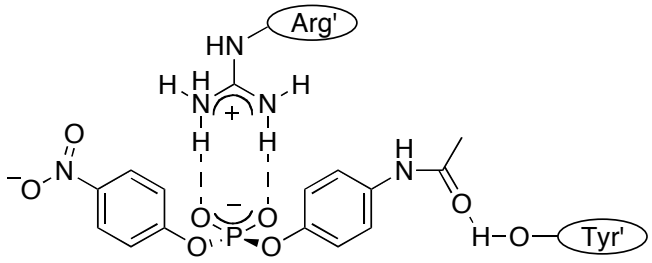

Figure 1.14 Pasetto et al. suggest that the interactions between the phosphate ester template and the Arg' and Tyr' monomers (Fig 1.15) (the NO_2 group of the phosphate ester may also provide hydrogen bond acceptors) create favourable catalytic sites for the hydrolysis of the target carbonate shown in (Fig 1.13).

In 2005, Pasetto et al. used a non-covalently linked complex between monomers **9** and **10** and a phosphate template (Fig 1.14 & 1.15) to stabilise a catalytic binding site. The imprinted microgels showed enhanced catalytic properties over non-imprinted polymers, or "blanks". [47] The catalytic behaviour of the polymer allowed the interaction to be quantified via kinetic studies. This does not allow for an exact quantification of the association constants involved, however, the experiments were carried out in a water:DMSO mixture at a rough concentration of 4 mg/mL of microgel. Therefore it can be assumed that the actual affinity is low. This does, never the less, remain an excellent example of how molecular imprinting and microgels can be used together to great effect.

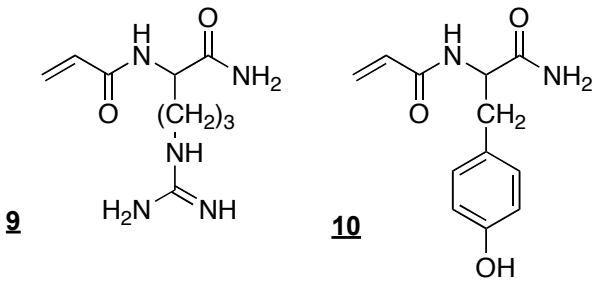

Figure 1.15 The monomers used by Pasetto et al. were intended to impart amino-acid-like functional groups into the polymer, monomer 9 are represented by the short hand *Arg'* and monomer 10 is represented by *Tyr'* in figure 1.5.

Metal coordinating sites have also been incorporated into molecularly imprinted polymers (MIPs) (Fig 1.16). [48] The polymerisation of monomer **11** provides a synthetic route towards tridentate *N*-donor ligands supported within a polymer matrix. These donor ligands were used to immobilise Cu^{2+} ions, which were then found to promote phosphoester hydrolysis.

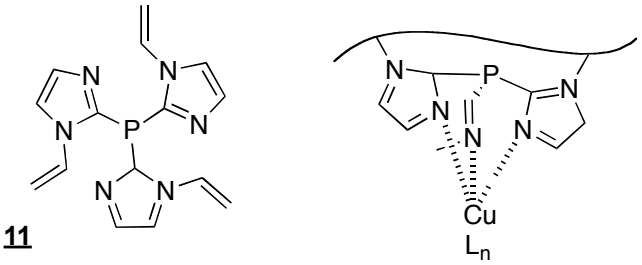

Figure 1.16 Schiller et al. used monomer 11 to introduce a tridentate ligand to immobilise Cu^{2+} ions and create catalytically active sites to promote hydrolysis of phosphoesters. [48]

A supported catalyst on a polymer network has various advantages: it could be stable, recoverable, reusable and exhibits good resistance to high temperature and pH. [49]

1.3.3 Applications in drug delivery

Since the introduction of drug loading by ion exchange by Kiser et al. in 1998, many attempts have been made to imprint binding sites for low-molecular-weight pharmaceutical agents. [12] One of the most inherent problems with this methodology is that, whilst the templating process works well when a template is available, many pharmaceutical agents have reactive functional groups that can interfere with the polymerisation process. If a radical polymerisation is taking place then any compound that has the ability to quench the radicals, such as thiols or polyphenols, or even the presence of a double bond within the targeted template, these would result in unfavourable side reactions. Many pharmaceutical agents may not be stable within the polymerisation reaction conditions or may not even be soluble in the polymerisation medium. A post polymerisation imprinting technique would be a distinct advantage.

Transport of bio-therapeutic agents into the body is a complicated process. Many parameters must be taken into consideration, and pH and hydrophobic/hydrophilic domains form only a small portion of the factors to be taken into account. [50, 51, 52] Microgels have been shown to be able to transport fragile bio-molecular drugs such as DNA and peptides into cells where a lower pH facilitates their entry into the cell through the membrane. [53] This could be applicable in areas such as cancer treatment where cancerous tissues exhibit a lower pH than healthy tissue. In 2002, Frechet introduced a novel method for protein encapsulation and release by using just such biological conditions. An acid-labile crosslinker was used in the synthesis of microgels, the crosslinker was easily broken up via acid hydrolysis in an environment similar to that found in cancerous cells at pH 5. (Fig 1.17) [54]

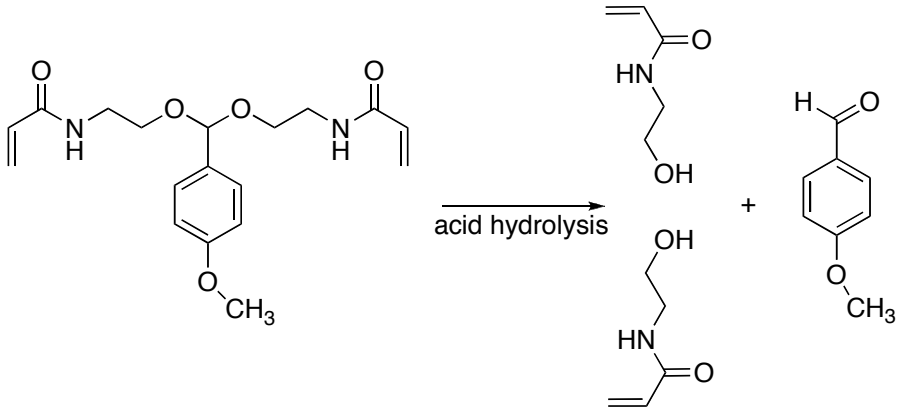

Figure 1.17 Acid hydrolysis of an acetal crosslink breaks down the internal structure of the microgels resulting in protein release.

The hydrophobic interiors inherent with polymeric particles may be exploited to deliver hydrophobic drugs into the body. [55] To date, most orally active drugs must be water-soluble in order to be effective. One of the challenges of modern drug delivery is to deliver hydrophobic entities into a biological environment, without the use of co-solvents, surfactants or emulsions. It has been postulated that hydrophobic drugs can be easily delivered to specific sites by loading them onto simple polymeric nano-particles. Zhu and McShane highlighted a new and straightforward method of loading hydrophobic materials into stabilised polymer colloids. [56] Surfactants and organic co-solvents were used to swell the polymer particles and the hydrophobic molecules were loaded onto the polymer matrix. The particles were then stabilised by removing the co-solvent.

1.3.4 Applications in chemical sensors

For use as chemical sensors the imprinting process must generate very high selectivity and affinity to compete with existing sensor technologies. Some suggested strategies have included the loading of fluorescent molecules into a polymer network. Fluorescence quenching can be very selective and indeed very sensitive, concentrations in the femto-molar range can be detected.[55]

Imprinting processes have been used to introduce selectivity to binding metal ions. In 2001, D'Oleo et al. employed a post-polymerisation "imprinting process". They used a disulfide crosslinker and then oxidatively cleaved the bonds to introduce sulfonic acid groups, which were then close enough to each other in the polymer network to be able to capture divalent metal ions. The metal ions could not only be bound, but also released by a swelling process. (Fig 1.18) [57]

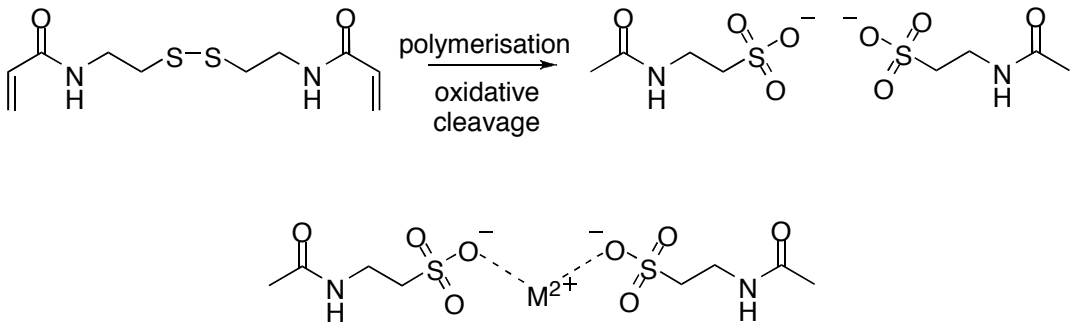

Figure 1.18 Divalent metal ions can be bound by the sulphonate groups present in the polymer, introduced by oxidative cleavage of *N,N'-cystaminebisacrylamide (CBA)*.

Similarly, Hiratani et al. used disulfide bonds to allow the post-polymerisation rearrangement of the structure of the polymer to allow functional groups to capture metal ions such as Ca^{2+}. [58] In this case, a methacrylic acid comonomer provided the acidic functional groups that were introduced during the polymerisation process which bound the Ca^{2+} ions.

The myriad methods available for the development of sensors via molecular imprinting have been reviewed elsewhere. [59]

1.3.5 Challenges of high solubility

The challenge that faces the next generation of polymeric supramolecular receptors is to initiate supramolecular binding of highly soluble ligand molecules in competitive environments at concentrations that can compete with natural systems.

At physiological pH (around 7.4) and in an aqueous environment, where the ionic strength is around 0.15 mol L^{-1}, competition for suitable binding sites is an inherent problem as supramolecular interactions are governed by a whole array of parameters. Inclusion of acidic functional groups is the most common method for trying to attract positively charged ligands; however, the degree of protonation of these groups is again dictated by the pH and incorporation of some of these monomers into the polymers has been shown to be less than ideal.

1.3.6 Solution dynamics

Supramolecular recognition in water is not just a natural progression from non-polar solvents such as hexane and pentane through to aprotic solvents such as dimethylformamide and dimethylsulfoxide. It is more complicated. Water is known for its "strange" properties, i.e. its unusually high boiling point for a compound of such low molecular weight and its expansion upon cooling below 4 °C to name a few. In more scientific terms the factors that govern these behaviours are a large dielectric constant (ε), small molar volume and its ability to form an extensive network of hydrogen bonds even in the liquid state. The result of these factors is the rather counter-intuitive statement that like charges can attract due to their favourable entropic contribution just as opposite charges attract due to the enthalpic contribution. [60] In addition to this, the free energy of solvation that governs the transfer of charged groups from areas of high dielectric constant to those of low dielectric constant, e.g. from the outside of a binding cavity to the inside, means that charged groups do not always contribute to the strength of the interaction. Sometimes they can be there merely to govern specificity. [61]

The ionic strength of a solution can also have a drastic effect on the affinity; a number of studies have taken this into consideration. [62, 63, 64] However, more specifically, Rotello has studied the effect of salt concentration on the binding of α-chymotrypsin to gold nanoparticle receptors. High concentrations were found to totally disrupt the electrostatic binding of α-chymotrypsin to carboxylic acid functionalised gold nanoparticles, but this activity was shown to be the result of the protein's structural change in the high salt concentration. [65] In a similar study, the effect of ionic strength of a solution on hydrophobic interactions was tested using myoglobin and the butyl- and octyl-sepharose adsorbent via isothermal titration calorimetry; the results showed that not only does the ionic strength of the solution enhance the hydrophobic interaction, but it also serves to decrease the heat required for dehydration. [66]

1.4 Dynamic combinatorial chemistry

1.4.1 Reversible bonds and thermodynamic control

Dynamic combinatorial chemistry has become a stalwart in the search for new, strongly binding macrocycles in the chemist's tool kit. One can easily trace the roots of this method back to metal-ion templated reactions. Coordinating metal ions such as Ni^{2+} can be used to stabilise a complex in order to allow bonds to form between its constituent parts. A rudimentary example is shown in Fig. 1.19. In the presence of Ni^{2+} the desired product is stabilised in a complex. The advantage of this process is clear: without the Ni^{2+} template a very low yield is obtained. [67]

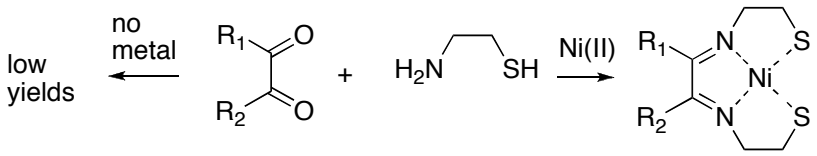

Figure 1.19 Thermodynamically controlled synthesis of a macrocycle using Ni(II) as a template.

It was not until the 1990's that dynamic combinatorial chemistry was conceived as an approach that would capture the combinatorial, selection and amplification elements exhibited by the mammalian immune system. Initial work was carried out on the base-catalysed transesterification reaction and hydrazone exchange, but it was not until the end of the decade that disulfide exchange reactions would mark the movement of dynamic combinatorial chemistry into aqueous solutions and mild conditions. Fully comprehensive studies on dynamic combinatorial chemistry can be found elsewhere. [68, 69, 70]

The principle behind dynamic combinatorial chemistry is that all the constituents in a "library" are under thermodynamic control. Therefore the composition of the library can be effected by external conditions. This responsiveness can be exploited to discover

compounds that have temperature, pressure and even magnetically responsive properties.

Developed as a method of creating and isolating novel macrocyclic host-guest systems predominantly for use as catalysts [71, 72], combinatorial libraries are usually obtained when a number of difunctional building blocks are introduced into a system together with a template under conditions that a macrocyclic system will be formed.

S. Otto's and J. K. M. Sanders' Dynamic Combinatorial Libraries (DCL's) differ from normal combinatorial chemistry in the formation of *reversible* covalent bonds. This idea has opened the door to creating systems, which are truly adaptable to their environment. When a template is introduced into a library, the free energy landscape is changed (Fig 1.20) and the lowest energetic configuration is obtained by interactions with the template. This process therefore creates an excess of macrocyclic species which interact favourably with the template. In much the same way that the templating process used to synthesise molecularly imprinted polymers creates binding cavities; the template creates a complex with the monomers chosen to interact with the template and optimises a binding cavity for the template molecule.

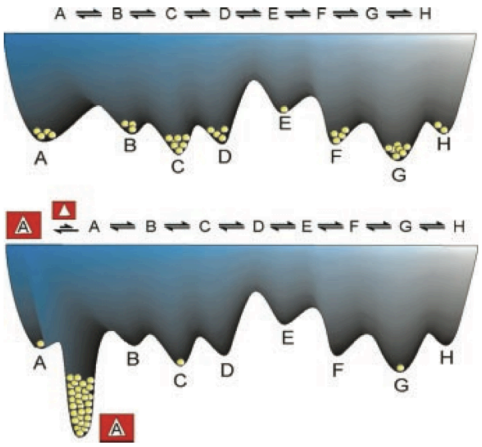

Figure 1.20 A free energy landscape of a dynamic library, the top image shows a thermodynamically stable Library in the absence of a template. After addition of a template molecule, the free energy landscape shifts the equilibrium towards the most favoured template/host complex. [73]

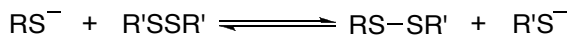

Figure 1.21 The reaction scheme for a disulfide exchange reaction. The thiol can be recycled and can go on to initiate another exchange reaction providing it is not mopped up by oxygen.

An elegant example of the usefulness of this procedure is the creation of extremely high-affinity receptors for the biologically relevant oligoamine spermine. [74] With a relatively rudimentary library consisting of only two members, a macrocyclic receptor with an association constant of 22 nM^{-1} was successfully isolated. The discovery of synthetic receptors with such high affinities is extremely rare but this method has shown that strong binding receptors can be made even with basic building blocks. (Fig 1.22)

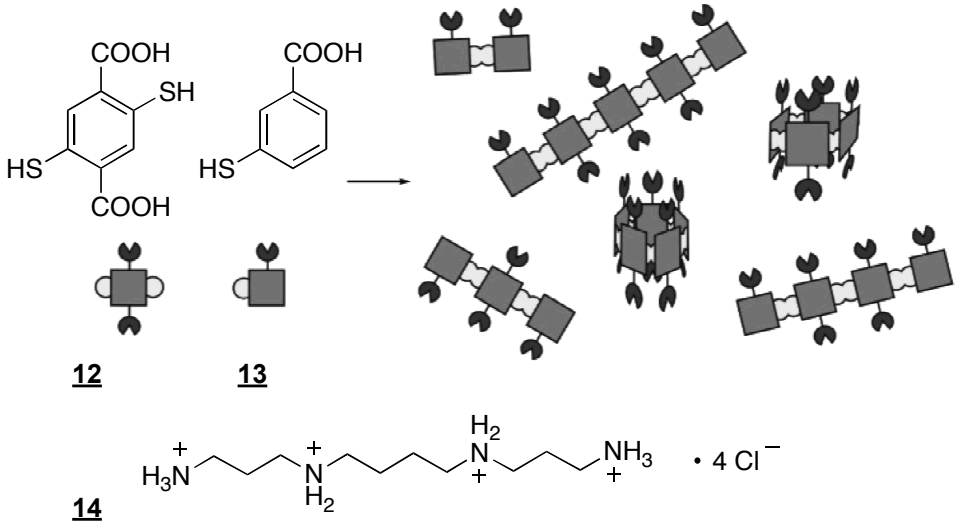

Figure 1.22 With only very rudimentary building blocks, 12 and 13, an extremely high-affinity macrocyclic receptor can be isolated for the spermine template 14.

1.5 Protein binding

1.5.1 Interactions of large molecules

1.5.1.1 Protein structure

When dealing with proteins it is important to realise that, in contrast to low molecular weight compounds, where a charge can be thought of as being localised at a specific point; proteins can be thought of as having charged surfaces, whilst the interior tends to be predominantly hydrophobic. [75] It is not uncommon for a protein to have a high concentration of positively or negatively charged groups within a particular area. These charges are generated by particular functional groups found in the side chains of certain amino acids e.g. NH_3^+ from lysine or CO_2^- from aspartic acid. The overall charge is dictated by the choice of pH relative to the isoelectric point (pI) of the protein. (Fig 1.23) [4, 6]

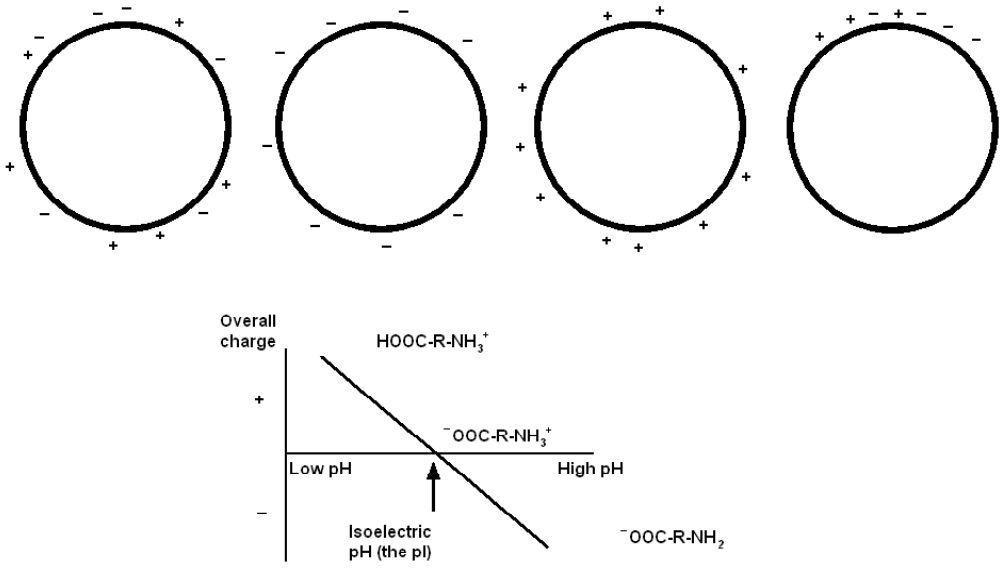

Figure 1.23 Above is a graphic representation of possible charge distribution scenarios along a protein surface. The overall charge of a protein is determined by the pH of the surrounding medium. At high pH, the carboxylic acid sites are de-protonated and therefore a negative charge dominates. Similarly for amine groups, where a positive charge is dominant at low pH. The point where the protein is considered neutral is known as the isoelectric point or pI.

Many of the structures that give proteins their highly specialised functions are formed and stabilised by hydrophobic interactions. In addition, a number of studies have highlighted the importance of hydrophobic interactions in protein-protein interactions, complemented by surrounding charged groups. In summary it is important to take into consideration the full range of interactions when trying to mimic nature and create highly specific systems. This is becoming all the more important with the realisation that many protein-protein interactions are biologically important and that being able to control them would be an extremely useful tool for many medical treatments. [79, 2]

If the model for protein-protein interactions were applied to the interactions of proteins with microgels, it would seem fitting to think of the two species as similar. Therefore many of the techniques that are used to investigate protein-protein interactions would remain valid when trying to quantify the affinity that microgels have for proteins. ^{1}H NMR and ITC are some of the most commonly used and adaptable techniques, although ^{1}H NMR, like UV titrations relies on the presence of a definable signal, from a chromophore or a definable proton. ITC does not have this draw back. In reality the most common microgels are of a much larger size than proteins, more comparable to viruses.

1.5.1.2 Points to consider with common proteins

Cytochrome C (cytC) (Fig 1.24) has a molecular weight of 16 kDa and is made up of a single peptide chain that coils under physiological conditions to give a globular structure with pendant residues. In the case of cytC the predominant residue on the surface is lysine (making up 10% of the composition). This gives an overall positive charge to the protein, which therefore has a pI of 9.55. [76]

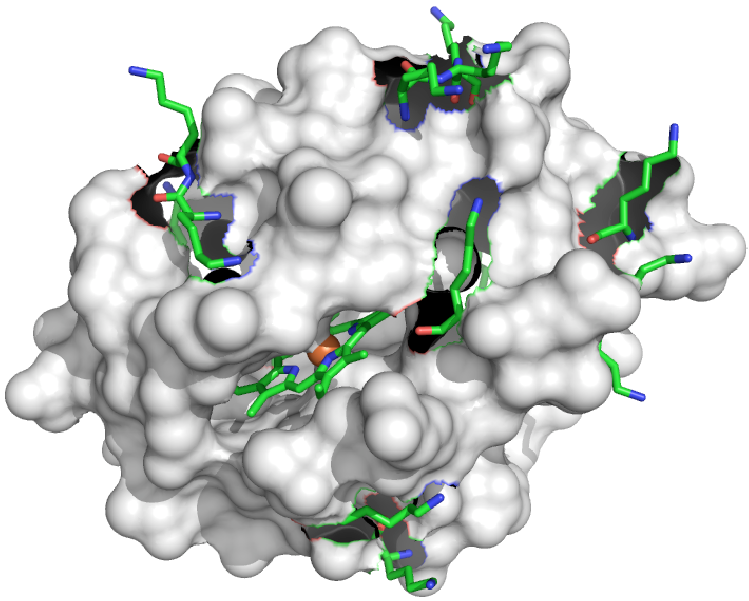

Figure 1.24 A representation of (horse heart) cytochrome C shows the solvent-exposed surface with a number of lysine residues represented as sticks. The Fe atom of the haem group is visible in the cavity.

Haemoglobin [77] (HGBN) (Fig 1.25) is another example of a globular protein with exposed basic residues. The HGBN tetramer is held together, tightly, by salt bridges,

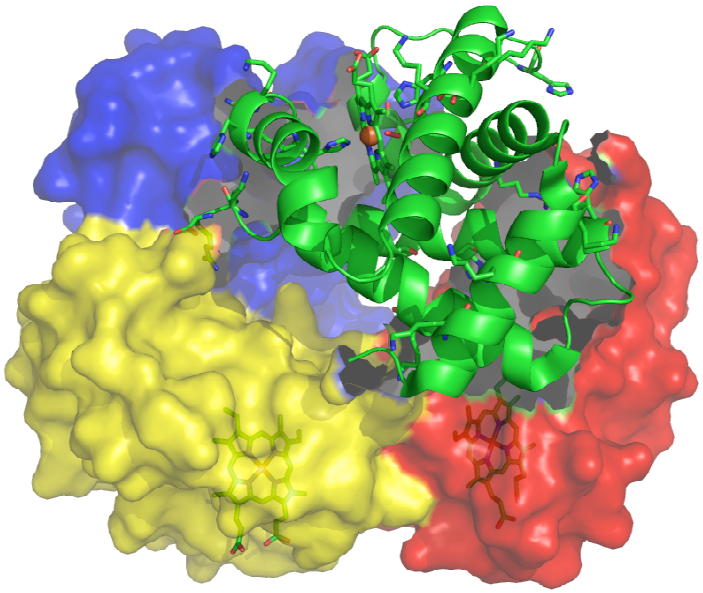

Figure 1.25 Haemoglobin tetramer. The different peptide chains are set out in different colours, with the basic residues on the green helix displayed as sticks.

van der Waals interactions and hydrophobic interactions, with a number of basic groups exposed to the exterior (Fig. 1.25). This can be thought of as an example of an extremely effective use of supramolecular interactions, whereas, fibrous proteins make more use of cysteine-cysteine disulphide bonds to form links between individual peptide chains. Like cytC, this large globular protein maintains a globular structure in solution with exposed positive charges, giving the protein a pI of 7.6. These basic proteins lend themselves very easily to investigation due to their availability and chromophores with high molar extinction coefficients.

1.5.2 Protein/amino acid specific systems

Protein specific receptors could be achieved not only by templating, but also by specifically designing large molecules (MW > 750 g mol^{-1}), such as polymers, that are equally able to complement the known amino acid residues on the surface of a protein target. The driving force behind this research is the potential for discovery of novel therapeutics; where low molecular weight drugs do not have the ability to disrupt protein-protein interactions. [78, 79]

Recent studies have shown patterns or "hot spots" with respect to certain amino acid residues being more involved predominantly in protein-protein interactions. Tryptophan, arginine and tyrosine appear more often than other residues such as serine and leucine. [80, 81] It stands to reason that the design of new receptors should take advantage of the presence of these certain amino acid residues or "hot spots" and thus create tailored binding to protein surfaces.

Schrader et al. have shown that arginine selectivity can be induced in polymer chains by using a methacrylamide based bis-phosphonate monomer. [6] The bis-phosphonate binding unit **1** gives good selectivity towards proteins that have a high level of arginine, e.g. lysozyme and proteinase K (Fig 1.3).

Jain and Hamilton demonstrated surface-specific binding to cytochrome C at roughly similar strengths to that of the cytochrome C-cytochrome C peroxidase. (Fig 1.4 and 1.5) This work suggests that these man-made polymer-based particles may be mimicking the binding surface of the cytochrome C peroxidase, a native partner of cytC. [8, 78] The success of this and others such as highly specific chymotrypsin inhibitors (Fig 1.6) and Rotello's work with protein specific nanoparticles [16, 17] indicates that there is great scope for the specific targeting of protein surfaces. In fact, there are numerous examples sited by Hamilton where rational design from X-ray crystallography, ^{1}H NMR spectroscopy and computational studies were used to anticipate structure and create high affinity partners. [78]

1.6 Aims

It is the aim of this thesis to describe the synthesis, characterisation and development of receptors for low molecular weight compounds and proteins with polymers.

An investigation into the precise mode of binding between tetrazolate compounds and guanidine-like amidines will be undertaken to elucidate the characteristics of the association between the tetrazole functional group and anionic amino acid residues with respect to pharmaceutical drugs. Conflicting reports in the literature have highlighted the need for a greater understanding of the affinity of tetrazoles for amino acids such as lysine and arginine.

Microgels incorporating a tetrazolate functional group will be synthesised and investigated for their potential as supramolecular hosts for protonated amines in aqueous buffer.

Microgels will also be investigated for their ability to bind proteins in a competitive environment, i.e. in aqueous buffer at pH 7 with an ionic strength of 0.15 M. A number of different monomers with functional groups are anticipated to instil a degree of selectivity to the microgels with respect to their interactions with different proteins will be used.

A living free radical polymerisation will be used to synthesise linear copolymers with defined molecular weights and low polydispersities for use as polymeric supramolecular hosts for proteins. Hydrophobic monomers will be incorporated into these polymers to try and increase the affinity of these hosts to their ligands via hydrophobic interactions. These linear copolymers will be investigated with respect to their composition to attempt to iterate a strongly binding host.

This thesis will also introduce a templating process similar to the Dynamic Combinatorial process described above which will be adapted and used to create polymeric hosts with strong affinity for biologically significant polyamines. Polymers synthesised via a living radical polymerisation with a disulfide containing monomer

will undergo a thiol exchange in the presence of a template to create highly specific polymeric host molecules.

2 Unusually weak binding interactions in tetrazole-amidine complexes

2.1 Background and concepts

In modern drug design a common motif is the iteration of different functionalities in the optimisation of pharmaceuticals. Small changes in a drug's structure can induce large changes in activity. One such change can come from replacing a carboxylic acid group with an acidic heterocycle such as a tetrazole. Since the tetrazole has a similar pK_a and binding properties as a CO_2H group, it is called a bioisoteric replacement for a carboxylic acid. [82, 83, 84] However, the use of a bioisoteric group does not always demonstrate increased activity. In the case of prostaglandin F2 analogues [85] and tyrosine phosphatase inhibitors [86] a decrease in activity is observed when tetrazole groups are used to replace the carboxylic acid group. In contrast, angiotensin II receptor antagonists such as losartan, [87] candesertan and valsartan [88, 89] all benefit from an increase in activity due to the choice of a tetrazole as an acidic H-bond acceptor. (Fig 2.1)

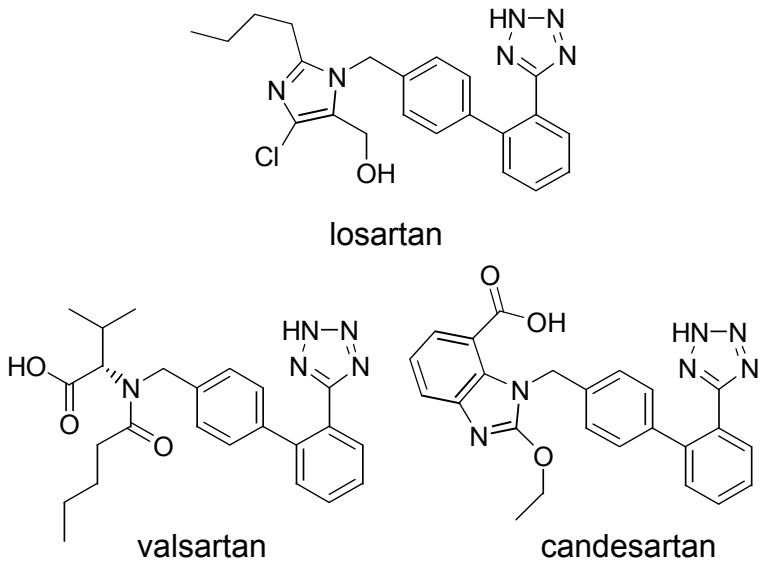

Figure 2.1 Losartan, candesartan and valsartan, three angiotensin II receptor antagonists that all have a tetrazole functional group.

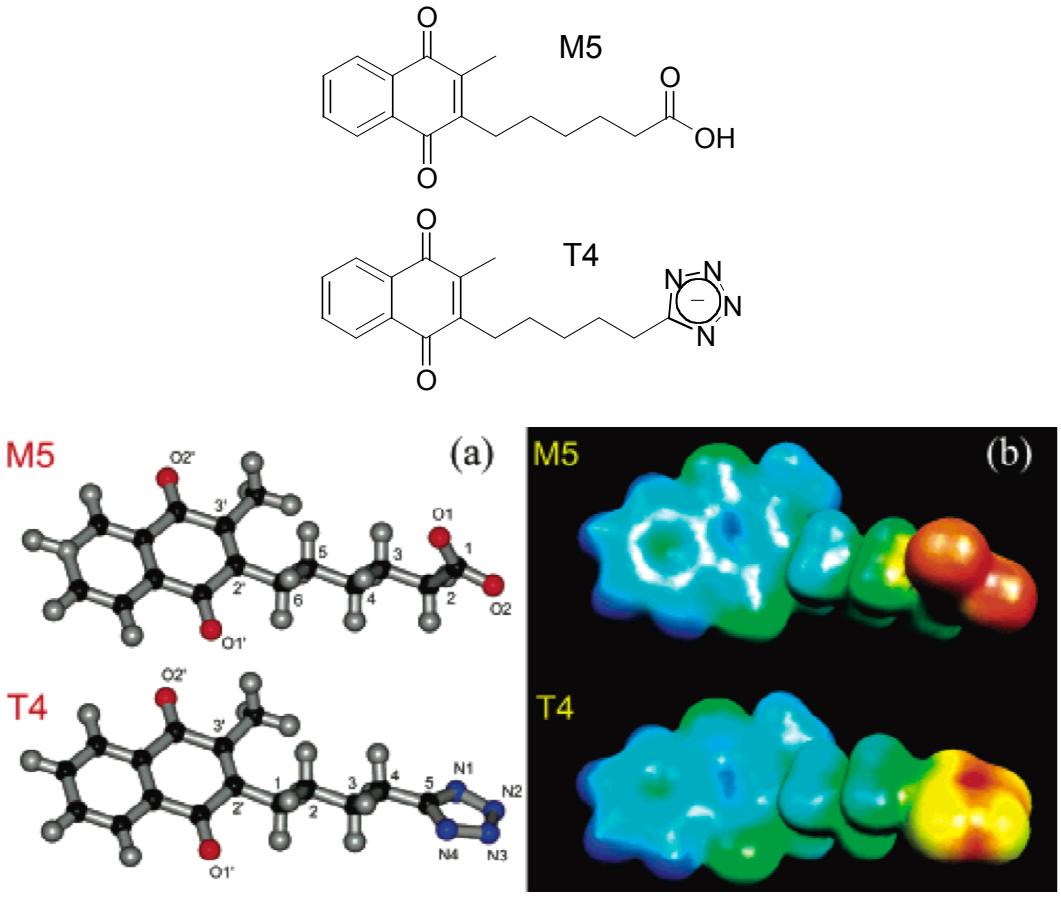

Figure 2.2 Structural and electronic profiles of a carboxylic acid glutathione reductase inhibitors (M5) and its more potent tetrazolate analogue (T4) [92].

In the literature there is some debate as to the exact mode of binding that these drugs exhibit, (Fig 2.1) and a number of differing theories have been put forward. In the case of angiotensin II receptor antagonists some reports suggest that the deprotonated tetrazole in losartan, for example, interacts with a lysine and a histidine [90] at the recognition site of the membrane receptor, whereas others conclude that the tetrazole binds instead to a guanidine group of a nearby arginine at the receptor binding site or that an interaction with both a lysine and an arginine [91] might play a role. What is clear is that the tetrazole, and other acidic heterocycles such as oxadiazolone, are efficient bioisoteric replacements in modern drug design. Tetrazoles, in particular, are a larger functional group, which is considered advantageous for an H-bond donor in supramolecular chemistry. [92] (Fig 2.2) Possibly leading to the tetrazoles having shorter and therefore stronger H-bonds with prospective H-bond donors.

Further evidence for tetrazole's use as an efficient replacement comes, again, from the tyrosine phosphatase inhibitor series. While some studies had seen a decrease in activity when a tetrazole was introduced, [86] more specifically when the tetrazole group is used as a replacement for the carboxylic acid attached to the C-3 of the thiophene, others have revealed an increase in potency and permeability when a tetrazole was used as a replacement for the terminal carboxylate. (Fig 2.3) In the crystal structure below the terminal C-2 tetrazole replacement can be seen binding to the Lys120 residue, this was thought to be responsible for the strong interaction observed. (Fig 2.4) [93] This all serves to show the complexity of the relationship between low-molecular-weight inhibitor structure and function.

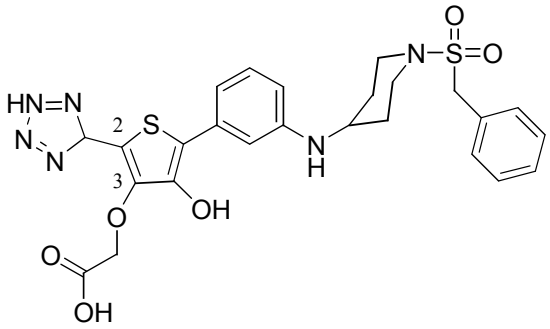

Figure 2.3 Tyrosine phosphatase inhibitor, the tetrazole group can be seen on the C2 terminus, this was associated with a significant increase in activity. The replacement of the carboxylic acid functionality attached to the C3 of the thiophene with a tetrazole had a detrimental effect. [93]

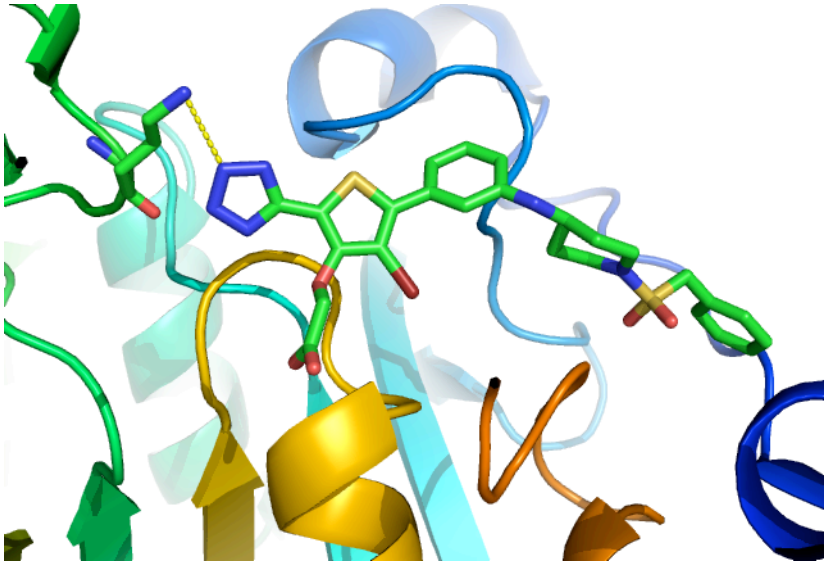

Figure 2.4 Tyrosine phosphatase inhibitor complexed with PTB1B protein. Terminal tetrazole is shown hydrogen bonded to Lys120 (dashed line). [93]

This debate serves to highlight the abundance of highly useful electrostatic groups that are available for incorporation into supramolecular systems. Nature takes full advantage of available anionic groups, e.g. phosphates, carboxylates and sulphates, which serve important functions in metabolic pathways of cells as well as in electrostatic interactions. It is clear that in the search for highly efficient pharmaceutical drugs (inhibitors and antagonists alike) and bio-mimetic receptors, the whole spectrum of anionic (and cationic) groups must be explored. In most of these examples from the literature where tetrazoles have been found effective, a lysine or histidine tends to be near the protein receptors binding site. [90]

2.2 Results and discussion

In an effort to shed some light on how tetrazoles bind and to determine whether a tetrazolate would be a reliable binding motif for supramolecular chemistry, a model system was investigated, using tetrazole and benzamidine or acetamidine (Fig 2.5). Amidines were chosen because of the close structural similarities they have with the guanidine functional group on an arginine residue. However, amidines are simpler to study since they present only a single binding mode whereas an *N*-substituted guanidine offers 3 different possible binding sites. Acetamidine and benzamidine also present the opportunity to probe different environments, the aromatic protons of benzamidine are in a different electronic environment from the methyl protons of the acetamidine. These structures allow the simplest method of probing the arrangement of any interactions with tetrazoles whilst remaining easy to interpret.

A clear pattern of strong binding of the tetrazoles to the amidines would indicate a similarly strong interaction between arginine and tetrazoles is likely.

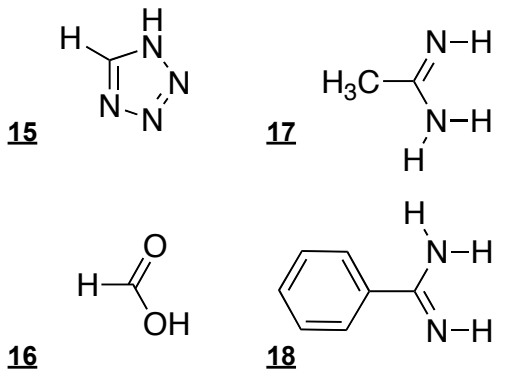

Figure 2.5 Structures of the model compounds used to study the binding strength of tetrazole 15 in relation to formic acid 16 to the guanidine-like amidines 17 &18.

The acetamidine hydrochloride was treated with sodium hydroxide in methanol to give the crude amidine base, which was then purified by gradient sublimation. The free bases were then combined with an equimolar amount of tetrazole to give a 1:1 complex (Fig 2.6). The resulting salt was then recrystallised. Crystals for X-ray crystallography were grown by slow evaporation of a methanol/acetonitrile mixture.

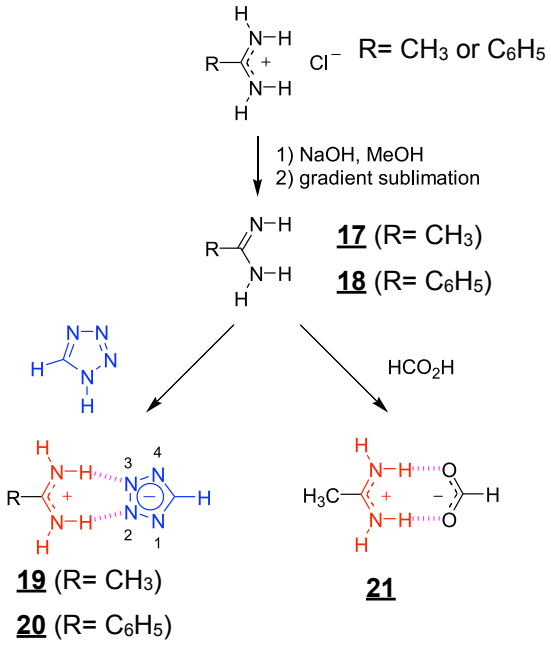

Figure 2.6 Synthetic scheme for tetrazole complexes.

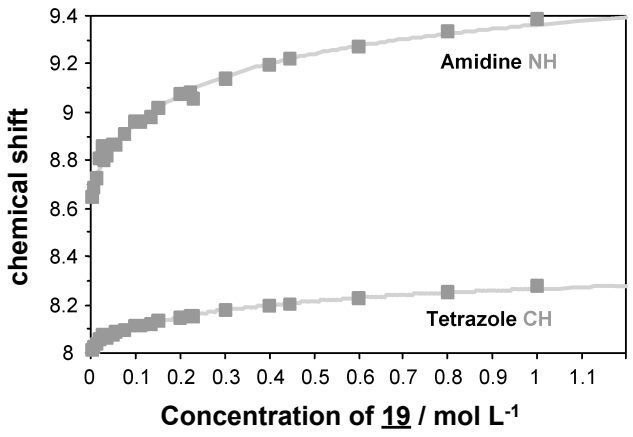

Figure 2.7 Concentration dependence for tetrazole-amidine complex 19 in DMSO. Binding curves were fitted for 1:1 binding.

^{1}H NMR dilution studies were carried out to determine the association constant, K_a, of the complexes. The results of a typical titration can be seen in Fig 2.7. The data was fitted using Equation 2 where δ_{free} and $\delta_{complex}$ is the observed chemical shift of the free species and the bound species, respectively, [*G*] is the concentration of the guest species and K_a is the association constant. [94, 95, 96] A 1:1 stoichiometry was confirmed by a Job plot (Fig 2.8). [97, 98] Since the observed chemical shift is a weighted average signal for the bound species and the free species (Equation 1), Equation 2 can be used to determine the strength of the association constant given that the concentrations are known and the binding is of a 1 : 1 stoichiometry.

$$\delta_{obs} = X_{free}\delta_{free} + X_{complex}\delta_{complex}$$

Equation 1

$$\delta = \delta_{free} - \frac{\delta_{free} - \delta_{complex}}{2[G]} \times 2[G] + \frac{1}{K_a} - \sqrt{\left(2[G] + \frac{1}{K_a}\right)^2 - 4[G]^2}$$

Equation 2

Table 1 Association constants of complexes shown in Fig. 2.6 determined using Equation 2. Details of association constant determination for compounds 20 and 21 can be found in Appendix B.

Complex	Association constant, K_a
19	2.5 ± 0.5 M^{-1}
20	18 ± 3 M^{-1}
21	1600 ± 100 M^{-1}

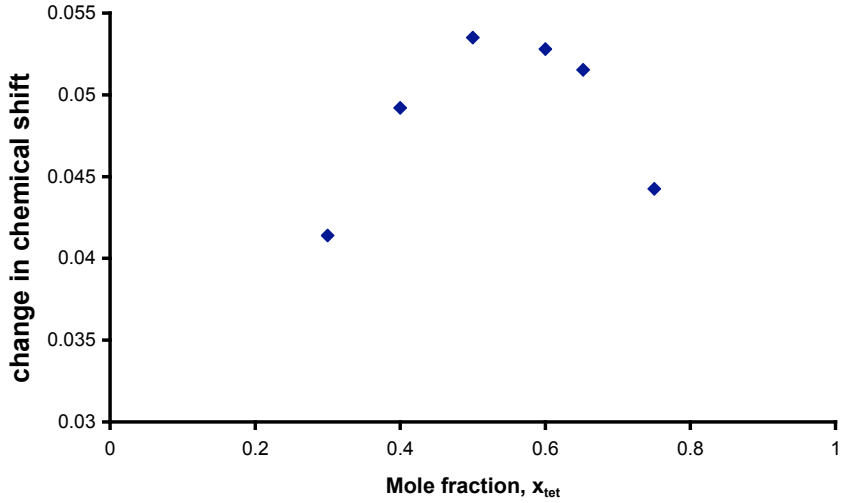

Figure 2.8 Job plot showing the stoichiometry of the tetrazole-acetamidine complex 19.

The results shown in Table 1 display a marked difference in association constants between amidinium tetrazolate and amidinium carboxylate complexes, determined by ^{1}H NMR titration. The crystal structure (Fig. 2.9) of the tetrazole-amidine complexes provided an answer for the surprisingly small association constants. (Table 1.)

Calculated errors for binding constants in Table 1 refer to mathematical error in the curve fitting technique, derived from sensitivity to binding constant and $\Delta\delta_{sat}$ values. Errors present from the chemical shift were thought to be small due to the resolution of the spectrometers and the consistency with other relevant shifts in the spectra.

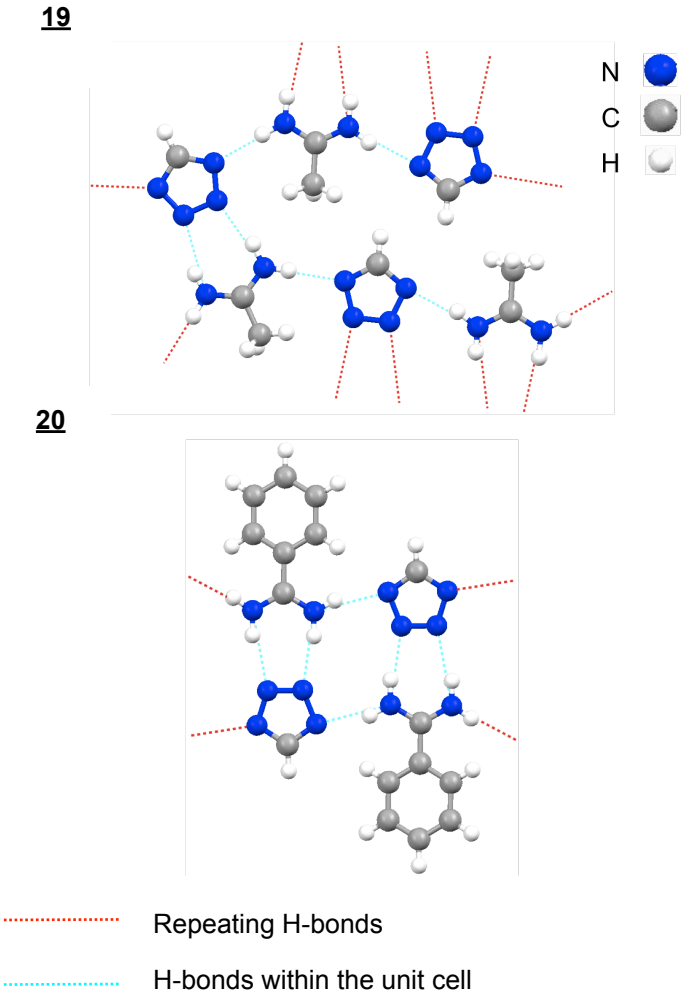

Figure 2.9 Crystal structure of (a) acetamidinium tetrazolate 19 and (b) benzamidinium tetrazolate 20.

Both complexes **19** (Fig 2.9) and **21** (Fig 2.10) are all almost co-planar, with torsion angles of 1.11° (**21**) and 5.5° (**19**). In the case of complex **20** only the benzene group has a slightly higher torsion angle of 22.8°. Complex **21** possesses almost linear hydrogen bonds between the formate oxygen and amidinium nitrogen, with O···H–N angles of 178.6° and 176.6°. The O···N distances of 2.841 Å and 2.870 Å. In the acetamidinium tetrazolate complex the corresponding hydrogen bonds are noticeably bent and N···H–N angles range from 161 to 169°. H-bonds in **19** are also significantly longer, with N···N distances of 2.919 – 2.985 Å. Similar angles and distances, corresponding to the H-bond interactions, to **19** are observed in complex **20**. In both amidinium–tetrazolate complexes, the tetrazole binds in the same way as a carboxylic acid but, both the nonlinear hydrogen bond angles and the longer H-bonds weaken the attraction between the tetrazolate and amidinium ions. Whilst the O···N distances of complex **21** and the N···N distances in compexes **19** and **20** are well within conventional

distances to be considered as H-bonds, the increase of 0.1 Å can have a significant impact on the strength of the bond. [99]

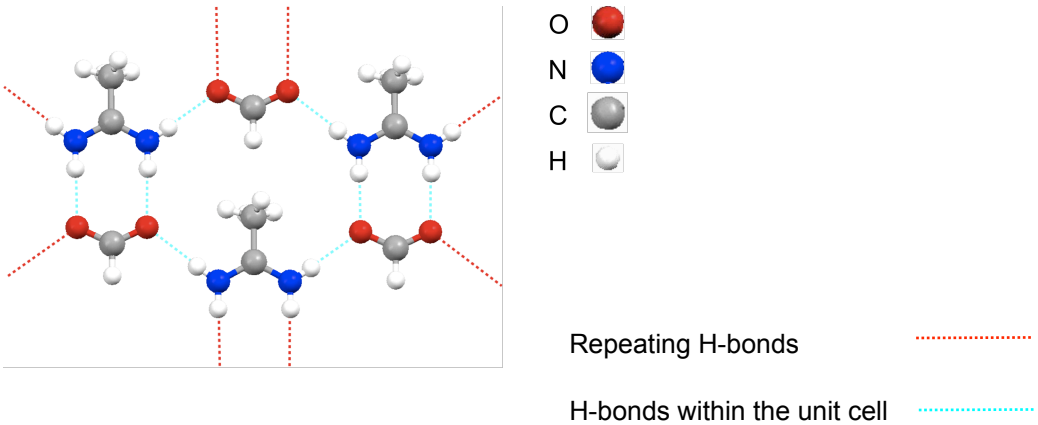

Figure 2.10 Crystal structure of acetamidinium formate 21.

Also worthy of note is the fact that in complex **21** both the inter-complex and intra-complex H-bonds are almost identical in distance, at 2.87 Å (O···N), and angle, 176.6° (O···H–N). Whilst in complex **19** and **20** the lateral, intermolecular H-bonds are in fact significantly shorter than the "binding" hydrogen bond interaction.

A purely structural interpretation would seem to suggest that the analogous structures and H-bonding motifs in the acetamidinium tetrazolate crystals to the acetamidinium formate crystals imply that the association constants should be similar. However since this is not the case, there is clearly a more complex underlying relationship.

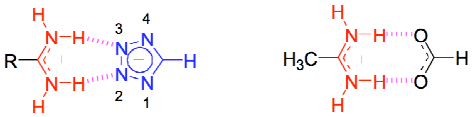

Figure 2.11 A structural break down of the amidinium tetrazolates, 19 and 20, and acetamidinium formate 21.

The charge distribution in the tetrazolate is more predominant on the nitrogen atoms closest to the primary carbon atom, (N^1/N^4) [92, 100] but the arrangement of the constituents in the crystal structure (Fig 2.8) indicates a large contribution from the planar, end-on arrangement of the species shown in Figure 2.11, similar to the salt-

bridge-like structure that is present in the acetamidinium formate **21**. This would seem to indicate that a significant portion of the charge is located on the N^2/N^3 locale or at least enough of a charge density to merit a similar binding behaviour to the carboxylic acid.

The crystal structure (Fig 2.9) also clearly shows evidence for an extensive network of hydrogen bonds, which includes the N^1/N^4 nitrogens and the peripheral hydrogens of the amidinium ion, similar to the side on intra-complex interactions that are observed in the crystal structure of **21**. In the structure of **21** (Fig 2.10) we see that all the hydrogen bonds are roughly the same length; however, in both **19** and **20** it appears that the side-on interactions, from N^1/N^4 to the neighbouring amidinium hydrogen that form the chains, are shorter in length than the intra-complex H-bonds. The distance from the N^2/N^3 of the tetrazole and the hydrogens of the amidine group is slightly increased, with respect to the side-on interactions. The weakening of the association constant may come from the extended length of the intra-complex hydrogen bonds, the tetrazolate N^2/N^3 (the two nitrogens furthest from the carbon) and the amidine. [101] The packing arrangement of the crystal structures showed a layered arrangement but there was no indication of hydrogen bonding between layers and was therefore not thought to be relevant to the discussion. The only significant interactions were planar in orientation.

The above findings do seem to hint at an explanation why the tetrazole is not always a successful replacement for the carboxylic acid when it comes to pharmocophores. The affinity of the acidic heterocycle for the amidine moiety is significantly lower when compared to the low dissociation constant of tetrazoles and amines, for example, ammonium phenyltetrazolate. [106]

Whilst it has been well established that the association constant of the amidinium carboxylate complexes in DMSO at room temperature are well in the order of 1000-3500 M^{-1} [102, 103, 104], this is perhaps not surprising when the structural importance of salt bridges formed by carboxylic acids and arginines in proteins is taken into consideration. It was rather surprising that the tetrazole-acetamidine complex was significantly weaker, even in DMSO. The actual association constant determined by ^1H NMR titrations was found to be 2.5 ± 0.5 M^{-1} (**19**) (Table 1). This small binding

constant in DMSO makes it clear that binding in water would require more than just favourable electrostatic interactions and H-bonds, i.e. a more complex binding site and/ or multiple residue interactions.

From the various literature examples of tetrazole-containing inhibitors it would seem that, when an arginine residue is primarily involved in binding, the tetrazole falls short of being an ideal replacement. When another cationic species is involved, such as a lysine or histidine, the tetrazole remains a highly effective acidic pharmacophore and a valuable bioisosteric replacement.

The results in this chapter support the continued use of tetrazoles in modern drug design but also in certain cases as a possible tool in the supramolecular chemists search for higher degrees of specificity. A tetrazole functional group; with its higher surface-charge distribution, higher lipophilicity, greater membrane mobility and aspects of selectivity, could be incredibly useful in systems where the selective binding of anionic compounds is favourable. [92, 105 , 93] Since tetrazolate-based inhibitors apparently show a significant affinity for lysines, a tetrazole supramolecular receptor should show a preference to amines (see later chapters). The small dissociation constant for ammonium phenyl tetrazolate (2.87×10^{-5} M in DMSO at 25 °C), determined by conductivity measurements is, at present, the only literature report that confirms this suggestion. [106] Further investigations into the binding behaviour of tetrazoles and amines were not carried out in this thesis. A simple system for study could not be formed since fast exchange between ammonium ions and residual water made ^{1}H NMR titrations of ammonium tetrazolates unreliable.

3 Supramolecular binding of protonated amines to microgels

3.1 Introduction

Tetrazoles have been demonstrated as efficient replacements for carboxylic acids in modern pharmaceutical design. The interaction of tetrazoles with protonated amines and amidines has also shown to be biased towards amines. This intrinsic selectivity could be exploited to create a supramolecular host, which could discriminate between functional groups. The following chapter will present the design of a microgel containing tetrazole-binding sites for the supramolecular recognition of low-molecular-weight amines and oligoamines.

3.2 Background

Since the initial report of an artificial secretory granule for doxorubicin (Fig 1.9) by Kiser *et al.* in 1998, microgels have seen a considerable upsurge in interest from research groups seeking to apply the many unique properties of microgels to the biomedicinal field. [22, 107] Indeed it has been widely recognised that the rapid swelling response of certain microgels to external stimuli combined with their small, sub micron size, which allows them to travel in the bloodstream without triggering a response from the immune system, has led to several successful studies outlining possible uses for, among others, non-viral vectors for biotherapeutic agents. [108, 33, 38] The sub micron size of the microgels essentially means that they are too large to trigger immune responses that would typically deal with viral particles and too small to be dealt with by mechanisms which deal with bacterial particles. There is also some evidence that some proteins become adsorbed onto the surface of the microgels *ad vivo* effectively camouflaging them.[109]

A popular method of introducing specificity to a polymer is the imprinting process (Fig 3.1) although highly successful for chromatographic separations with macroscopic gels,

the largest drawback is the low intrinsic solubility in an aqueous medium. [10] Since one of the most significant properties of microgels is their high solubility and low solution viscosity, they have attracted a great deal of interest from groups seeking to utilise the imprinting process with a highly soluble polymer. There have been a number of reports that have suggested an extension of Wulff's [11] imprinting process to microgels (see Chapter 1). [109, 110, 111, 110, 111]

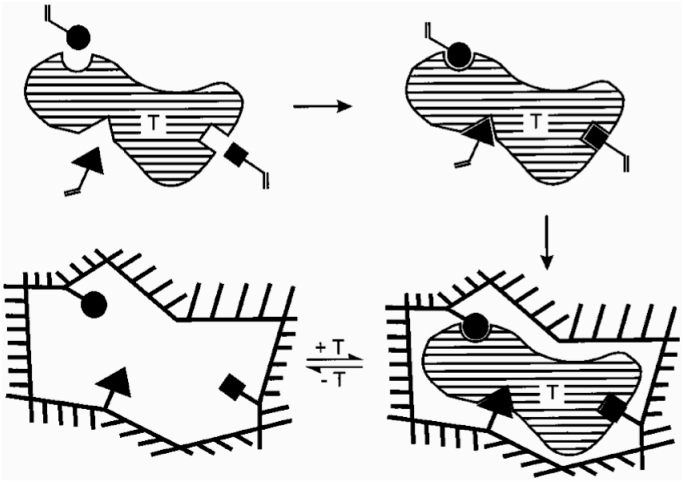

Figure 3.1 Schematic drawing of the imprinting process. Monomers with suitable binding groups (■, ▲, ●) are copolymerised in the presence of a template (T), a crosslinker and a porogen. The polymer, a lightly crosslinked network, is then extracted to remove the template, leaving well-defined cavities behind that possess a suitable shape and binding groups for re-binding the template.

The molecular-imprinting process relies on a template molecule creating a favourable arrangement within a polymeric host during polymerisation. (Fig 3.1) A number of different complementary interactions can be used to allow a template molecule to "arrange" a favourable binding site. In macroscopic gels, such binding sites can be thought of as a physical cavity where a guest molecule can be adsorbed. In microgels, solvent molecules swell the polymer network so the binding sites must rely more heavily on favourable functional group interactions, although the hydrophobicity or polarity of the polymer would still play a role. In the majority of cases the templated ligands that were investigated have been poorly soluble in an aqueous medium. Although a hydrophobic ligand would already show a propensity to occupy the polymer matrix in an aqueous medium, binding via electrostatic interactions would be more

predictable. Frequently, large hydrophobic groups and well recognised and understood H-bond donors and acceptors are used to maximise the possibility of rebinding. (Fig 3.2) [112, 113]

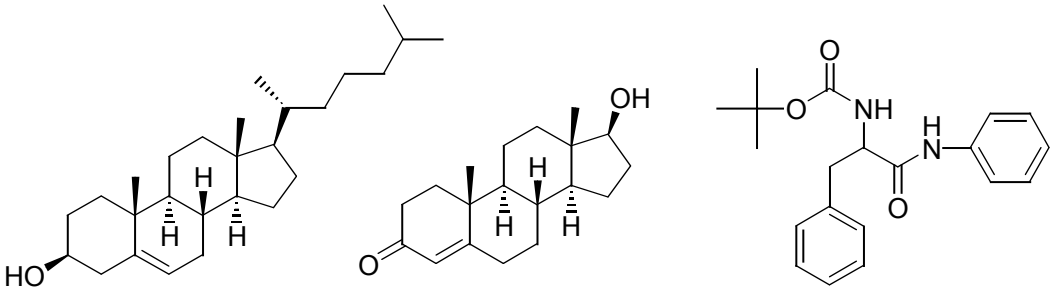

Figure 3.2 Structure of some typical templates used in the imprinting process. cholesterol (left) [112], testosterone (centre) [113] and L-Boc protected phenylalanine (right) [111].

Template molecules are typically chosen because of their rigid structure and the ability to form hydrogen bonds. (Fig. 3.2) However, many templates reported in the literature have a low intrinsic aqueous solubility. This low solubility aids the rebinding process but also necessitates the use of a co-solvent in the rebinding measurements. One goal of the supramolecular chemist is to achieve rebinding of highly soluble molecules in a purely aqueous environment, ideally similar to that found under physiological conditions.

3.2.1 Co-polymerisation properties of NIPAAM

Sodium methacrylate and methacrylic acid have been shown to be poor co-monomers for copolymerisation with NIPAAM. The uptake of the acidic monomers can be sluggish and heavily dependent on whether the acidic group is protonated or not. A high affinity for NIPAAM homopolymerisation leads the formation of polymer chains, which have a very low methacrylic acid content at the initial stages of the polymerisation, whereas later the copolymer becomes very rich in methacrylic acid once most of the NIPAAM has been consumed.

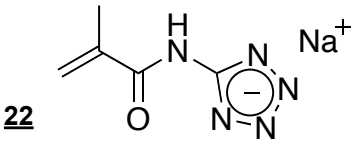

22

Figure 3.3 Sodium 5-(methacrylamido) tetrazolate monomer 22 has been shown to polymerise favourably with NIPAAM.

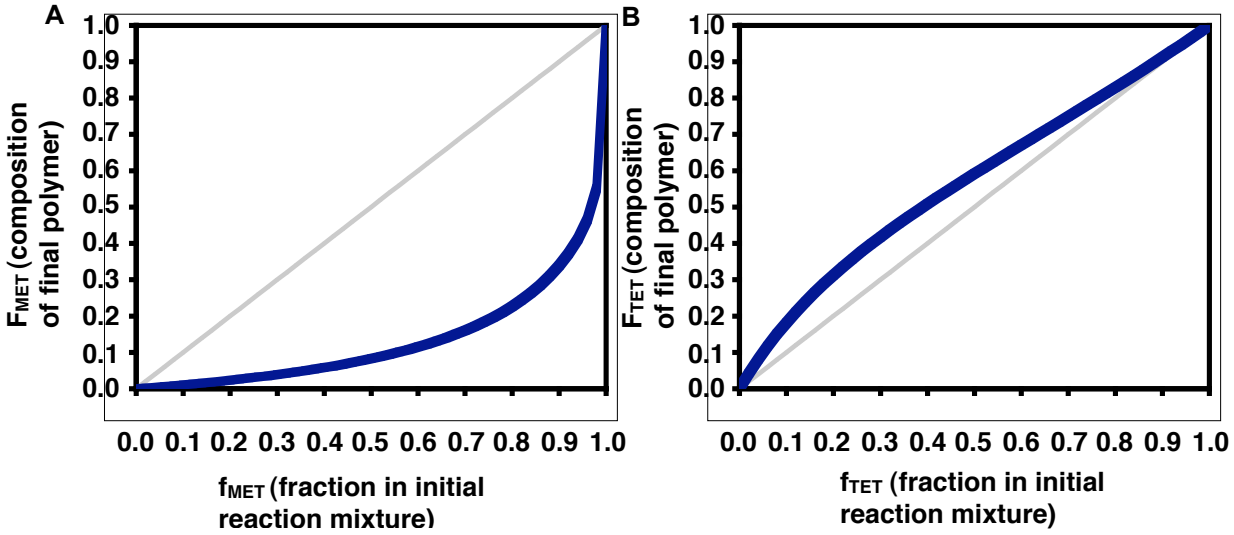

Figure 3.4 In an unfavourable co-polymerisation the homopolymer is preferred and uptake of the co-monomer is sluggish, even at high comonomer concentrations. This is the case for the copolymerisation of NIPAAM with methacrylic acid. (A) In a more favourable example the final composition of the polymer (F_{TET}, y-axis) is closer to the initial reaction mixture (f_{TET}, x-axis). This situation is observed for the copolymerisation of monomer 22 with NIPAAM. (B)

This leads to highly functionalised "shells" surrounding microgels created towards the end of a polymerisation [114, 115] and creates an unfavourable environment for the formation of microgels with a homogenous structure. In order to synthesise microgels with a homogenous structure a monomer with more favourable reactivity ratios is needed. The tetrazolate monomer **22** (Fig 3.3) has an amide group separating the acidic functionality and the polymerisable double bond, it has been postulated that this separation has a stabilising effect, meaning, the reaction is almost independent of whether the tetrazole is deprotonated or not [116].

Favourable reactivity ratios lead to a greater degree of control over the final composition and the polymer.[116] Figure 3.4 demonstrates how the polymerisation of methacrylic acid deviates significantly from the ideal line shown as the diagonal where as **22** hold closer to the ideal polymerisation showing a more favourable reaction. (Table 2)

3.3 Microgel synthesis and characterisation

Microgels were chosen as targets for possible supramolecular receptors due to their ease of synthesis and purification. They are spherical particles with monodisperse size ranges (0.1 to several μm); control over dimensions, and hence physical properties are easily achieved by controlling the reaction conditions. Simple changes in the temperature at which the reaction is kept can have huge effects on the size distribution when temperature sensitive monomers are used. [31] This is achieved when a critical point is reached and the microgel becomes insoluble in the reaction medium crashing out of solution. Altering the initial concentrations of any of the reactive species drastically alters the properties of the microgel; using different concentrations of emulsifying agent and usually sodium lauryl sulphate can also change the size and density of the microgels. [26]

N-isopropylacrylamide, NIPAAM **2** was chosen as the principal monomer for synthesising receptor microgels, due to the wealth of literature available on the reaction conditions and the resultant properties of the microgels. Previous work within the group has focused on the reactivity of NIPAAM with tetrazole containing monomer **22** and found that the radical copolymerisation of the two monomers in water is significantly more favourable to that of the copolymerisation with methacrylate monomers **3** and **4**, with the latter's reactivity ratio differing by three orders of magnitude (Fig 3.4). It was postulated that the replacement of the methacrylic acid component by the polymerisable tetrazolate would give greater control over the negative charge distribution in the resultant microgels. [117] The use of an acrylamide-based monomer was also seen to be advantageous because it introduced amide functional groups to the polymer backbone similar to that found in proteins, creating possible H-bonding sites.

N,N'-methylene-bisacrylamide was chosen as crosslinker to preserve the NIPAAM-like backbone. This monomer is a commonly used crosslinker for environmentally sensitive polymers. The microgels were synthesised by precipitation polymerisation in deionised water at 70 °C with sodium dodecylsulfate as an emulsifying agent. The precipitation of the polymers at a critical size, where they are no longer stable in solution, ensures a narrow size distribution. The addition of an emulsifying agent is also a common method of controlling the dimensions of the final microgel. [118, 119]

Microgels were purified initially by dialysis to remove the unreacted monomer but this lengthy procedure was soon replaced by ultrafiltration using a 100 000 kDa filter. This was followed by another purification step using ultrafiltration through a 0.2 μm filter. The second filtration step was necessary to remove any macroscopic impurities such as aggregates and macroscopic gel particles. It drastically improved the solubility of the polymer and ensured that only microgels were collected from the reaction. The microgels were then isolated after freeze-drying. These samples were highly soluble and formed clear, highly fluid solutions when dissolved in aqueous medium. It was noted that the aqueous solutions were not at all highly viscous as would be expected of linear polyelectrolytes.

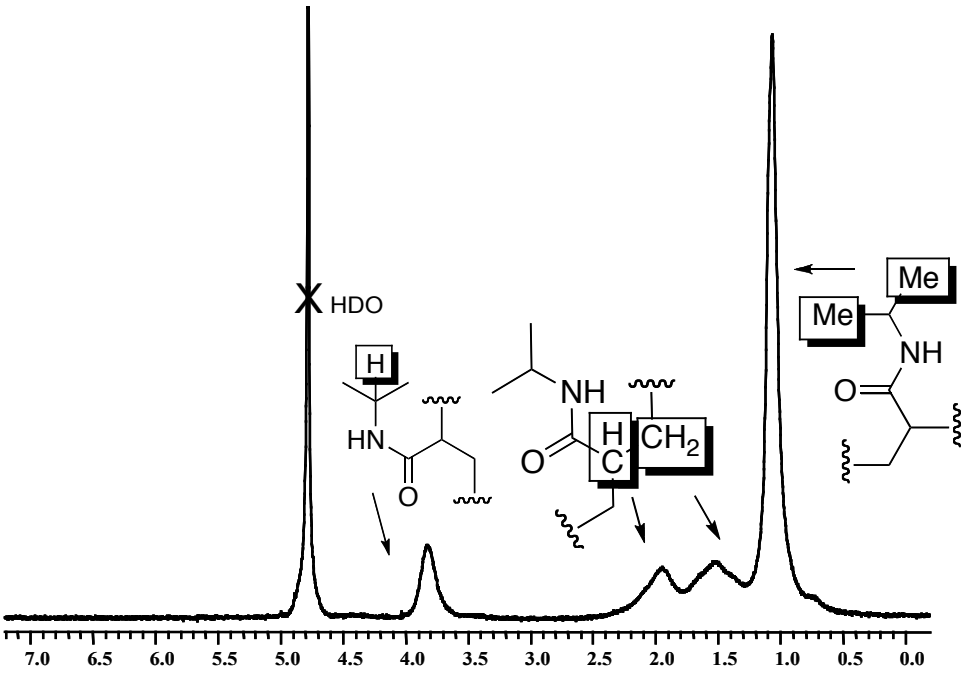

Figure 3.5 A typical ^{1}H NMR spectrum of microgel MG-TET (400 MHz, D_2O) showing characteristically broad polymer signals.

Typical microgel characterisation included FT-IR and ^{1}H NMR spectroscopy. Broad signals in the ^{1}H NMR spectra are typical for a polymer. (Fig 3.5) The absence of acrylic proton signals in the ^{1}H NMR spectrum and lack of a defined C=C double bond signature in the FTIR spectrum indicate the absence of monomer and/or partially reacted crosslinker. Light scattering measurements (David Andrew, Project student), carried out previously within the group, have indicated that the size of the microgel particles peaked at around 0.28 μm, samples for this measurement were not filtered through a 0.2 μm filter. Ultrafiltration, whilst highly efficient at removing macroscopic impurities, does have some degree of error in the actual size cut off. It can be sxpected that whilst some of the larger particles (≥ 0.2 μm) would be filtered out, a significant portion would still pass through the filter. Potentiometric titrations also showed that an initial reaction composition of 8 mol% w/w (tetrazolate **22**/NIPAAM) gave microgels containing 6 mol% anionic monomer, compared to 4 mol% final composition from similar reaction conditions with the methacrylate monomer **4**. (Table 2) The lower methacrylate content confirmed again the differences in reactivity between the two monomers.

Table 2 Comparison of monomer feed percentage and final microgel % composition.

Reaction feed % composition	5%	8%	15%	20%
% composition (**4**)	3	4	8	9
% composition (**22**)	-	6	12	14

The final size, density and thermal characteristics can be controlled by the careful choice of reaction mixture and conditions but have been shown to be heavily dependent on both the crosslinker-monomer ratio and the concentration of emulsifying agent, sodium dodecylsulfate. From the relevant concentrations in the reaction mixture a molecular weight of 2.5×10^{9} g mol^{-1} can be extrapolated with an average diameter of around 250 nm. [32, 120, 121] Light scattering measurements have shown previously that the average diameter was in a good agreement with this figure.

3.4 Supramolecular binding between tetrazolate anions and protonated amines

A number of protonated amines were used to probe the supramolecular affinity of the microgels. The polyamines spermine and spermidine both have multiple positive charges of the amine groups at neutral pH that would create a strong interaction. Dibucaine and propranolol, two commercially available drugs, were chosen as substances in this study because they have UV chromophores. Spermine and spermidine are important polyamines involved in cellular metabolism and are found in all eukaryotic cells. Spermine is associated with nucleic acids and is thought to be important in the life cycles of various cancers and viruses. [122]

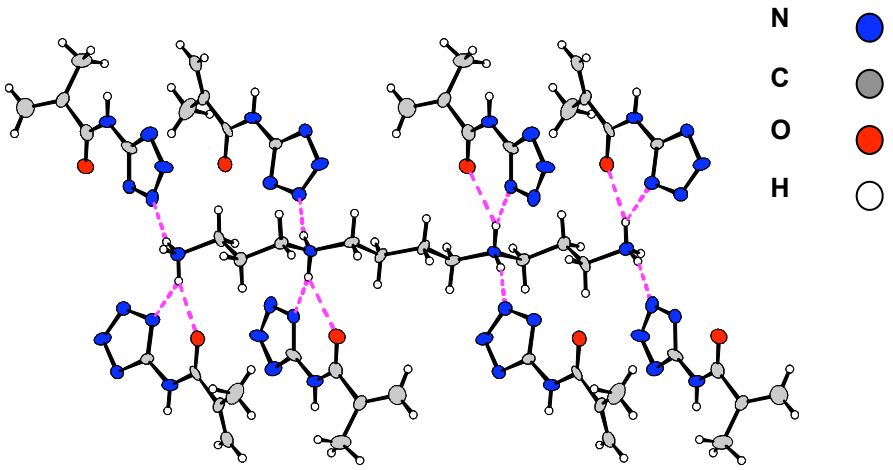

Figure 3.6 Crystal structure of spermine and the tetrazolate monomer 22. (Andrew McIver, Miniproject report, Heriot Watt University, 2002.)

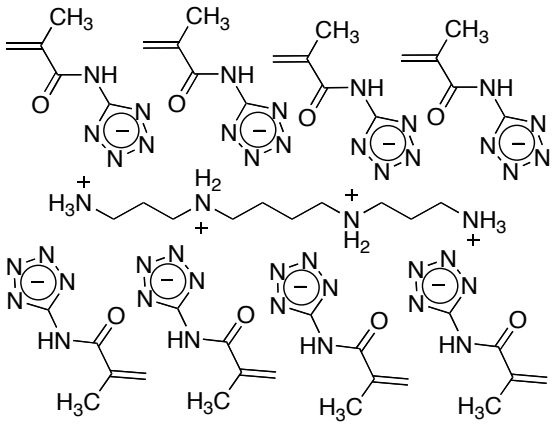

Figure 3.7 Chemical structure of the complex formed from monomer 22 and spermine. (Fig 3.5) This represents a theoretical binding site which could be created within a polymer by reacting the acrylic groups to form a polymer backbone.

Propranolol methacrylate (Fig 3.9) was prepared by precipitating the propranolol base from propranolol hydrochloride in sodium hydroxide and combining it with methacrylic acid in methanol. Slow evaporation in methanol and hexane yielded crystals. This model crystal structure bears a similarity to the spermine methacrylamidotetrazolate crystal structure (Fig 3.6 & 3.7) and also to a structure prepared previously within the group. (Fig 3.10) From these crystal structures we can see that both the methacrylic acid and the tetrazolate monomer are able to bind to protonated amines in a similar manner. Figure 3.9 shows that the carboxylate anion H-bonds to both the hydrogen on the quaternary nitrogen and the proton on the OH group, thus forming a nine membered ring (H12, O2, C20, O3, H13D, N13, C13, C12, O12). This kind of dual interaction is not unusual with carboxylic acids.

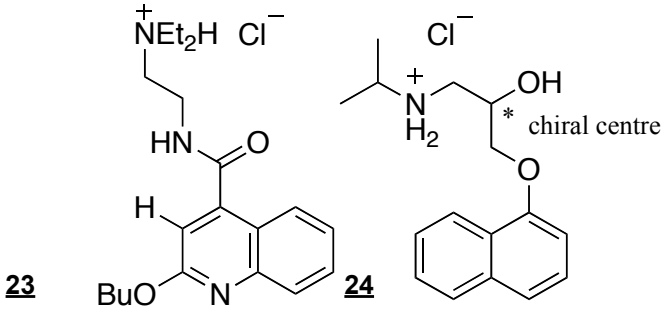

23 **24**

Figure 3.8 Structures of the local anaesthetic dibucaine 23 and β-blocker propranolol 24.

Interestingly, in both structures involving the tetrazolate two different types of interaction can be seen, in one case the carbonyl and the nitrogen α to the tetrazole carbon are both binding to the propranolol molecule this is shown by the red dashed line in Figure 3.10. In the other case, the β nitrogen of the tetrazole is involved solely in binding (the blue dashed line in Figure 3.10). The structures shown in figures 3.6, 3.9 and 3.10, represent ideal configurations for binding sites between carboxylate anions, tetrazolates and the protonated amines, e.g. propranolol and spermine.

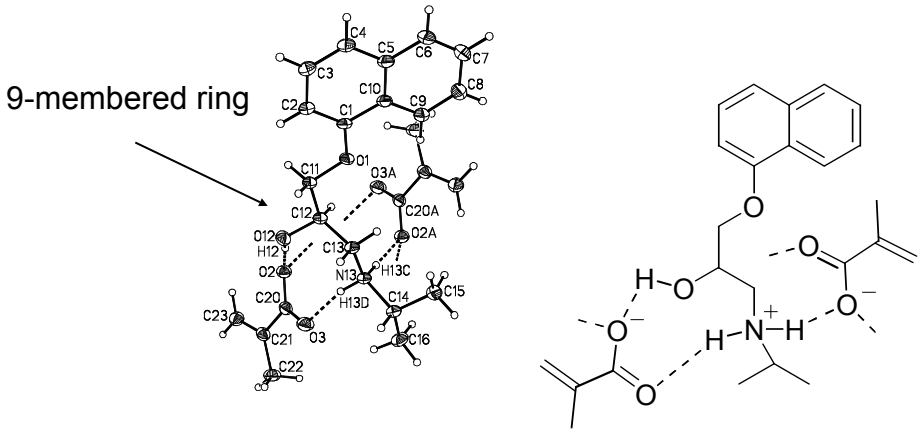

Figure 3.9 Propranolol methacrylate crystal structure.

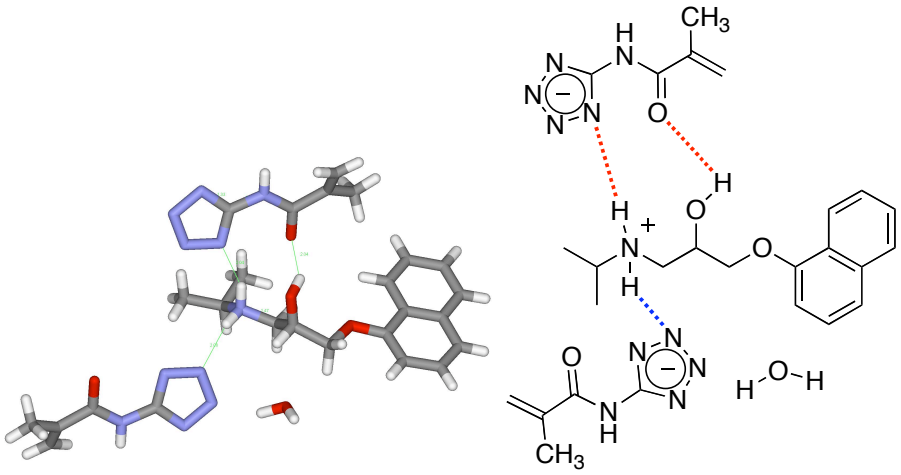

Figure 3.10 Propranolol methacrylamidotetrazolate crystal structure. (Lewis Oliphant, BSc (hons) dissertation, Heriot Watt University, 2003.)

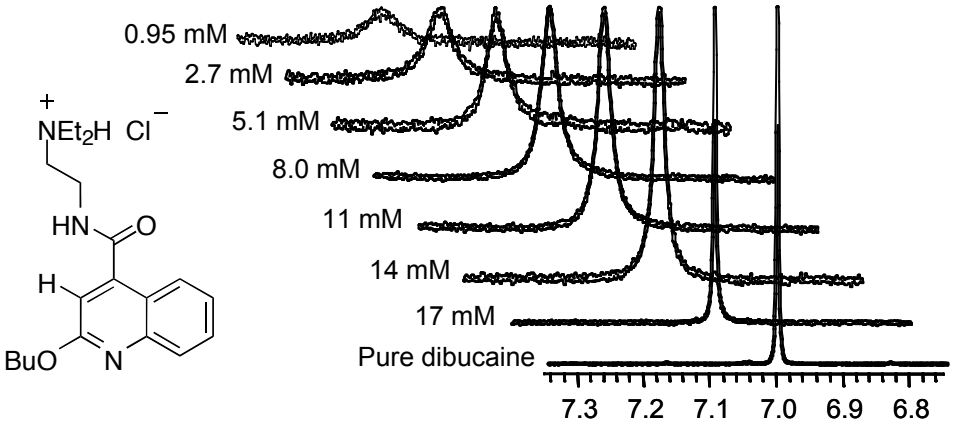

Figure 3.11 Stack plot of dibucaine's aromatic 3-H signal at various concentrations. Dibucaine concentrations are shown in millimoles per litre (microgel concentration: 2.2 mg in 0.70 mL). Spectra are offset to show line broadening with respect to concentration; no significant signal shift was observed upon binding.

Preliminary binding measurements were undertaken using ^{1}H NMR titrations. The interaction of the low-molar-mass ligand with the microgel induced broadening of the ligand signals in the ^{1}H NMR spectrum. Line broadening of the ^{1}H NMR signals was consistent with binding. [123] The broadening was brought on by the decrease of the T_2 relaxation time as the ligand took on the lower tumbling rate of the microgel. [124] Line broadening is a relatively common effect in the NMR spectra of polymer solutions; it can also be due to a high solution viscosity or an artefact of shimming errors. The characteristically high degree of solubility and relatively low viscosity of the microgel solutions ruled out this cause for any line broadening.

The most noticeable result from these experiments was for dibucaine's aromatic 3-H signal (Fig 3.10) in D_2O at pD 7.4. Line broadening can clearly be seen at millimolar concentrations in the ^{1}H NMR spectra (Fig 3.11). This was an encouraging sign of supramolecular binding of the amine drug to the microgel in a phosphate buffer at physiological ionic strength (0.15 mol/L).

In other cases, supramolecular binding leads to a complexation-induced shift in the signals of the NMR spectrum. Complexation-induced shifts refer to a change in the chemical shift of the host/guest system when binding occurs under fast exchange on the

NMR time scale. (Fig 3.12) This change is brought about by the changing electronic environment of the free, solvated ligand to the fully bound guest in a binding cavity. [94, 95, 96]

NMR titrations were carried out using a phosphate buffer at a pD of 7.4 and an ionic strength of 0.15 M. The pD of 7.4 in D_2O corresponds to a pH of 7.0 in H_2O due to the deuterium ion affinity being offset by 0.4 from the pH scale. Figure 3.12 shows how the signals of spermine shift by up to 0.3 ppm with increasing microgel-to-spermine ratio.

Binding between microgels and spermine was further confirmed by isothermal microcalorimetry. The results were in agreement with the observations in the NMR titrations (Fig 3.12). The binding constant for the spermine-microgel system was determined by fitting the data to an *n* : 1 binding model which gave an estimated binding constant of about 700 M^{-1}, with a stoichiometry close to that of the value expected for four tetrazoles per binding site. This binding constant confirmed the observed binding evidence in the NMR titrations at millimolar concentrations.

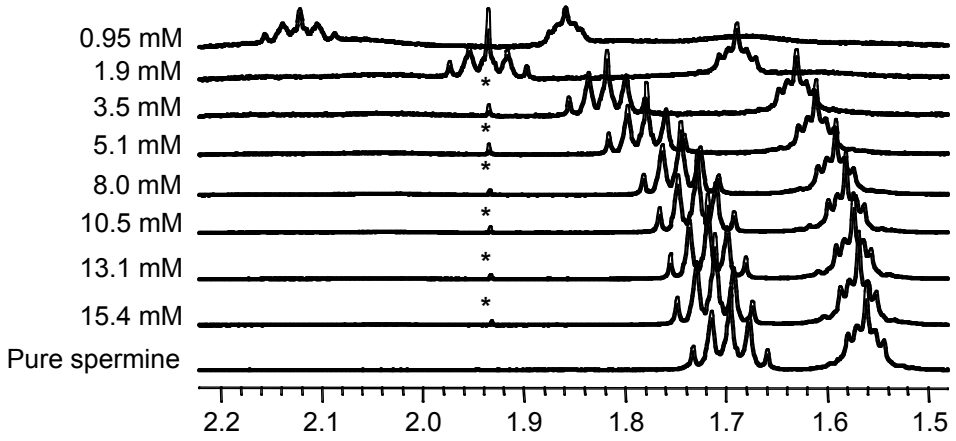

Figure 3.12 ^{1}H NMR (400 MHz, D_2O, pD 7.4) spectra of a typical NMR titration of spermine tetrahydrochloride guest into a solution of microgel (3.0 mg/0.70 mL) showing characteristic complexation induced shifts of several spermine CH_2 signals. An asterisk (∗) marks the signal of an acetone impurity.

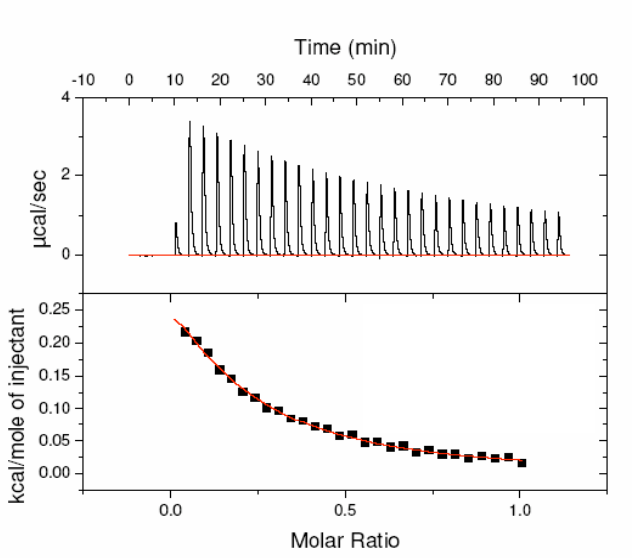

Figure 3.13 Isothermal calorimetry titration of spermine into a solution of microgel in pH 7 phosphate buffer. Molar ratio refers to the ratio of spermine to tetrazole in solution. (ITC measurements were carried out by Dr. Sijbren Otto at Cambridge University).

Positive values for ΔH and $T\Delta S$ (3.2 kJ mol^{-1} and 19.2 kJ mol^{-1}, respectively) accounted for an endothermic, entropy-driven process. This could be indicative of water being released from the binding cavity. It is also possible that some kind of rearrangement of the binding cavity, allowed by the flexible nature of the polymer backbone, is responsible for the positive enthalpy. Driving highly soluble ligands from aqueous solution into the body of the microgels, a slightly more hydrophobic environment would still require some significant attractive contribution from the microgels. A possible cavity rearrangement combined with the release of water molecules from the site of binding could explain the perceived *endothermic* ΔH whilst still allowing for a significant and possibly more important electrostatic binding event. These processes are not unheard of in Nature where certain protein-ligand systems show similar effects upon binding.[125, 4] Entropy-driven processes are not unusual for small molecules complexing to proteins. An example is the case of alpenolol binding to the cellulase Cel7A, where the entropically driven process is attributed to the inclusion of the ligand into a cavity and the loss of water.[126] A similar effect has also been seen in the conformational change when berberine binds to polyriboadenylic acid.[127]

To confirm that binding was not solely due to the positive charge of the ligands, two further experiments were undertaken. When tetramethylammonium salt (NMe4Cl) was combined with the microgel, no evidence of binding was observed although binding of the cation to the negatively charged microgel could still be possible (ion exchange). In this case, the absence of binding was attributed to the inability of the cations to hydrogen bond to the microgel. Similarly, benzamidinium hydrochloride [128] did not bind to the microgel. This was consistent that the positive charge alone was not sufficient to effect binding. NMe_4^+ is an alkyl ammonium salt with an alkyl group which provides steric hindrance to any supramolecular bonding but would still allow for an ion exchange process to take place. No evidence of such an ion exchange was observed in a ^1H NMR titration. The high ionic strength of the aqueous medium in which the tests were carried out would also explain the lack of ion exchange, since the 154 mM KCl is far in excess of the concentration of the NMe_4^+.

Benzamidinium hydrochloride was also used to investigate the possibility of ion exchange being the major contribution to the observations. Previous work, discussed in Chapter 2, had shown that the amidine functional group would have relatively little affinity for the tetrazoles in aqueous medium, since they only showed a weak affinity in DMSO.

The absence of an ion-exchange process points towards supramolecular binding as the dominant mechanism. The difference in concentration between the non-complexing salts and the salt concentration of the buffer means that it would be unlikely that ion exchange takes place. It should also be noted that these salts have a slightly more hydrophobic nature than some of the ligands used in this study and, would in theory, prefer the non polar environment inside the shell of the microgel. It can therefore be postulated that an ion exchange effect was too weak to be noticed, or was not present.

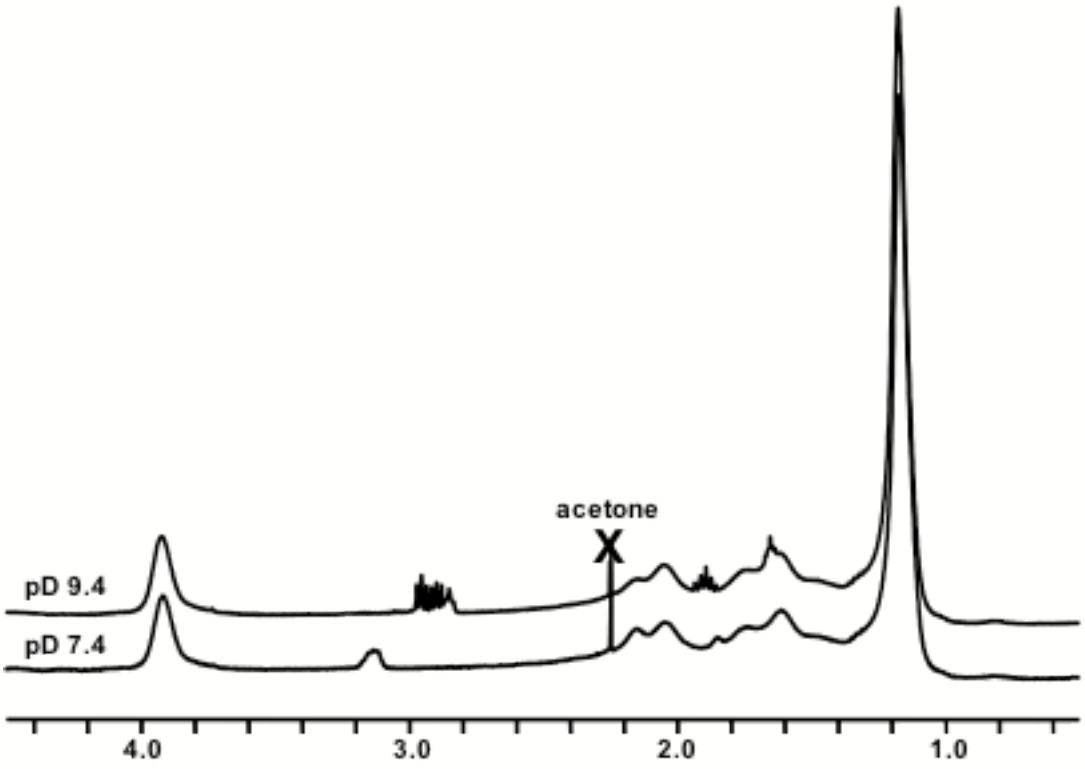

Figure 3.14 Spermidine-microgel at pD 7.4 shows characteristic line broadening and complexation-induced shift. At pD 9.4 the fine structure of the proton signals becomes clear again (400 MHz, D_2O).

Further investigations were carried out into the nature of the host/guest interaction. NMR measurements at pD 9.4 revealed neither line broadening of spermidine nor complexation-induced shift. (Fig 3.14)

Spermine has 4 pK_a's and at pH 7 spermine would be nearly fully protonated, since the pK_a's for spermine are 10.8, 10.0, 8.9 and 8.0 (at 100 mM ionic strength and 25 °C). [129] At a pH of 9, however, spermine would hold predominantly 1 proton with only a fraction of the spermine being doubly protonated. Protonation of the amine was therefore assumed to be an important factor; the neutral species does not bind to the microgel. This points towards electrostatic interactions being the major component of the observed behaviour.

3.5 Conclusion

In conclusion, these results demonstrated supramolecular binding of protonated amines in a competitive aqueous environment using microgels with tetrazolate binding groups. ^{1}H NMR evidence from line broadening and complexation-induced shifts pointed towards supramolecular binding of, among others, spermine, spermidine, propranolol and dibucaine in the millimolar range. This was in agreement with isothermal titration calorimetry measurements (in the case of spermine).

An electrostatic contribution to binding was evident from the observation that deprotonation of the oligoamine, spermidine, at high pH saw a return of the fine structure of the ^{1}H NMR signals, representing a loss of line broadening and, therefore, binding behaviour. Ion exchange was unlikely due to the relatively high concentration of ions in solution (154 mmol L^{-1}) compared to the concentration of the target ligand (*ca.* 1-15 mmol L^{-1}). Titrations with a tetramethylammonium salt and benzamidinium salt also demonstrated that ion exchange was not the driving force for the affinity of the microgels towards the selected ligands. Where simply the most charged species is being bound but rather a supramolecular interaction is taking place. [130, 131]

The supramolecular binding of protonated amines in water at pH 7 and at an ionic strength of 0.15 M was a significant step towards artificial polymeric receptors for low-molecular-weight compounds in a competitive aqueous environment.

These results suggest that both hydrophobic and electrostatic contributions play an important role in the supramolecular binding of protonated amines to microgels. Microgels therefore should not only be good at binding small molecules but it may also be possible to bind larger guests, particularly if they are multiply charged. The next chapter will therefore look at the suitability of the microgels for protein binding. The ability of the microgels to be tailored to bind specific guests (proteins) selectively will also be investigated.

4 Microgels for protein specific recognition

4.1 Background

Proteins have a wide array of roles in Nature, from purely structural materials to highly functional catalysts and receptors, where binding sites afford selectivity unrivalled by most modern catalysts. The surface interactions of proteins have been studied in great detail recently.[2, 4, 5] The electrostatic attraction of oppositely charged groups is often supplemented by the complementary interaction of hydrophobic "patches" on the surface of proteins where areas of low hydrophilicity are usually surrounded by charged residues.[3] Currently, there is growing interest in the understanding and the manipulation of protein–protein interactions.[79, 2] Synthetic polymer model systems remain at the forefront of these investigations, due to their perceived ability to disrupt protein–protein interactions, in a manner not available to low-molecular-weight compounds.[79]

A number of possibilities present themselves as motifs to promote protein binding to polymeric materials. Both electrostatic interactions involving ionic groups, and hydrophobic interactions, are important factors in protein structure and protein–protein binding and can not be overlooked. Recognition, of targeted proteins on a molecular level, is also one of the challenges that many supramolecular chemists are currently tackling.

A few reports have suggested that molecular imprinting [132] can be used to target proteins for binding. Wang *et al.* recently reported the creation of surface molecularly imprinted nano-wires and postulated possible uses such as in chromatography and biochemical sensing. [133] In principle, most molecularly-imprinted polymers (MIPs) tend to be insoluble, and any re-binding experiments take place in a chromatographic fashion where the imprinted polymer acts as a stationary phase and the target proteins are solvated in a mobile phase. These MIPs are typically packed into an empty column and measurements are then carried out on protein uptake. [134, 135, 136] Similarly, a

thin film approach has also been taken by Ratner and co-workers who used a deposition technique to create molecularly imprinted thin films on mica surfaces. The binding behaviour of these thin films was quantified by observing the protein uptake onto the film and competition adsorption studies showed a high level of specificity.[137] These chromatographic separations and thin film MIPs rely greatly on surface absorption and complex surface cavity interactions between the polymer and the protein.

The use of hydrogels as MIPs presents the possibility of 3-dimensional binding sites, which should lead, in principle, to better selectivity and stronger affinity. A hydrogel, i.e. a network polymer that is fully solvated in the aqueous phase, would allow the protein full access to its internal structure and therefore would be able to "envelop" the protein more fully. A hydrogel would also have the advantage that aqueous media can easily be used in both synthesis and binding characterisation. It has also been suggested that this should ensure the stability and solubility of the protein.[138] Supramolecular binding of proteins in an aqueous medium is made trickier since the polymer, which is to bind the protein, should be soluble in water to aid transport in a biological system and administration, should these become successful treatments. Although it has been suggested that hydrogels would show all these improvements, very little work has been done to confirm these statements.

In recent years substantial progress has been made by Schrader *et al.* who achieved selective, albeit in some cases irreversible, binding of highly charged linear polymers to basic proteins, such as histone and ferritin, in aqueous solution. This success was attributed to monomer **1** [6, 139, 140, 141] which gave the copolymer a high affinity to arginine-rich proteins, such as cytochrome C (6×10^6 M^{-1}) and ferritin (2×10^6 M^{-1}).[6] This represents a deliberate and targeted approach to bind arginine-rich proteins. This kind of selectivity, without the need to imprint the polymer, seems to have the ability to create highly efficient protein binding polymers. (Fig 4.1)

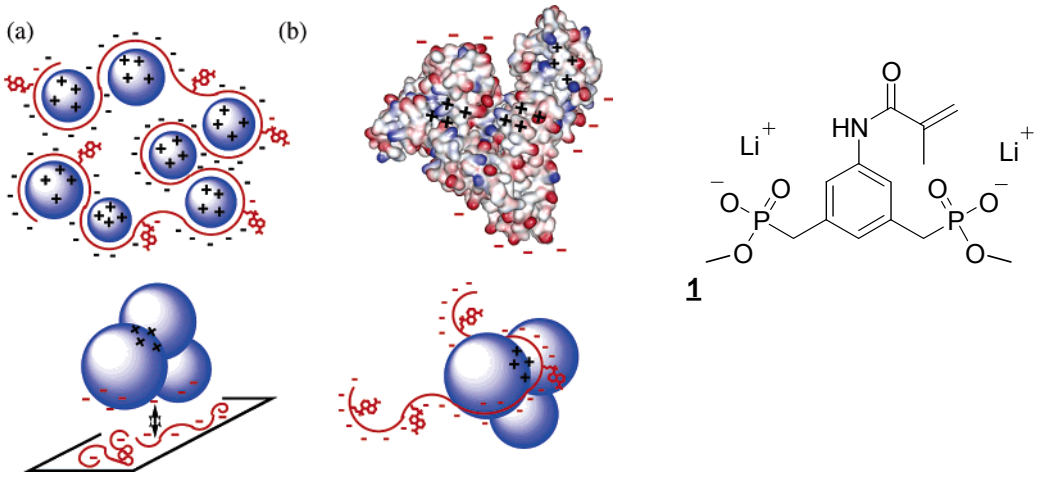

Fig 4.1 (a) Schematic diagram of the postulated binding mode between a fluorescently labelled linear copolymer and cytochrome C (b) A representation of bovine serum albumin's protein topology; the lysine rich domain of the protein is only accessable by the polymer in solution and not by the deposited thin film. [6]

Rotello *et al.* have shown that gold and cadmium selenide (CdSe) nanoparticles coated with amino acid groups can bind to chymotrypsin and display inhibition of the enzyme's catalytic behaviour. [142, 143, 144, 145] No attempt has been made to use an imprinting technique on these nanoparticles yet, but they already show very high affinities towards certain target proteins. Some nanoparticles have even demonstrated control over the facial orientation of the bound protein after tailoring the functional groups used to bind different binding surfaces. [16] Rotello and Knapp showed that facial selectivity of cytochrome C (cytC) was achievable with functionalised gold nanoparticles. By tuning the nanoparticle surface with different functionalities to mimic the functional binding sites for redox partners, it was possible to select the orientation of the protein that was bound to the surface. (Fig 4.2)

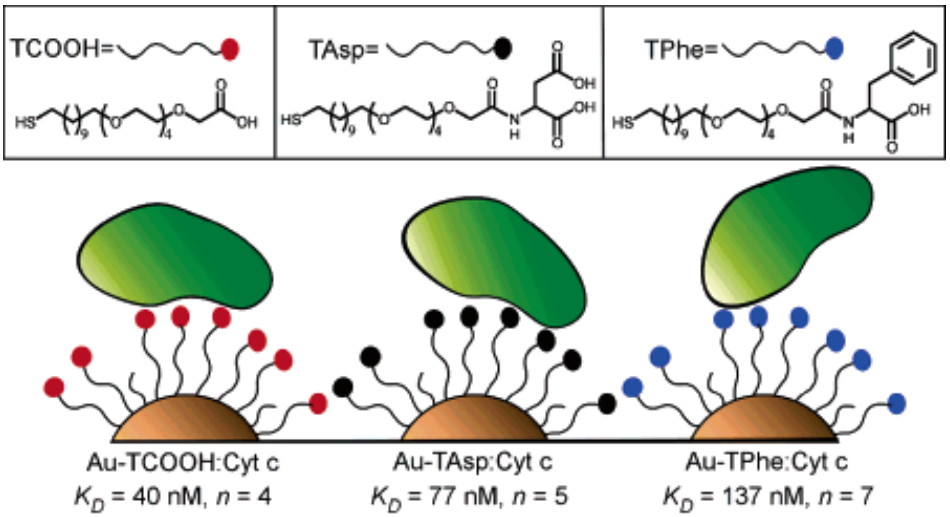

Figure 4.2 Chemical structure of the functionalised gold nanoparticles used by Rotello and Knapp and a schematic representation of the surface-specific interactions with cytochrome C. [16]

Microgels, too, have been considered for interactions with proteins. Linse and co-workers were among the first to investigate the binding of proteins to poly-NIPAAM microgels, although binding was essentially due to hydrophobic interactions. [146] This study highlighted the phenomenon where nanoparticles in biological fluids became coated with proteins and the toxicological effects of this. They found that polymer nanoparticles bound proteins depending on their hydrophobicity and radius of curvature. ITC turned out to provide a simple way of measuring the adsorption in a quantitative manner.

The supramolecular binding of proteins in aqueous media by microgel particles would present another step towards the deliberate and designed binding of important biomacromolecules in a highly competitive environment (Fig 4.3). The following chapter will present the results of an investigation into the use of different co-monomers in the synthesis of microgels for protein binding. Following on from the results in previous chapters, where tetrazoles have shown a marked bias for protonated amines, the following investigation will also attempt to determine whether or not a degree of selectivity can be instilled onto a microgel by the careful selection of the co-monomer.

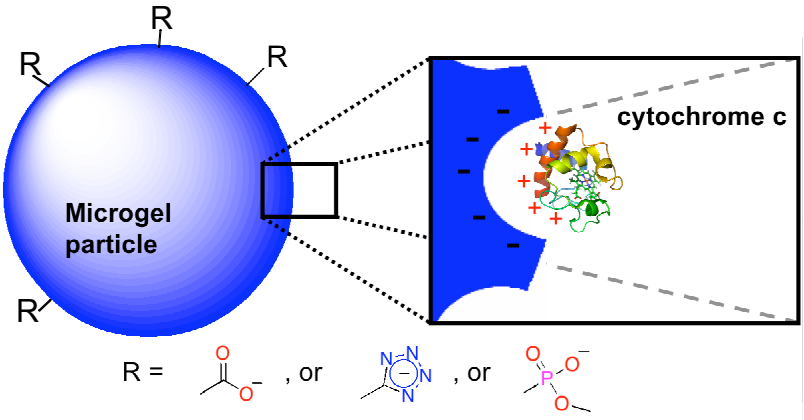

Figure 4.3 Schematic of microgel particle interacting with a cytochrome C molecule. It should be noted that the microgel particle (average diameter ~200 nm) is significantly larger than the protein.

4.2 Characterisation of supramolecular binding of proteins to microgels in an aqueous medium

Many common, commercially available proteins such as haemoglobin, cytochrome C and ferritin possess strong chromophores. (Fig 4.4) In addition to the aromatic amino acid residues,tryptophan, phenylalanine and tyrosine, haemoglobin has four porphyrins and, as a result, absorbs strongly in both the near and far UV spectrum (*ca.* 300-400 nm and 200-300 nm, respectively) and on into the visible spectrum. The strong Soret band of the haem group in haemoglobin can be used as an extremely sensitive method of haemoglobin detection. [147]

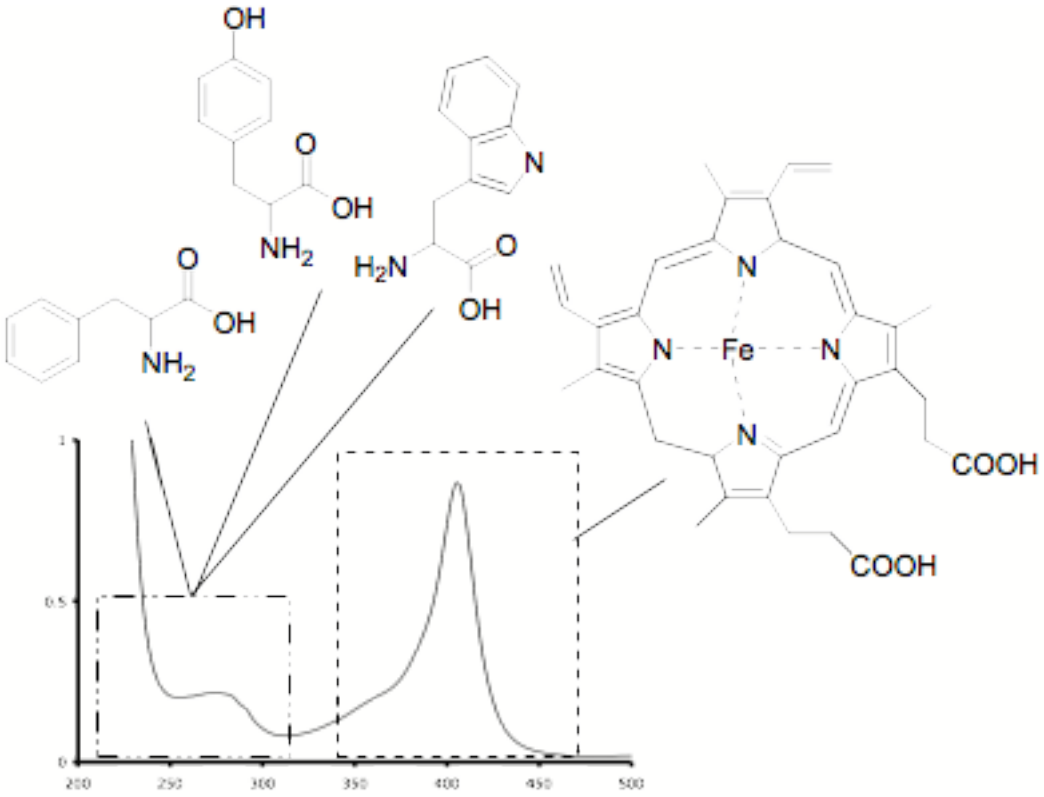

Figure 4.4 Aromatic amino acids give proteins a degree of UV absorption but the haem group in haemoglobin also has a strong Soret band at 410 nm (2.19×10^{-5} mol/ L in aqueous phosphate buffer at pH 7).

The fundamental principle behind a UV-Vis titration is that, upon binding, the change in environment of the protein changes the peak absorbance for the Soret band. Plotting the change in the UV absorbance spectrum throughout the titration, with respect to concentration, can be used to determine whether or not binding is taking place. These titrations were carried out in aqueous pH 7 buffer at physiological ionic strength of 0.15 mol L^{-1} to properly mimic the serum conditions and insure the native charge and structure of the protein would be preserved for realistic binding studies.

Incorporation of a polymerisable carboxylate **4**, tetrazolate **22** or bisphosphonate **1** (Fig. 4.5) into the microgel was anticipated to promote electrostatic interactions with positively charged residues on the protein surface. It was hoped that the inclusion of a large number of charged groups on the surface of the microgel would create favourable interactions with positively charged proteins whereas the choice of the anionic co-monomer (SMA, TET or BP) (Table 3) would provide an element of selectivity, e.g. for arginine or lysine-rich proteins.

Microgel	NIPAAM /mol%	MBA (crosslinker) / mol%	10% anionic co-monomer /mol%
MG-SMA	80	10	4
MG-TET	80	10	22
MG-BP	80	10	1

Table 3 Microgel reaction composition

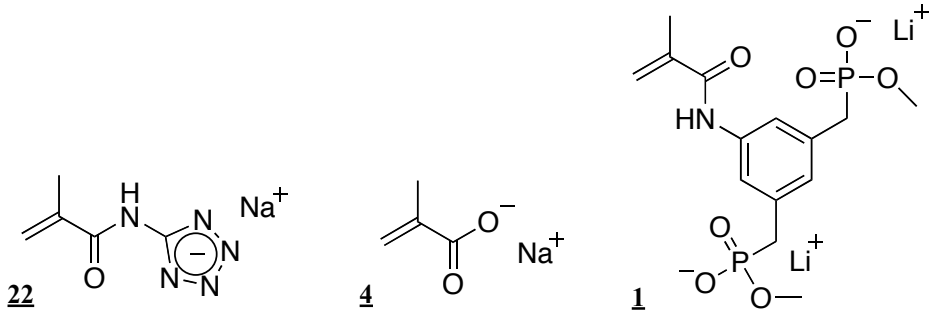

Figure 4.5 Monomers used to promote supramolecular binding of proteins to microgels.

Three microgels (MG-SMA, MG-TET and MG-BP) were prepared using the same procedure as described in Chapter 3. ^{1}H NMR and potentiometric titrations were performed in order to determine the compositions of the various microgels.

4.3 UV-vis titrations

The addition of microgel to a protein solution during UV-Vis titrations led to UV spectra of poor quality initially, owing to the microgel particles having a size (~ 0.2 μm) large enough to scatter UV and visible light. This increased the background noise of in the measurement and hindered consistent analysis. This was overcome by using the second derivative method developed by Savitzky and Golay. [148, 149] The second derivative of the UV absorbance is still concentration-dependent but the mathematical tranformation negates any baseline offset and therefore produces a higher quality spectrum (Fig 4.6 and 4.7). Isosbestic points were clearly displayed in the second derivative UV-Vis spectra. A bathochromic shift in the wavelength of the Soret band was also more easily observed for the titration of cytochrome C and **MG-SMA** (Fig 4.8).

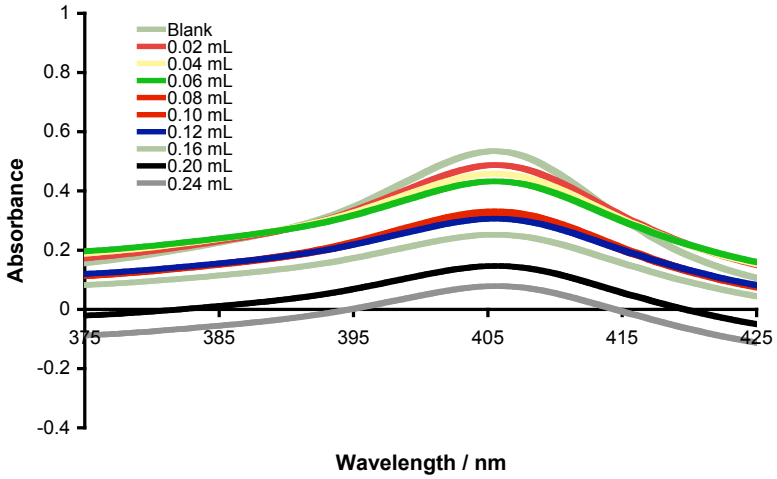

Figure 4.6 UV absorbance data for a typical UV titration. In this example a solution of haemoglobin (1.24×10^{-5} mol/L) in phosphate buffer (pH 7) was titrated with a microgel solution (MG-BP). Although the change in peak height can clearly be seen, serious problems with baseline offset causes the quality of the spectrum to decrease. The inset (and colour code) refers to how much of the microgel stock solution (in mL) has been added to the protein solution. For further details, see Experimental.

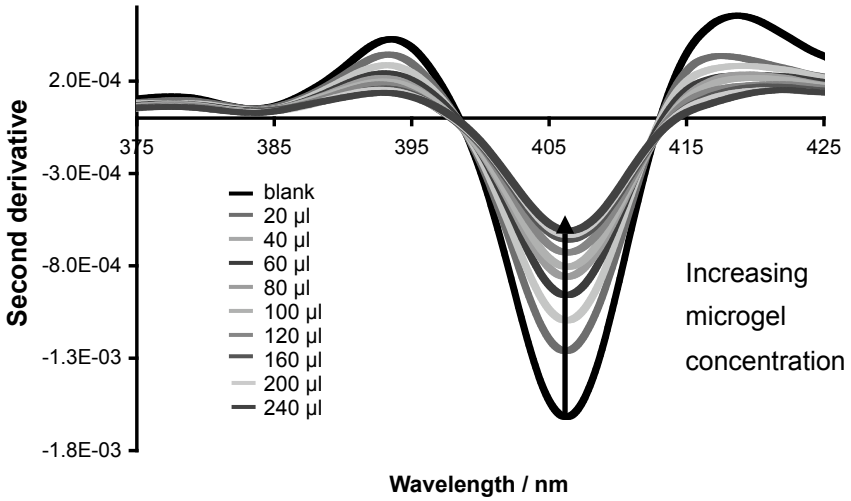

Figure 4.7 The second derivatives of the UV spectra shown in Fig 4.6 demonstrate the advantage of using this technique. Clear isosbestic points at 397 and 413.5 nm are now visible.

Titrating a solution of **MG-SMA** into buffer solution containing cyt-C displayed clear evidence of binding (Fig 4.8). Isosbestic points were visible at 398 nm, 412 nm and 423 nm, indicating that two species were present in the solution. These were thought to represent the bound and unbound species. The presence of isosbestic points, the bathochromic shift of the peak absorbance moving from (410 nm to 413 nm) and the decrease in peak height are all evidence of binding of the protein to the microgel.

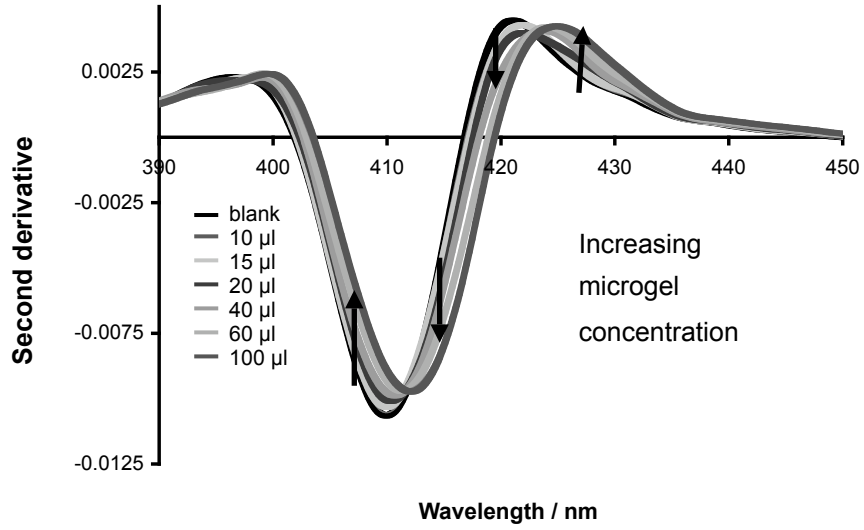

Figure 4.8 Second derivative UV spectra of a titration of MG-SMA solution (10 mg/mL) into cytochrome C (1.02×10^{-5} mol/L) in 20 mM phosphate buffer (KCl 0.15 M).

MG-TET showed a much higher degree of binding to haemoglobin (Fig 4.9). The second derivative spectra showed a larger change in peak height but there did not seem to be any bathochromic shift involved. This became characteristic of haemoglobin binding to microgels and was thought to be brought about by the porphyrin rings being buried deeper into the structure of the protein in haemoglobin than in cyt C and therefore being shielded from the same change in electronic environment changes that brings about the bathochromic shift in cyt C.

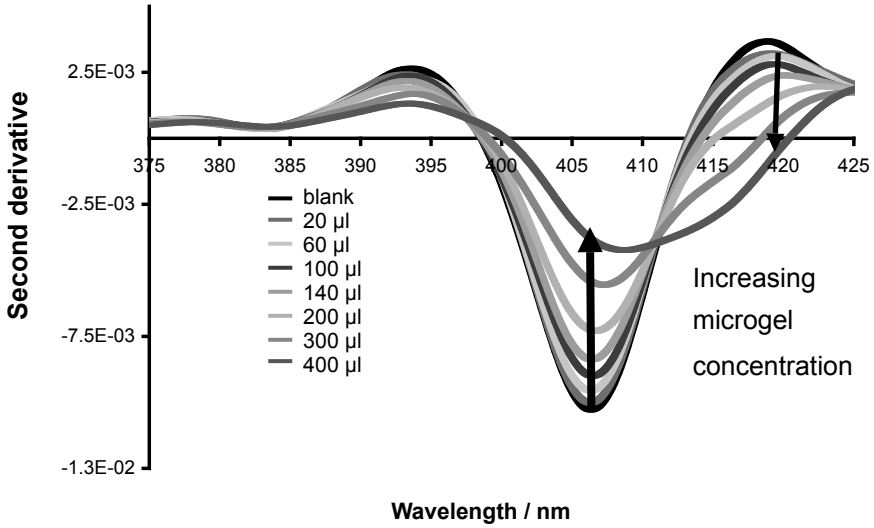

Figure 4.9 Second derivative UV spectra of a titration of MG-TET solution (10 mg/ mL) into haemoglobin (1.24×10^{-5} mol/L) in 20 mM phosphate buffer (KCl 0.15 M).

Whilst **MG-TET**, containing tetrazole binding groups, showed binding to both cytochrome C and haemoglobin, microgels **MG-SMA** and **MG-BP** demonstrated a remarkable degree of selectivity.

MG-SMA only displayed affinity for cyt C (Fig 4.8), whereas little or no evidence of supramolecular binding to haemoglobin was observed (Fig 4.10). This result was confirmed by ITC measurement.

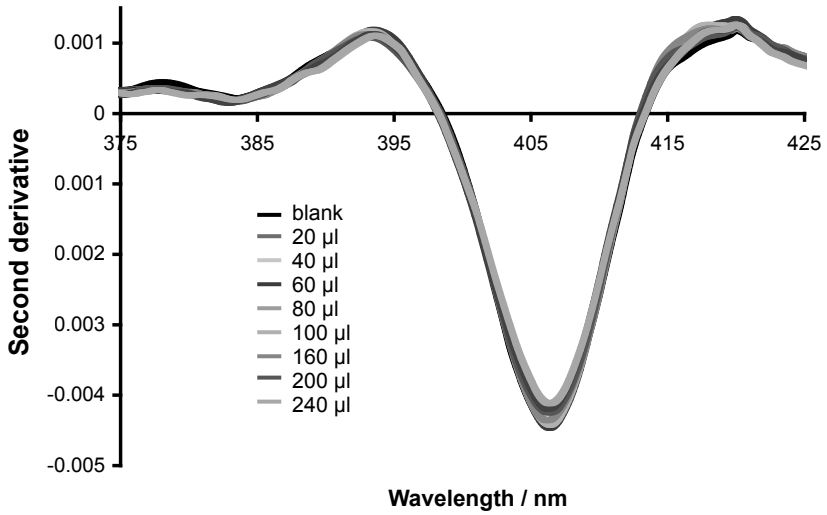

Figure 4.10 MG-SMA titrated into haemoglobin solution shows little change in the spectrum; this is indicative of weak or no binding.

Similarly **MG-BP** only showed an affinity for haemoglobin (Fig 4.11).

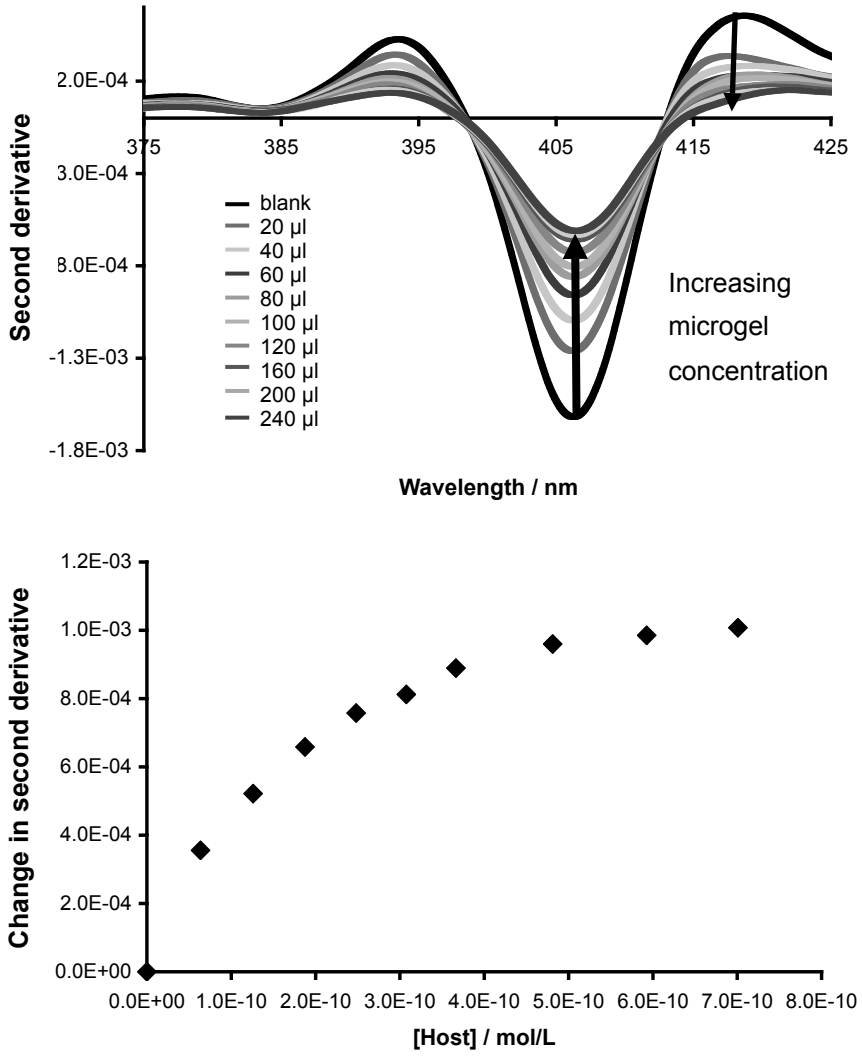

Figure 4.11 Titrating MG-BP solution (10 mg/mL) into haemoglobin (2.4×10^{-6} mol/ L) in 20 mM phosphate buffer (KCl 0.15 M) (top) and plotting the difference in the second derivative (Δd) with respect to the concentration shows a characteristic binding curve (bottom).

The Scatchard equation is typically used to calculate the affinity constant of a ligand for a protein. (Equation 3). Where *B* is the ratio of bound ligands to available binding site, *L* is the concentration of free ligand and *n* is the number of binding sites per receptor.

$$\frac{B}{L} = nK_a - BK_a$$

Equation 3

Plotting *B/L vs B* gives a Scatchard plot, which has a slope of $-K_a$ and an x-intercept of nK_a. The Scatchard plot is a reliable estimation of binding affinity; however, it has

fallen out of favour among supramolecular chemists who now prefer a non-linear least squares regression, because it assumes identical, independent binding sites and also is unreliable when not dealing with 1:1 binding. B and L are estimated from spectroscopic data using the beer lambert relationship, this estimation does, however add significant error to the calculation and an association constant extracted from this data would be flawed. It does however show typical binding behaviour and can therefore be thought of as a "first pass" look to see whether the observed trends in the titrations are indeed supramolecular binding.

A Scatchard plot (Fig 4.12) for the titration of **MG-BP** into a solution of haemoglobin (Fig 4.11) shows a characteristic linear plot, from which a binding constant or Ka of 1×10^{-5} M^{-1} can be calculated. However the Scatchard plot in this case can only be used as an indication or estimation as with UV titrations there is no way of determining the stoichiometry of the association and therefore the ratios generated for the graph remain only an estimate.

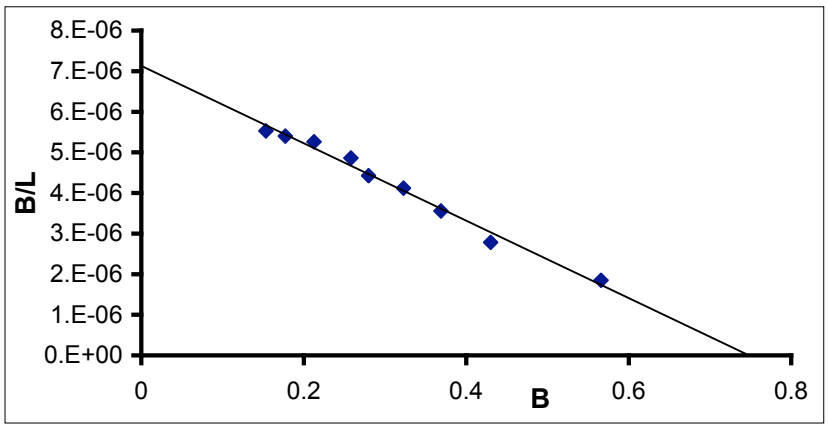

Figure 4.12 A Scatchard plot for the above titration, MG-BP and haemoglobin, shows a typical binding response.

4.4 Isothermal microcalorimetry measurements

Isothermal titration calorimetry was also used to probe the thermodynamics of the interaction between protein and microgel. ITC has the advantage that it does not require any chromophore and therefore has the ability to determine binding between a wider array of proteins and microgels. It also has the added advantage that it has a larger effective window. However, ITC measurements could only be performed on selected samples in collaboration with Prof. Dr. Thomas Schrader and Sun Wei at the University

of Duisburg-Essen. Most of the preliminary work was therefore carried out using second derivative UV spectroscopy, which was easily implemented, as it required only a UV spectrometer and a precision pipette for the measurement. In addition, the data analysis only required an Excel spreadsheet and a modified macro for calculating the second derivative.[145, 146, 150] In the case of UV titrations, the concentrations that can be used are governed by the molar absorption coefficient of the target ligand (this means that a typical concentration range is between 10^{-4} and 10^{-6} mol/L).

Figure 4.13 shows a typical titration curve for the titration of cyt C with **MG-SMA.** Microcalorimetry measurements (Table 4) corroborated the UV-vis results and provided estimated association constants for microgel–protein complexes in the range consistent to those estimated from the UV-vis titrations.

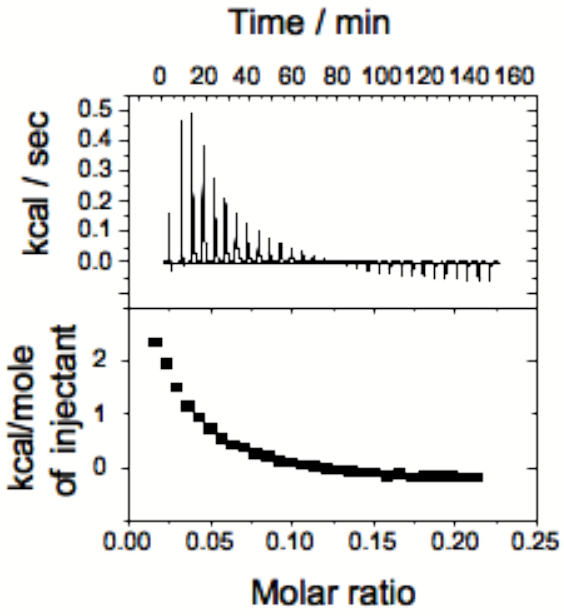

Figure 4.13 A typical ITC curve for a titration with MG-SMA and cyt C (Table 3).

Table 4 Isothermal titration microcalorimetry data

Microgel / (host)	Protein / (Guest)	Binding Constant / single residue (M^{-1})	Stoichiometry	ΔH / $kJmol^{-1}$	ΔS / $kJmol^{-1}$	ΔG / $kJmol^{-1}$
MG-SMA	cytochrome C	1.14×10^3	11 : 1	14.41	0.062	-4.09
MG-TET	cytochrome C	N/A*	N/A*	N/A*	N/A*	N/A*
MG-BP	cytochrome C	-	-	-	-	-
MG-SMA	haemoglobin	N/A*	N/A*	N/A*	N/A*	N/A*
MG-TET	haemoglobin	5.91×10^3	92 : 1	0.41	0.018	-5.07
MG-BP	haemoglobin	2.41×10^5	20 : 1	2.33	0.031	-7.23

*N/A = unable to fit data

Using a typical molecular weight of 2.5×10^9 g mol^{-1} for the microgel, which was taken from literature data,[143, 32, 151, 152] a calculated binding constant could be computed in the nanomolar range for binding of a single protein to a single microgel(Table 5). The calculated binding constants assume non-cooperative, independent binding. The values are remarkably high and competitive with some of the most prominent results in the literature.

In proteins, cooperative binding takes place due to long-range interactions along the surface or through the structure of the protein. In a microgel, which is significantly larger than the target proteins, these long-range interactions are likely to be negligible due to the separation of the bound proteins. The shear scale of the microgels results therefore in the binding of many proteins to a microgel molecule. This is emphasised by the stoichiometries which range from 11:1 to 92:1. In an extreme case, a conformational rearrangement of the microgel upon association could, theoretically, create a more favourable local environment for another protein to bind. It is reasonable to assume that the opposite effect could take place elsewhere. Therefore the calculated macroscopic binding constants are a realistic estimate of the observed binding behaviour.

Table 5 Calculated macroscopic binding constants

Microgel / (host)	Protein / (Guest)	Binding Constant / single residue (M^{-1})	Calculated macroscopic binding constant (M^{-1})
MG-SMA	cytochrome C	1.14×10^3	1.18×10^9
MG-TET	cytochrome C	NA	NA
MG-BP	cytochrome C	-	-
MG-SMA	haemoglobin	NA	NA
MG-TET	haemoglobin	5.91×10^3	3.06×10^9
MG-BP	haemoglobin	2.41×10^5	1.57×10^{11}

The stoichiometry involved in the association is also a significant result (Table 4). It should be noted that 11 methacrylate residues per cyt C are involved in the association. This is not far from the number of lysine residues on the surface of cyt C (Table 6).[75] A stoichiometry of 92:1 was observed for the interaction of **MG-TET** with haemoglobin, which was again intuitive when the larger size of haemoglobin is taken into account, offering a larger number of surface contacts. **MG-BP** displayed the

highest binding constant with respect to haemoglobin, and interestingly only to haemoglobin, placing the dissociation constant beyond the nanomolar range.

The effective concentration of anionic comonomer (*ca.* 10 mol% with respect to the microgel) in solution was relatively high for the ITC titrations. If this is taken into account, then a binding constant between an arginine residue and a single anionic comonomer residue was found to be in the 10^3 M^{-1} range. Only **MG-BP** displayed a much higher binding constant, which was attributed to the bidentate structure of the bisphosphonate groups and the increased (doubled) negative charge compared to tetrazolate or carboxylate binding sites.

4.5 Origin of binding selectivity

At this point it is still unclear as to which factors contribute to the selectivity of the microgels. Linear polymers containing a high concentration of bisphosphonate monomer **1** have a strong affinity for proteins with a large number of lysine residues, whilst the tetrazole moiety has also shown a bias towards protonated amines, see chapters 2 &3.[6] These results would seem to indicate that **MG-TET** and **MG-BP** should bind to proteins with a high ratio of lysine to arginine but this was not proven to be the case. What is apparent is that proteins with a higher isoelectric point bind strongly.

Table 6 Protein properties [153]

Protein	Molecular weight / g mol^{-1} (Total residues)	Theoretical pI	No. of lysine residues	No. of arginine residues	No. of negatively charged residues
Cytochrome C	11832.7 (105)	9.59	19	2	12
Haemoglobin α-chain♦	15184.3 (142)	8.07	11	3	13
Haemoglobin β-chain♦	15954.3 (145)	7.02	13	4	17
Ferritin light-chain◊	20019.6 (175)	5.51	12	10	29
Ferritin heavy-chain◊	27538.2 (242)	6.79	20	9	30
Albumin	69293.4 (607)	5.82	60	26	99

♦ Haemoglobin consists of 2 α and 2 β chains.
◊ Native ferritin protein consists of 24 subunits consisting of both light and heavy chains

Ferritin and albumin, two proteins with relatively low pI's (see Table 6) showed little or no evidence of binding to microgels containing any of the anionic monomers. Although

a small change was observed in the titration of **MG-SMA** into a solution of ferritin (1.2 × 10^{-5} mol/L) the results were not reproducible and could not be quantified. ITC was also unable to determine if any binding was taking place. (Fig. 4.14) A similar case was observed with **MG-TET** and albumin (Fig. 4.15), despite the large number of lysine and arginine residues for the protein. Given their low pI values, these proteins will be negatively charged at pH 7 and electrostatic repulsion between the protein and the microgel presumably predominates.

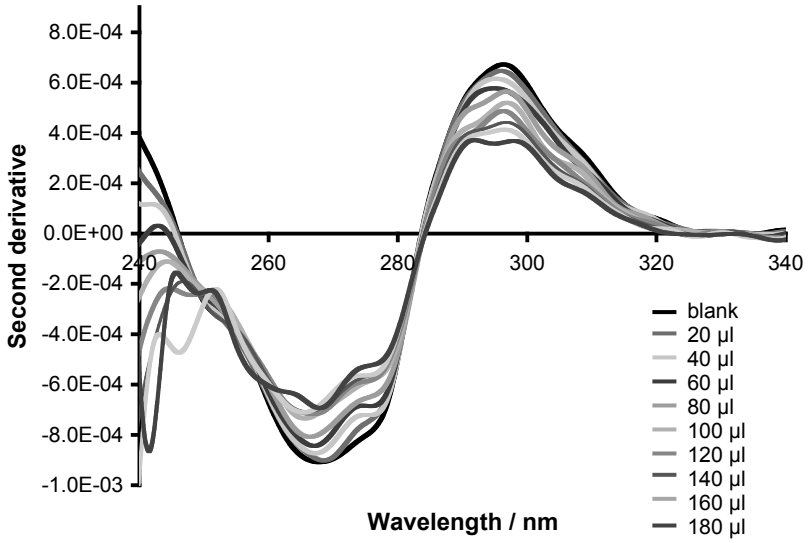

Figure 4.14 Ferritin (1.2×10^{-5} mol/L) does show some signs of binding to MG-SMA (20 mg/mL) in 20 mM phosphate buffer (KCl 0.15 M). It should be noted that the second derivative values change only slightly.

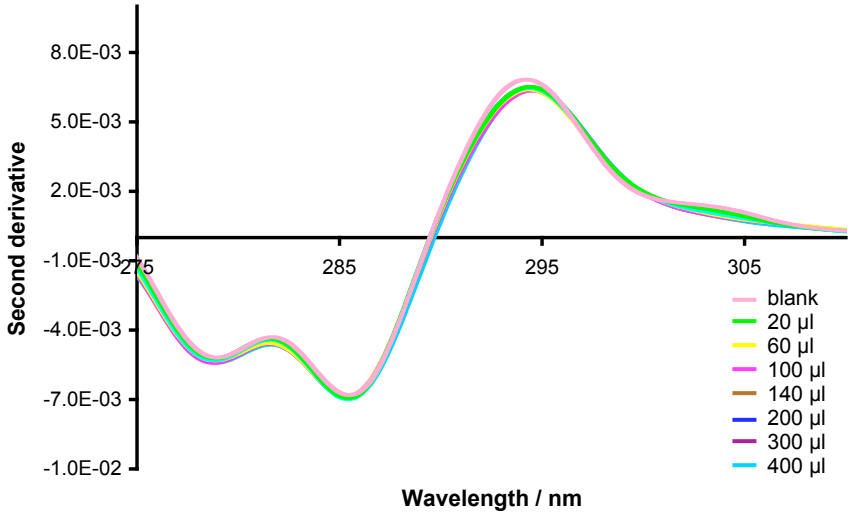

Figure 4.15 Albumin (1.6 × 10^{-5} mol/L in 10 mM phosphate buffer, 0.15 M KCl) displays no affinity to MG-TET (20 mg/mL) even at high concentrations.

The microcalorimetry measurements revealed again a large entropic contribution to the binding. Large endothermic binding processes are not uncommon for protein–protein interactions and protein–ligand systems when a rearrangement or closure of the binding site is necessary. [124] Similarly, this type of behaviour is observed when a highly solvated ligand moves from an aqueous environment into a less hydrophilic situation. This is the case when a protein is incorporated into a microgel. The flexible structure of the microgels would also demand some degree of rearrangement upon binding to a large protein, which helps to explain why the binding of proteins by microgels would be dominated by an entropic contribution. Also, the large size of the proteins and the porous nature of the microgel's outer layer would require a large number of water molecules to be evacuated upon binding. In fact, water's large dielectric constant, its negative value of $\partial\varepsilon/\partial T$ (where ε is the dielectric constant and T is the temperature), small molar volume and highly structural nature (even in the liquid state) can make entropic processes favourable in water and explain the prevalence of an entropy-driven process.[4] All of these properties contribute to the positive ΔS observed in the microcalorimetry titrations.

4.6 Unusual redox behaviour of cytochrome C with microgel binding

A reversible change in the absorbance of the α-band of the porphyrin was also observed during UV titrations of cyt C (Fig 4.16). This indicates a change in the oxidation state of the iron within the porphyrin ring, from Fe (III) to Fe (II). [154] Cyt C is an electron transport protein which transports electrons from complex III to complex IV. The reduction of cyt C takes place through a number of residues along the chain of the protein in association with complex III (Fig 4.17). The change in the absorbance at 550 nm is therefore indicative of some kind of supramolecular interaction which mimics the actual interaction in complex III. The exact mechanism is uncertain but the reduction of the Fe atom is clear evidence of an intermolecular interaction between the microgel and the cyt C molecule. However, there is no explanation yet as to the exact mode of interaction between the microgel and cyt C and the redox reaction that takes place. This

change in oxidation state of the iron does hint at a complex interaction which could mimic that of complex III.

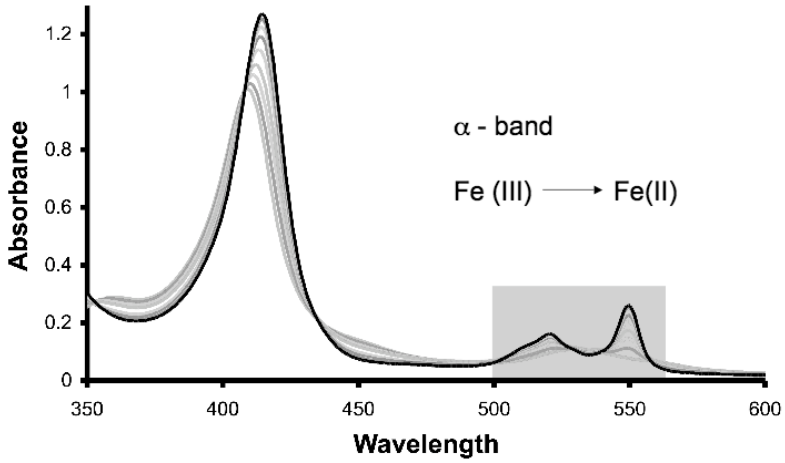

Figure 4.16 UV-vis spectra recorded during the titration of MG-SMA into cyt C. The appearance of peaks at 520 nm and 550 nm is characteristic of reduction of Fe (III) to Fe (II).

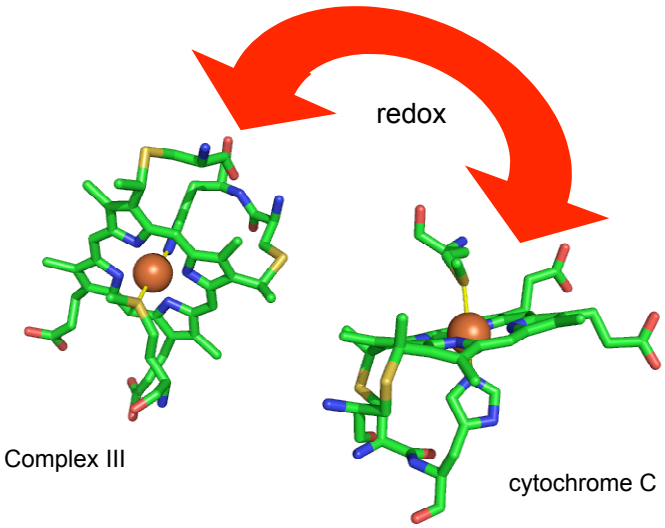

Figure 4.17 Electron transfer occurs from the cytochrome C1 porphyrin in complex III to the water-soluble cytochrome C. The amino acid residues interacting with the Fe atom are involved in the electron transfer.

4.7 Conclusion

In conclusion, these findings have illustrated the development of microgels as supramolecular hosts for protein binding in a highly competitive aqueous environment. Microgels **MG-TET**, **MG-SMA** and **MG-BP** have displayed a high affinity to proteins with a high pI such as HMGN and cyt C. Proteins with low pI values like ferritin and albumin showed little or no affinity.

Interestingly, **MG-SMA** only bound cyt C and displayed no affinity to any other proteins. Similarly, **MG-BP** and **MG-TET** only bound to HMGN.

The initial working hypothesis that a microgel with tetrazole binding groups might bind preferentially to a lysine-rich protein and a microgel made from bisphosphonate monomer **1** would favour arginine-rich proteins proved to be incorrect. There was little or no correlation between the individual arginine/lysine residue content of protein and the protein affinity to the microgels. Proteins such as cyt C or haemoglobin that bound to microgels typically had high pI values, whereas ferritin and albumin (which both have pIs < 7) showed hardly any supramolecular binding to the negatively charged microgels. Further investigation is needed to determine the source of this apparent selectivity.

Dissociation constants in the millimolar range have been observed for individual anionic residues (Table 4), which corresponded to dissociation constants for microgel-protein interactions down in the nanomolar range in some cases. These values are competitive with examples in the literature, linear polymers synthesised by Schrader et al. show dissociation constants in the same range.[6] The degree of selectivity, although only tested on a few proteins does seem to be of the same order as the functionalised nanoparticles of Rotello and Knapp.[16]

The next chapter will look into the possibility of replicating the results reported in this chapter with microgels by using linear copolymers of defined composition and molecular weight instead.

5 Linear copolymers as protein specific receptors

5.1 Introduction

Molecular recognition in aqueous solutions remains an important challenge in supramolecular chemistry. Recent developments have seen our understanding of the interactions of macromolecular receptors with a wide variety of ligands grow.

In the field of protein recognition, substantial progress has been made towards the selective recognition of proteins with high affinity in an aqueous environment using synthetic polymers. Schrader et al. have reported irreversible binding of highly charged linear polymers to basic proteins such as histone and ferritin in aqueous buffer using bisphosphonate monomer **1** (Fig 1.3).[6] High affinity and selectivity are attained by fine-tuning the composition of the polymers. In particular, the choice of anionic binding sites and the inclusion of hydrophobic groups can drastically improve the binding strength of the polymer. (Fig. 5.1) Examples in the literature concentrate on carboxylic acid functional groups and phosphonates, for creating non-covalent host-guest binding sites. [155] Inclusion of hydrophobic groups such as *N*-alkyl and *N*-cyclohexyl acrylamide into the polymer chains serves to mimic natural protein receptors which rely, not only on electrostatic interactions, but also on hydrophobic attractions between nonpolar domains. [4] The latter are often the driving force for the formation of many of the higher order protein structures i.e. α-helices, β-sheets and tertiary structures.

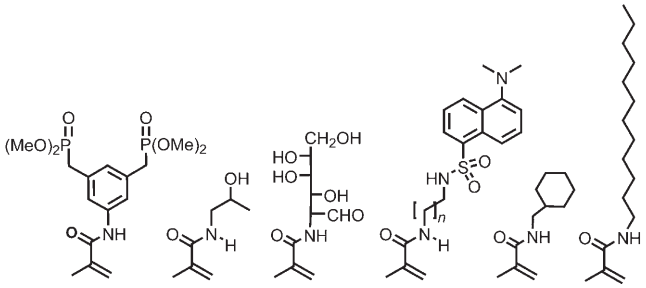

Polymer	Bisphosphonate **a**	Alcohol **b**, **c**	Dansyl **d**	Cyclohexyl **e**	Dodecyl **f**
1	1	–	0.1	–	–
2	1	3[b]	0.4	–	–
3	1	1[c]	1	–	–
4	3	1[c]	0.5	1	–
5	1	1[c]	0.3	–	1
6	3	1[c]	0.5	–	1

[a] Each row indicates the relative ratio of co-monomers for a given copolymer. [b] Alcohol monomer from 2-hydroxypropylamine **b**. [c] Alcohol monomer from 2-glucosamine **c**.

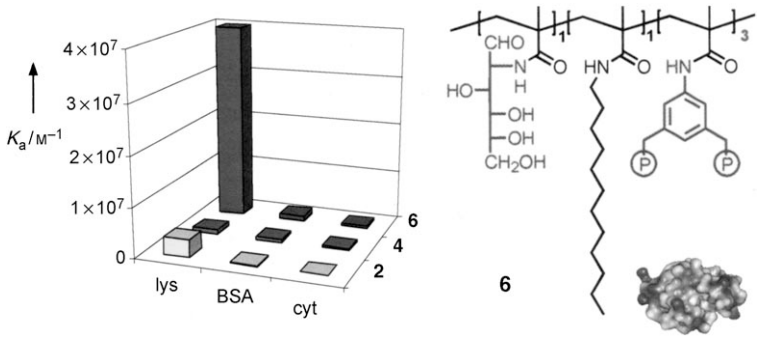

Figure 5.1 Exceptional increase in selectivity towards lysozyme (lys) was observed with small changes in a copolymer. No change can be seen with regard to bovine serum albumin (BSA) and cyt C. [156]

The previous chapter discussed how microgels could be used for protein binding. This chapter will discuss linear polymers that possess a similar NIPAAM: anionic monomer composition as the microgels, but with no crosslinker. In addition, the linear polymers for protein binding were made by a controlled radical polymerisation, which had not been used for this purpose before, to allow the molecular weight of the polymer to be more precisely controlled.

5.2 RAFT polymerisation

Controlled radical polymerisation techniques such as reversible addition-fragmentation chain transfer (RAFT) polymerisation are an extremely useful tool for the controlled synthesis of a wide range of polymers. The RAFT technique was first developed by Rizzardo et al. in 1998.[157, 158] It has been shown to be an extremely robust method for controlling the molecular weight distribution and the architecture of the polymer. [159] Thiocarbonyl compounds, such as dithioesters, dithiocarbamates, trithiocarbonates and xanthates, mediate the polymerisation via a reversible chain-transfer process. The thiocarbonyl compound is used as a chain transfer agent (CTA) that "inserts" an additional step into the polymerisation reaction. (Fig 5.2) This additional reaction step serves to decrease the number of active chains and therefore slows down termination reactions. Chain growth thus becomes more controlled. This gives rise to narrow polydispersity and allows the polymer molecular weight to be controlled. Unlike atom-transfer radical polymerisation (ATRP) [160] and nitroxide mediated polymerisation (NMP) [161], RAFT can be used in a variety of solvents and, most importantly, it is compatible with NIPAAM. Whilst ATRP is an extremely versatile method in itself, there have been very few reports of the successful use of ATRP with acrylamides. For this reason, RAFT was chosen as the preferred method for controlled synthesis of linear polymers in this chapter.

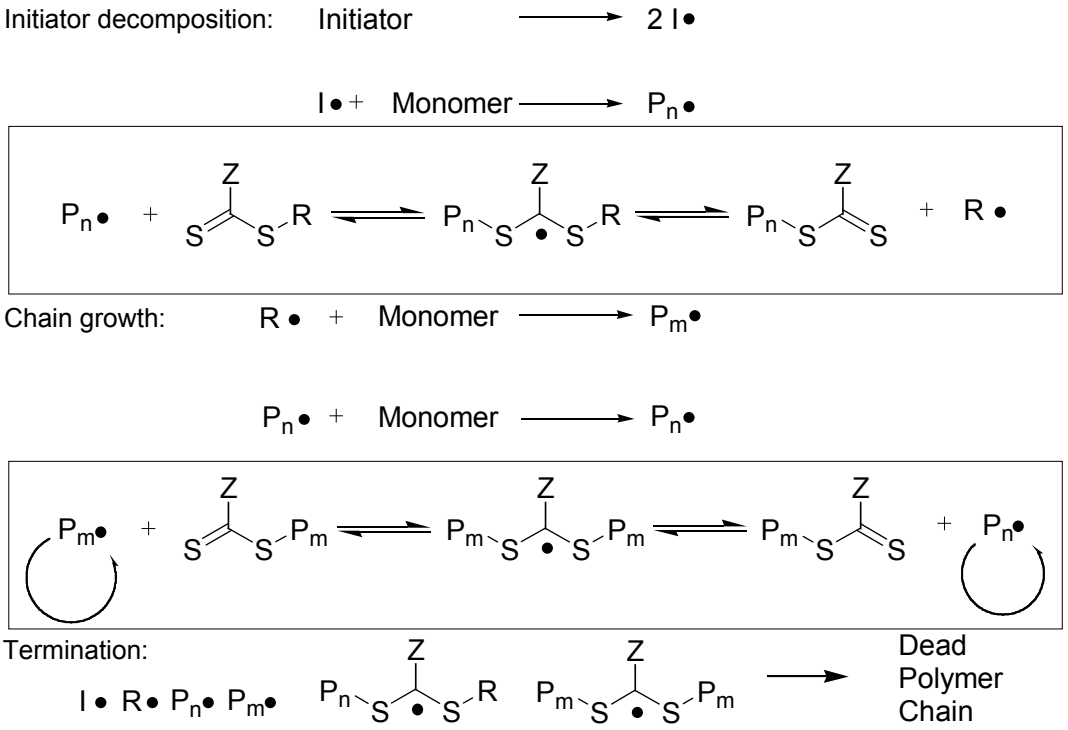

Figure 5.2 RAFT polymerisation reaction mechanism. Additional steps created by the presence of a CTA are shown in boxes.

An extremely important part of the RAFT polymerisation is the choice of RAFT reagent, or CTA. Myriad papers have been published describing the synthesis of CTAs and some are now commercially available.[162, 154, 163] The reactivity of each CTA is important, and so is the effective cleavage of a leaving group and the ability of the subsequent radical to initiate a polymerisation chain reaction. Shea et al. reported a facile synthesis of a carboxyl-terminated trithiocarbonate with high yields and an extremely high chain transfer rate (Fig 5.3).[164] Trithiocarbonates typically have high chain-transfer efficiency and show control over the radical polymerisation in common solvents such as acetone, toluene and water (for acrylic acid), because of the stabilised tertiary carbon next to the trithiocarbonate which also bears a radical-stabilising carboxylic acid. This initiator was known to be compatible with NIPAAM and the copolymerisation of NIPAAM and acrylic acid.[162]

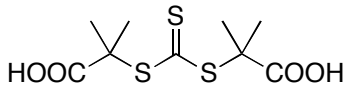

25

Figure 5.3 Trithiocarbonate CTA for RAFT polymerisation of NIPAAM.

The trithiocarbonate **25** was synthesised by reacting a 50% aqueous solution of NaOH with a mixture of carbon disulfide, acetone, chloroform and decyltrimethylammonium bromide (a phase transfer catalyst), followed by stirring overnight. The reaction proceeds via an intermediate dichloroethyl oxide (formed from chloroform, acetone and NaOH) with a trithiocarbonate (CS_3^{2-}). (Fig 5.4) The resulting yellow solid was characterised by NMR, mass spectroscopy and CHN analysis. Initial synthesis was carried out by Julia Liese under supervision as part of an exchange project.

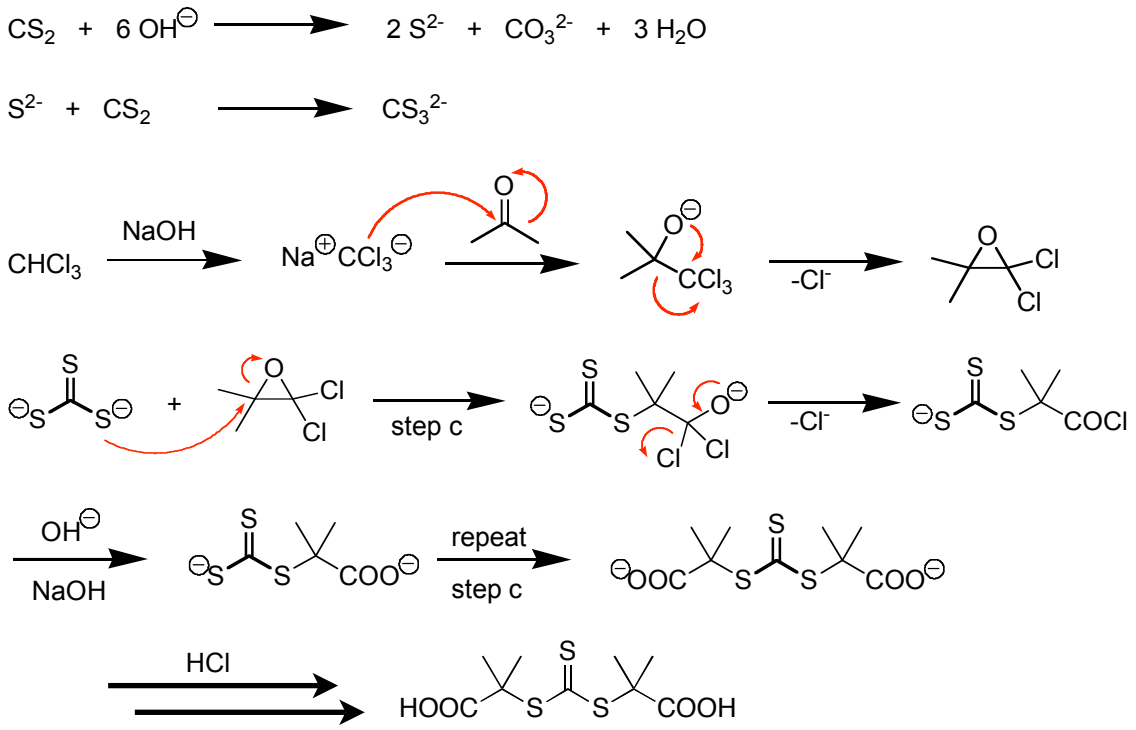

Figure 5.4 Reaction scheme for the synthesis of trithiocarbonate CTA.

The final molecular weight and polydispersity of a polymer synthesized by RAFT polymerisation is dependent on the concentrations and the molecular weights, Mw, of the CTA, radical initiator and monomers as defined in Equation 4. Assuming ideal reactivity ratios between the monomers used. The molecular weight of the polymer is therefore calculated as the sum of the molecular weights of the monomers multiplied by the ratio of that monomer over the CTA.

$$Mw = \left[\left[\frac{mols\,NIPAM}{mols\,CTA}\right] \times Mw\ NIPAM\right] + \left[\left[\frac{mols\,comonomer}{mols\,CTA}\right] \times Mw\ comonomer\right]\ldots\ \Big] + Mw\ CTA$$

Equation 4 Relationship between the molecular weight of the final polymer (after full conversion) and the initial reaction composition. [155, 156]

A typical RAFT polymerisation was carried out in methanol with 15 mmols of total monomer, 0.25 mmol of CTA, and 0.08 mmol of radical initiator to give a polymer with a molecular weight of 7000 g mol^{-1}. The reaction mixture was heated to 60 °C for 48 hours in methanol. Methanol was used as solvent as previous reports had suggested it to be a more suitable solvent for the reaction.[155] Methanol would also guarantee that a wide variety of monomers would be soluble. Furthermore, NIPAAM polymers did not show any LCST behaviour in methanol. The resulting polymer was simply purified by precipitation in hexane.

Characterisation of the RAFT polymers was carried out initially by ^{1}H NMR spectroscopy. End-group analysis proved unsuccessful in determining the molecular weight of the polymer due to the poor quality of spectra. This was most likely a side effect of the high viscosity of the samples and the poor resolution of the spectrometer. The purity of the polymers could be ascertained. In addition, the inclusion of various comonomers was also established by ^{1}H NMR spectroscopy.

Table 7 Composition and molecular weights of selected RAFT polymers

Polymer	Anionic monomer	Target molecular weight	GPC determined M_n / g mol^{-1}	Polydispersity / M_w/M_n
Met-1	methacrylate	3000	3211	1.13
Tet-2	tetrazolate	3000	3129	1.15
Met-3	methacrylate	15000	11148	1.56
Met-4	methacrylate	17500	12111	1.52

Aqueous gel permeation chromatography (GPC), carried out by Dr. Steven Rimmer at Sheffield University, was used to determine the molecular weight and the polydispersity of the RAFT copolymers (Fig 5.5). The target molecular weight of each polymer can be seen in Table 7, the resultant number average molecular weight of each polymer turned out to be close to the estimated target Mw. Polydispersity ranged from 1.13 to 1.56.

Small amounts of low-molecular-weight-impurity were observed and were attributed to small oligomers (n=2 or 3). The polydispersity of Met-1 and Tet-2 came close to some of the highly efficient results present in the literature, where values are sometimes around 1.10. Figure 5.5 (inset) also displays the highly precise nature of the RAFT polymerisation. Met-1 and Tet-2 had the same targeted molecular weight; their peak molecular weights show a strong correlation. Met-4 and Met-3 were targeted slightly further apart; their peak molecular weights are still rather close together, perhaps hinting that the polymerisation needs optimisation at higher molecular weights. Many of the best literature results with respect to polydispersity were achieved by fine-tuning the composition of the reaction mixture and by tailoring a specific CTA agent to the monomers used. This was beyond the scope of this investigation. Typically, higher polydispersities are seen for co-polymerisations.

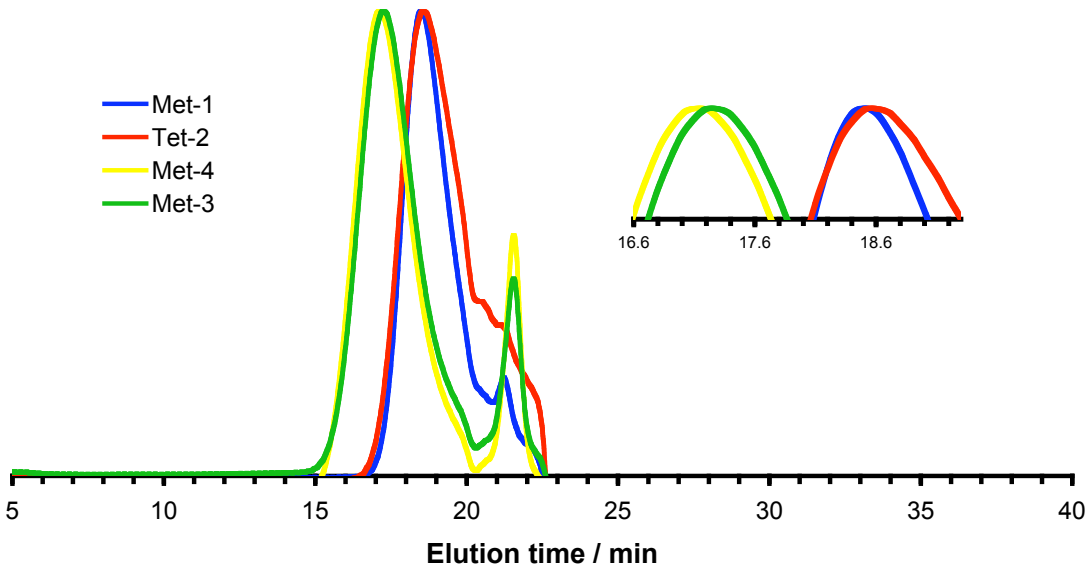

Figure 5.5 Normalised aqueous GPC chromatograms for Table 7. Inset is a close up of the peaks, showing the precision of the RAFT polymerisation. Some low molecular weight impurities are present but were not included in the analysis of the molecular weight averages and polydispersity. The solvent front has been deleted for clarity.

Of particular interest to this study were the different values available for the molecular weight of each polymer. M_w, M_n and M_{peak} are values that are familiar to a polymer

chemist but each individual value can vary significantly. The M_w (weight average molecular weight) is a weighted mean value for the molecular weight of the polymer chains and the number average, whereas M_n is the arithmetic mean of the molecular weights for each chain. M_{peak} refers to the most likely molecular weight corresponding to the peak of the GPC trace. Determining an association constant relies upon using the most relevant value for the molecular weight of each polymer. A narrow polydispersity (< 1.2) is highly desirable, as it would mean that the polymer chains all have similar molecular weights.

For the purposes of this study, the M_n was used as the molecular weight in calculations of binding constants.

5.3 Supramolecular interactions with proteins

UV-vis titrations were again used to study binding between RAFT copolymers and proteins. UV-vis titrations were initially carried out with cyt C and a linear RAFT polymer based on the 10% sodium methacrylate and 90% NIPAAM with a targeted molecular weight of 7000 g mol^{-1}. This polymer will be given an abbreviated code S1-7000 where “S1” and “-7000” refer to the sodium methacrylate content (in mol%) and the targeted molecular weight (in g mol^{-1}) respectively.

The UV titration of this polymer into a solution of cyt C in a phosphate buffer (pH 7, 0.15 M KCl) showed characteristic second derivative spectra, similar to the those observed in the titrations of microgels into protein solutions. Isosbestic points are clearly visible along with a bathochromic shift in absorbance peak (Fig 5.6).

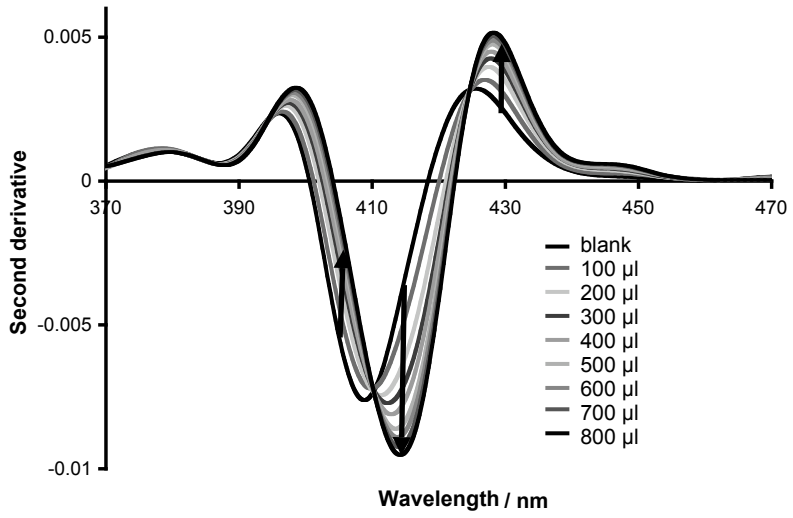

Figure 5.6 Second derivative UV-vis titration of methacrylate polymer S1-7000 (the inset refers to ml of 5.33×10^{-3} mol/L of RAFT copolymer solution added) into a solution of cyt C (1.11×10^{-5} mol/L) in phosphate buffer (pH 7, 0.15 mol/L KCl)

When the second derivative values of the protein at 415 nm were plotted against the RAFT polymer concentration, a dissociation constant of 1.63×10^{3} M^{-1} can be fitted using a modified version of equation 2 (Fig 5.7).

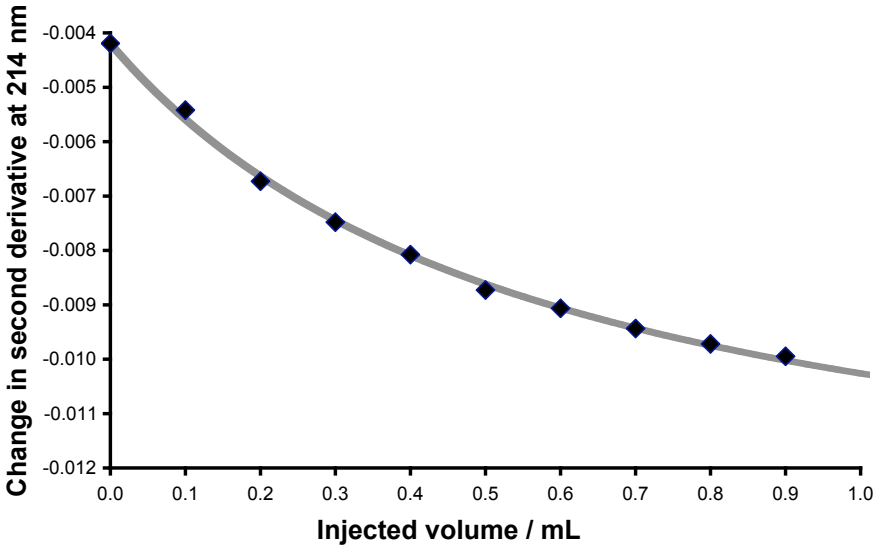

Figure 5.7 The change in absorbance at 415 nm against the concentration of RAFT copolymer S1-7000 injected can be fitted to a hyperbolic binding curve.

5.3.1 Hydrophobic contributions to supramolecular binding

Since hydrophobic contributions to supramolecular binding are becoming more and more understood in protein-protein binding, [2, 4] it was suggestive that hydrophobic groups could have a similar effect on the interaction of linear RAFT copolymers with proteins. The investigation described in this thesis concentrated on binding of RAFT copolymers with cyt C for two reasons:

1) Cyt C already showed noticable and selective binding to sodium methacrylate based microgels which made it likely that it would also bind to the various SMA derived RAFT copolymers.
2) Cyt C has a relatively small molecular weight, similar to the RAFT copolymers so that 1:1 binding was anticipated.

Acrylamides offer the advantage that they are easily functionalised. A simple reaction between acryloyl chloride and almost any primary of secondary amine yields an *N*-substituted acrylamide monomer. Three hydrophobic monomers were prepared by reacting octylamine, cyclohexylamine and benzylamine with acryloyl chloride. (Fig 5.8) [165, 166, 167] These monomers were used to create a second generation of RAFT polymer with a dual, hydrophobic-anionic, functionality (Table 8). Only 10 mol% of the hydrophobic monomer was incorporated to preserve the water solubility of the copolymer.

Table 8 Composition of RAFT polymers made with hydrophobic monomers "S1" stands for a 10 mol% sodium methacrylate content, "O10" for 10 mol% *N*-octyl acrylamide, "B10" for 10 mol% *N*-benzyl acrylamide and "cH10" for 10 mol% *N*-cyclohexyl acrylamide. "-7000" refers to the approximate (targeted) molecular weight.

Polymer	Hydrophobic monomer	% Hydrophobic monomer	Targeted M_n
S1-7000	N/A	N/A	7000
S1O10	*N*-octyl acrylamide	10	7000
S1B10	*N*-benzyl acrylamide	10	7000
S1cH10	*N*-cyclohexyl acrylamide	10	7000

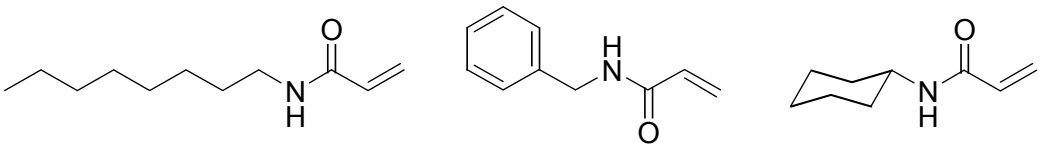

N-octyl acrylamide *N*-benzyl acrylamide *N*-cyclohexyl acrylamide

Figure 5.8 Hydrophobic monomers used in the synthesis of second generation anionic/hydrophobic RAFT polymers.

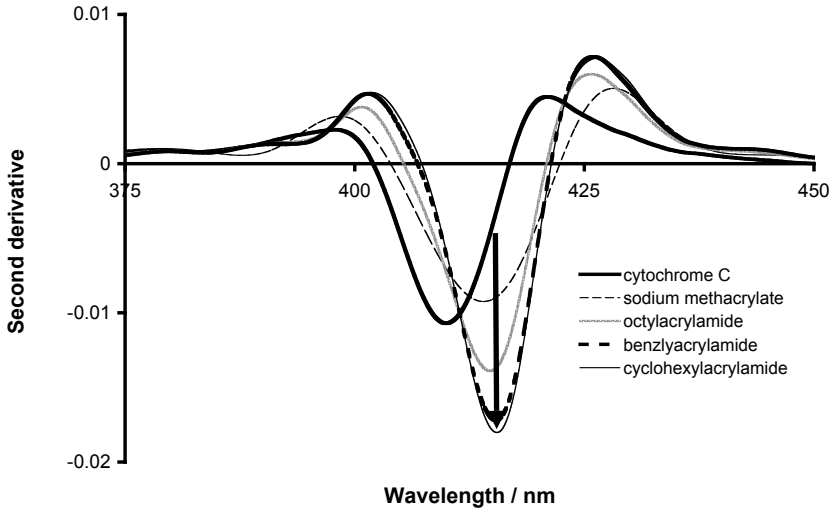

Figure 5.9 Comparison of the changes in strength of binding with the addition of hydrophobic monomer. RAFT polymer (1.2×10^{-3} mol/L) and cyt C (9.8×10^{-6} mol/L) in a phosphate buffer (pH 7, 0.15 mol/L KCl).

To determine the most efficient hydrophobic comonomer, the second derivative spectra of the three copolymers were measured in the presence of cytC (Fig. 5.9) The same amount of RAFT polymer (either a 1st generation sodium methacrylate or the 2nd generation polymer with hydrophobic comonomer) was added in each case. A greater change in the second derivative indicated a higher affinity for the protein. At the same concentration, a polymer that binds more strongly would exhibit a trace that is closer to the end-point of the titration than a polymer with weaker affinity. The mid-titration concentration was chosen as it would be most sensitive to change in affinity.

Figure 5.9 clearly shows a bathochromic shift and decreases in peak height when sodium methacrylate RAFT polymer S1-7000 was titrated into cytochrome C solution. The incorporation of *N*-octyl acrylamide resulted in the same bathochromic shift but the peak height was closer to that of the end-point. This effect was even more pronounced for the RAFT copolymers with an *N*-benzyl acrylamide and *N*-cyclohexyl acrylamide which went much further towards saturation. The comparison shows that incorporation of *N*-cyclohexyl acrylamide increased the affinity of the methacrylate polymer more significantly than *N*-benzyl acrylamide and *N*-octyl acrylamide.

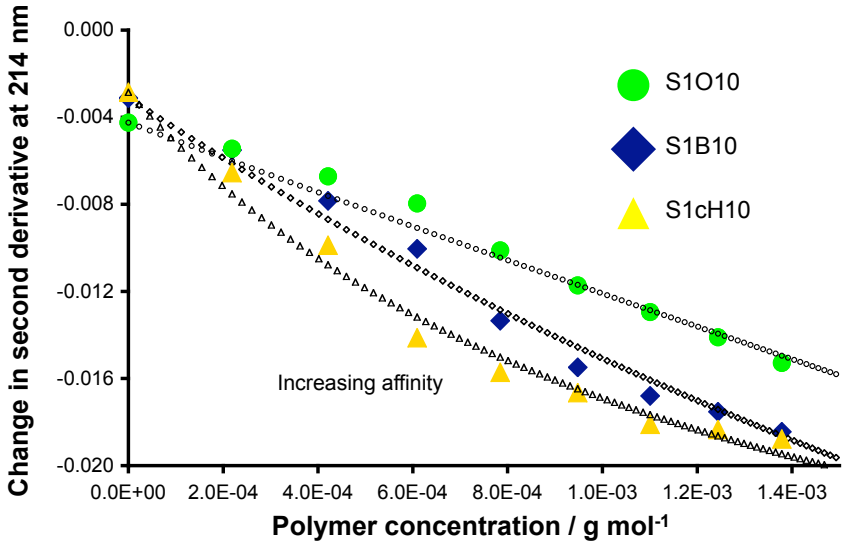

Figure 5.10 Binding curve plotting the change in the second derivative against the concentration of S1O10, S1B10 and S1cH10 added into a solution of cyt C (9.85×10^{-6} mol/L in phosphate buffer, pH 7, 0.15 mol/L KCl).

Table 9 Dissociation constants calculated from binding curves in Fig 5.9

Polymer	Dissociation constant, K_d / M
S1O10	$3.33 \times 10^{-2} \pm 0.6$
S1B10	$5.30 \times 10^{-3} \pm 0.9$
S1cH10	$2.69 \times 10^{-3} \pm 0.4$

Plotting the change in the second derivative of UV absorbance against the concentration of polymer added gives a binding curve that can be fitted using a modified version of Equation 2. Table 9 shows an increase of an order of magnitude from S1O10 to S1B10 and S1cH10. This can also be seen in Figure 5.10, where a more pronounced and

steeper binding curve is evident for S1cH10, whilst S1O10 has a shallower change and does not appear to move towards saturation as quickly.

5.3.2 Effect of polymer composition on supramolecular affinity

At this point a combinatorial approach was employed to identify the ideal composition of the copolymer with respect to the anionic comonomer (MET) and the hydrophobic monomer, *N*-cyclohexyl acrylamide. Previous studies, by Schrader et al., have reported much higher affinity for polymers containing both charged and hydrophobic repeat units. In their case linear polymers with an anionic comonomer concentration of around 80% [6] have shown extremely high binding. However, the RAFT copolymers in this thesis possessed a methacrylate content of only 10%, which was significantly lower. It was anticipated that there was scope for improving receptor-polymer binding by optimising the polymer composition with respect to the active functional groups.

RAFT polymers were prepared with range of different compositions to determine the best composition for supramolecular binding of linear polymers to cyt C via an iterative process. Anionic monomer composition was varied from 10% to 50%, in increments of 10%, while the hydrophobic monomer content was set to 10, 20 and 30 %. A narrower range of hydrophobic monomer (≤ 30%) was investigated in order to maintain water solubility of the final polymer.

Table 10 shows the composition of a series of RAFT copolymers prepared for this purpose. The target molecular weight was initially kept at 7000 g mol^{-1} as this M_n value would correspond approximately to the molecular weight of cyt C, which was the target protein for this new generation of protein receptor.

UV titrations were limited to a single point titration, similar to that shown in Figure 5.9, to provide an efficient screening method and determine the best composition. UV titrations with RAFT polymers were highly reproducable and therefore a single point titration was thought to be a quick and effective method of testing a large volume.

Table 10 Composition of a series of RAFT polymers synthesised in order to identify the ideal composition for a cyt C-binding linear polymer.

Name	mol% sodium methacrylate	mol% *N*-cyclohexyl acrylamide	Target molecular weight / g mol^{-1}
S10-7000	10	-	7000
S1cH10	10	10	7000
S1cH15	10	15	7000
S1cH20	10	20	7000
S2cH10	20	10	7000
S2cH15	20	15	7000
S2cH20	20	20	7000
S3cH10	30	10	7000
S3cH15	30	15	7000
S3cH20	30	20	7000
S4cH10	40	10	7000
S4cH15	40	15	7000
S4cH20	40	20	7000
S5cH10	50	10	7000
S5cH15	50	15	7000
S5cH20	50	20	7000

An identical concentration of polymer (*ca*. 5×10^{-4} mol/L) was added to a solution of cytC in buffer (6.3×10^{-3} mol/L, in 10 mM NaH_2PO_4, pH 7, 0.15 mol/L KCl).

The results of this investigation would seem to indicate that a higher concentration of charged functional group within a polymer chain has in fact a detrimental effect on the binding strength. Figure 5.11 shows the relationship between the observed strength of polymers with different contents of sodium methacrylate compared to a polymer with sodium methacrylate content of 10%. The graph shows a slight increase relative to S10-7000 and then it begins to drop off. This may have been linked to the viscoscity effect seen with the higher loading of charged groups onto a polymer, as polyelectrolytes are well known for their increased viscosity in solution, leading to slower diffusion and aggregates forming in solution. This would lead to polymer interactions becoming more dominant in solution and protein binding becoming not so prominant.

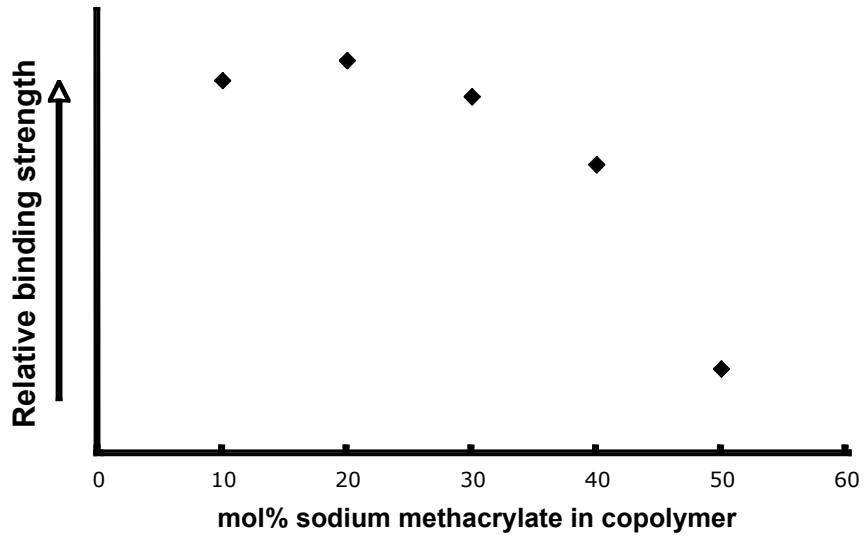

Figure 5.11 A comparison of the different binding strengths as a function of the % content of sodium methacrylate, normalised against S1cH10. The polymers used in this experiment were S1cH10, S2cH10, S3cH10, S4cH10 and S5cH10.

The difference between the strongest binding interaction and the weakest interaction was a shift in peak absorbance of 2 nm and a difference in in absorbance of 0.1 this represents a significant change and is well above the resolution of the spectrometer.

A similar trend was observed with hydrophobic comonomers (Fig 5.12). The relative strength of association had a maximum for polymers with an *N*-cyclohexyl acrylamide content of 15%. At 20% content the binding strength seemed to drop slightly, possibly due to a decreased solubility from the high content of the cyclohexyl group. It is also possible that these polymers behave differently in solution because of their more hydrophobic character. The measurements were carried out at room temperature, well below the LCST of the copolymers. The cyclohexyl groups may encourage the polymers to collapse into aggregates when a critical w/w % is reached therefore the topology of the copolymer may inhibit any interaction with the protein, as has been observed by Schrader *et al*. with polymer thin films.[6]

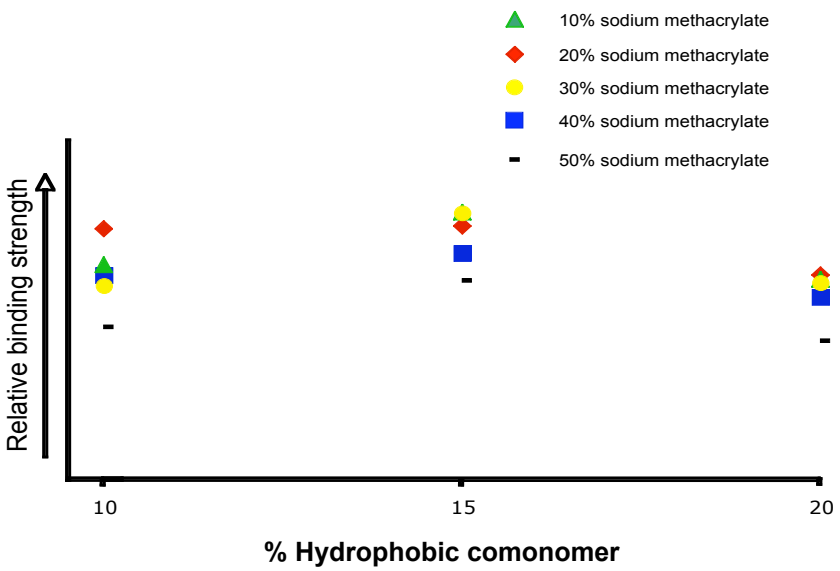

Figure 5.12 A comparison of the relative binding strengths of each polymer listed in Table 10. Each individual data point represents a polymer with a specific hydrophobic monomer content (x-axis) and anionic monomer content (legend). For a more detailed comparison see Appendix B.

Through this combinatorial approach it was possible to elucidate the strongest binding polymer. The RAFT polymer S3cH15 with 30% sodium methacrylate and 15% *N*-cyclohexyl acrylamide demonstrated a great improvement from the initial S1 polymer. Figure 5.13 shows a typical binding curve for the titration of S3cH15 into cyt C.

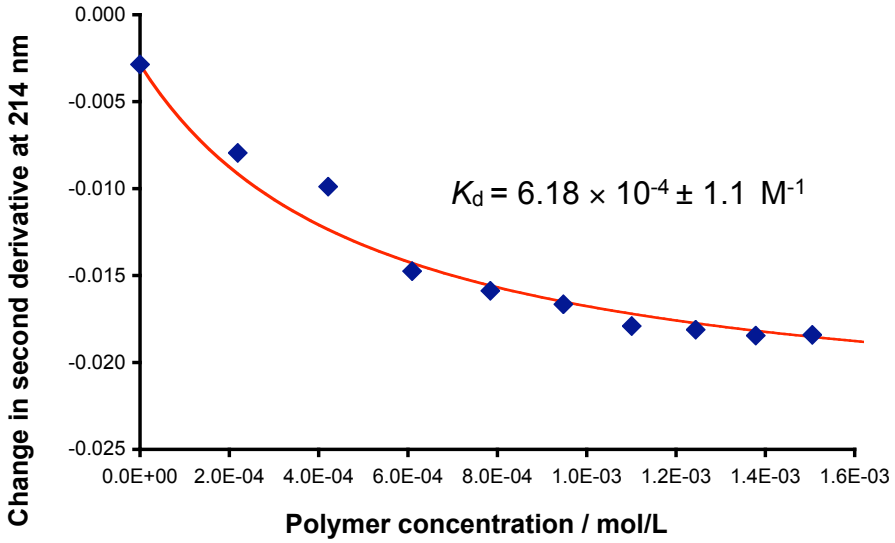

Figure 5.13 Binding curve for the titration of S3cH15 into cytochrome C (9.8×10^{-6} mol/L, 10mM phosphate buffer pH 7, 0.15 M KCl)

5.4 Conclusion

The results in this chapter provide an insight into the parameters that create a good protein-binding polymer.

Linear polymers were synthesised via a RAFT polymerisation process yielding defined molecular weights and good polydispersities (Table 7). The RAFT process allowed more accurate binding constants to be calculated by defining the M_n of the polymers. To my knowledge this is the first report of RAFT polymers being used as supramolecular receptors for proteins.

Like MG-SMA, the RAFT polymers (which all possessed SMA as the anionic comonomer) only showed an affinity for cyt C. The specificity observed in Chapter 4 for microgels was also evident in linear polymers.

Inclusion of hydrophobic monomers served to increase the affinity of the linear polymers for the protein. *N*-Octyl acrylamide only displayed a mild increase in affinity whereas *N*-benzyl and *N*-cyclohexyl acrylamide displayed a much larger increase (Table 8), with *N*-cyclohexyl acrylamide being the most efficient comonomer.

A combinatorial approach was then used to determine the optimum polymer composition for binding to cytC. It demonstrated an increase in the dissociation constant by 1 order of magnitude, from of 1.63×10^{-3} M^{-1} (S1-7000) to 6.18×10^{-4} M^{-1} (S3cH15).

These results demonstrate that it is possible to iterate the composition for a polymer and optimise its protein binding properties. It turned out that even small changes in polymer composition had drastic effects on the strength of the association. These dissociation constants are not yet compettitive with some of the literature values (for example, those presented by Schrader *et al.*) but the new RAFT copolymers have a much lower anionic monomer content as well as a much narrower molecular weight distribution.[152]

6 Dynamic combinatorial chemistry with polymers

6.1 Introduction

Dynamic combinatorial chemistry (DCC) has had a considerable amount of success in recent years, particularly for the synthesis and identification of macrocyclic receptors. [68] Interconversion of library members into one another allows a system to reach equilibrium. It is this equilibrium mixture that can be altered by the addition of a template; any library member that is favoured by complementary interactions with the template will be amplified. Therefore, a combinatorial library under thermodynamic control allows amplification of synthetic receptors such as macrocyclic receptors or molecular capsules (Fig 6.1).[68]

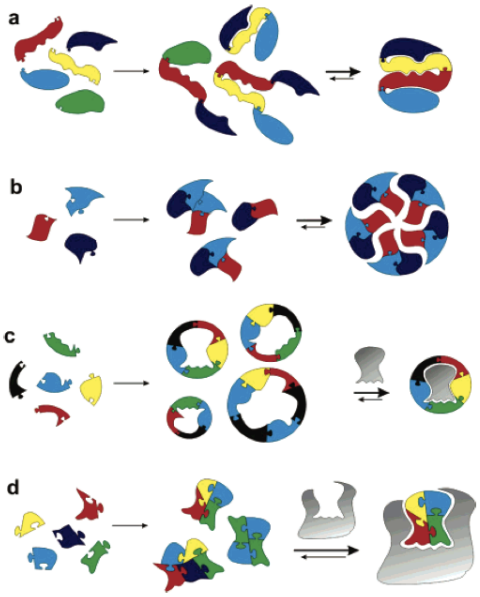

Figure 6.1 A number of different ways of using DCLs for the synthesis of a) foldamers, b) the self-assembly of larger molecules, c) host selection by introduced guests and d) guest selection. [68]

A number of exchange reactions have been reported in DCL synthesis, ranging from the covalent hydrazone exchange [168] to non-covalent metal-ligand exchange.[169] The exchange reactions are only constrained by the conditions that a desired template can

tolerate, i.e. a template must be stable under the conditions necessary for the exchange reaction to take place.

In this chapter the DCC concept will be applied to linear copolymers similar to those studied in Chapter 5 with a view to introducing high affinity and high selectivity towards polyamines.

6.2 Dynamic combinatorial chemistry with polymers

6.2.1 A post-polymerisation imprinting process based on dynamic combinatorial synthesis

Dynamic combinatorial chemistry and the molecular imprinting technique have a number of similarities; the use of a template molecule to determine the final configuration of its binding site is a common theme. Where the two techniques differ is that with molecular imprinting, the reaction to form the host polymer is not reversible, effectively freezing the binding sites into the polymer as they were at the moment of polymerisation. This makes it almost impossible to isolate any single binding site or high affinity host configuration and this may not create the most favourable arrangement. In DCC, the reversible bonds allow a more favourable host to be created by multiple transformations.

A post-polymerisation process based on the dynamic combinatorial method would be a highly useful tool for supramolecular chemists. It would allow a degree of fine tuning to be applied or optimising the host-guest interactions.

Based on the successful supramolecular interactions of microgels with protonated amines reported in Chapter 4, efforts were made to enhance the affinity of microgels towards low-molecular-weight ligands, such as protonated amines, via a post-polymerisation imprinting process. Disulfide exchange was selected as a suitable exchange reaction due to the compatibility of the protonated amines used as guests and

the reaction conditions necessary (pH ~8 in an aqueous buffer) to engage the exchange reaction. Microgels crosslinked with a mixture of *N,N'*-methylenebisacrylamide (MBA) and a disulfide containing analogue, *N,N'*-cystaminebisacrylamide (CBA) (Fig 6.3) were synthesised. The total amount of crosslinker was kept at 10 mol%. It was postulated that reconfiguration of the fine structure of the microgel via an exchange reaction between the disulfide group and a thiol to create favourable binding sites for a template. (Fig 6.2)

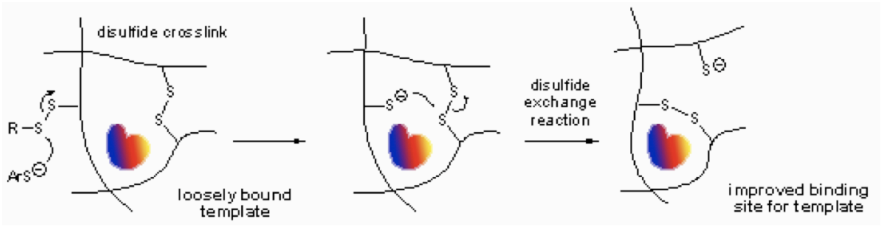

Figure 6.2 A disulfide exchange reaction can optimise the binding site for a template in a crosslinked polymer, such as a microgel.

The synthesis of a disulfide microgel yielded a highly soluble white powder which was purified by ultrafiltration. Both ^{1}H NMR and FTIR spectra were typical of NIPAAM-based polymers synthesised in chapter 5. The exchange reaction was initiated with *m*-mercaptobenzoic acid in a pH 7 phosphate buffer in the presence of spermine and dibucaine as template.

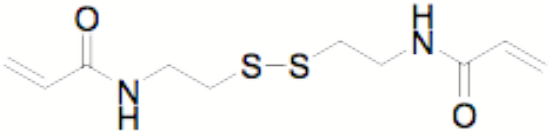

***N,N'*-cystaminebisacrylamide (CBA)**

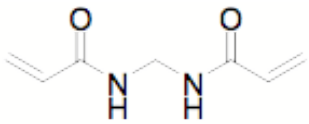

***N,N'*-methylenebisacrylamide (MBA)**

Figure 6.3 Structures of crosslinkers used in the synthesis of disulfide microgels.

Initial exchange reactions resulted in decomposition of the microgel. It was suspected that mercaptobenzoic acid might have cleaved too many disulfide groups. A great deal of aggregation and intermolecular crosslinking was accompanied by a large amount of insoluble polymer being recovered after equilibration. Preliminary reactions were conducted in a thoroughly degassed solution. The absence of dissolved oxygen meant that the reaction would continue at equilibrium and it is possible that this slowly

destroyed the polymer's internal crosslinks and led to the poor yields observed. What little microgel was recoverable was used to probe for the presence of high affinity binding sites via ^{1}H NMR spectroscopy and UV-vis titrations. Of the three templates studied, only dibucaine showed any evidence of improved binding after the microgel had been subjected to DCL conditions in the presence of the template (Fig 6.4)

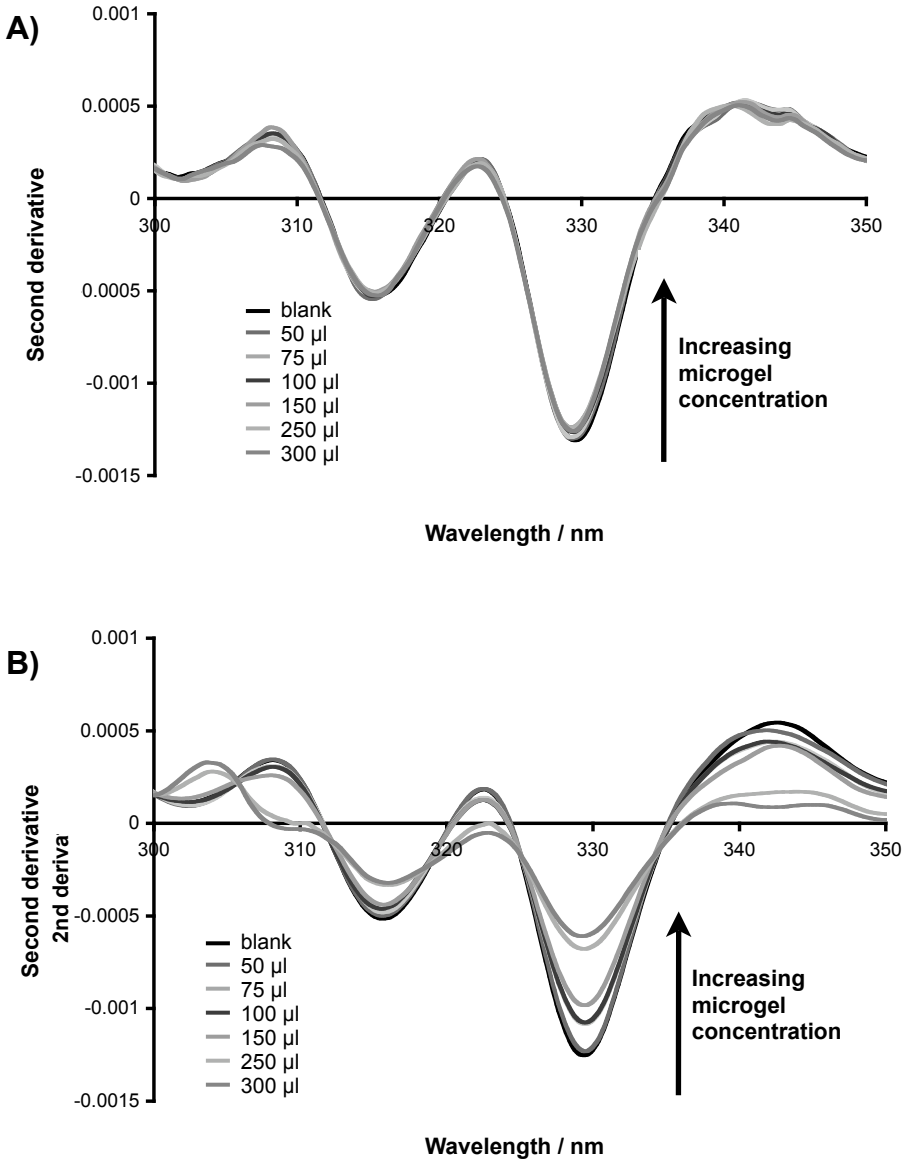

Figure 6.4 UV titration of unexchanged microgel (3.1 mg in 0.3 mL pH 7.0, 0.15 M KCl) into a solution of dibucaine (2.5×10^{-5} M^{-1}, pH 7.0, 0.15 M KCl) shows no evidence of binding (A). After a successful exchange process had taken place, titration of microgel (3.0 mg in 0.3 mL pH 7.0, 0.15 M KCl) into a dibucaine solution (2.5×10^{-5} M^{-1}, pH 7.0, 0.15 M KCl) displayed a change which indicated improved binding (B).

These results were promising, but proved to be difficult to reproduce. Work on microgel templating through dynamic combinatorial chemistry was therefore not pursued.

6.2.2 Linear polymers as dynamic combinatorial library members

As a result of the unsuccessful templating process with microgels it was postulated that linear polymers containing pendant disulfide groups might be more suitable for DCL chemistry (Fig. 6.5). This would represent a "bottom-up" approach, by building intramolecularly "crosslinked" polymer systems based on a template rather than attempting to rearrange existing crosslinks within a polymer network. It was hoped that this approach would avoid the losses through gelation and low yields that were associated with the exchange process with microgels.

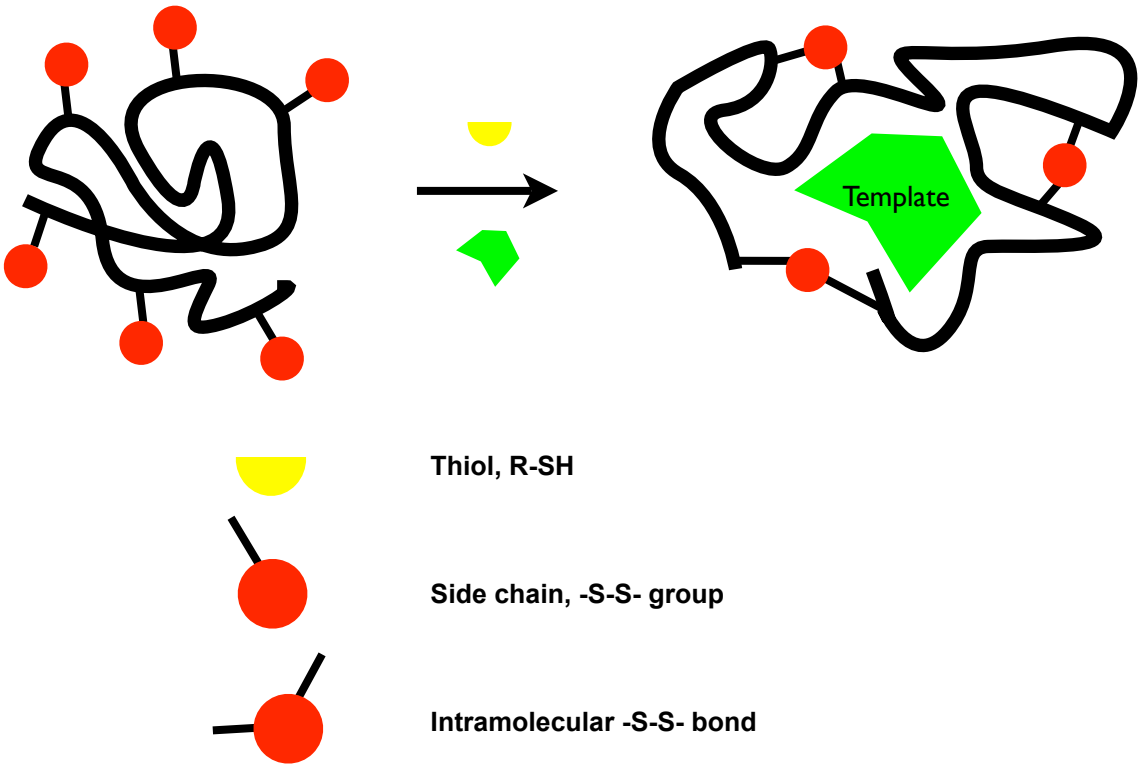

Figure 6.5 A linear polymer with pendant disulfide groups can undergo a thiol exchange reaction and form fixed improved binding sites around a template. This type of disulfide "crosslink" was designed to be reminiscent of cystine crosslinks in proteins

In order to insert a disulfide functional group into a linear polymer, a disulfide monomer similar to the *N,N'*-cystaminebisacrylamide crosslinker was synthesised (Fig 6.6).

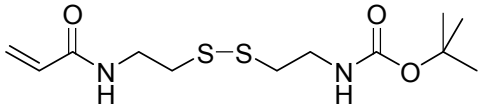

Figure 6.6 (*N*-boc)-*N*-acryloyl cystamine.

For this, cystamine hydrochloride was monoprotected with Boc anhydride (Boc_2O) and then reacted with acryloyl chloride to add a polymerisable group (Fig 6.7). The Boc protecting group was not cleaved, thus providing a diagnositic ^{t}Bu singlet that could be identified in an ^{1}H NMR spectrum as evidence for incorporation of the monomer into the polymer.

RAFT copolymerisation of NIPAAM, **26** and tetrazolate monomer **23** yielded a polymer with a targeted molecular weight of 7000 g mol^{-1}. The polymer was purified by precipitation in pentane. ^{1}H NMR spectra were taken to ascertain the absence of any unreacted monomer. A broadened peak that corresponded to the Boc-protecting group signalled the inclusion of the disulfide monomer into the polymer chain.

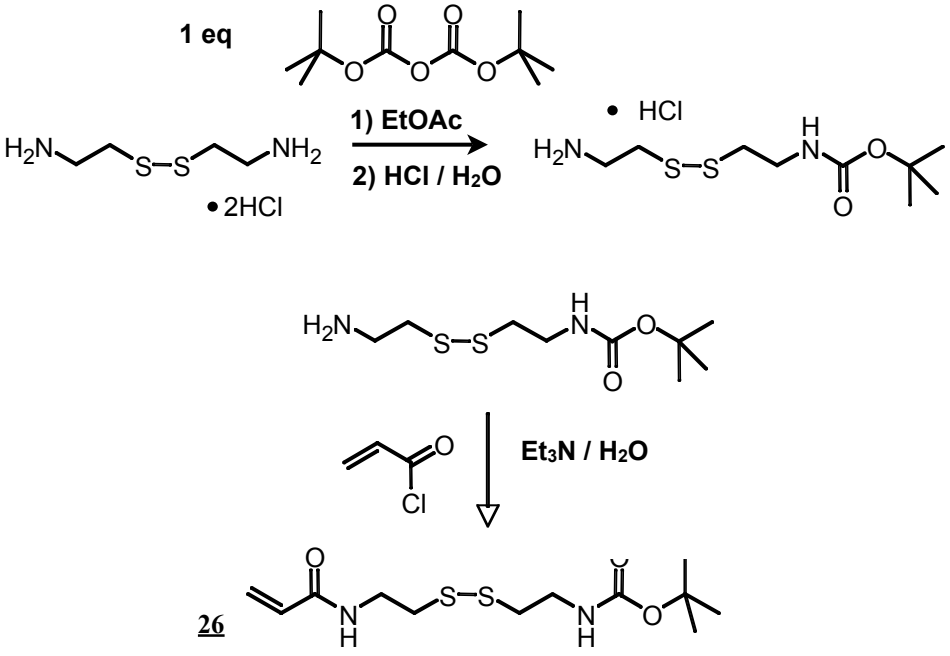

Figure 6.7 Synthesis of monomer 26.

6.3 Thiol exchange reaction with polymers

6.3.1 Dynamic combinatorial polymer libraries

A dynamic combinatorial polymer library (DCPL) was set up using aromatic thiols in a pH 7.5 phosphate buffer. Aromatic thiols were selected as their pK_a values are significantly lower than those of aliphatic thiols (*ca.* 10); this means that there will be a significant amount of deprotonated thiolate in neutral solution to initiate the exchange reaction. Libraries containing 4-mercaptobenzoic acid, 3-mercaptobenzoic acid, 4-mercapto nitrobenzene (Fig 6.8), polymer and template were prepared in a phosphate buffer at pH 8 and left to equilibrate for 24 hr.

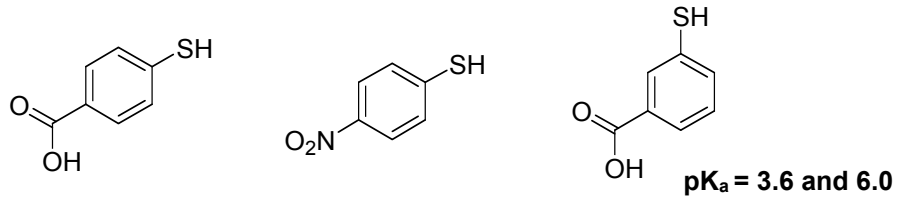

Figure 6.8 Aromatic thiols choosen as thiol exchange initiators.

Spermine was chosen as template since it had already shown binding to microgels containing tetrazolate functional groups. Spermine is also highly soluble in aqueous buffer and supramolecular binding in a competitive environment would be a significant development, as the unexchanged linear polymer showed absolutely no binding prior to the exchange reaction.

Polymer libraries were investigated with HPLC and LC-MS, for the presence of the fully reduced disulfides, indicating the exchange reaction was taking place. HPLC chromatographs showed only slight changes in the composition of the libraries with polymer in the presence of template and polymer alone. In a standard DCL, a change in the composition of the library indicates that a change in the equilibrium state of the library has taken place. This change should be due to library constituents interacting with the template, or guest, forming a new host. Any change in the HPLC chromatogram, in the polymer library would not arise from a new library member being formed. Essentially any new host would still be polymer and since the polymer was

filtered using a pre-column, these would not be visible in the chromatogram. Any change in the composition of the polymer library would not, therefore, come from a new host but from the exchange reaction taking place between the thiolates and the disulfide side chain. (Fig 6.9)

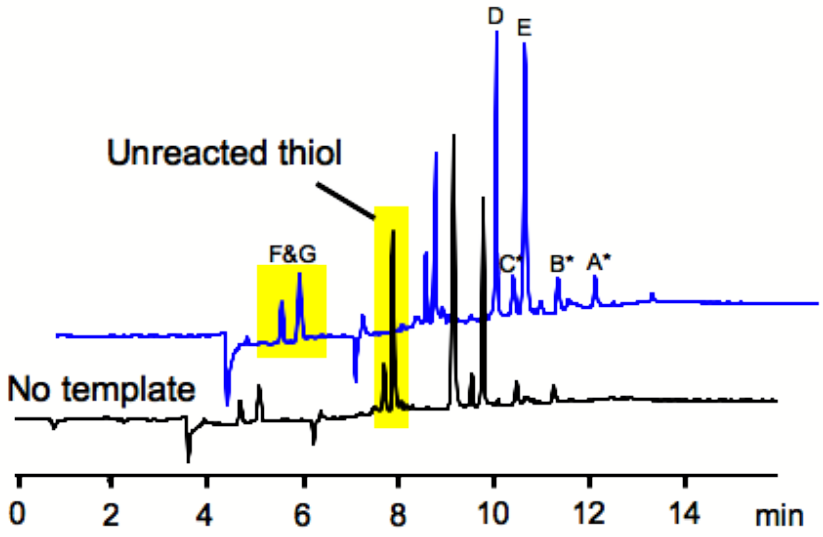

Figure 6.9 Chromatograms of the spermine DCPL. The unreacted thiol present in the reaction mixture indicates that the library has not reached equilibrium.

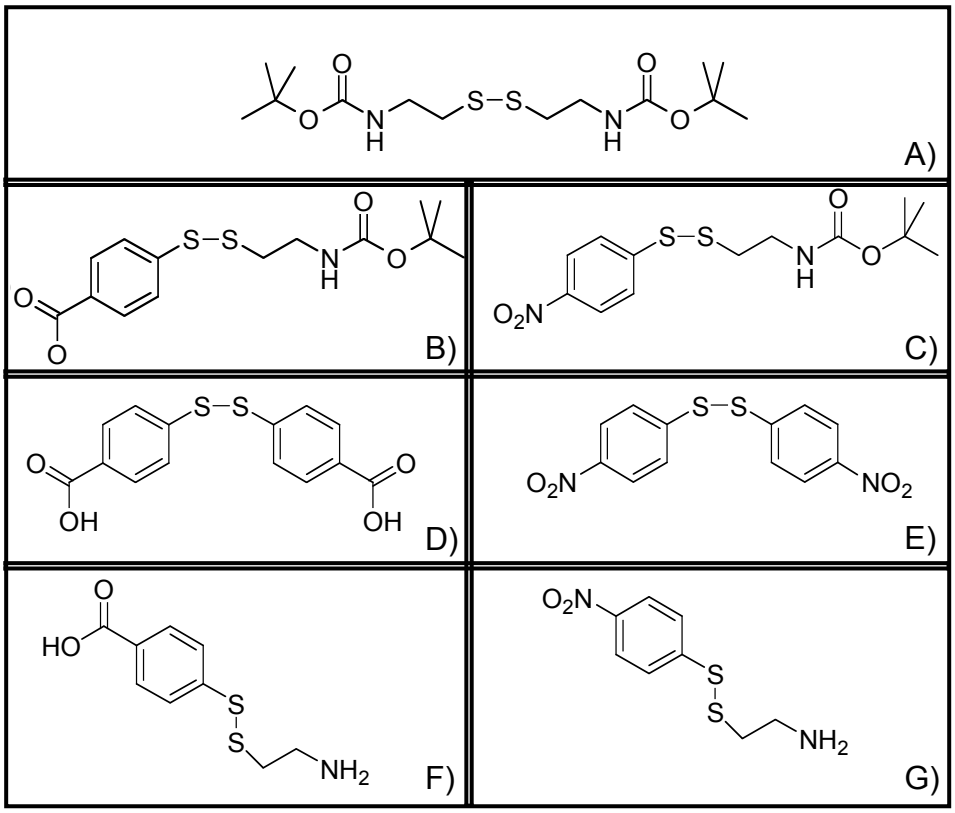

Figure 6.10 Various disulfides identified by LC-MS (performed by Zaida Rodriguez Docampo, Cambridge University). The most significant is compound A, as it demonstrates that the disulfide monomer (Fig 6.6) is readily exchanging with the thiolates.

HPLC analysis was therefore an ineffective tool for the analysis of polymer libraries despite its previous success in the identification of new hosts in standard dynamic combinatorial chemistry.[69, 70, 71, 72, 73, 74] LC-MS, however, proved to be much more useful. It allowed the molecular ion peaks for the expected disulfide library members to be identified. In addition, ion peaks were also visible for the disulfides that would form when the labile portion of the disulfide side chain and a thiol exchanged. These molecular ion peaks were the first conclusive evidence that the exchange reaction was taking place (Fig 6.10).

No change in library composition was observed by HPLC or LC-MS for template libraries and the control libraries set up with no template. This was not unexpected because an exchange reaction would take place even in the absence of a template and

result in intramolecular crosslinking of the polymer. Any evidence of an actual templating process would have to come from elsewhere.

6.3.2 Selective supramolecular binding with linear polymers

A ^{1}H NMR spectrum of the DCPL gave evidence of supramolecular binding between the polymer and the spermine template. The ^{1}H NMR signals for spermine appeared shifted upfield which was similar to the behaviour observed with spermine and microgels, (Fig 6.11) despite the concentrations being significantly lower. The initial concentration (Fig 6.11a) of the DCPL was 4.7×10^{-4} mol L^{-1} (polymer host) and 5.4×10^{-4} mol L^{-1} (spermine guest). Dilutions close to the detection limit of the NMR spectrometer showed no change in the NMR spectrum that would be expected for unbound spermine. This was either an indication of the spermine being incased in the polymer or that strong supramolecular binding was taking place.

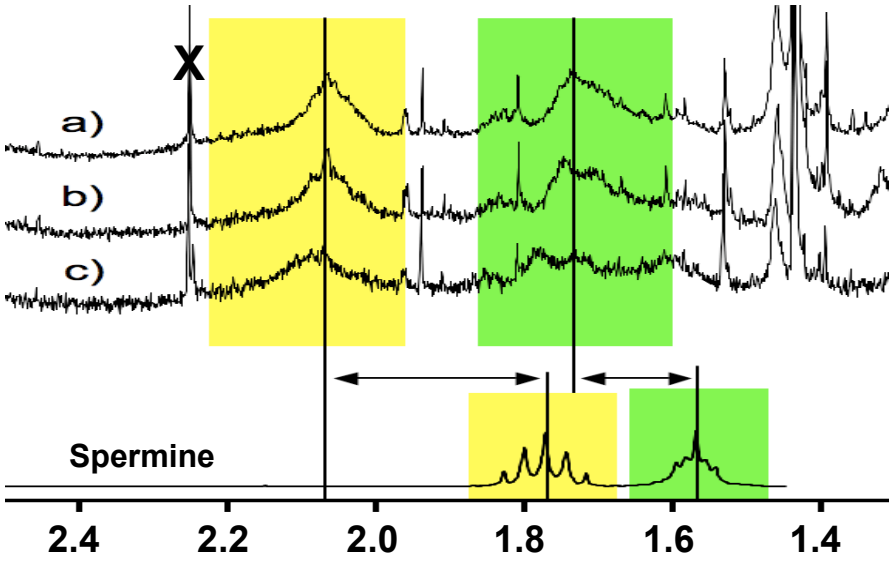

Figure 6.11 ^{1}H NMR spectrum (D_2O, 200 MHz, pD 8.0) of spermine DCPL (a) shows spermine signals shifted significantly relative to the position of pure spermine signals. Subsequent dilutions display no shift towards the unbound signal suggesting that binding is too strong to be quantified by ^{1}H NMR at 4.5×10^{-4} mol L^{-1} polymer host, 5.0×10^{-4} mol L^{-1} spermine guest. Concentrations: b) 2.3×10^{-4} mol L^{-1} polymer host, 2.5×10^{-4} mol L^{-1} spermine guest, c) 1.15×10^{-4} mol L^{-1} polymer/

host, 1.6×10^{-4} mol L^{-1} spermine/guest, each step was diluted with phosphate buffer (pD 8.0). The signals of an impurity (acetone) are marked with an "X".

After bulk preparation of the DCPL, the exchanged polymer was recovered by either filtration through an ion exchange resin or centrifugation through a filter with a molecular weight cut-off of 3000 g mol^{-1}. The ^{1}H NMR spectrum of the purified polymer displayed no peaks that would indicate the presence of spermine.

Isothermal titration calorimetry was used to further investigate the exchanged polymers. A 2 mM solution of spermine guest was titrated into a 0.2 mM solution of polymer in a 10 mM TRIS•HCl buffer (pH 7.5). The templated polymer showed a sub-millimolar affinity for its template, spermine, in an aqueous environment whereas the un-templated polymer showed no affinity for spermine.

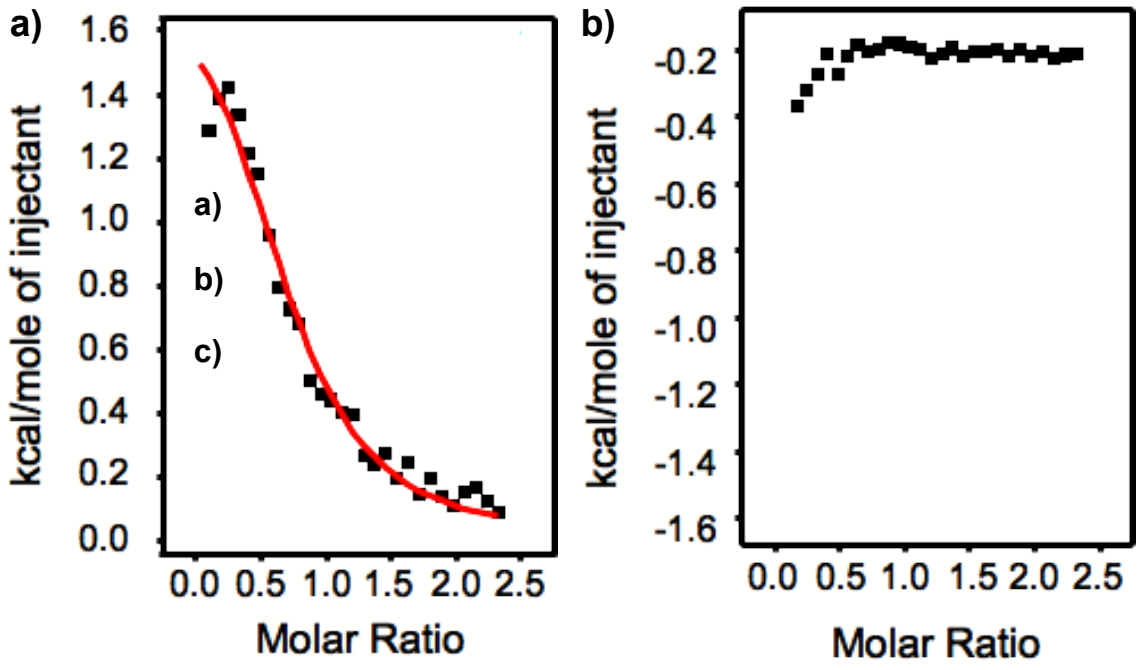

Figure 6.12 a) ITC data for the titration of spermine into a solution of spermine-exchanged polymer in 10 mM TRIS•HCl buffer (pH 7.5) at 25 °C. The experimental data were fitted using an n:1 model from which a binding constant of 2.61×10^{4} M^{-1} could be calculated. Average thermodynamic parameters are given in table 11. b) ITC data for the same titration using unexchanged polymer shows no affinity.

A number of titrations were carried out to determine what degree of selectivity the polymer displayed. Spermidine, *N,N*-bis(3-aminopropyl)-1,3-propanediamine, triethylenetetraamine and diethylenetriamine were chosen owing to their structural similarity to spermine (Fig 6.13).

The results of the ITC titrations of spermine exchanged polymer with *N,N*-bis (3-aminopropyl)-1,3-propanediamine, triethylenetetraamine and diethylenetriamine showed no binding, just like the unexchanged polymer and spermine.

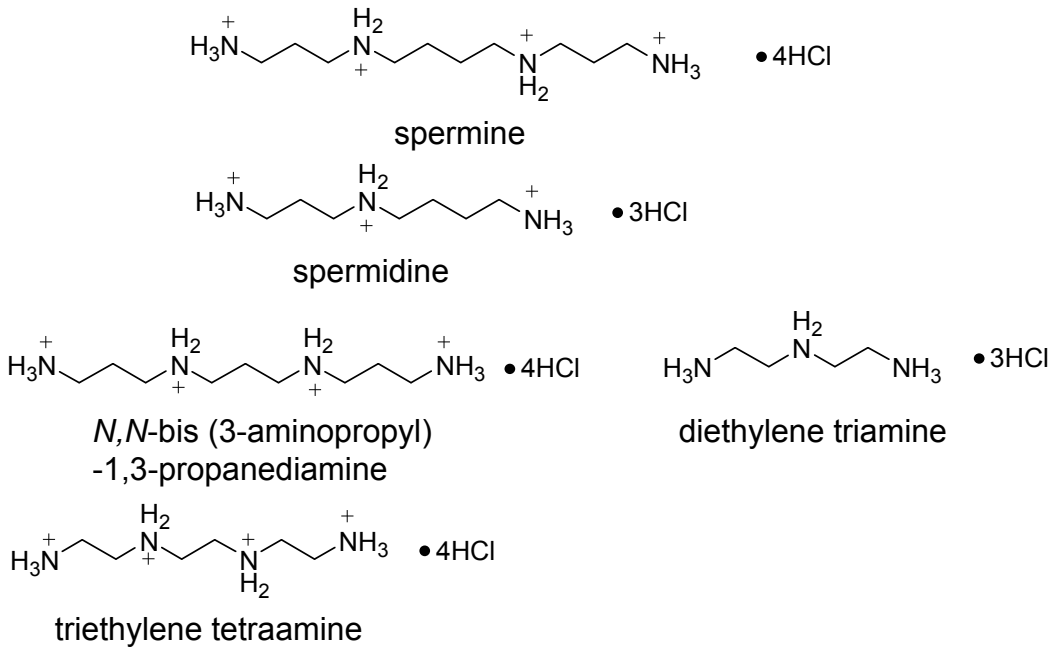

Figure 6.13 Spermine, spermidine and some structurally related compounds used to test the specificity of the spermine-exchanged polymer.

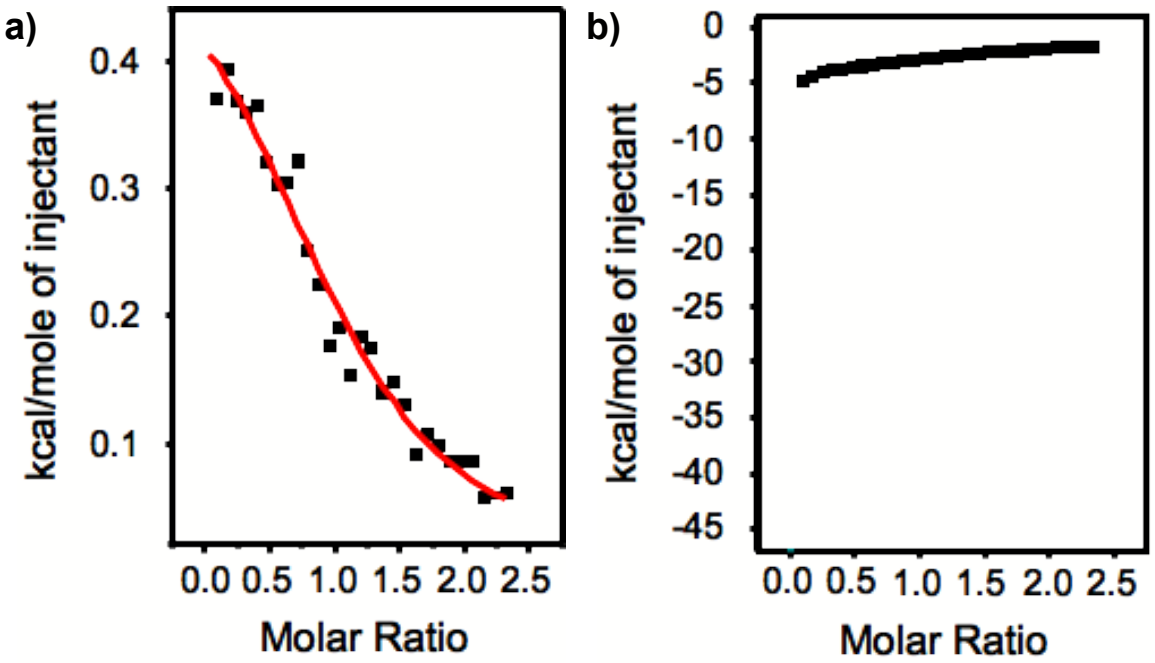

Figure 6.14 a) ITC data for the titration of spermidine into a solution of spermine exchanged polymer in 10 mM TRIS•HCl buffer (pH 7.5) at 25 °C, from which a binding constant of 1.4×10^4 M^{-1} could be calculated. b) ITC titration of the structurally related compound *N,N′*-bis(aminopropyl)-1,3-propanediamine with spermine-exchanged polymer.

The selectivity displayed by the exchanged polymer for the template (spermine) was surprising. It would seem that the binding "cavity" is extremely selective towards spermine and spermidine which both share the 4-3 carbon chains separated by a protonated amine. Spermidine has a decreased affinity towards the polymer, which would also seem to indicate that the fourth amino group present on the spermine molecule contributes to the binding event. Spermine and spermidine titrations showed an entropic contribution similar to that displayed by microgels and spermine. The entropic contribution could be due to the template molecule occupying a cavity, formed by the templating process. A small exothermic character was visible in the titrations of the structural analogues that could be an indication of some kind of ion exchange / adsorption to the polymer particles. In particular, for triethylene tetramine, which showed the strongest binding behaviour for the analogues. It is possible that the presence of four protonated amines allows this structurally similar compound to bind to the exchanged polymers slightly better, although it is still and order of magnitude weaker than the template spermine. (Table 11)

Table 11 Table of ITC results

Polymer / [host]	Guest	Association constant / M^{-1}	ΔH / $kJmol^{-1}$	ΔS / $kJmol^{-1}$	Stoichiometry
Spermine exchanged	Spermine	2.61×10^{4}	1.88±0.134	0.027	0.755
Spermine exchanged	Spermidine	1.43×10^{4}	0.535±0.047	0.021	1.11
Spermine exchanged	N,N'-bis (aminopropyl)-1,3-propanediamine	N/A	N/A	N/A	N/A
Unexchanged	Spermine	N/A	N/A	N/A	N/A
Spermine exchanged	diethylene triamine	N/A	N/A	N/A	N/A
Spermine exchanged	triethylene tetraamine	1.03×10^{3}	-1.96±2.35	-52	1.08

6.4 Conclusion

Highly selective polymer hosts have been modified from a linear RAFT copolymer by dynamic combinatorial chemistry. The DCL method has been applied to copolymers to create hosts for spermine for the first time. This represents the possibility for development of a new class of macroscopic hosts for low-molecular-weight compounds.

Isothermal titration calorimetry and ^{1}H NMR spectroscopy have both shown that the polymeric hosts possess strong affinity to the templated molecule in a competitive aqueous environment. Titrations with structurally related compounds indicated that a change in the chain length of the guest molecule by as little as two CH_2 has a drastic effect on the affinity.

As such a degree of selectivity and an association constant in the sub-millimolar range has been created in a linear polymer by a process based on the templated the crosslinking of a polymer to define a binding site within an intramolecularly crosslinked polymer.

7 Summary and outlook

The results presented in this thesis support the successful use of the tetrazole group as recognition element in Supramolecular Chemistry. Although tetrazoles are widely known as bioisosteric replacements for carboxylic acids, there has been a long-standing discussion whether or not tetrazoles bind to arginine sites in protein receptors. The binding of tetrazoles to amidines (which served as a simple model for an arginine) was considered in Chapter 2. While the binding modes of tetrazolate and carboxylate anions in amidinium complexes turned out to be similar, the association constant of the former was only 2.5 – 10 M^{-1} in DMSO, about 2–3 orders of magnitude smaller than that of amidinium carboxylates. (Fig 7.1) Crystal structures revealed that the N···H–N hydrogen bonds in amidinium tetrazolates tend to be bent and noticeably longer than corresponding hydrogen bonds in amidinium carboxylates. These findings seemed to explain why replacement of a crucial carboxylic acid by a tetrazole (e.g. in the case of inhibitors of the fibrinogen receptor or prostaglandin transporter) caused their inhibitor efficiencies to be lowered by at least two orders of magnitude while, on the other hand, tetrazoles are highly effective in tetrazole-containing angiotensin II receptor antagonists when binding involved other cationic sites such as lysine or histidine.

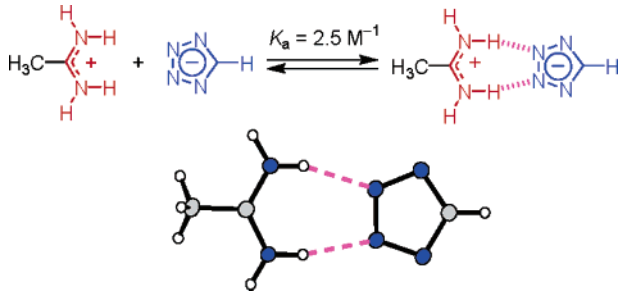

Figure 7.1 Simple model studies which simulated the interactions between carboxylic acids and arginine residues 21, tetrazoles and arginines 19.

The thesis then concentrated on the design of polymeric supramolecular receptors based on crosslinked microgels and linear copolymers that were prepared by a controlled radical polymerisation (RAFT). Chapter 3 details the synthesis and characterisation of microgels that bound protonated amines in a competitive aqueous environment (pH 7,

0.15 mol/L KCl) with association constants in the millimolar range (700 M^{-1} [f]or spermine). ITC measurements gave positive values for ΔH and $T\Delta S$ (3.2 kJ mol^{-1} and 19.2 kJ mol^{-1}, respectively) which accounted for an endothermic, entropy-driven process. (Fig 7.2) This was indicative of water being released from the binding cavity. It is also possible that some kind of rearrangement of the binding cavity, or that flexible nature of the polymer backbone, is responsible for the positive enthalpy. ^{1}H NMR measurements with non-complexing ligands (NMe_4Cl and acetamidine hydrochloride) ruled out an ion-exchange process and pointed towards supramolecular binding.

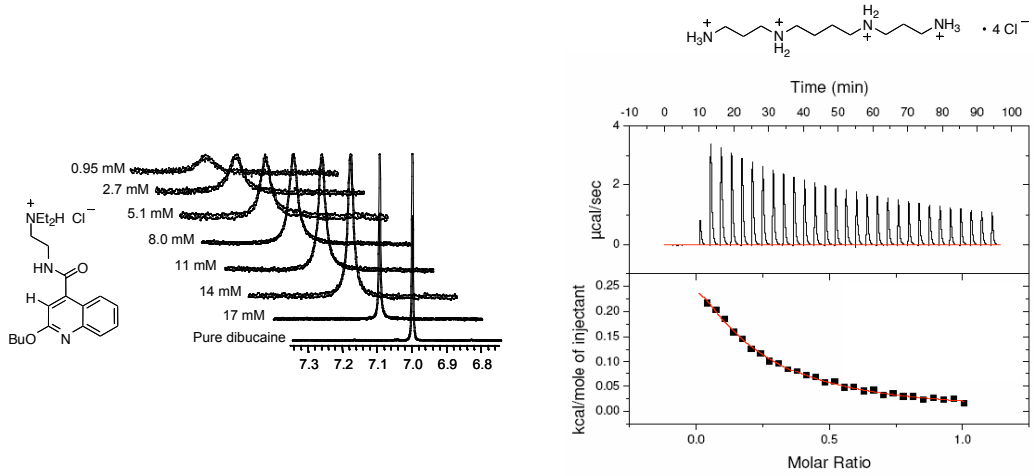

Figure 7.2 Supramolecular binding of protonated amines to microgels was evident from line broadening or complexation-induced shifts in the 1H NMR spectra and microcalorimetry measurements.

Chapter 4 describes the successful use of microgels as supramolecular hosts for proteins in aqueous buffer. The inclusion of different functional groups instilled an unexpected degree of selectivity to the microgels. Proteins with high pI bound strongly to the microgels with association constants that were competitive with other polymers designed for protein recognition that have been published in the literature. (Table 12)

Table 12. Calculated macroscopic binding constants for microgels binding to selected proteins.

Microgel / (host)	Protein / (Guest)	Binding Constant / single residue (M^{-1})	Calculated macroscopic binding constant (M^{-1})
MG-SMA	cytochrome C	1.14×10^3	1.18×10^9
MG-TET	cytochrome C	NA	NA
MG-BP	cytochrome C	-	-
MG-SMA	haemoglobin	NA	NA
MG-TET	haemoglobin	5.91×10^3	3.06×10^9

MG-BP	haemoglobin	2.41×10^5	1.57×10^{11}

Chapter 5 discusses linear copolymers that were prepared by a controlled radical polymerisation and showed a similar selectivity to the microgels. The inclusion of hydrophobic monomers into these RAFT copolymers increased the binding strength even further. Association constants ranged from 18 L/mol for S1O10 to 1600 L/mol for the fully optimised S3cH15. (Fig 7.3)

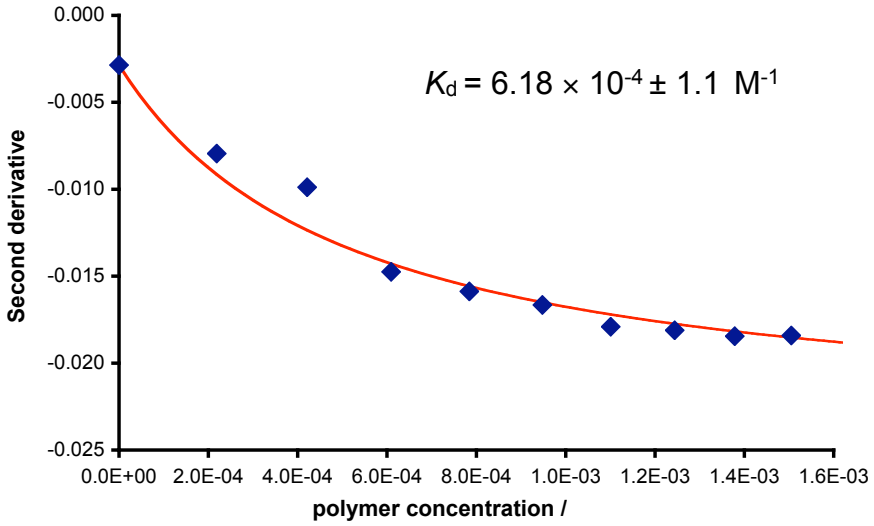

Figure 7.3 Binding curve for the titration of S3cH15 into cytochrome C (9.8×10^{-6} mol/L, 10mM phosphate buffer pH 7, 0.15 M KCl). This proved to be the strongest binder determined by a combinatorial process.

Highly selective polymer hosts were then obtained from a linear RAFT copolymer with the help of dynamic combinatorial chemistry (Chapter 6). This is, to my knowledge, the first time that DCC has been used to enhance a polymer's affinity for a template. It led to a significant increase in the affinity of the polymers for spermine as well as a surprising degree of selectivity.

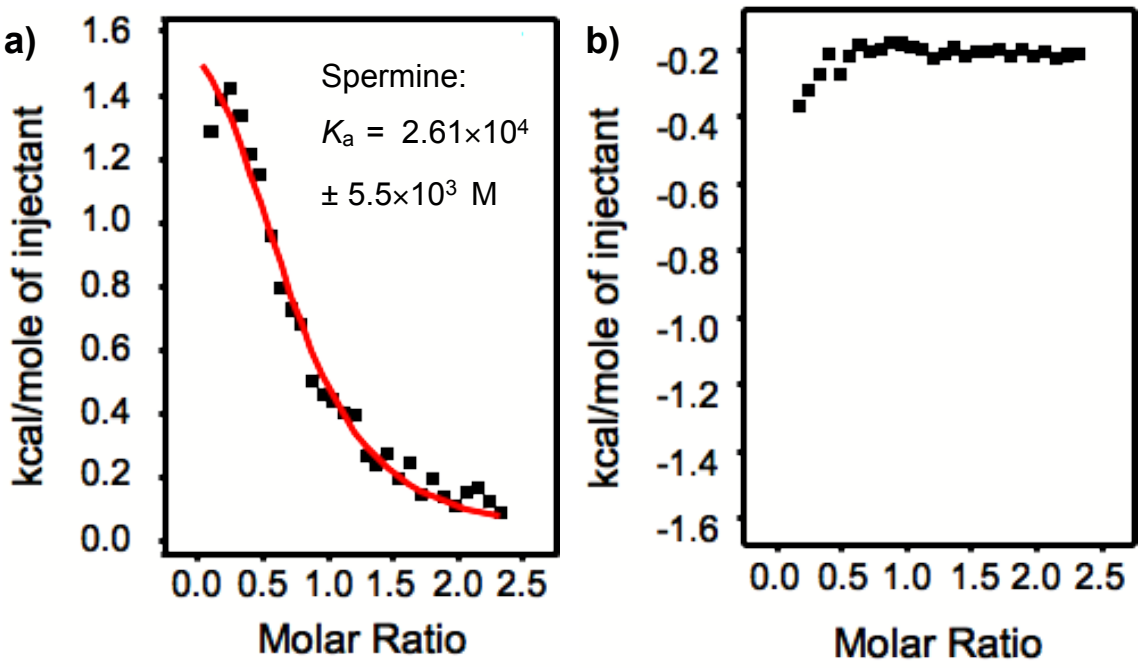

Figure 7.4 Dynamic combinatorial chemistry was used to adapt highly selective supramolecular hosts for polyamines in an aqueous buffer. Isothermal microcalorimetry provided evidence of a) shows a significant increase in binding strength for a template over b) the unexchanged polymer.

In summary, these results demonstrate that polymers are extremely versatile tools in supramolecular chemistry. I see no reason why polymeric receptors cannot continue to be at the forefront of supramolecular chemistry. Future work could include investigation into microgels and RAFT copolymers and their affinity for other proteins such as chymotrypsin, histone and lysozyme. If polymeric receptors continued to show binding to specific proteins, then it would be feasible to use them in diagnostic devices or in protein separations. Coating an electrode with a RAFT polymer which specifically binds a certain protein would, for example, provide easy access to a highly sensitive biochemical sensor. Different polymers could be used to create an extremely compact device with a high degree of sensitivity.

Dynamic combinatorial chemistry with polymers is certainly still in its infancy. There are a number of possible areas which could be concentrated on to fully exploit the potential of these highly selective systems. A combinatorial approach similar to the method used for the linear copolymers could be used to quickly find an ideal composition. It is interesting to note that others (Schrader, Rotello) have been using a

significantly higher mol% of anionic monomer.[6] It is possible that further improvements could be achieved by decreasing the amount of NIPAAM in the copolymerisation. It would also be interesting to see whether or not dynamic combinatorial chemistry could be used to optimise polymers for protein recognition.

8 Experimental

8.1 General materials and instrumentation

All chemicals used were reagent-grade and used without further purification. Haemoglobin, cytochrome C and ferritin were purchased from Fluka Biochimica. Lithium bisphosphonate monomer **1** was kindly supplied by T. Schrader from the University of Duisburg-Essen (Germany).

A Masterflex 7518-00 peristaltic pump with Vivaflow 50, 100,000 MWCO polyether sulfone (PES) and 0.2 μm PES filters were used for ultrafiltration. ^{1}H NMR (400 MHz) spectra were obtained with a Bruker DPX400 spectrophotometer and 200 MHz ^{1}H NMR spectra were recorded on a Bruker AC200 spectrometer. UV-Vis spectroscopy was carried out using a Shimadzu UV-1601 UV-Vis spectrometer. All UV measurements were taken at room temperature (circa 21 ^{o}C). Potentiometric studies were conducted with a Metrohm 702 Titrino autotitrator using a Metrohm 6.0222.100 combined pH glass electrode with a 3 M KCl internal filling. Differential scanning calorimetry was used to determine melting points; the DSC used was a Thermal Advantage DSC 2010. Infrared spectra were obtained with a Perkin Elmer RX Fourier transform infrared spectrometer.

HPLC analysis was performed on an Agilent 1100 system coupled to a UV detector with a Agilent ZORBAX C8 Eclipse, 150 mm × 4.6 mm, 3.5 μm. Data was analysed with Agilent Chemstation software (Rev A.10.0.2).

LC-MS analysis was performed using an Agilent XCT ion trap MSD mass spectrometer with an Agilent Eclipse XDB-C8 3.5 μm, 2.1 x 150 mm column. Agilent Chemstation software (Rev A.10.02) and Bruker Daltonik LC/MSD Trap software 5.2 (Build 374) was used to operate the LC-MS and analyse the data.

GPC analysis was carried out on a Waters model 510 GPC chromatograph with a differential refractometer, model 410 and a Rheodyne injector model 7125 by P. Sarker

at Sheffield University.

ITC was carried out on an MCS-ITC from Microcal LLC, Northampton, MA . Data were recorded at 298 K.

8.2 Synthesis and characterisation of monomers and reagents

8.2.1 Tetrazole-amidine complexes

8.2.1.1 Benzamidine

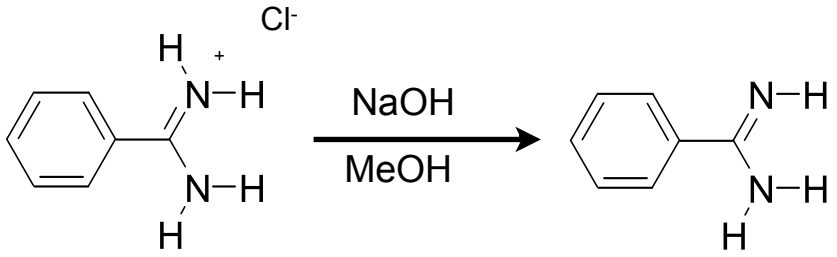

Benzamidinium hydrochloride (1.38 g, 8.81 mmol) was dissolved in methanol (3 mL). To this, a solution of NaOH (352 mg, 8.85 mmol) in methanol (10 mL) was added. The mixture was then concentrated in vacuum, and the residue was sublimed at 110 °C/0.4 mbar. Yield: 180 mg of a colourless oil (1.50 mmol, 17%).

8.2.1.2 Benzamidinium tetrazolate **21**

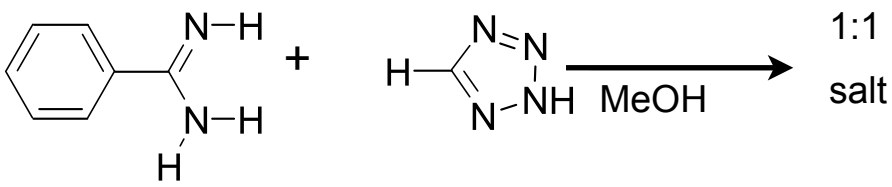

A solution of tetrazole in acetonitrile (0.45 M, 3.3 mL, 1.5 mmol) was added to a solution of benzamidine (180 mg, 1.50 mmol) in methanol (2 mL). The mixture was concentrated in vacuum, and the residue was recrystallised from hot MeOH/MeCN (1 mL/5 mL). Yield: 178 mg (63%), colourless solid. DSC: T_m = 150 °C (broad, 44 J g^{-1}).

^{1}H NMR (200 MHz, d_6-DMSO): δ 7.56–7.89 (m, 5 H), 8.17 (s, 1 H), 9.56 (br s, 4 H). IR (KBr, cm^{-1}): ν 3260, 3064, 1670, 1480, 1137, 882, 788. Anal. Calcd. for $C_8H_{10}N_6$ (190.21): C, 50.53; H, 5.40; N, 43.96. Found: C, 50.52; H, 5.30; N, 44.18.

8.2.1.3 Acetamidine

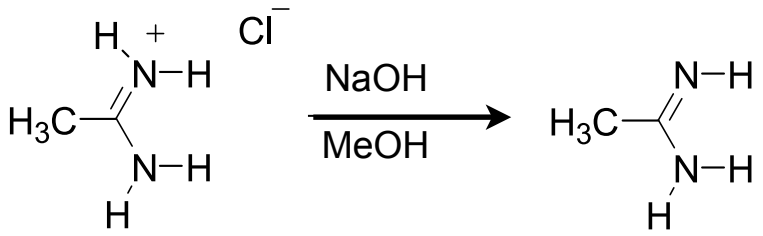

Acetamidinium hydrochloride (2.00 g, 21.2 mmol) was dissolved in methanol (20 mL). To this, a solution of NaOH (853 mg, 21.3 mmol) in methanol (60 mL) was added. The mixture was then concentrated in vacuum, and the residue was sublimed at 60 °C/0.4 mbar. Yield: 150 mg of a colourless oil (2.59 mmol, 23%). ^{1}H NMR (200 MHz, d_6-DMSO): 1.75 (s, 3 H), 5.36 (br s, 3 H).

8.2.1.4 Acetamidinium tetrazolate **19**

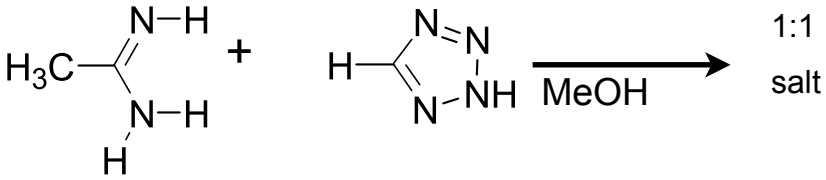

A solution of tetrazole in acetonitrile (0.45 M, 5.45 mL, 2.45 mmol) was added to a solution of acetamidine (142 mg, 2.45 mmol) in methanol (2 mL). The mixture was concentrated in vacuum, and the residue was recrystallised from hot MeOH/MeCN. Yield: 165 mg (53%), colourless solid. DSC: 149 °C (145 J g^{-1}). ^{1}H NMR (400 MHz, d_6-DMSO, 60 mg/0.7 mL): 2.19 (s, 3 H), 8.23 (s, 1 H), 9.28 (br s, 4 H). ^{13}C NMR (50 MHz, d_6-DMSO, 60 mg/0.7 mL): 18.69 (CH_3), 149.16 (tetrazole H), 168.42 (amidine C=N). IR (KBr, cm^{-1}): ν 3277, 1703, 1530, 1442, 1377, 1281. Anal. Calcd. for $C_3H_8N_6$ (128.14): C, 28.24; H, 6.36; N, 64.61. Found: C, 28.12; H, 6.29; N, 65.59.

8.2.1.5 Sodium tetrazolate

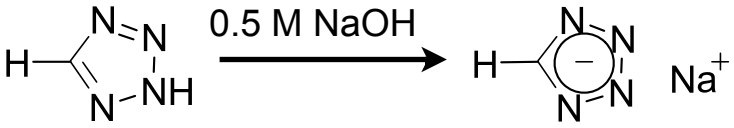

Tetrazole (102 mg, 1.45 mmol) was dissolved in water (30 mL) and then titrated with 0.5 M aqueous NaOH until neutralised using an automated titrator. The solution was then concentrated in vacuum and dried. ^{1}H NMR (200 MHz, d_6-DMSO): 8.09 (s).

2.2.1.5 Acetamidinium tetrakis[3,5-bis(trifluoromethyl)phenyl]borate

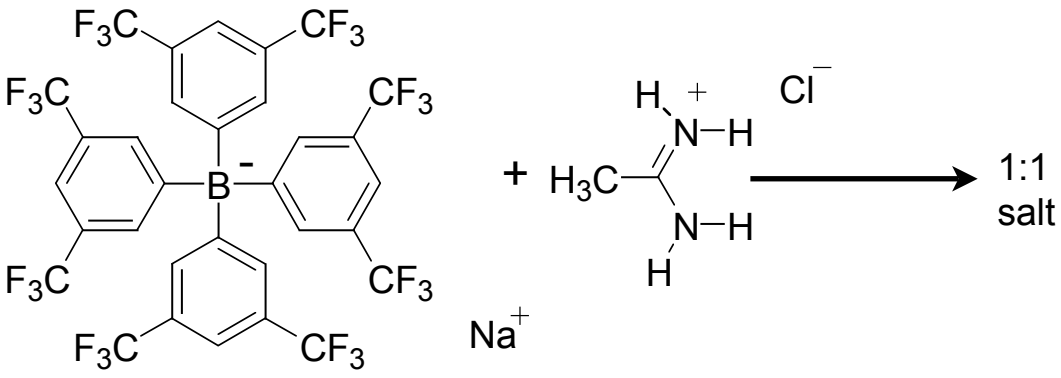

Acetamidinium hydrochloride (50 mg, 0.53 mmol) was dissolved in methanol (50 mL). Sodium tetrakis[(3,5-bistrifluoromethyl)phenyl]borate (468.7 mg, 0.53 mmol) was then added and the solvent was removed under a vacuum. The resulting solid was dissolved in acetonitrile (20 mL), filtered and then the filtrate was concentrated in vacuum and dried. Yield: 336 mg (70%). ^{1}H NMR (200 MHz, d_6-DMSO): 2.10 (s, 3H), 7.60 (br s, 2H) 7.65 (s, 1H), 8.62 (bs, *NH*)

8.2.2 Monomers and reagents for the synthesis of microgels and linear copolymers

8.2.2.1 Sodium 5-(methacrylamido)tetrazolate **23** [117]

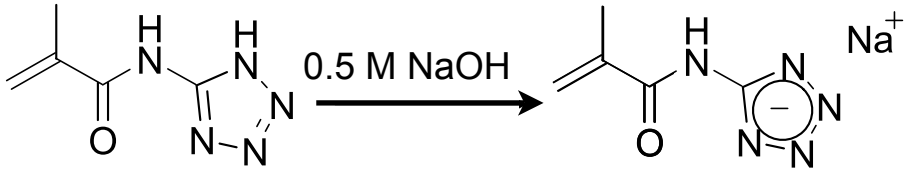

Sodium hydroxide (0.59 g, 15 mmol) was dissolved in hot methanol (25 mL) under reflux. 5-(Methacrylamido)tetrazole (2.00 g, 13.1 mmol) was added and the mixture was heated to 64 °C for 1-2 minutes until everything dissolved. The solution was concentrated under a vacuum. The resulting liquid was dissolved in propan-2-ol and stored at 4 °C overnight. The colourless precipitate was collected by suction filtration and dried. Yield: 1.90 g (83%); ^{1}H NMR (200 MHz, d_6-DMSO): δ 1.93 (s, 3H, CH_3), 5.46 (s, 1H, NH), 5.87 (s, 1H, CH_2).

8.2.2.2 *N, N'*-Bis(acryloyl)cystamine [58]

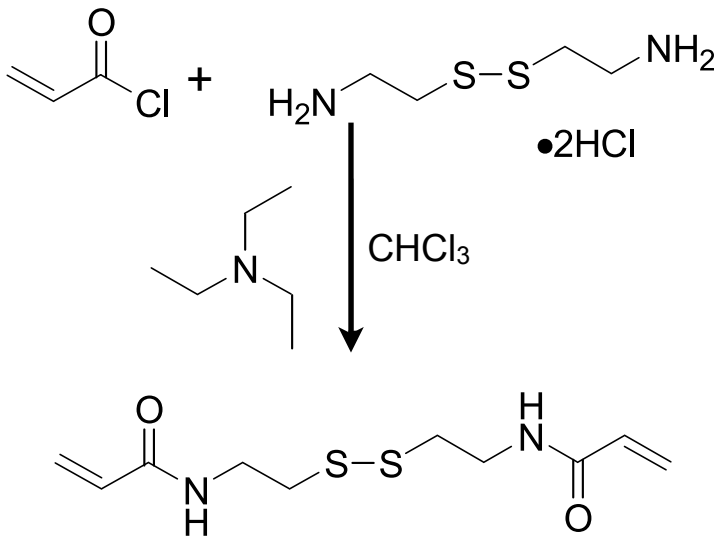

Cystamine dihydrochloride (1.98 g, 8.79 mmol) was dissolved in a 3 M solution of NaOH (20 ml). The solution was then combined with chloroform (20 ml) containing acryloyl chloride (2.15 ml, 34 mmol) at 0 °C. The mixture was stirred at 50 °C for 30 minutes. After cooling, the product was collected by suction filtration and recrystallised

from chloroform. Yield: 1.81 g (90%); ^{1}H NMR (200 MHz, $CDCl_3$): δ 2.92 (t, 2H, CH_2, J = 6.6), 3.72 (q, 2H, CH_2, J = 6.7), 5.17 (dd, H, CH, J = 3.7, 8.2), 6.32 (m, 2H, CH_2), 6.77 (bs, 1H, NH). DSC: T_m 122 °C (lit. m.p. = 125°C).

8.2.2.3 Propranolol, methacrylic acid salt

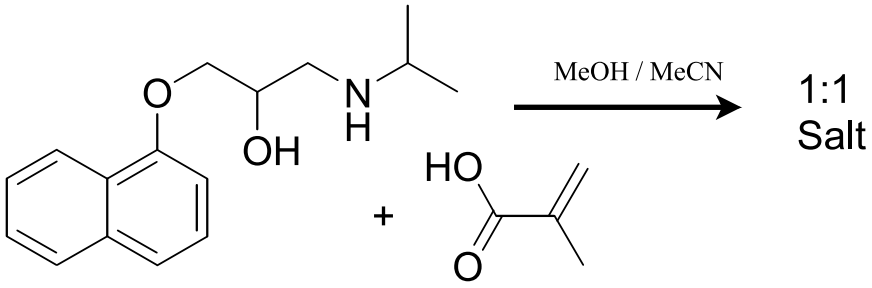

Propranolol hydrochloride (300 mg, 1 mmol) was dissolved in aqueous NaOH (44 mg, 1.1 mmol in 20 ml) and the propranolol base was extracted twice with $CHCl_3$ (40 ml). The resulting solution was dried with anhydrous $MgSO_4$ and concentrated under a vacuum to give a colourless solid (116 mg, 26%). Propranolol base was combined with methacrylic acid (33.3 mg, 0.38 mmol) in methanol (20 ml). Recrystallisation from MeOH/MeCN yielded crystals of sufficient quality for X-ray crystallography. ^{1}H NMR (200 MHz, CD_3OD): δ 1.15 (dd, 6H, 2 x CH_3, J = 2.0, 6.2), 2.75 (m, 3H), 3.2 (m, 2H), 4.1 (m, 3H), 4.87 (bs, 2H), 6.82 (dd, 2H, J = 1.6, 7.0), 7.3 (m, 3H), 7.7 (m, 3H), 8.2 (m, 3H). Anal. Calcd. for $C_{20}H_{27}NO_4$ (346.39): C, 69.34; H, 7.85; N, 4.04. Found: C, 69.05; H, 7.96; N, 4.13.

8.2.2.4 *S,S′*-Bis(α,α'-dimethyl-α''-acetic acid)-trithiocarbonate chain transfer agent [156]

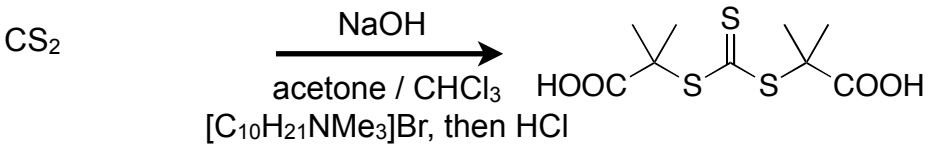

Carbon disulfide (6.85 g, 90.0 mmol), acetone (12.1 g, 0.23 mol), chloroform (26.9 g, 0.23 mol) and decyltrimethylammonium bromide (0.50 g, 1.78 mol) were mixed with hexane (30 mL) under nitrogen. The solution was cooled to ~10 °C in an ice-water bath. Sodium hydroxide solution (50.4 g in 50 mL, 0.63 mol) was added dropwise over 60

minutes to keep the temperature below 25 °C. The solution was stirred overnight. Water (200 mL) was added, followed by concentrated HCl (30 mL) with vigourous stirring under a nitrogen purge for 30 minutes. The yellow solid was filtered, washed with water and dried under vacuum. Yield: 2.66 g (21%). ^{1}H NMR (200 MHz) δ 1.59 (s, 12 H). ^{13}C NMR (50 MHz, CD_3OD): δ 25.65 (CH_3), 57.14 (CMe_2), 176.13 (COOH), 220.29 (C═S). MS *m*/*z*: M^+ 282, $HOOCC(CH_3)_2SC(S)S^+$ 195, $HOOCC(CH_3)_2SCS^+$ 162, $HOOCC(CH_3)_2^+$ 87, $COOH^+$ 45.

8.2.2.5 *N*-Octyl acrylamide [162]

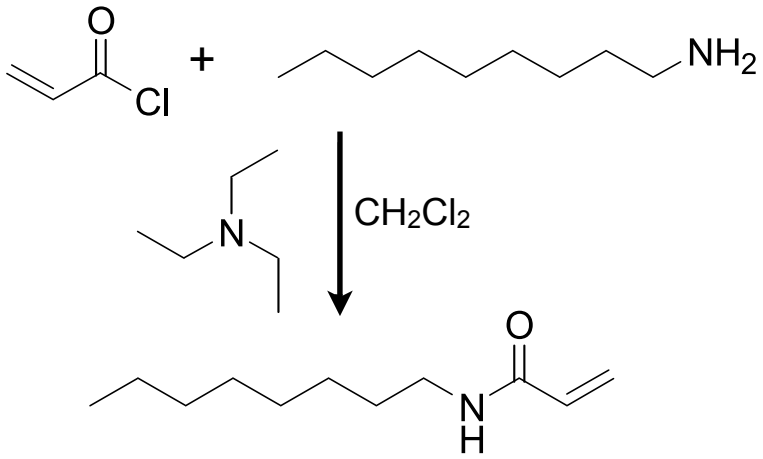

Octylamine (34.2 g, 0.26 mol) and triethylamine (26.8 g, 0.26 mol) were dissolved in dichloromethane (50 ml) and cooled over ice with intense mixing. A solution of acryloyl chloride (20.0 g, 0.22 mol) in dichloromethane was added dropwise over a period of 1 hour. The solution was left to warm to room temperature and stirred overnight. The solvent was evaporated under vacuum resulting in a pale yellow, waxy powder. The residue was then recrystallised from hexane to provide off-white crystals. Yield: 38.4 g (95%). ^{1}H NMR (200 MHz, DMSO-d_6): δ 0.84 (t, 3H, CH_3, J = 6.7), 1.4 [m, 12H, $(CH_2)_6$], 3.95 (q, 2H, CH_2, J = 6.6, 12.7), 5.53 (dd, 1H, =CH, J = 2.8, 9.6), 6.14 (m, 2H, $=CH_2$), 8.07 (t, 1H, NH, J = 6.6). DSC: T_m 34.5 °C (Lit. m.p. 35-36 °C).

8.2.2.6 *N*-Benzyl acrylamide [163]

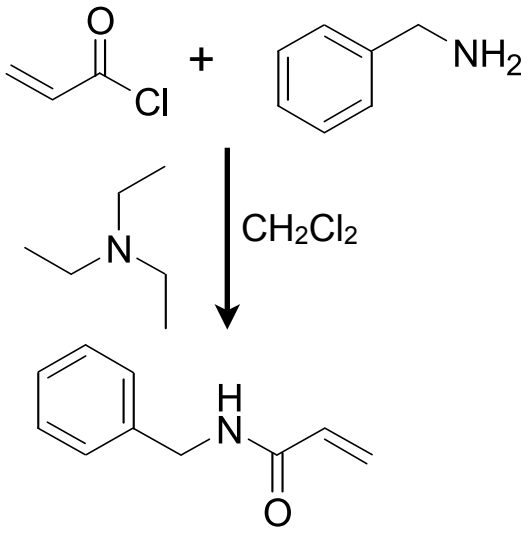

Benzylamine (27.9 g, 0.26 mol) and triethylamine (26.8 g, 0.26 mol) were dissolved in dichloromethane (50 ml) and cooled over ice with intense mixing. A solution of acryloyl chloride (20.0 g, 0.22 mol) in dichloromethane was added dropwise over a period of 1 hour. The solution was left to warm to room temperature and stirred overnight. The solvent was evaporated under vacuum resulting in pale yellow, waxy powder. The residue was then recrystallised from hexane to provide off-white crystals. Yield: 30.6 g (86%). ^{1}H NMR (200 MHz, DMSO-d_6): δ 4.35 (d, 2H, CH_2, J = 6.0), 5.53 (dd, 1H, CH, J = 2.5, 9.9), 6.14 (m, 2H, CH_2, J = 2.5, 9.9, 7.1, 17.3), 7.25 (m, 5H, C_6H_5), 8.73 (t, 1H, NH, J = 4.8). DSC T_m 63 °C (Lit. m.p. 65-65.7 °C).

8.2.2.7 *N*-Cyclohexyl acrylamide [164]

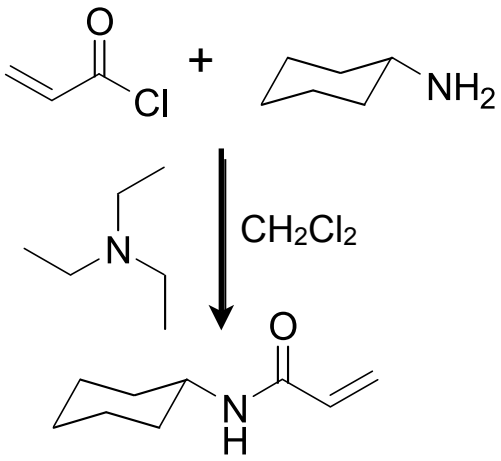

Cyclohexylamine (25.8 g, 0.26 mol) and triethylamine (26.8 g, 0.26 mol) were dissolved in dichloromethane (50 ml) and cooled over ice with intense mixing. A solution of acryloyl chloride (20.0 g, 0.22 mol) in dichloromethane was added dropwise over a period of 1 hour. The solution was left to warm to room temperature and stirred overnight. The solvent was evaporated under vacuum resulting in pale yellow waxy powder. The residue was then recrystallised from hexane to provide of off-white crystals. Yield: 31.6 g (94%) ^{1}H NMR (200 MHz, d_6-DMSO) δ 1.16 (m, 5H, -CH_2-), 1.63 (m, 5H, -CH_2-), 2.50 (q, H, CH J = 1.8, 3.6, 11.2), 5.49 (dd, H, CH, J = 2.6, 12.3), 6.14 (m, 2H, CH_2), 8.03 (d, 1H, NH J = 7.7). DSC: T_m 112 °C (Lit. mp. 112-113 °C).

8.2.2.8 (*N*-Boc)-*N'*-acryloyl cystamine

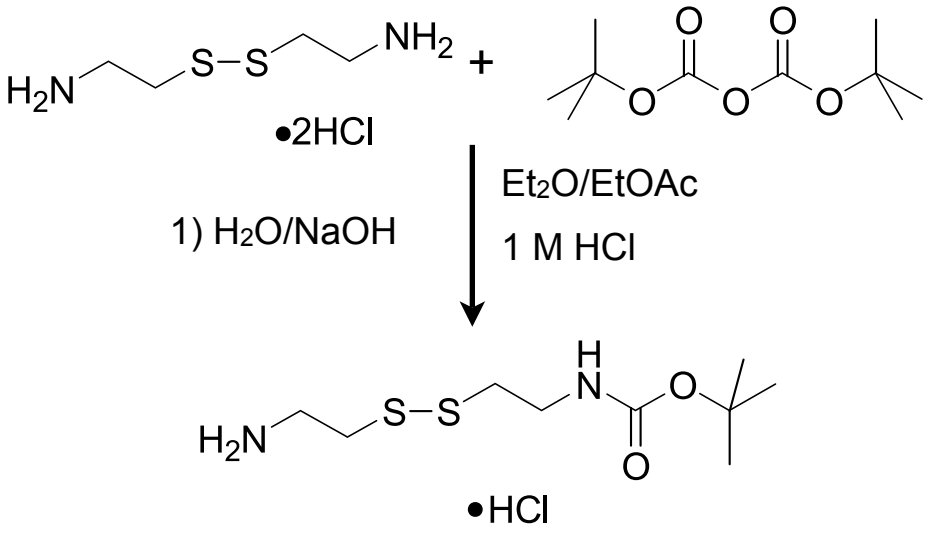

A solution of boc anhydride (0.44 g, 2.0 mmol) in H_2O (50 mL) was added dropwise into a solution of cystamine dihydrochloride (0.50 g, 2.2 mmol, in water (50 mL). The mixture was stirred at room temperature overnight. The solution was then brought to pH 11 with NaOH (0.5 M) and extracted twice with diethylether. The aqueous portion was then extracted twice with ethylacetate, which was then evaporated under vacuum. The resulting oily residue was titrated to pH 7 with 1.0 mM HCl and dried under vacuum to yield the mono-protected cystamine. Yield: 0.21g (41%). ^{1}H NMR (200 MHz, D_2O): δ 1.37 (s, 9H $-CH_3$), 2.80 (t, 2H, CH_2), 2.96 (q, 2H, CH_2) 3.35 (m, 4H, CH_2-CH_2) 7.77 (bs, 1H CONH). ^{13}C NMR (50 MHz, D_2O): δ 159.16 (NCO_2), 118.36 (CMe_3), 82.12 (CNH), 38.67 (CH_2), 34.18 (CH_2), 28.68 (CH_3). MS *m*/*z*: MH^+ 253.1, $H_3N(CH_2)_2S_2(CH_2)_2NHCO_2{}^tBu^+$

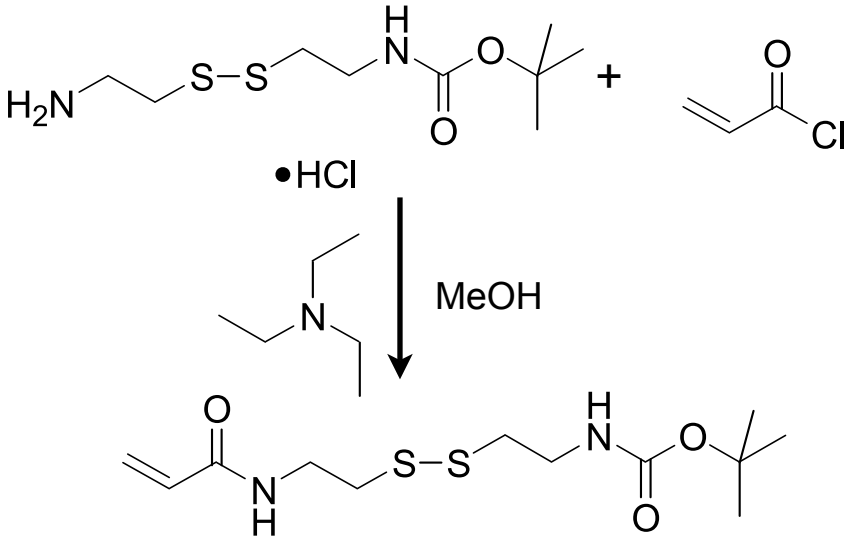

The mono-protected cystamine (0.240 g, 0.8 mmol) was dissolved in MeOH (50 mL) together with triethylamine (0.29 mL, 2.1 mmol). A solution of acryloyl chloride (0.10 g, 1.1 mmol, 1.5 eq) in MeOH was added dropwise with vigourous stirring at 0 °C over 1.5 hours. The mixture was then left at room temperature overnight and the solvent was evaporated under vacuum to give a crude beige residue. The residue was recrystallised in hexane to yield an off-white, oily residue. Yield: 0.21g (97%). ^{1}H NMR (200 MHz, D_2O): δ 1.41 (s, 9H, CH_3), 3.54-3.31 (m, 4H, CH_2), 2.83 (m, 4H, CH_2) 5.64, 6.12, 6.19 (ABX). ^{13}C NMR (50 MHz, D_2O): δ 168.20 (NCO_2), 131.87 (CO), 126.87 (CMe_3), 80.16, 71.17 (C=C), 39.58, 38.31, 39.02, 38.41 (CH_2), 28.75 (CH_3).

8.3 Polymerisations

8.3.1 Synthesis of microgels

8.3.1.1 **MG-TET**

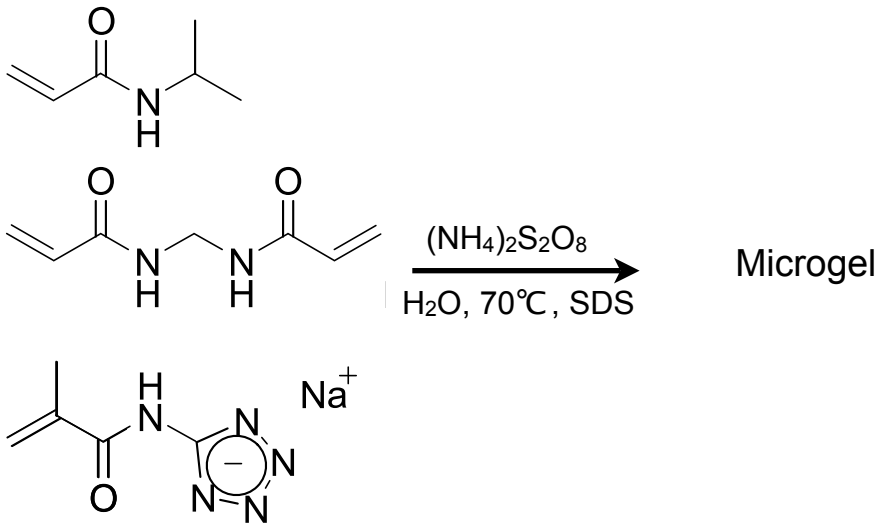

MG-TET microgels were synthesised according to the following general procedure. Sodium 5-(methacrylamido)tetrazolate (0.14 g, 0.8 mmol), NIPAM (1.13 g, 10 mmol), *N,N'*-methylene bisacrylamide (155 mg, 10 mmol) and SDS (60 mg, 0.2 mmol) were dissolved in water (200 ml) in a three-necked round bottomed flask fitted with a septum

cap. The solution was heated to 70 ˚C and degassed by bubbling nitrogen through for 30 minutes. Ammonium persulphate (60 mg, 0.5 mmol in 1 mL) aqueous solution was added and the reaction mixture was stirred and heated at 70 °C overnight. Ultrafiltration against 1 L of distilled water followed by a second ultrafiltration through a 0.2 μm PES membrane filter was used to purify the reaction mixture. The microgel solution was then concentrated under vacuum and freeze-dried (room temperature, 0.8 mbar). The yields of this procedure were typically in the range of 25-45% (of monomer mass used). ^{1}H NMR (200 MHz, D_2O): δ 1.07 (bs, CH_3), 1.53 (bt, CH_2), 1.96 (bm, CH), 3.83 (bs, CH), 7.77 (bm, NH). IR (KBr, cm^{-1}): ν 3300, 1650, 1500, 1400, 1225, 1200, 1050.

8.3.1.2 **MG-BP**

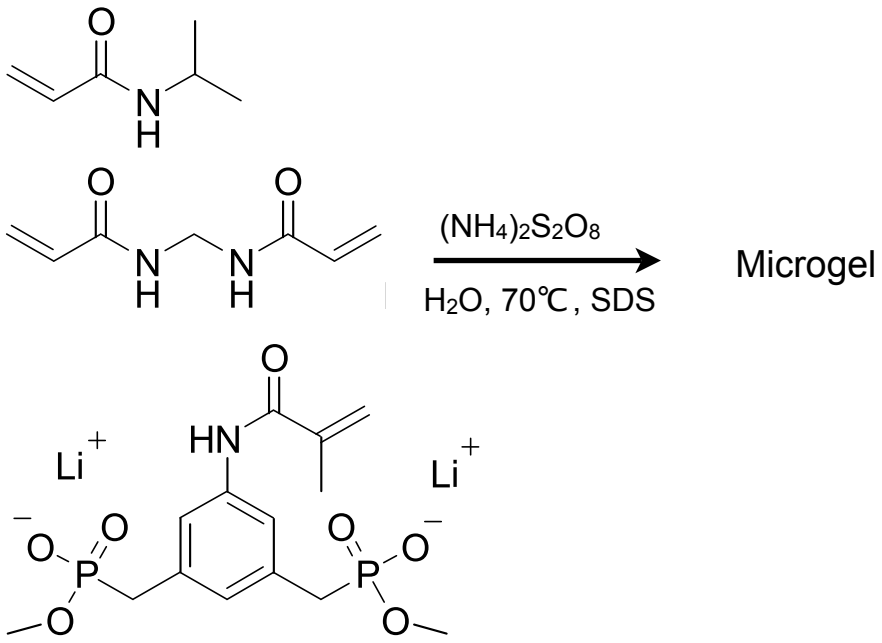

The lithium salt of the bisphosphonate monomer (0.31 g, 0.8 mmol), NIPAM (1.13 g, 10 mmol), methylene bisacrylamide (46 mg, 3.0 mmol), bis(acryloyl) cystamine (182 mg, 7.0 mmol) and SDS (60 mg, 0.2 mmol) were dissolved in water (200 ml) in a three necked round bottomed flask. The solution was heated to 70 °C and degassed by bubbling nitrogen through for 30 minutes. Ammonium persulphate (60 mg, 0.5 mmol) in aqueous (1 mL) solution was added with a syringe and the reaction mixture was stirred and heated at 70 °C overnight. Ultrafiltration against 1 L of distilled water followed by a second ultrafiltration through a 0.2 μm PES membrane filter yielded a purified microgel solution. The microgel solution was concentrated under vacuum and

freeze-dried (room temperature, 0.8 mbar) to give a yellow, amorphous solid. The yields of this procedure were typically in the range of 45-65% (of monomer mass used). ^{1}H NMR (200 MHz, D_2O): δ 1.09 (bs, CH_3), 1.54 (bt, CH_2), 1.97 (bm, CH), 3.05 (bd, J_{HJ}=9.4 Hz, CH_2) ,3.55 (bd, J_{HJ}=17.8 Hz, CH_3) 3.84 (bs, CH), 7.03-7.18 (bm, aromatic). IR (KBr, cm^{-1}): ν 3300, 1650, 1500, 1400, 1225, 1200, 1050, 890, 790.

8.3.1.3 **MG-SMA**

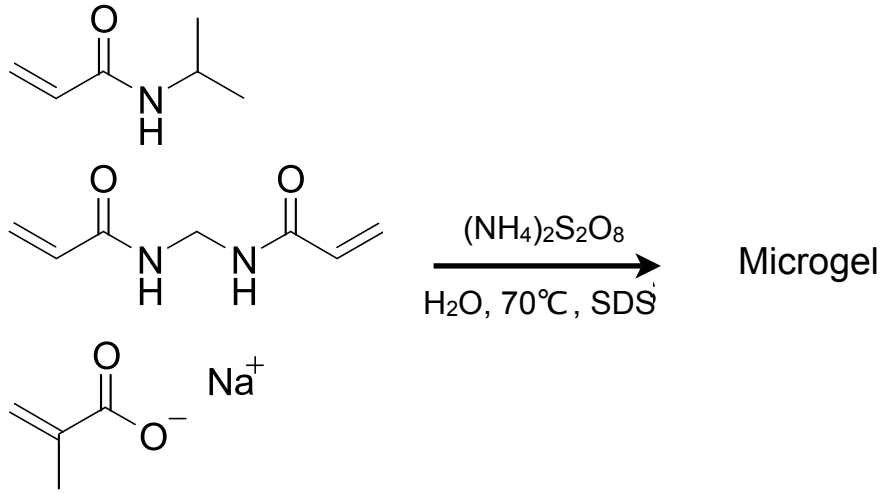

Sodium methacrylate (86.5 mg, 0.8 mmol), NIPAM (1.13 g, 10 mmol), *N,N'*-methylene bisacrylamide (155 mg, 10.0 mmol) and SDS (60 mg, 0.2 mmol) were dissolved in water (200 ml) in a three necked round bottomed flask. The solution was heated to 70 ^{o}C and degassed by bubbling nitrogen through for 30 minutes. Ammonium persulphate (60 mg, 0.5 mmol) in aqueous solution (1 mL) was added and the reaction mixture was stirred and heated at 70 ^{o}C overnight. Ultrafiltration against 1 L of distilled water followed by ultrafiltration through a 0.2 μm PES membrane filter produced a purified microgel solution. Concentration under vacuum and freeze-dried (R.T, 0.8 mbar) gave an off-white powder. The yields of this procedure were typically in the range of 25-45% (of monomer mass used). ^{1}H NMR (200 MHz, D_2O): δ 1.14 (bs, CH_3), 1.58 (bt, CH_2), 2.01 (bm, CH), 3.89 (bs, CH) IR (KBr, cm^{-1}): ν 3300, 1650, 1500, 1400, 1225, 1200, 1050.

8.3.1.4 Disulfide-containing microgels

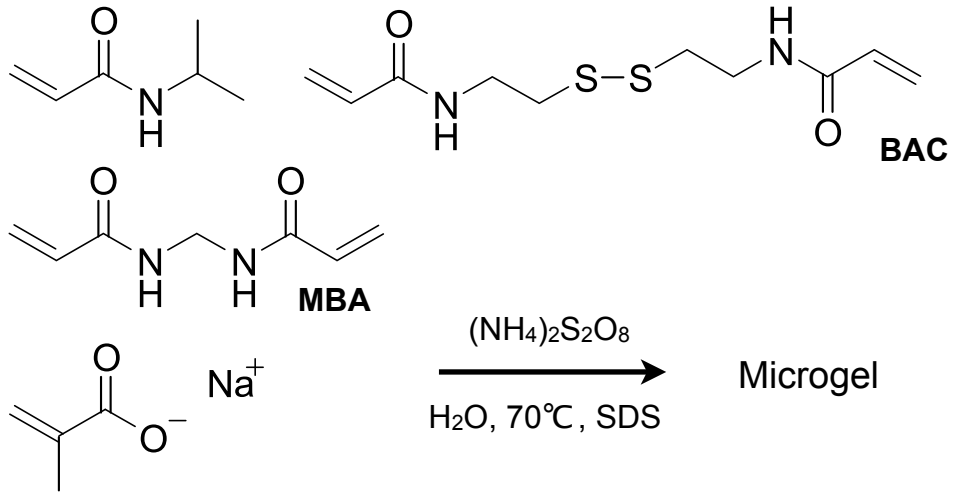

Disulfide microgels were synthesised according to the following general procedure. Sodium 5-(methacrylamido)tetrazolate (0.14 g, 0.8 mmol), NIPAM (1.13 g, 10 mmol), *N,N'*-methylene bisacrylamide (46 mg, 3.0 mmol), bis(acryloyl) cystamine (182 mg, 7.0 mmol) and SDS (60 mg, 0.2 mmol) were dissolved in water (200 ml) in a three necked round bottomed flask. The weights were altered as detailed in Table 13 to produce microgels of varying compositions. The solution was heated to 70 ^{o}C and degassed by bubbling nitrogen through for 30 minutes. Ammonium persulphate (60 mg, 0.5 mmol) was added, in aqueous solution (1 mL), and the reaction mixture was stirred and heated at 70 ^{o}C overnight. Ultrafiltration against 1 L of distilled water followed by ultrafiltration through a 0.2 μm PES membrane filter provided the purified microgel solution. Concentration under vacuum and followed by freeze drying (R.T, 0.8 mbar) gave an off-white solid. The yields of this procedure were typically in the range of 25-45% (of monomer mass used). ^{1}H NMR (200 MHz, D_2O): δ 1.09 (bs, CH_3), 1.54 (bt, CH_2), 2.01 (bm, CH), 3.82 (bs, CH), 7.78 (bm, NH). IR (KBr, cm^{-1}): ν 3300, 1650, 1500, 1400, 1225, 1200, 1050.

Table 13 Different weights of crosslinkers used to make microgels with different % w/w disulfide composition.

Composition (BAC)	20%	30%	50%	70%	80%
Crosslinker	Mass of monomer added / mg				
MBA	124.0	92.7	77.0	46.2	30.8
BAC	52.6	103.7	130.1	182.6	208.1

8.3.2 Preparation of linear copolymers by RAFT

8.3.2.1 Linear copolymers for protein binding

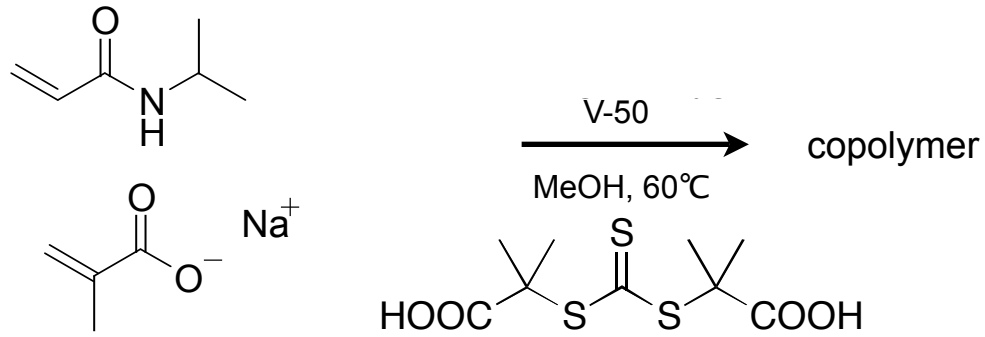

S1:

NIPAM (1.488 g, 13.1 mmol) and sodium methacrylate (0.142 g, 1.3 mmol) was dissolved in methanol (20 mL) in a polymerisation tube (Fig. 8.1). The mixture was degassed by bubbling nitrogen through for 30 mins. *S,S'*-Bis(α,α'-dimethyl-α"-acetic acid)-trithiocarbonate (74.4 mg, 0.26 mmol) and V−50 (23.8 mg, 0.08 mmol) were then added and the mixture was heated to 60 °C for 48 hours. The polymer was collected by evaporating the solvent. It was dissolved in THF and precipitated in pentane, then left to dry to give a pale yellow, odorous powder. ^{1}H NMR (200 MHz, D_2O): δ 1.02 (bs, CH_3), 1.14 (bs, 9H, CH_3), 1.47 (bt, CH_2), 1.96 (bm, CH), 3.84 (bs, CH), 7.53-7.88 (bm, NH) IR (KBr, cm^{-1}): ν 3300, 1650, 1500, 1400, 1225, 1200, 1050.

S1cH15:

NIPAM (1.488 g, 13.1 mmol), sodium methacrylate (0.142 g, 1.3 mmol) and *N*-cyclohexyl acrylamide (0.209 g, 1.3 mmol) was dissolved in methanol (20 mL) in a polymerisation tube (Fig. 8.1). The mixture was degassed by bubbling nitrogen through for 30 mins. *S,S'*-Bis(α,α'-dimethyl-α"-acetic acid)-trithiocarbonate (74.4 mg, 0.26 mmol) and V−50 (23.8 mg, 0.08 mmol) were then added and the mixture was heated to 60 °C for 48 hours. The polymer was collected by evaporating the solvent. It was dissolved in THF and precipitated in pentane, then left to dry to give a pale yellow, odorous powder. ^{1}H NMR (200 MHz, D_2O): δ 1.07 (bs, CH_3), 1.37 (bm, 9H, CH_3), 1.50

- 1.90 (bm, CH + CH_2), 3.80 (bs, CH) IR (KBr, cm^{-1}): ν 3300, 1650, 1500, 1400, 1225, 1200, 1050.

Figure 8.1 A polymerisation tube consisting of a thick-walled test-tube with a septum cap, was used in the preparation of the RAFT copolymers.

Combinatorial synthesis of RAFT copolymers (Table 14):

The following solutions (Table 13) were prepared in methanol (4 mL) in polymerisation tubes, the tubes were degassed by bubbling nitrogen through them for 15 minutes and suspended in a covered water bath at 60 °C.

Table 14 Composition of reaction mixtures for combinatorial synthesis of RAFT copolymers.

Polymer	NIPAAM / mg	Sodium methacrylate / mg	*N*-Cyclohexyl acrylamide / mg
S1cH10	372.3	35.3	52
S1cH15	370.9	32.7	78.9
S1cH20	370.8	35.5	103.5
S2cH10	371.4	71.4	52.3
S2cH15	372	70.8	78.1

Polymer	NIPAAM / mg	Sodium methacrylate / mg	*N*-Cyclohexyl acrylamide / mg
S2cH20	372.7	69.9	103.8
S3cH10	372.2	106.5	52.9
S3cH15	372.5	103.2	80.1
S3cH20	373.2	108.3	102.9
S4cH10	374.5	142.9	53.4
S4cH15	371	140.1	78.5
S4cH20	372.6	143.5	106
S5cH10	372.8	177.8	52.1
S5cH15	370.9	175.6	76.8
S5cH20	372.1	178.7	106.5

A solution of *S,S'*-Bis(α,α'-dimethyl-α"-acetic acid)-trithiocarbonate (372.4 mg, 1.3 mmol) and V−50 (119.4 mg, 0.4 mmol) was prepared in methanol and degassed by bubbling nitrogen through for 15 minutes. 1 mL of this solution was then injected into each polymerisation tube and the mixture was left to stir for 48 hours.
Each preparation was then processed by the same method to isolate the polymer as detailed for S1cH15. The yields were typically in the range of 65-80%.

8.3.2.2 DCLP

In a typical RAFT polymerisation, NIPAM (1.488 g, 13.1 mmol), sodium 5-(methacrylamido)tetrazolate (0.227 g, 1.3 mmol) and (*N*-boc)-*N*-acryloyl cystamine (0.398 g, 1.3 mmol) were dissolved in methanol (20 mL). The mixture was degassed by bubbling nitrogen through for 30 mins. *S,S'*-Bis(α,α'-dimethyl-α"acetic acid)-trithiocarbonate (74.4 mg, 0.26 mmol) was then added together with V−50 (23.79 mg, 0.08 mmol) and the mixture was heated to 60 °C for 48 hours, to ensure a high conversion. The polymer was collected by evaporating the solvent. It was dissolved in THF and precipitated in pentane, then left to dry to give a pale yellow, odorous powder.

2.3.2.3 Dynamic combinatorial libraries with polymers

Stock solutions of thiol, polymer (DCPL) and template (spermine) were prepared in phosphate buffer (10 mM, pH 8) with compositions according to Table 15. Libraries were prepared by pipetting aliquots of stock solution (Table 15) into HPLC vials. The resulting samples were made to volume with buffer.

Table 15 Weights and concentrations of stock solutions used in polymer libraries.

Compound	Weight / mg	Volume / mL	Concentration / mM^{-1}	Named
4-Mercapto benzoic acid	0.67	1.09	4.35	Carb.
Thiocynaminic acid	0.73	1.01	4.01	Thiocyn.
4-Thio nitrobenzene	0.73	1.18	4.71	Nitro.
Polymer	11.1	1.01	1.57	Polymer
Spermine HCl	1.13	1.56	2.08	Template

Table 16 Library compositions and solution volumes used to make DCLPs.

	Carb	Thiocyn	Nitro	Template	Polymer	Buffer
Library No.	uL of stock solution					
Markers						
1	250					750
2		250				750
3			250			750
4	125	125				750
5		125	125			750
6	125		125			750
Controls						
7	125	125		250		500
8		125	125	250		500
9	125		125	250		500

	Carb	Thiocyn	Nitro	Template	Polymer	Buffer
DCLs						
10	125	125		250	500	
11		125	125	250	500	
12	125		125	250	500	
Controls						
13	125	125			500	250
14		125	125		500	250
15	125		125		500	250

2.3.2.4 Spermine exchanged DCPL

DCLP (100 mg) and spermine (3 mg, 1.48×10^{-5} mol) was dissolved in a 10 mM phosphate buffer solution (22.5 mL, pH 8) in a polymerisation tube fitted with an airtight septum. Solutions of 2-mercaptobenzoic acid (4 mM) and 3-mercaptobenzoic acid (4 mM) were prepared in 10 mM phosphate buffer (Table 17) and 3.75 mL of each was injected to initiate the reaction. The final volume of the solution was 26.25 mL. This solution was stirred for 1 week to ensure an equilibrium point was reached.

Table 17 Thiol solutions prepared for the exchange process

Compound	Weight / mg	Volume / mL	Conc. / mM
2-Mercapto benzoic acid	6.2	10	4
3-Mercapto benzoic acid	6.3	10	4

The resulting solution was concentrated under vacuum and the polymer was extracted with THF (100 mL) and then precipitated into pentane. A further purification step was carried out using an ion exchange resin (Lewatit AF 5) to completely remove the template.

8.4 Characterisation and quantification of results

8.4.1 ^{1}H NMR binding studies

8.4.1.1 Tetrazolate-amidine complexes

NMR dilution experiments were carried out with complexes **3a–b**, which contained exactly equimolar amounts of amidinium and tetrazolate ions. Non-linear regression analysis [with Microsoft Excel 2003] was used to fit the concentration *C* of complexes **3a–b** and the experimental ^{1}H NMR chemical shifts δ of the tetrazole CH singlet in the unbound (δ_0) and the complexed form (δ_c) to the equation. The hyperbolic shape of the dilution curve was fitted to 1:1 host–guest complexation by non-linear regression analysis. [94, 95, 96] Standard deviations were derived using the macro Solvstat. [170]

8.4.1.2 Binding of protonated amines to microgels

Microgel (3 mg) was dissolved in 0.7 mL of D_2O containing a phosphate pD 7.4 buffer with a constant ionic strength (0.15 M). A stock solution of ligand was also prepared in D_2O at a concentration of 0.454 M in a phosphate pD 7.4 buffer of ionic strength 0.15 M. The stock solution of ligand was titrated into the microgel solution with a digital microliter syringe, and ^{1}H NMR spectra were recorded after each addition.

8.4.1.3 Job plot

A Job plot for the complex between sodium tetrazolate and acetamidinium tetrakis[3,5-bis(trifluoromethyl)phenyl]borate was carried out to determine the stoichiometry of the complex between tetrazole and acetamidine. A solution of sodium tetrazolate was prepared (0.44 g, 4.8 mmol) was dissolved in d_6-DMSO (10 mL). In a seperate flask acetamidinium tetrakis[3,5-bis(trifluoromethyl)phenyl]borate (4.43 g, 4.8 mmol) was dissolved in d_6-DMSO (10 mL). Samples for ^{1}H NMR were prepared by adding portions of the above solutions into NMR tubes. The two solutions were combined in NMR tubes in varying compositions (0.4:0.4 mL, 0.35:0.45 mL...) while the total volume was kept constant. The change in chemical shift of the amidine NH and amidine

CH_3 signal was determined for these compositions. The total concentration of acetamidinium + tetrazolate was kept to 0.48 M. The mole fraction x_{tet} which is defined as [**Tet**]/([**Tet**] + [**Ace**]), that of x_{ace} as [**Ace**]/([**Tet**] + [**Ace**]), was then plotted against the change in chemical shift.

8.4.2 Potentiometric titrations

Microgel (300 mg) was dissolved in 0.15 M KCl (30 mL) and concentrated HCl (1 mL) was added, the pH of the resulting solution was then adjusted to 2, to fully protonate all acidic groups. The solution was then titrated against sodium hydroxide (0.5 M) at 25 °C until pH 11. After correcting for he ionic strength the bound H^+ concentration was calculated using a theoretical Bjerrum function with non-linear least squares regression. [117]

8.4.3 UV-Vis titrations

A pH 7.0 phosphate buffer with an ionic strength of 0.15 mol L^{-1} (KCl) was prepared by dissolving NaH_2PO_4 (0.920 g, 7.67 mmol), Na_2HPO_4 (0.567 g, 3.99 mmol) and KCl (9.848 g, 0.132 mol) in 1 L of de-ionised water.

A stock solution of ligand (protein) was prepared in pH 7.0 phosphate buffer. A sample solution of 20 mg of microgel in 0.5 mL of protein stock solution was prepared; this was the sample solution for the titration. A solution of microgel in buffer solution was also prepared (20 mg in 0.5 mL); this was the blank solution.

Table 18 A table of typical concentrations of protein stock solutions used in UV-Vis protein binding measurements

Protein	Concentration of stock solution / mol L^{-1}
haemoglobin	1.24×10^{-5}
cytochrome C	1.02×10^{-5}
ferritin	1.20×10^{-5}
albumin	1.26×10^{-5}

A reference cell was filled with 2.5 mL phosphate buffer in a quartz cuvette for comparison. The sample cuvette was filled with 2.5 mL of protein stock solution (Table 18). Equal aliquots of sample solution and blank solution were titrated into the sample cuvette and the blank cell, respectively, to maintain an equal concentration of microgel in each cuvette UV-Vis spectra were recorded after allowing the solution to equilibrate during 15 minutes of stirring using a small magnetic stirrer. Titrations were carried out at room temperature.

8.4.4 HPLC/LC-MS

HPLC was carried out on dynamic combinatorial polymer libraries prepared in Waters HPLC vials. HPLC was carried out on Agilent 1100 LC systems:

Column:	Agilent Zorbax Eclipse C8, 150 mm × 4.6 mm, 3.5 μm		
Column oven:	40°C		
Flow rate:	1 mL/min		
Stop time (Post run):	16 min (5 min)		
Injection volume:	5.00 μL		
Mobile phase A:	0.1 % w/w formic acid, 0.1 mM HCl		
Mobile phase B:	Acetonitrile 0.1% w/w formic acid		
Gradient parameters:	Time (min)	% A	% B
	0.0	95	5
	10.0	5	95
	15	95	5
	16	95	5

Detection Wavelengths: 230 nm, 260 nm, 290 nm, 320 nm and 350 nm.

LC-MS was carried out on an Agilent 1100 LC with an Agilent XCT ion trap mass spectrometer. LC parameters were as above.

Mass range mode:	Ultra Scan
Ion polarity:	Negative
Ion source:	ESI
Dry temperature:	350 ºC
Nebuliser pressure:	39.97 psi
Dry gas flow:	7.97 L/min
HV capillary:	3500 V

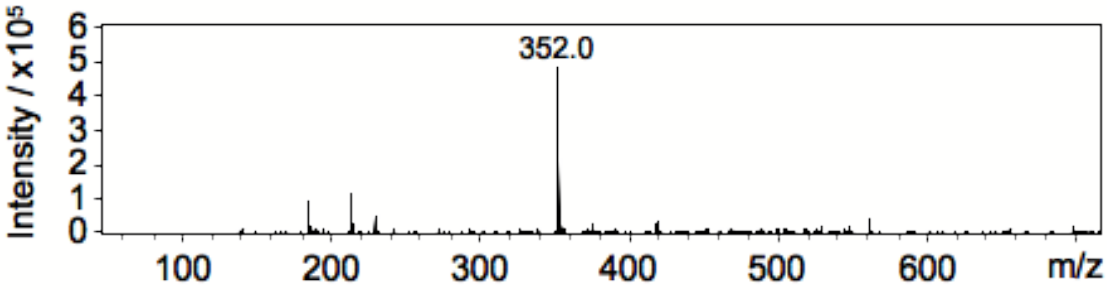

A M^+ ($C_{14}H_{28}N_2O_4S_2$), R.T 8.9-9.1 mins (M_w calculated 352.506) - spectral background

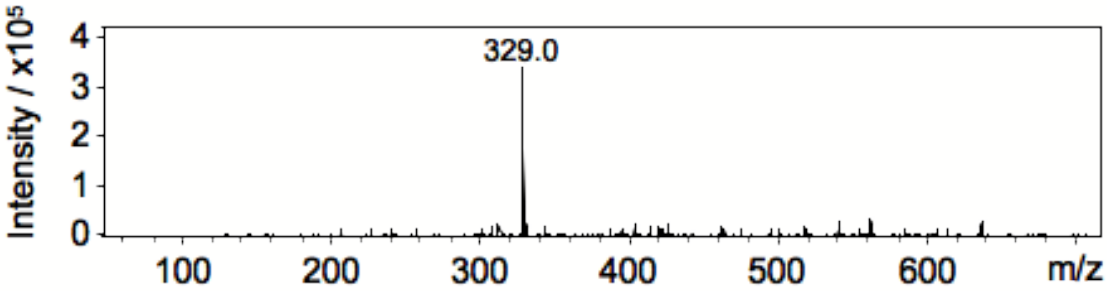

B M^+ ($C_{14}H_{19}NO_4S_2$), R.T 7.8-8.1 mins (M_w calculated 329.428) - spectral background

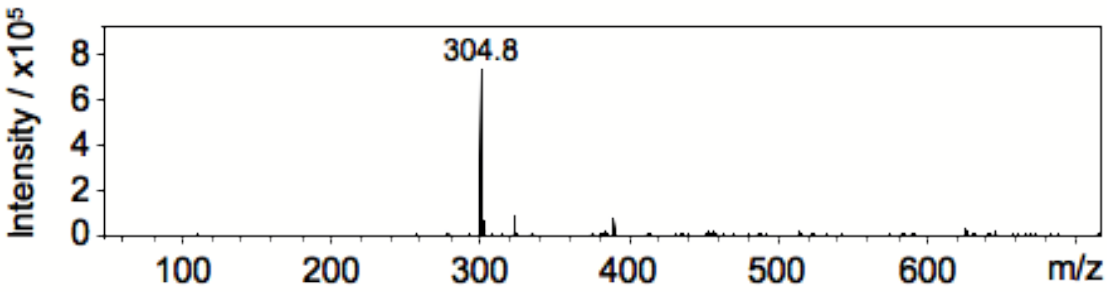

D $[HO_2C(C_6H_4)S_2(C_6H_4)CO_2]^-$ ($C_{14}H_9O_4S_2$), R.T 9.5-9.6 mins (M_w calculated 306.351) - spectral background

Figure 8.2 A sample of mass spectroscopy traces from LC-MS measurements at given retention times (R.T). A, B and D correspond to the structures shown in Fig 6.10.

8.4.5 ITC

In a typical ITC titration, 13.9 mg of polymer was dissolved in 10 mL of 10 mM TRIS buffer (pH 7.5) to give a 0.2 mM 'host' solution. Spermine tetrahydrochloride (7.0 mg) was dissolved in TRIS buffer (10 mL, 10 mM, pH 7.5) to give a 2 mM 'guest' solution.

The ITC titrations were carried out by titrating guest solution into the host solution and fitting the data using Origin 7.0 ITC software.

8.4.6 Reactivity ratios

A solution of NIPAAM (2.8 mg, 2.5×10^{-5} mol) in D_2O (1 mL) and a solution of bisphosphonate monomer (10.1 mg, $2.5x10^{-5}$ mol) in D_2O (1 mL) were prepared, tetrazole (1.8 mg, $2.5x10^{-5}$ Mol) as an internal standard was prepared. 0.35 mL of each solution was added to an NMR tube. The test tube was placed in the ^1H NMR spectrometer and heated to 75 °C. After the test tube had stabilised, 3 mg of $(NH_4)_2S_2O_8$ was added to initiate the reaction.

The reaction was followed by recording a ^1H NMR spectrum every 60 seconds, the resulting spectra were analysed using Mestre C and Excel. Reactivity ratios were calculated using an iterative macro developed by J. Dupré (Project student, 2003)

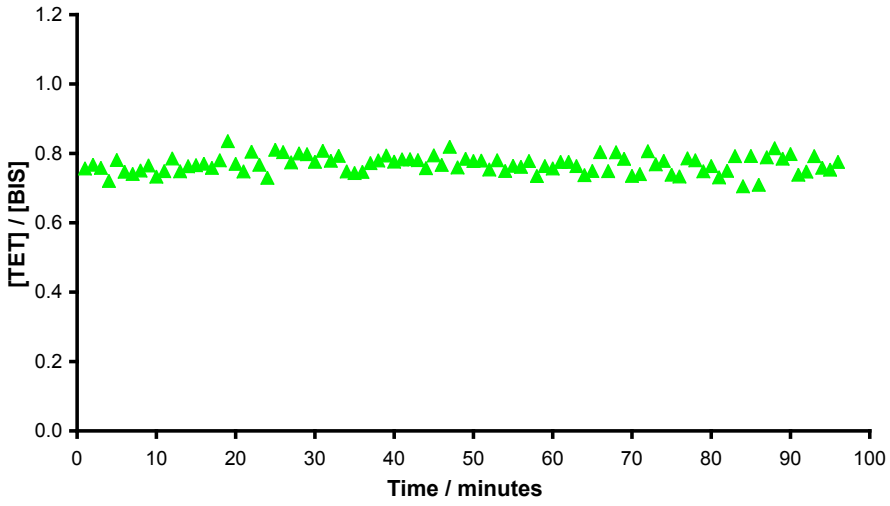

Figure 8.3. A plot of the NIPAAM-to-bisphosphonate monomer ratio first 100 minutes of the copolymerisation shows virtually no change in composition.

9 Appendix A: Crystallographic data

9.1 acetamidinium tetrazolate crystal structure

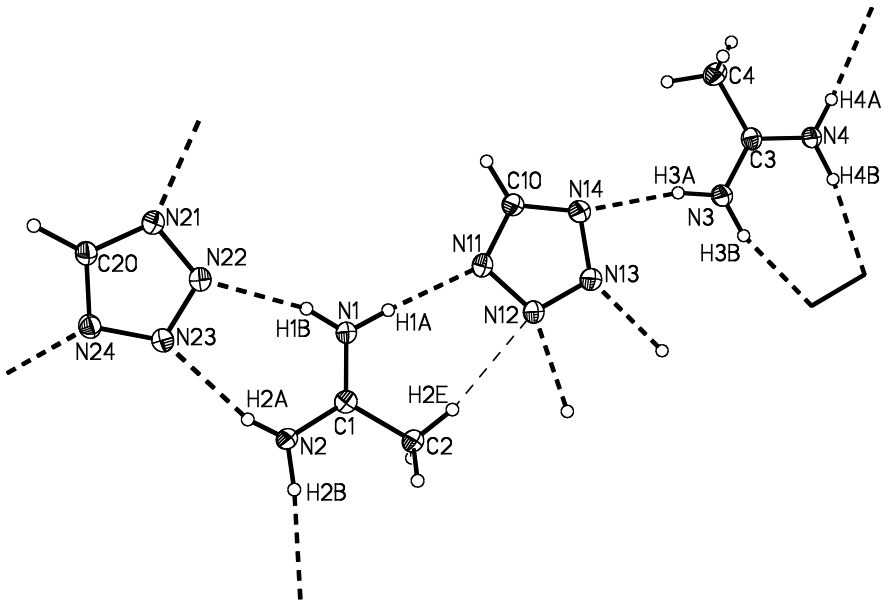

1:1 ratio amidine:tetrazole

Table 1. Crystal data and structure refinement for x80508.

Identification code	x80508	
Empirical formula	$C_3 H_8 N_6$	
Formula weight	128.15	
Temperature	100(2) K	
Wavelength	0.71073 Å	
Crystal system	Monoclinic	
Space group	C2/c	
Unit cell dimensions	a = 13.574(4) Å	a= 90°.
	b = 4.9473(13) Å	b= 96.297(3)°.
	c = 36.772(10) Å	g = 90°.
Volume	2454.4(11) $Å^3$	
Z	16	
Density (calculated)	1.387 Mg/m^3	
Absorption coefficient	0.102 mm^{-1}	
F(000)	1088	

Crystal size	0.18 x 0.15 x 0.12 mm^3
Theta range for data collection	1.11 to 28.02°.
Index ranges	-16<=h<=17, -6<=k<=6, -48<=l<=48
Reflections collected	17225
Independent reflections	2907 [R(int) = 0.0429]
Completeness to theta = 25.00°	96.9 %
Absorption correction	Semi-empirical from equivalents
Max. and min. transmission	0.988 and 0.873
Refinement method	Full-matrix least-squares on F^2
Data / restraints / parameters	2907 / 0 / 195
Goodness-of-fit on F^2	1.007
Final R indices [I>2sigma(I)]	R1 = 0.0540, wR2 = 0.1287
R indices (all data)	R1 = 0.0681, wR2 = 0.1333
Largest diff. peak and hole	0.247 and -0.260 e.$Å^{-3}$

Table 2. Bond lengths [Å] and angles [°] for x80508.

N(1)-C(1)	1.303(3)
N(1)-H(1A)	0.89(3)
N(1)-H(1B)	0.94(3)
C(1)-N(2)	1.308(3)
C(1)-C(2)	1.492(3)
N(2)-H(2A)	0.84(3)
N(2)-H(2B)	0.94(3)
C(2)-H(2C)	0.9800
C(2)-H(2D)	0.9800
C(2)-H(2E)	0.9800
N(3)-C(3)	1.304(3)
N(3)-H(3A)	0.92(3)
N(3)-H(3B)	0.91(3)
C(3)-N(4)	1.313(3)
C(3)-C(4)	1.486(3)
N(4)-H(4A)	0.91(3)
N(4)-H(4B)	0.95(3)
C(4)-H(4E)	0.9800
C(4)-H(4D)	0.9800
C(4)-H(4C)	0.9800

C(10)-N(11)	1.328(3)
C(10)-N(14)	1.331(3)
C(10)-H(10)	0.98(3)
N(11)-N(12)	1.347(3)
N(12)-N(13)	1.314(2)
N(13)-N(14)	1.340(3)
C(20)-N(21)	1.324(3)
C(20)-N(24)	1.333(3)
C(20)-H(20)	0.99(3)
N(21)-N(22)	1.349(3)
N(22)-N(23)	1.311(2)
N(23)-N(24)	1.342(3)
C(1)-N(1)-H(1A)	119.5(17)
C(1)-N(1)-H(1B)	118.5(16)
H(1A)-N(1)-H(1B)	121(2)
N(1)-C(1)-N(2)	122.1(2)
N(1)-C(1)-C(2)	119.58(19)
N(2)-C(1)-C(2)	118.27(19)
C(1)-N(2)-H(2A)	122.8(18)
C(1)-N(2)-H(2B)	116.3(16)
H(2A)-N(2)-H(2B)	121(2)
C(1)-C(2)-H(2C)	109.5
C(1)-C(2)-H(2D)	109.5
H(2C)-C(2)-H(2D)	109.5
C(1)-C(2)-H(2E)	109.5
H(2C)-C(2)-H(2E)	109.5
H(2D)-C(2)-H(2E)	109.5
C(3)-N(3)-H(3A)	117.8(17)
C(3)-N(3)-H(3B)	120.0(17)
H(3A)-N(3)-H(3B)	122(2)
N(3)-C(3)-N(4)	122.0(2)
N(3)-C(3)-C(4)	118.8(2)
N(4)-C(3)-C(4)	119.21(19)
C(3)-N(4)-H(4A)	120.8(17)
C(3)-N(4)-H(4B)	118.0(16)
H(4A)-N(4)-H(4B)	121(2)
C(3)-C(4)-H(4E)	109.5
C(3)-C(4)-H(4D)	109.5

H(4E)-C(4)-H(4D)	109.5
C(3)-C(4)-H(4C)	109.5
H(4E)-C(4)-H(4C)	109.5
H(4D)-C(4)-H(4C)	109.5
N(11)-C(10)-N(14)	112.6(2)
N(11)-C(10)-H(10)	122.5(15)
N(14)-C(10)-H(10)	124.9(15)
C(10)-N(11)-N(12)	104.21(18)
N(13)-N(12)-N(11)	109.26(17)
N(12)-N(13)-N(14)	109.83(18)
C(10)-N(14)-N(13)	104.08(17)
N(21)-C(20)-N(24)	112.5(2)
N(21)-C(20)-H(20)	127.3(14)
N(24)-C(20)-H(20)	120.1(14)
C(20)-N(21)-N(22)	104.30(17)
N(23)-N(22)-N(21)	109.32(17)
N(22)-N(23)-N(24)	109.65(17)
C(20)-N(24)-N(23)	104.19(17)

Symmetry transformations used to generate equivalent atoms:

Table 6. Hydrogen bonds for x80508 [Å and °].

D-H...A	d(D-H)	d(H...A)	d(D...A)	<(DHA)
N(1)-H(1A)...N(11)	0.89(3)	2.06(3)	2.948(3)	176(2)
N(1)-H(1A)...N(12)	0.89(3)	2.87(3)	3.674(3)	151(2)
N(1)-H(1B)...N(22)	0.94(3)	2.04(3)	2.955(3)	165(2)
N(1)-H(1B)...N(23)	0.94(3)	2.70(3)	3.450(3)	137(2)
N(2)-H(2A)...N(23)	0.84(3)	2.15(3)	2.955(3)	161(2)
N(2)-H(2A)...N(22)	0.84(3)	2.76(3)	3.394(3)	134(2)
N(2)-H(2B)...N(24)#1	0.94(3)	2.03(3)	2.963(3)	177(2)
N(3)-H(3A)...N(14)	0.92(3)	2.03(3)	2.930(3)	167(2)
N(3)-H(3A)...N(13)	0.92(3)	2.46(3)	3.174(3)	135(2)
N(3)-H(3B)...N(13)#2	0.91(3)	2.06(3)	2.939(3)	164(2)
N(3)-H(3B)...N(12)#2	0.91(3)	2.77(3)	3.483(3)	137(2)
N(4)-H(4A)...N(21)#3	0.91(3)	2.01(3)	2.919(3)	176(2)
N(4)-H(4A)...N(22)#3	0.91(3)	2.87(3)	3.690(3)	151(2)

N(4)-H(4B)...N(12)#2	0.95(3)	2.05(3)	2.985(3)	169(2)
N(4)-H(4B)...N(13)#2	0.95(3)	2.60(3)	3.380(3)	139(2)

Symmetry transformations used to generate equivalent atoms:

#1 -x,y-1,-z+1/2 #2 -x+1/2,-y+1/2,-z+1 #3 -x,-y+2,-z+1

9.2 Propranolol methacrylate

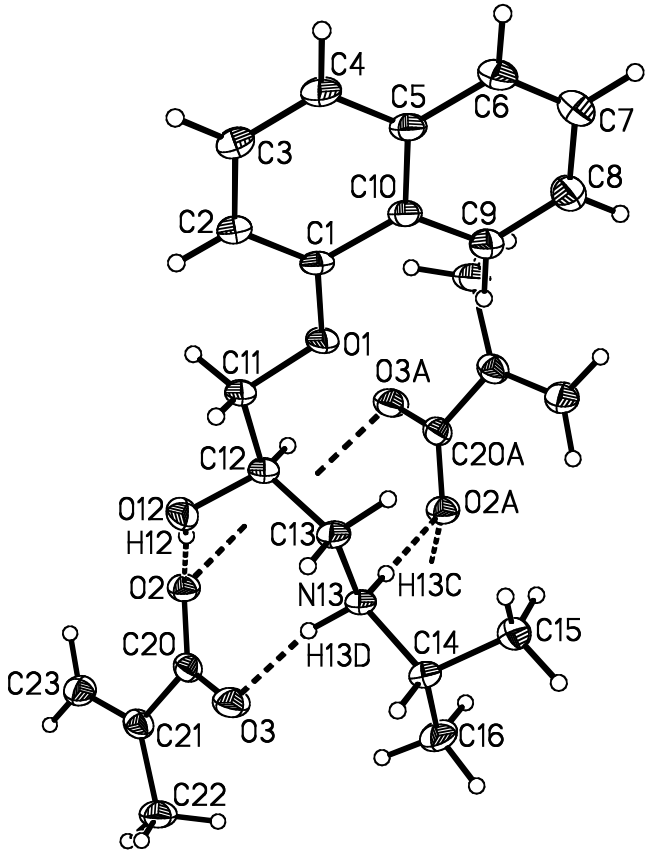

There is a nine-membered ring formed by hydrogen bonding interactions between the vinyl carboxylate and the hydrogen atoms on the quaternary nitrogen . The hydrogen bonding is extended as a chain through the other N bound H atom to O2 on a symmetry related vinyl carboxylate.

Molecule containing O2a O3a is a symmetry related to the molecule containing O2,O3.

Table 1. Crystal data and structure refinement for x80509.

Identification code	x80509
Empirical formula	$C_{20}\,H_{27}\,N\,O_4$
Formula weight	345.43
Temperature	100(2) K
Wavelength	0.71073 Å
Crystal system	Triclinic

Space group	P-1	
Unit cell dimensions	a = 8.0034(10) Å	a= 105.683(7)°.
	b = 9.0338(11) Å	b= 93.245(7)°.
	c = 14.1824(17) Å	g = 98.781(7)°.
Volume	970.5(2) $Å^3$	
Z	2	
Density (calculated)	1.182 Mg/m^3	
Absorption coefficient	0.082 mm^{-1}	
F(000)	372	
Crystal size	0.40 x 0.36 x 0.18 mm^3	
Theta range for data collection	2.38 to 33.09°.	
Index ranges	-12<=h<=8, -13<=k<=13, -21<=l<=21	
Reflections collected	20796	
Independent reflections	7155 [R(int) = 0.0414]	
Completeness to theta = 25.00°	99.1 %	
Absorption correction	None	
Refinement method	Full-matrix least-squares on F^2	
Data / restraints / parameters	7155 / 0 / 239	
Goodness-of-fit on F^2	1.176	
Final R indices [I>2sigma(I)]	R1 = 0.0649, wR2 = 0.1839	
R indices (all data)	R1 = 0.0828, wR2 = 0.2029	
Largest diff. peak and hole	0.786 and -0.394 $e.Å^{-3}$	

Table 2. Bond lengths [Å] and angles [°] for x80509.

C(1)-O(1)	1.3719(12)
C(1)-C(2)	1.3731(14)
C(1)-C(10)	1.4319(13)
O(1)-C(11)	1.4265(11)
C(2)-C(3)	1.4156(14)
C(2)-H(2)	0.9500
C(3)-C(4)	1.3673(15)
C(3)-H(3)	0.9500

C(4)-C(5)	1.4181(16)
C(4)-H(4)	0.9500
C(5)-C(10)	1.4210(14)
C(5)-C(6)	1.4218(15)
C(6)-C(7)	1.3679(17)
C(6)-H(6)	0.9500
C(7)-C(8)	1.4071(17)
C(7)-H(7)	0.9500
C(8)-C(9)	1.3724(14)
C(8)-H(8)	0.9500
C(9)-C(10)	1.4145(15)
C(9)-H(9)	0.9500
C(11)-C(12)	1.5156(14)
C(11)-H(11A)	0.9900
C(11)-H(11B)	0.9900
C(12)-O(12)	1.4137(12)
C(12)-C(13)	1.5270(14)
C(12)-H(12A)	1.0000
O(12)-H(12)	0.89(2)
C(13)-N(13)	1.4903(13)
C(13)-H(13A)	0.9900
C(13)-H(13B)	0.9900
N(13)-C(14)	1.5149(13)
N(13)-H(13C)	0.906(15)
N(13)-H(13D)	0.985(13)
C(14)-C(15)	1.5168(14)
C(14)-C(16)	1.5222(16)
C(14)-H(14)	1.0000
C(15)-H(15A)	0.9800
C(15)-H(15B)	0.9800
C(15)-H(15C)	0.9800
C(16)-H(16A)	0.9800
C(16)-H(16B)	0.9800
C(16)-H(16C)	0.9800
O(2)-C(20)	1.2801(12)
O(3)-C(20)	1.2502(13)
C(20)-C(21)	1.5084(15)
C(21)-C(23)	1.3585(15)

C(21)-C(22)	1.4785(15)
C(22)-H(22A)	0.9800
C(22)-H(22B)	0.9800
C(22)-H(22C)	0.9800
C(23)-H(23A)	0.9500
C(23)-H(23B)	0.9500

O(1)-C(1)-C(2)	124.38(9)
O(1)-C(1)-C(10)	114.46(8)
C(2)-C(1)-C(10)	121.14(9)
C(1)-O(1)-C(11)	116.97(8)
C(1)-C(2)-C(3)	119.57(9)
C(1)-C(2)-H(2)	120.2
C(3)-C(2)-H(2)	120.2
C(4)-C(3)-C(2)	121.06(10)
C(4)-C(3)-H(3)	119.5
C(2)-C(3)-H(3)	119.5
C(3)-C(4)-C(5)	120.40(9)
C(3)-C(4)-H(4)	119.8
C(5)-C(4)-H(4)	119.8
C(4)-C(5)-C(10)	119.59(9)
C(4)-C(5)-C(6)	122.19(9)
C(10)-C(5)-C(6)	118.20(10)
C(7)-C(6)-C(5)	121.31(10)
C(7)-C(6)-H(6)	119.3
C(5)-C(6)-H(6)	119.3
C(6)-C(7)-C(8)	120.03(10)
C(6)-C(7)-H(7)	120.0
C(8)-C(7)-H(7)	120.0
C(9)-C(8)-C(7)	120.47(10)
C(9)-C(8)-H(8)	119.8
C(7)-C(8)-H(8)	119.8
C(8)-C(9)-C(10)	120.57(10)
C(8)-C(9)-H(9)	119.7
C(10)-C(9)-H(9)	119.7
C(9)-C(10)-C(5)	119.41(9)
C(9)-C(10)-C(1)	122.34(9)
C(5)-C(10)-C(1)	118.23(9)

O(1)-C(11)-C(12)	108.02(8)
O(1)-C(11)-H(11A)	110.1
C(12)-C(11)-H(11A)	110.1
O(1)-C(11)-H(11B)	110.1
C(12)-C(11)-H(11B)	110.1
H(11A)-C(11)-H(11B)	108.4
O(12)-C(12)-C(11)	105.62(8)
O(12)-C(12)-C(13)	112.05(8)
C(11)-C(12)-C(13)	110.87(8)
O(12)-C(12)-H(12A)	109.4
C(11)-C(12)-H(12A)	109.4
C(13)-C(12)-H(12A)	109.4
C(12)-O(12)-H(12)	108.4(11)
N(13)-C(13)-C(12)	111.10(8)
N(13)-C(13)-H(13A)	109.4
C(12)-C(13)-H(13A)	109.4
N(13)-C(13)-H(13B)	109.4
C(12)-C(13)-H(13B)	109.4
H(13A)-C(13)-H(13B)	108.0
C(13)-N(13)-C(14)	115.36(8)
C(13)-N(13)-H(13C)	108.9(9)
C(14)-N(13)-H(13C)	107.8(9)
C(13)-N(13)-H(13D)	110.3(8)
C(14)-N(13)-H(13D)	109.3(8)
H(13C)-N(13)-H(13D)	104.5(11)
N(13)-C(14)-C(15)	110.61(8)
N(13)-C(14)-C(16)	108.06(9)
C(15)-C(14)-C(16)	111.50(9)
N(13)-C(14)-H(14)	108.9
C(15)-C(14)-H(14)	108.9
C(16)-C(14)-H(14)	108.9
C(14)-C(15)-H(15A)	109.5
C(14)-C(15)-H(15B)	109.5
H(15A)-C(15)-H(15B)	109.5
C(14)-C(15)-H(15C)	109.5
H(15A)-C(15)-H(15C)	109.5
H(15B)-C(15)-H(15C)	109.5
C(14)-C(16)-H(16A)	109.5

C(14)-C(16)-H(16B)	109.5
H(16A)-C(16)-H(16B)	109.5
C(14)-C(16)-H(16C)	109.5
H(16A)-C(16)-H(16C)	109.5
H(16B)-C(16)-H(16C)	109.5
O(3)-C(20)-O(2)	123.77(9)
O(3)-C(20)-C(21)	117.79(9)
O(2)-C(20)-C(21)	118.44(9)
C(23)-C(21)-C(22)	123.48(10)
C(23)-C(21)-C(20)	119.81(10)
C(22)-C(21)-C(20)	116.69(9)
C(21)-C(22)-H(22A)	109.5
C(21)-C(22)-H(22B)	109.5
H(22A)-C(22)-H(22B)	109.5
C(21)-C(22)-H(22C)	109.5
H(22A)-C(22)-H(22C)	109.5
H(22B)-C(22)-H(22C)	109.5
C(21)-C(23)-H(23A)	120.0
C(21)-C(23)-H(23B)	120.0
H(23A)-C(23)-H(23B)	120.0

Symmetry transformations used to generate equivalent atoms:

Table 3. Torsion angles [°] for x80509.

C(2)-C(1)-O(1)-C(11)	-4.10(15)
C(10)-C(1)-O(1)-C(11)	177.31(8)
O(1)-C(1)-C(2)-C(3)	-179.79(9)
C(10)-C(1)-C(2)-C(3)	-1.29(16)
C(1)-C(2)-C(3)-C(4)	0.15(17)
C(2)-C(3)-C(4)-C(5)	0.93(18)
C(3)-C(4)-C(5)-C(10)	-0.87(17)
C(3)-C(4)-C(5)-C(6)	177.40(11)
C(4)-C(5)-C(6)-C(7)	-177.93(11)
C(10)-C(5)-C(6)-C(7)	0.36(17)
C(5)-C(6)-C(7)-C(8)	-0.01(18)
C(6)-C(7)-C(8)-C(9)	-0.73(18)
C(7)-C(8)-C(9)-C(10)	1.09(17)

C(8)-C(9)-C(10)-C(5)	-0.72(16)
C(8)-C(9)-C(10)-C(1)	177.78(9)
C(4)-C(5)-C(10)-C(9)	178.34(10)
C(6)-C(5)-C(10)-C(9)	0.00(15)
C(4)-C(5)-C(10)-C(1)	-0.23(15)
C(6)-C(5)-C(10)-C(1)	-178.57(9)
O(1)-C(1)-C(10)-C(9)	1.44(14)
C(2)-C(1)-C(10)-C(9)	-177.20(10)
O(1)-C(1)-C(10)-C(5)	179.95(9)
C(2)-C(1)-C(10)-C(5)	1.31(15)
C(1)-O(1)-C(11)-C(12)	-178.24(8)
O(1)-C(11)-C(12)-O(12)	-175.94(8)
O(1)-C(11)-C(12)-C(13)	62.47(11)
O(12)-C(12)-C(13)-N(13)	67.51(11)
C(11)-C(12)-C(13)-N(13)	-174.75(8)
C(12)-C(13)-N(13)-C(14)	-175.44(8)
C(13)-N(13)-C(14)-C(15)	-60.73(11)
C(13)-N(13)-C(14)-C(16)	176.97(9)
O(3)-C(20)-C(21)-C(23)	164.90(10)
O(2)-C(20)-C(21)-C(23)	-14.39(15)
O(3)-C(20)-C(21)-C(22)	-13.49(15)
O(2)-C(20)-C(21)-C(22)	167.23(10)

Symmetry transformations used to generate equivalent atoms:

Table 4. Hydrogen bonds for x80509 [Å and °].

D-H...A	d(D-H)	d(H...A)	d(D...A)	<(DHA)
N(13)-H(13D)...O(2)	0.985(13)	2.771(13)	3.5654(12)	138.1(10)
N(13)-H(13D)...O(3)	0.985(13)	1.794(14)	2.7597(12)	166.0(12)
N(13)-H(13C)...O(2)#1	0.906(15)	1.863(15)	2.7649(12)	173.0(13)
O(12)-H(12)...O(2)	0.89(2)	1.79(2)	2.6690(12)	172.5(17)
O(12)-H(12)...O(3)	0.89(2)	2.695(19)	3.2431(13)	121.2(14)

Symmetry transformations used to generate equivalent atoms:
#1 -x+1,-y+1,-z+1

10 Appendix B: Supplementary data

Determination of association constants for 20 and 21

The association constant for **20** was determined by 1H NMR titration on a Bruker 400 MHz spectrometer according to the same procedure set out in 8.4.1.1.

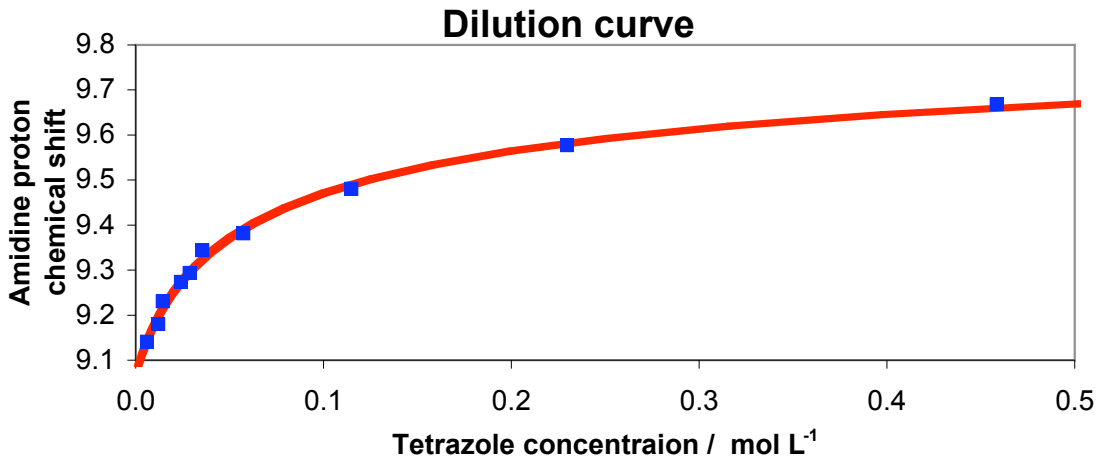

Figure B.1 A dilution curve showing the complexation induced chemical shift of 20. Experimental data (■) and the modeled response (▬)

Table B.1 Parameters used to calculate model parameters shown in Figure B.1. Errors were calculated from SOLVSTAT

Parameter	Result	Error
$\delta_{free\ amidine}$	9.068	± 0.021
$\delta_{complex}$	9.907	± 0.032
K_a	17.7	± 3.4

The determination of an association constant for **21** was complicated by the low solubility of the complex in DMSO, this was another strong indication of the higher association constant. Figure B.2 shows the dilution curve which is in excellent agreement with the 1 to 1 binding model and the corresponding literature values. [102, 103, 104]

1H NMR dilution experiments on **21** were carried out by measuring 40.0 mg of the 1:1 salt in deuterated DMSO (1 mL). Subsequent dilutions were then made using a micro-gas syringe and analysed on a Bruker 400 MHz spectrometer. Non-linear regression analysis [with Microsoft Excel 2003] was used to fit the concentration *C* of complexes

21 and the experimental ^{1}H NMR chemical shifts δ of the formate proton in the unbound (δ_0) and the complexed form (δ_c) to the equation. The dilution curve was fitted to 1:1 host–guest complexation by non-linear regression analysis. [94, 95, 96] Standard deviations were derived using the macro Solvstat. [170]

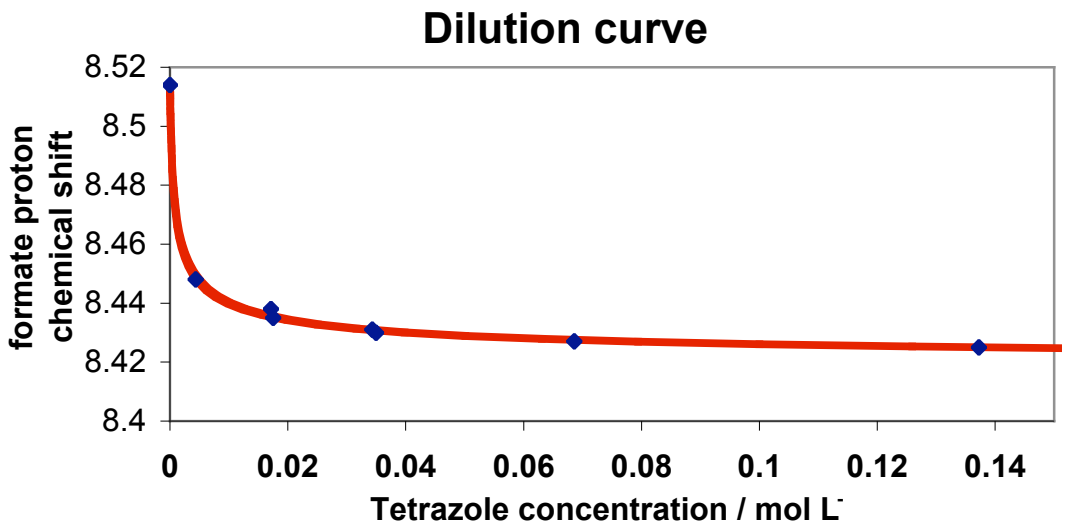

Figure B.2 A dilution curve for the ^{1}H NMR titration of 21. Experimental data (■) and the modeled response (—)

Table B.2 Parameters used to calculate model parameters shown in Figure B.2. Errors were calculated from SOLVSTAT

Parameter	Result	Error
$\delta_{free\ formate}$	8.515	± 0.005
$\delta_{complex}$	8.419	± 0.001
K_a	1639	± 100

3 Dimensional comparison of linear copolymers binding to cyt C

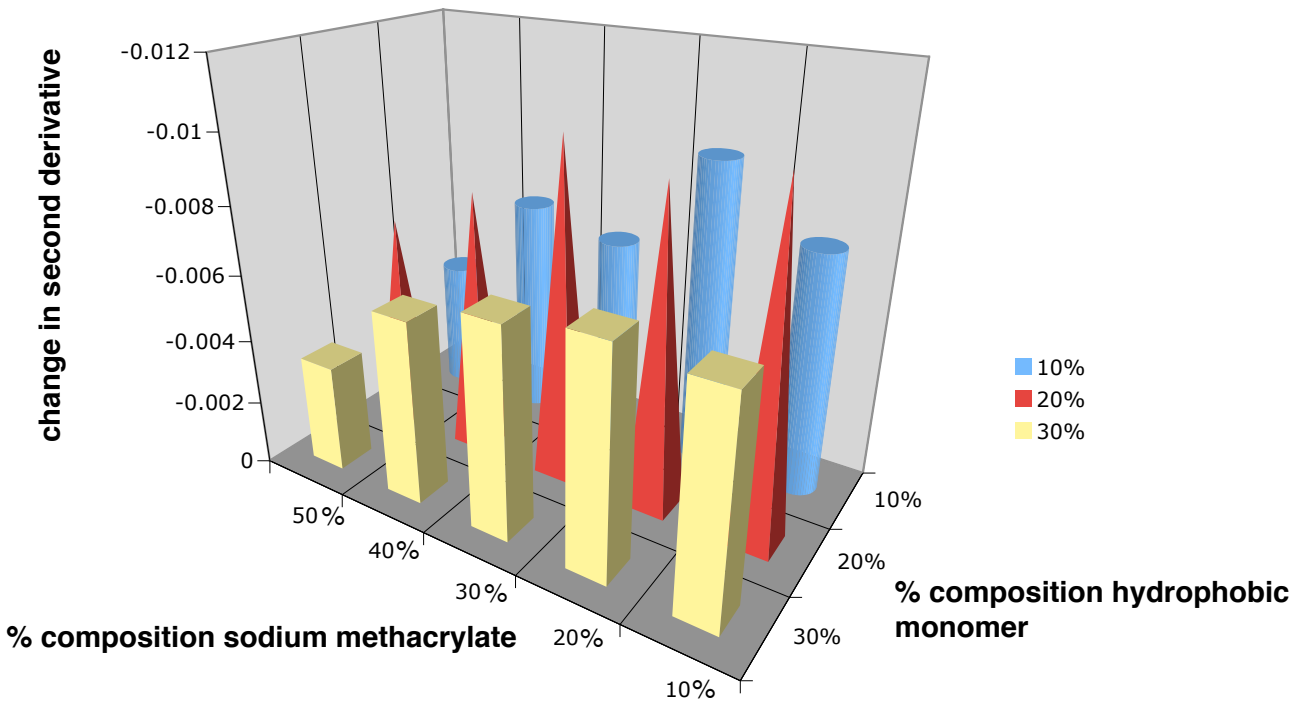

	10	20	30	40	50
10%	-0.007326697	-0.00925035	-0.006220059	-0.006780053	-0.004048108
20%	-0.010136964	-0.009395303	-0.010096625	-0.007955912	-0.00651496
30%	-0.006561549	-0.006790121	-0.006380921	-0.005616862	-0.0033139

Plotting all of the second derivative values for single point titrations allows a comparison (Table 10, Figures 5.11 & 5.12). The height of the peaks are representative of the relative strength of interaction. These values were calculated using the second derivative algorithm from the UV spectrum. These data points represent the second derivative at 415 nm in the cyt C spectrum with the addition of identical concentrations of linear copolymer.

Polymer ^{1}H NMR spectra

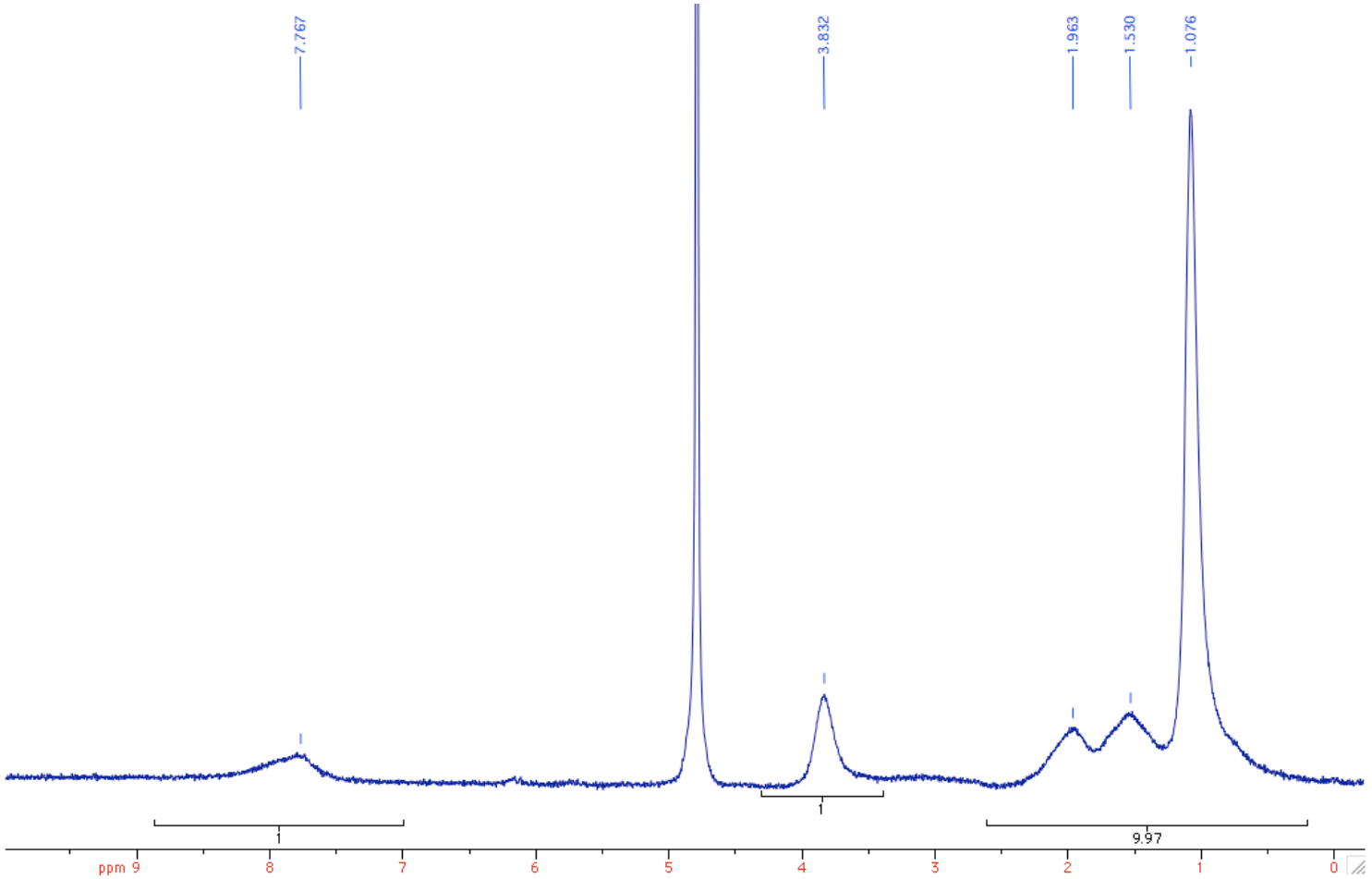

Figure B.3 MG TET ^{1}H NMR spectrum.

Polymer ^{1}H NMR spectra

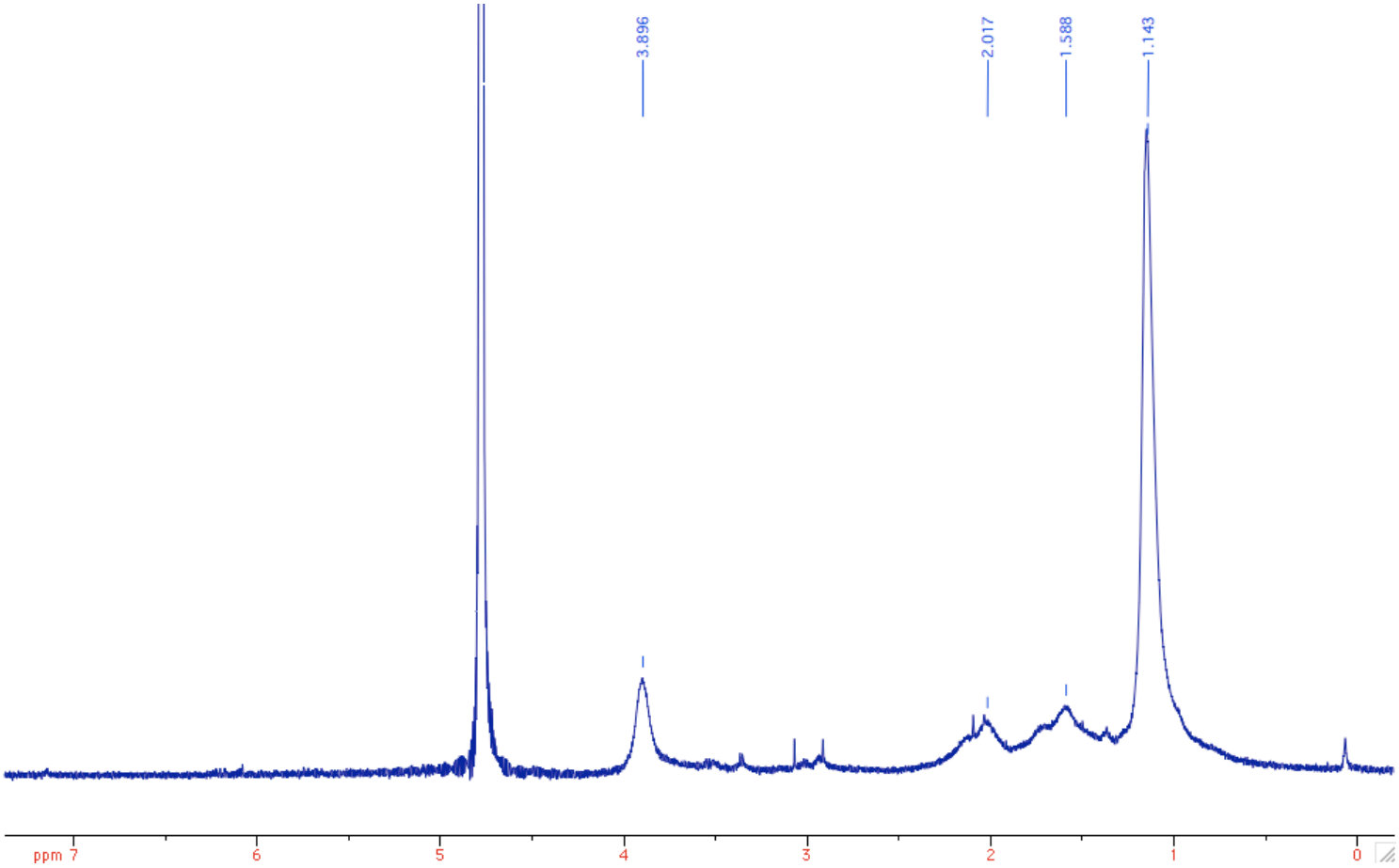

Figure B.4 MG SMA ^{1}H NMR spectrum.

Polymer ^{1}H NMR spectra

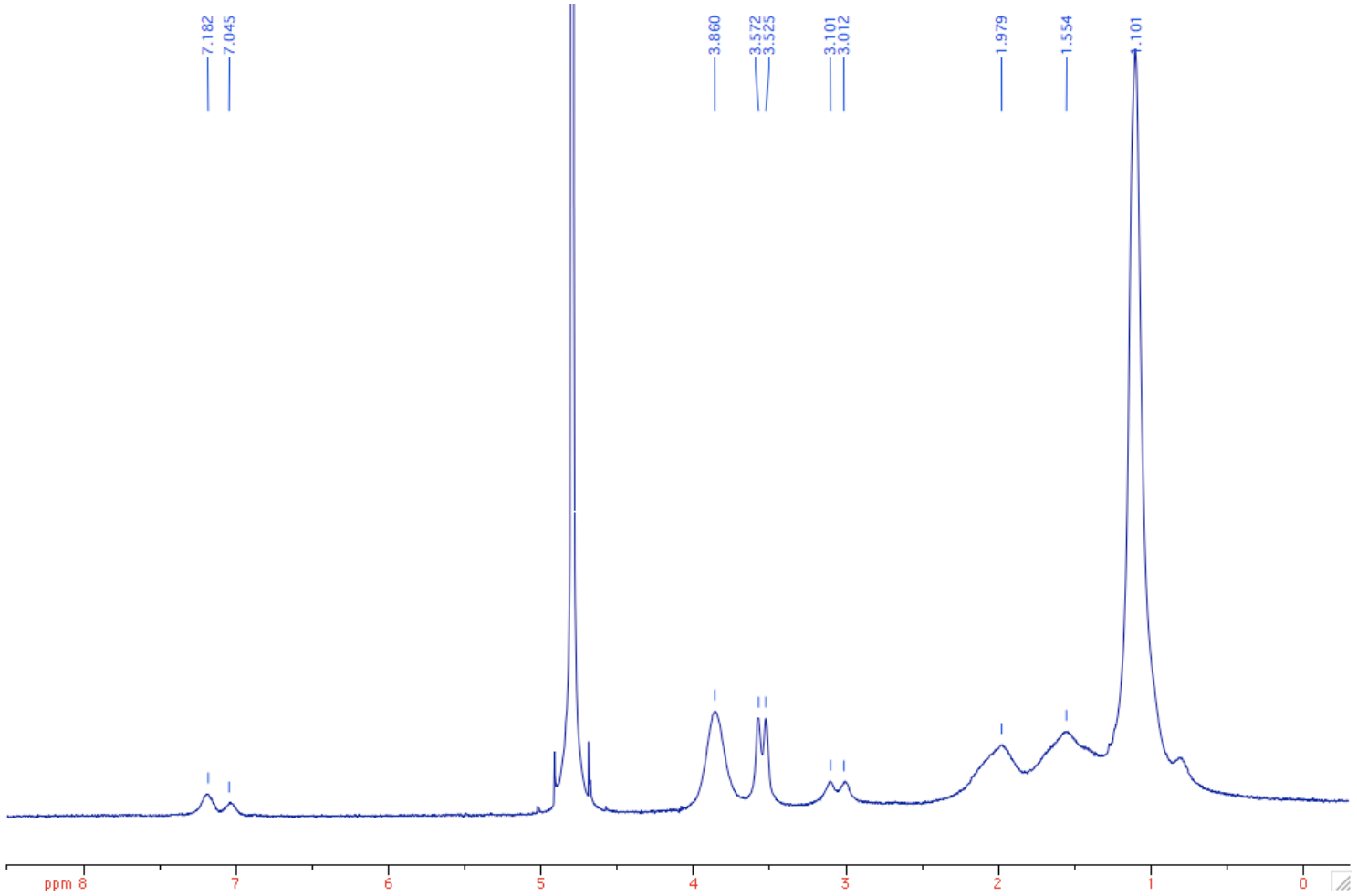

Figure B.5 MG BP ^{1}H NMR spectrum.

Polymer ^{1}H NMR spectra

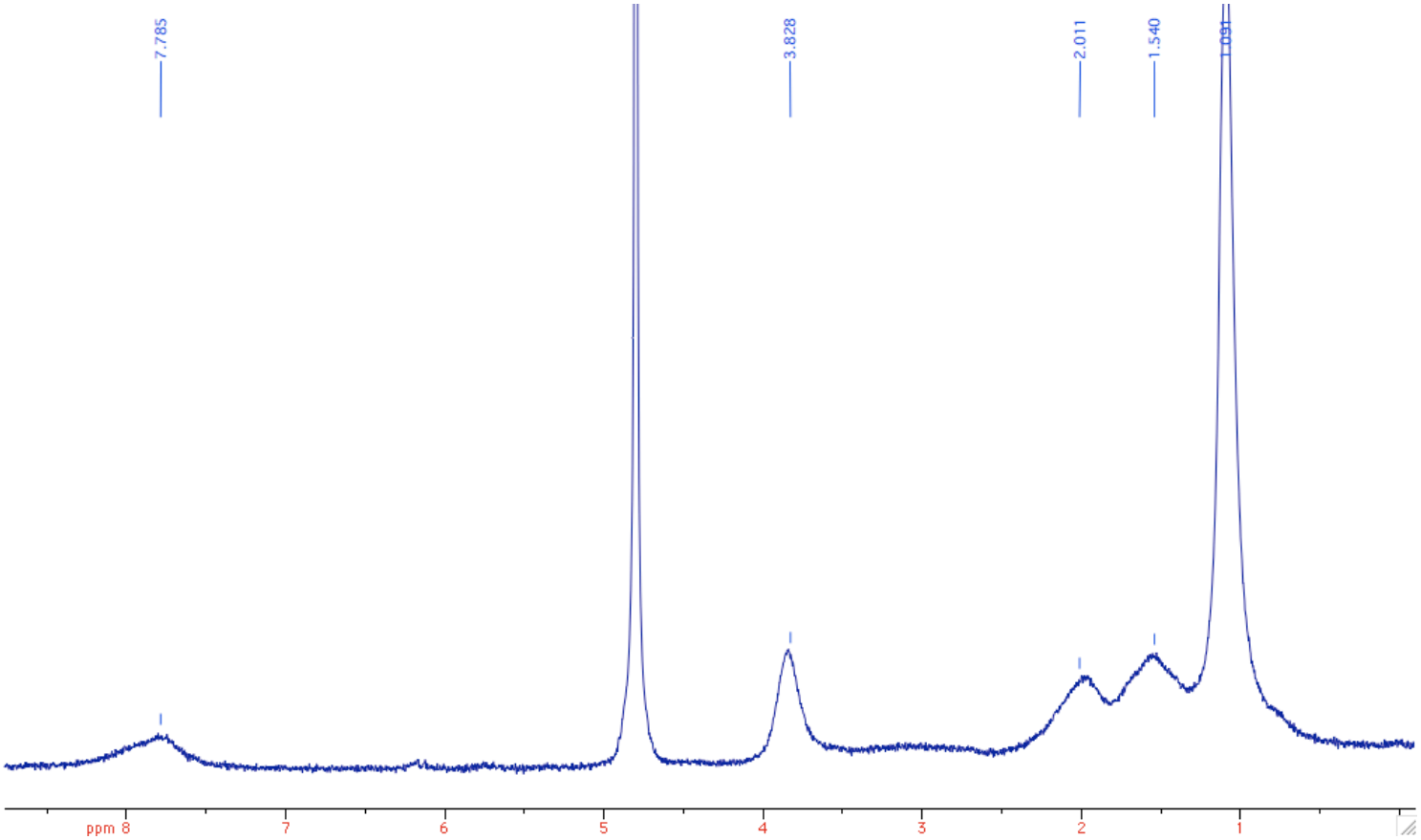

Figure B.6 ^{1}H NMR spectrum of a disulfide containing microgel. The chemical shifts show no noticable change from MG TET (Fig. B.3).

ITC data for titrating MG-SMA into a solution of Cytochrome C

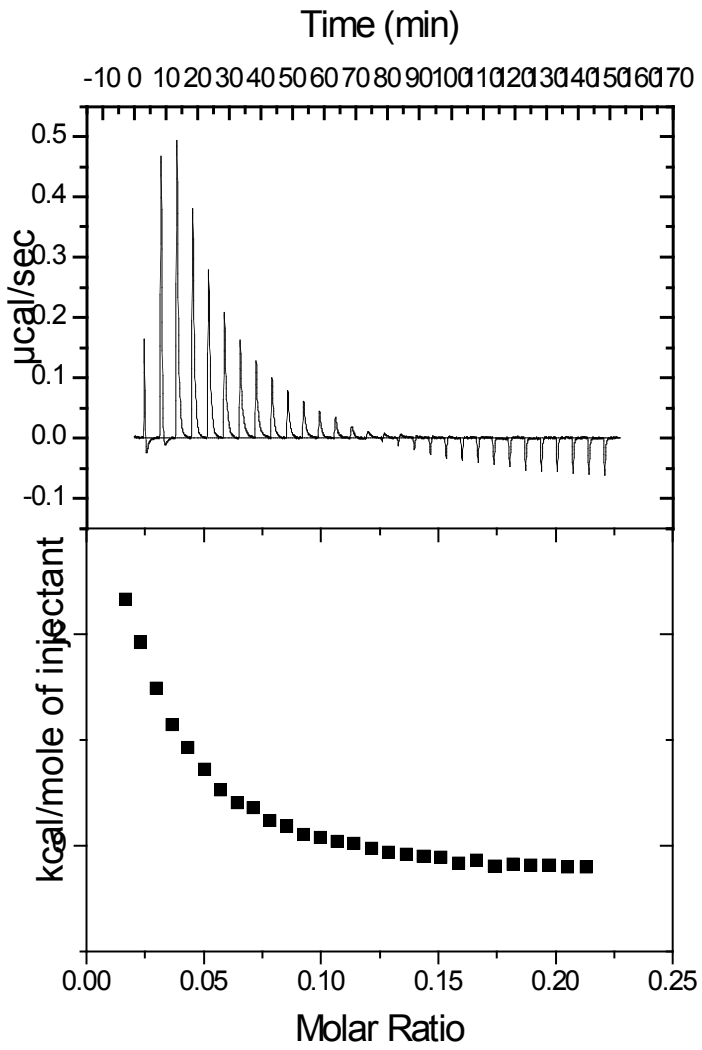

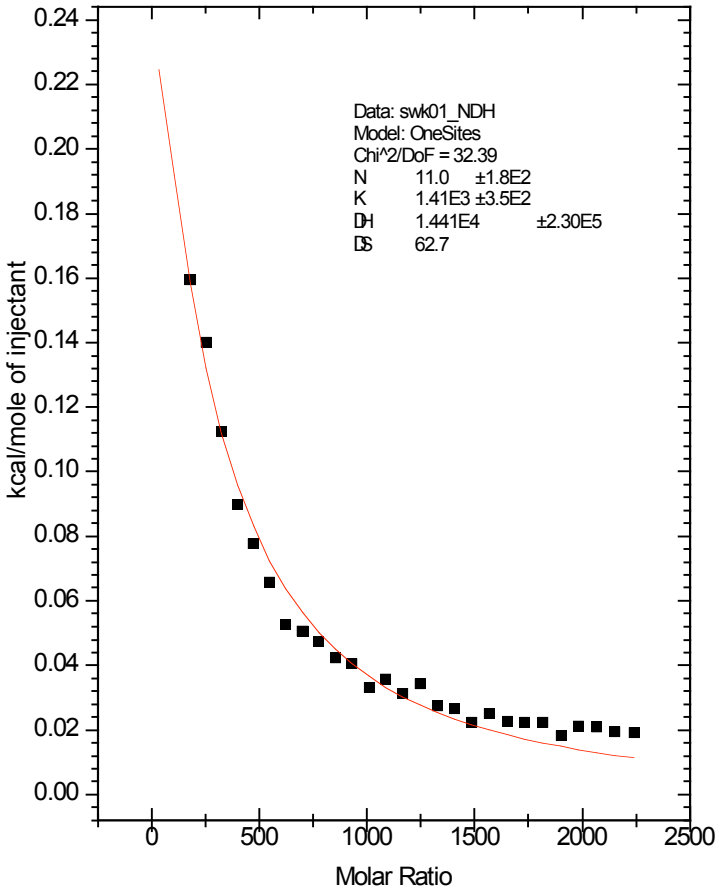

ITC data for titrating MG-TET into a solution of Cytochrome C

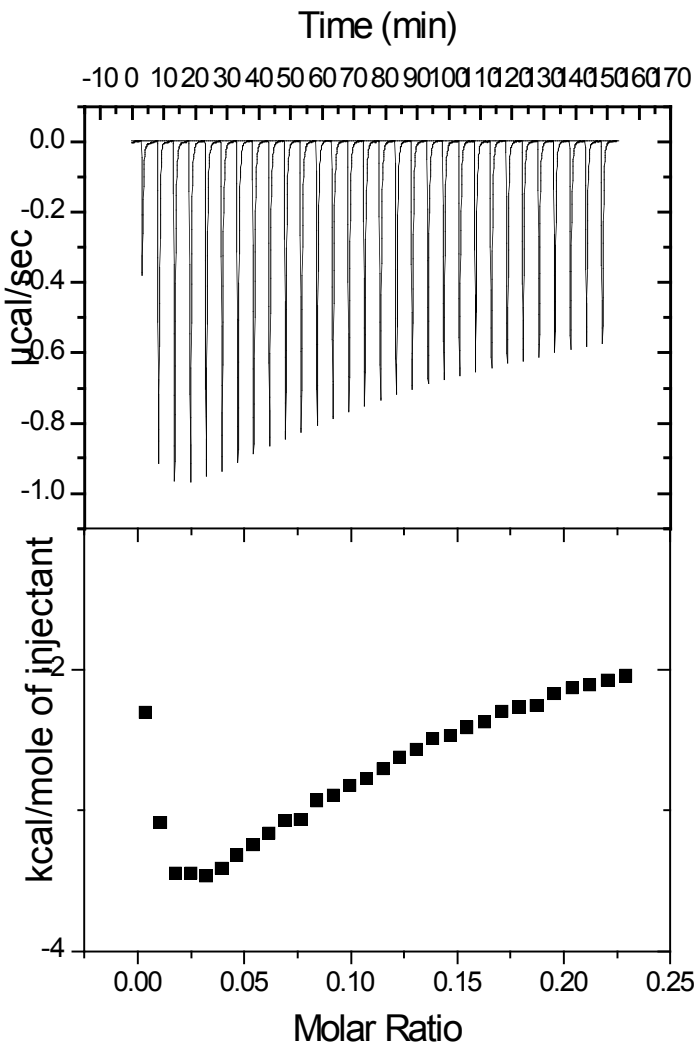

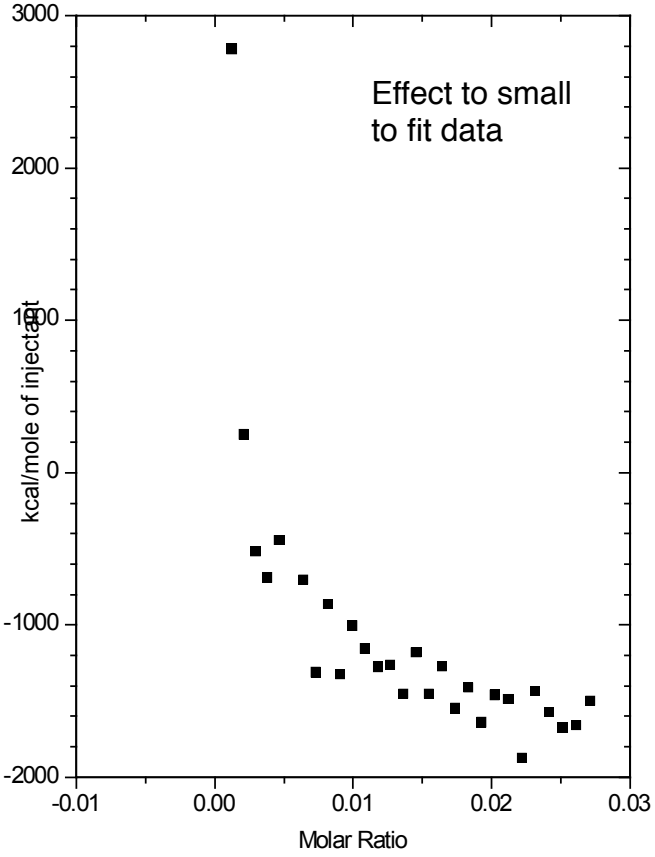

ITC data for titrating MG-TET into a solution of haemoglobin

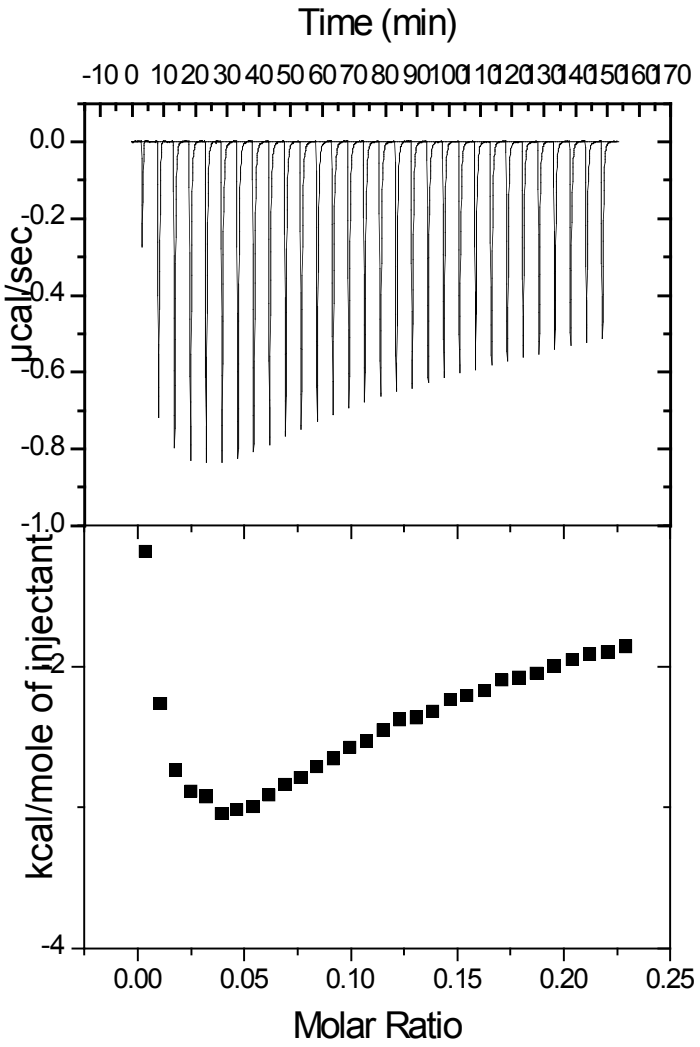

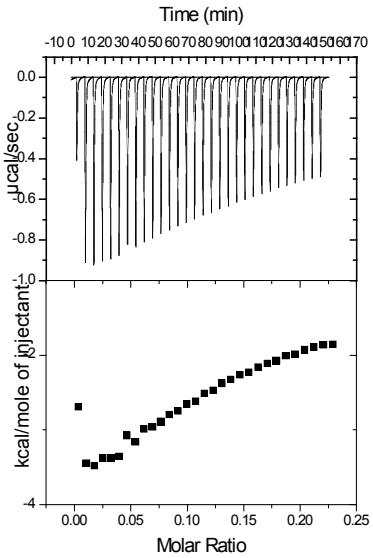

ITC titration of dilution

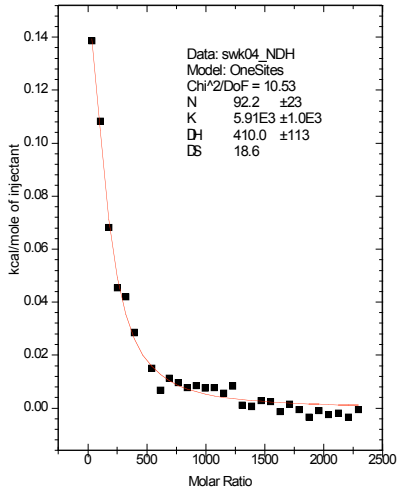

Data fitted after heat effect of dilution was subtracted

ITC data for titrating MG-TET into a solution of haemoglobin

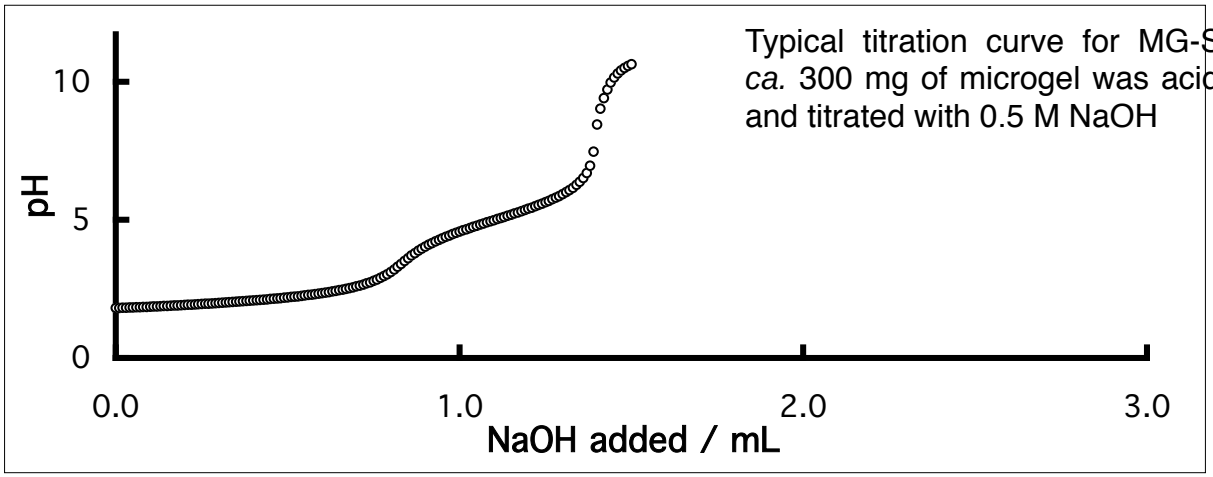

Typical titration curve for MG-SMA, *ca.* 300 mg of microgel was acidified and titrated with 0.5 M NaOH

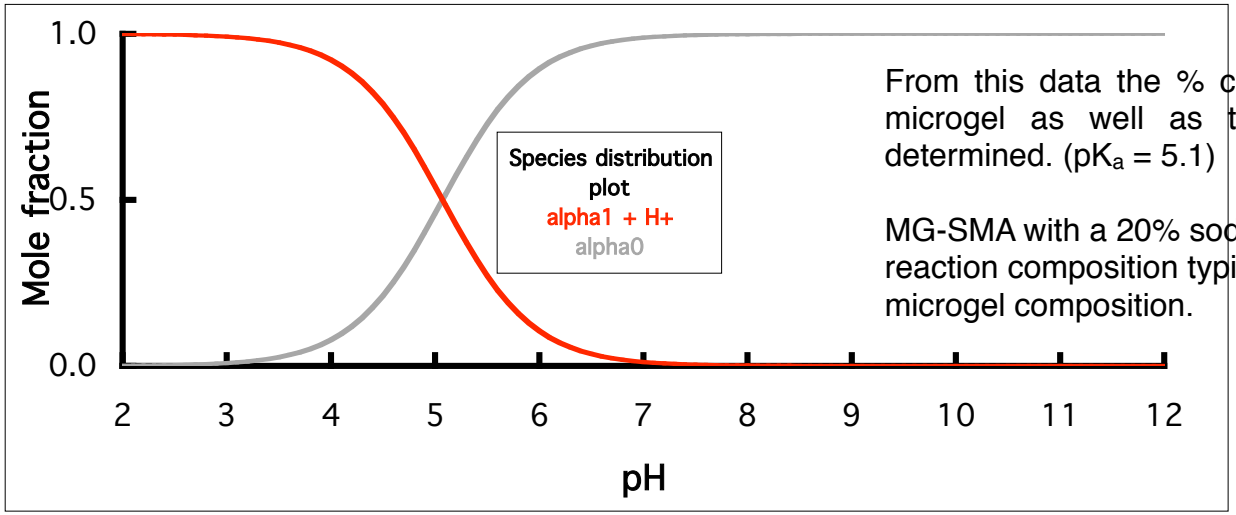

From this data the % compostion of the microgel as well as the pK_a can be determined. (pK_a = 5.1)

MG-SMA with a 20% sodium methacrylate reaction composition typically has 9% final microgel composition.

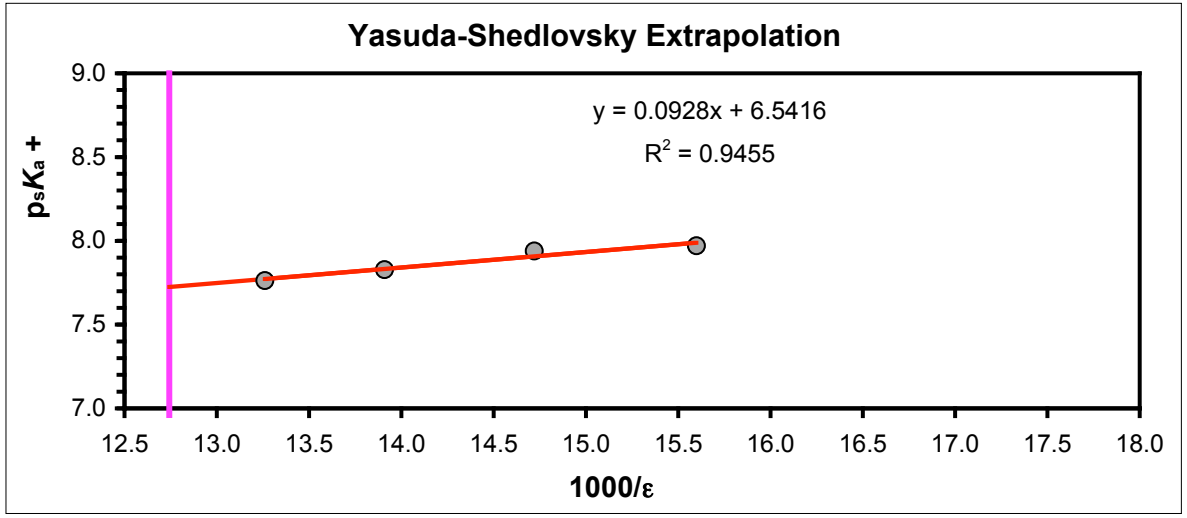

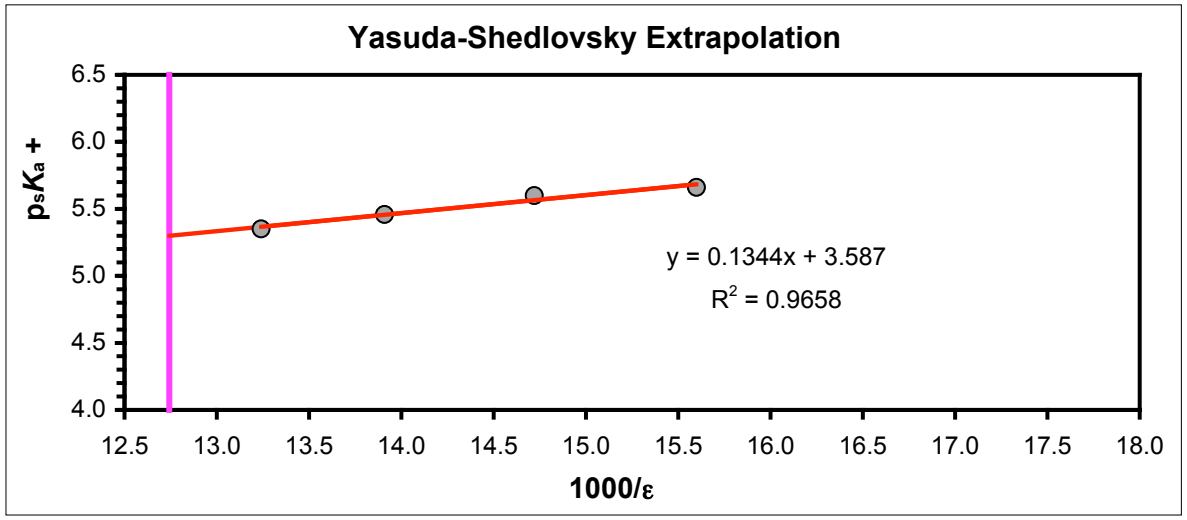

$pK_a1 = 5.3$

$pK_a2 = 7.7$

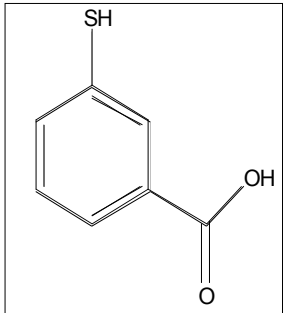

3-Mercapto-benzoic acid

$C_7H_6O_2S$

Mol. Wt.: 154.19

Yasuda-Shedlovsky extrapolation of the pK_a's of 3-mercapto-benzoic acid (pictured).

This method can be used to give the aqueous pK_a's of poorly soluble compounds. [i]

The compound is dissolved in varying solutions of water/methanol and titrated to determine the pK_a the Yasuda-shedlovsky plot allows the regression of this data using the dielectric constants for water-methanol mixtures.

i) Avdeef, A. *Quant. Struct. -Act. Relat.* **1992**, *11*, 510.

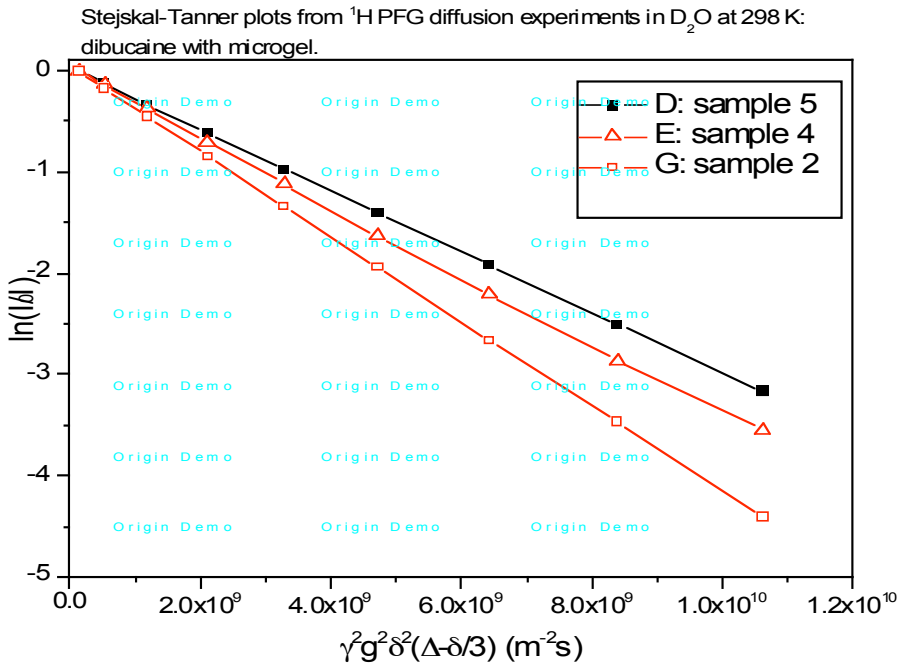

^{1}H PFG NMR diffusion measurements were used to determine the diffusion coefficient and thus the size of the microgel particles.

It was hoped that an association constant could be determined for low molecular weight compounds but the relatively high viscosity of the solution meant that we were not able to determine an association constant was.

The microgel's diffusion coefficient was determined to be 5.85 × 10^{-12} m^2s^{-1}

sample	2	3	4	5
D (10^{-10} m^2s^{-1})	4.53	3.75	3.50	3.11

Sample 1: 20 mg microgel in 0.7 mL D2O;
Sample 2: dibucaine•HCl in 0.7 mL D2O (45.4 mM);
Sample 3: 20 mg microgel in 0.7 mL D2O + 3.405 mmol dibucaine•HCl (final concentration equals 3.405 mM or 4.864 M?);
Sample 4: 20 mg microgel in 0.7 mL D2O + 13.62 mmol dibucaine•HCl;
Sample 5: 20 mg microgel in 0.7 mL D2O + 45.4 mmol dibucaine•HCl.

^{1}H NMR titration of acetamidinium methanoate. The data is fitted using linear least squares regression.

Titration	Mass Complex	[Complex]	$\delta_{obs\ (NH)}$	δ_{calc}	R2	Log C	$f\delta_{calc}/f\delta_h$	$f\delta_{calc}/f\delta_c$	$f\delta_{calc}/fK_a$
1	20	0.274435	9.727	9.7419095	0.000222	-0.56156	0.081661	0.918339	0.052238
2	10	0.137218	9.692	9.7148273	0.000521	-0.86259	0.113469	0.886531	0.042328
3	5	0.068609	9.62	9.6781685	0.003384	-1.16362	0.156524	0.843476	0.033153
4	2.5	0.034304	9.661	9.6294685	0.000994	-1.46465	0.213721	0.786279	0.019163
5	1.25	0.017152	9.6	9.566496	0.001123	-1.76568	0.287681	0.712319	-0.01029
A	2.55	0.03499	9.668	9.6310488	0.001365	-1.45605	0.211865	0.788135	0.019708
B	1.275	0.017495	9.609	9.5685074	0.00164	-1.75708	0.285319	0.714681	-0.00907
D	0.3125	0.004288	9.379	9.3960537	0.000291	-2.36774	0.487863	0.512137	-0.22502
E	0.1593	0.002186	9.261	9.2986936	0.001421	-2.66037	0.60221	0.39779	-0.53384

$$\delta = \delta_0 - \frac{\delta_0 - \delta_c}{2K_aC} \cdot \left[2K_aC + 1 - \sqrt{4K_aC + 1}\right]$$

		Error ±
$\delta_{free\ amidine}$ (δ_h)	8.960	0.396
$\delta_{complex}$ (δ_c)	9.811	0.052
logK_a	2.701	0.685
Ka	502	

Sum of R2 0.01096

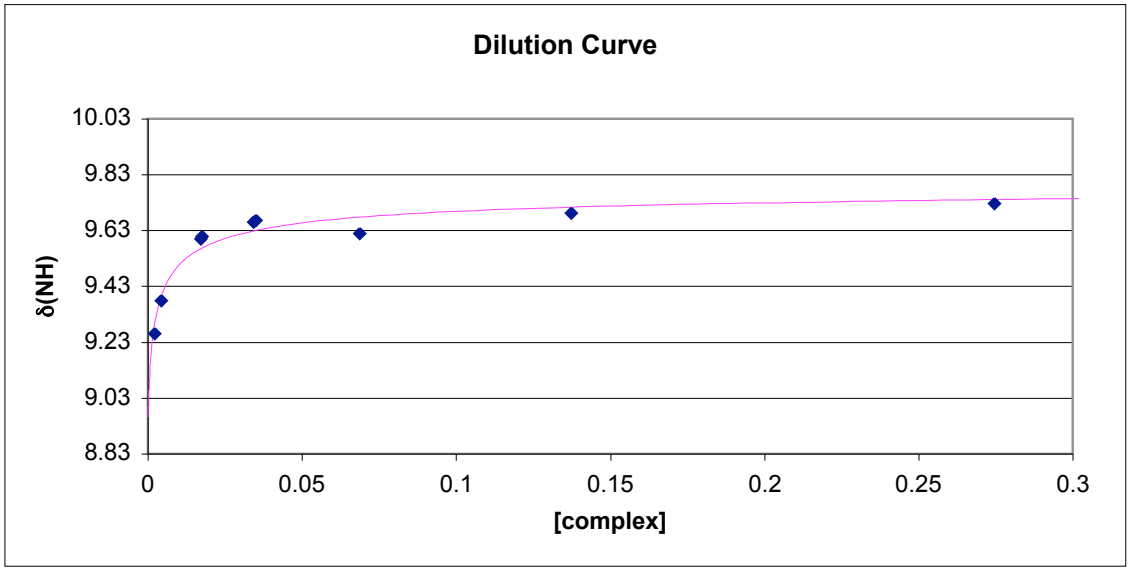

	Parameters from SOLVSTAT		
	$\delta_{free\ amidine}$ (δ_h)	$\delta_{complex}$ (δ_c)	logK_a
	8.96	9.811439	2.700532
std. dev.	0.396195	0.052432	0.685568
R^2/SE(y)	0.940216	0.04274	

UV-Vis titration of S1cH15 and cytochrome C. The data is fitted using linear least squares regression.

Ligand-substrate L-S binding

Wavelength, nm	**414**
Start volume V_0, mL	2.5
Protein	Cytochrome C
MW, g/mol	13500
Weight, g	0.0133
Volume, L	0.1
[Protein], mol/L	**9.852E-06**
Polymer	RAFT
MW, g/mol	7000
Weight, g	0.045
Volume, L	0.00102
[Polymer], mol/L	**6.303E-03**

K_a [L/mol]	1619	
K_d [mol/L]	6.176E-04	Error
log K_d	**-3.21**	± 0.04
d_{SL}	**-0.02087**	± 0.00072
Sum of Residuals Squared	**6.793E-07**	

		From Solvstat
Coefficients	-2.786628584	-0.016790532
Error	0.040381212	0.000721327
R2, SE(y)	0.99679034	9.07474E-05

	g	mol
NIPAM	1.488	0.01315
Na methacrylate	0.142	0.00131
Cyclohexylacrylam	0.199	0.00130
CTA	0.0744	0.00026

Ligand added, *v* [mL]	**[S_{tot}]**	**[L_{tot}]**	**d_{exp}**	**d_{calc}**	**Residuals squared**	**log [L_{tot}]**
0	9.852E-06	0.000E+00	**-0.00592**	-0.00592		
0.1	9.852E-06	2.424E-04	**-0.00962**	-0.01010	2.25991E-07	-3.615
0.2	9.852E-06	4.669E-04	**-0.01074**	-0.01232		-3.331
0.3	9.852E-06	6.753E-04	**-0.01411**	-0.01370	1.64995E-07	-3.171
0.4	9.852E-06	8.693E-04	**-0.01468**	-0.01464	1.77064E-09	-3.061
0.5	9.852E-06	1.050E-03	**-0.01527**	-0.01531	2.41044E-09	-2.979
0.6	9.852E-06	1.220E-03	**-0.01609**	-0.01583	6.89502E-08	-2.914
0.7	9.852E-06	1.379E-03	**-0.01638**	-0.01623	2.40059E-08	-2.861
0.8	9.852E-06	1.528E-03	**-0.01650**	-0.01655	2.60722E-09	-2.816
0.9	9.852E-06	1.668E-03	**-0.01639**	-0.01682	1.88532E-07	-2.778

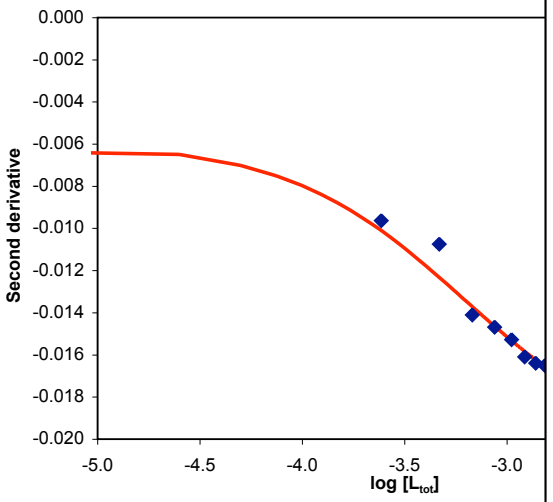

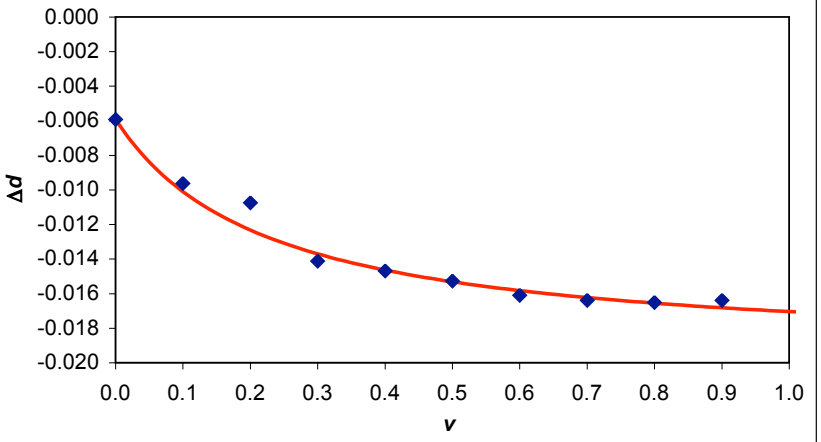

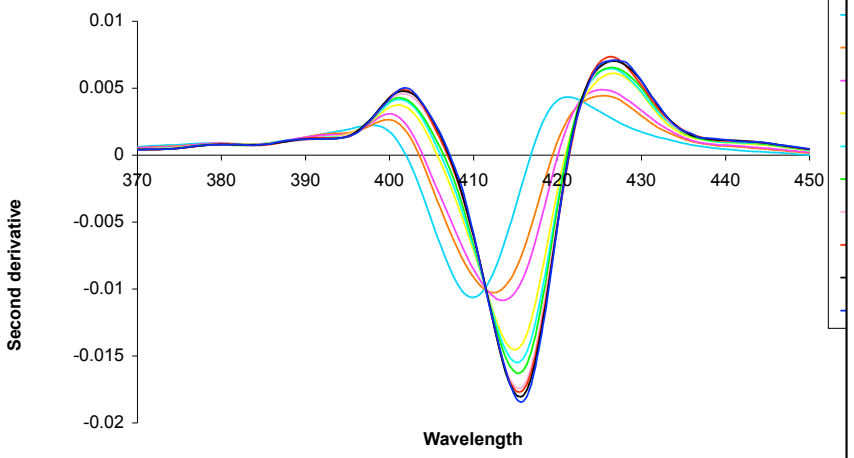

Sample: Spermine DCPL

UV traces taken at 260 and 290 nm and Base peak chromatograms for + and – modes.

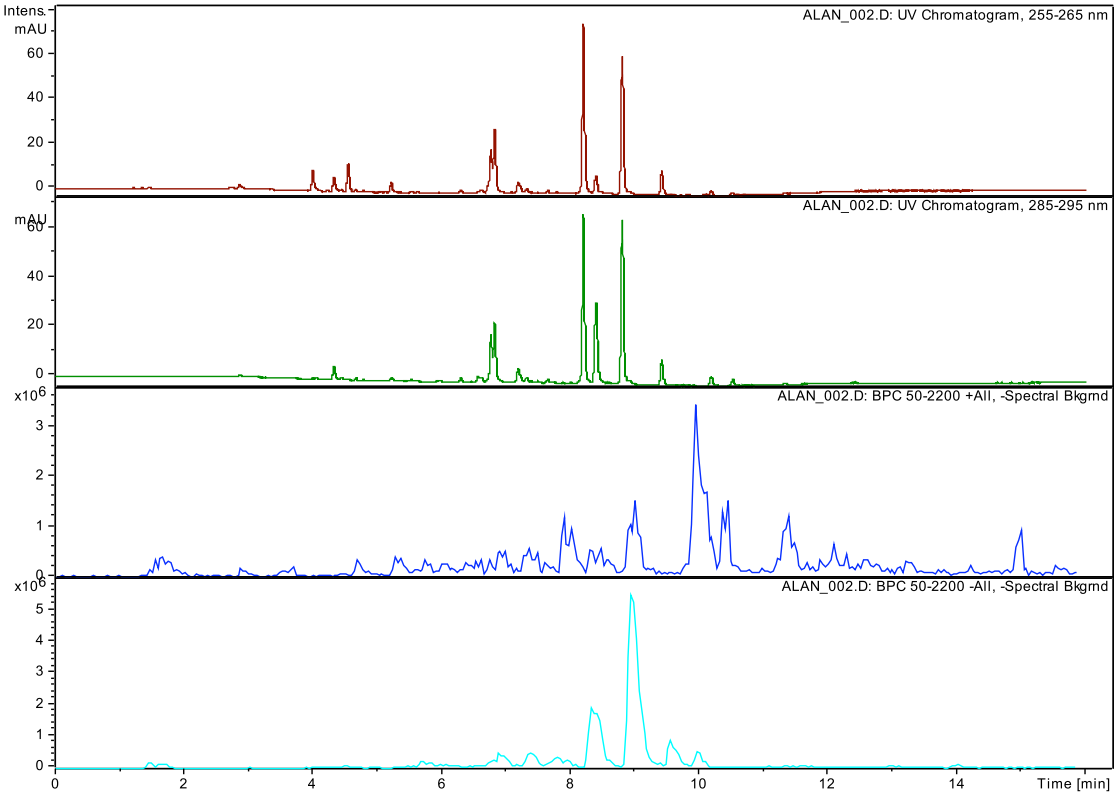

Extracted ion Chromatograms for + mode

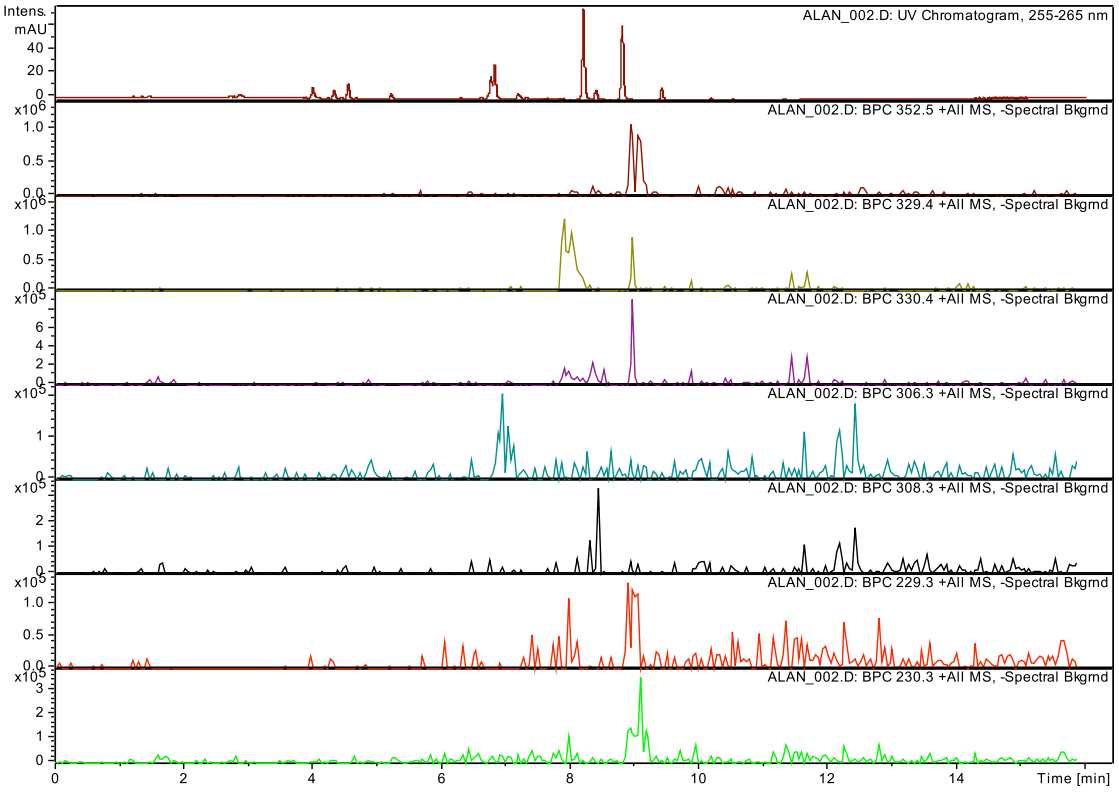

Extracted ion Chromatograms for - mode

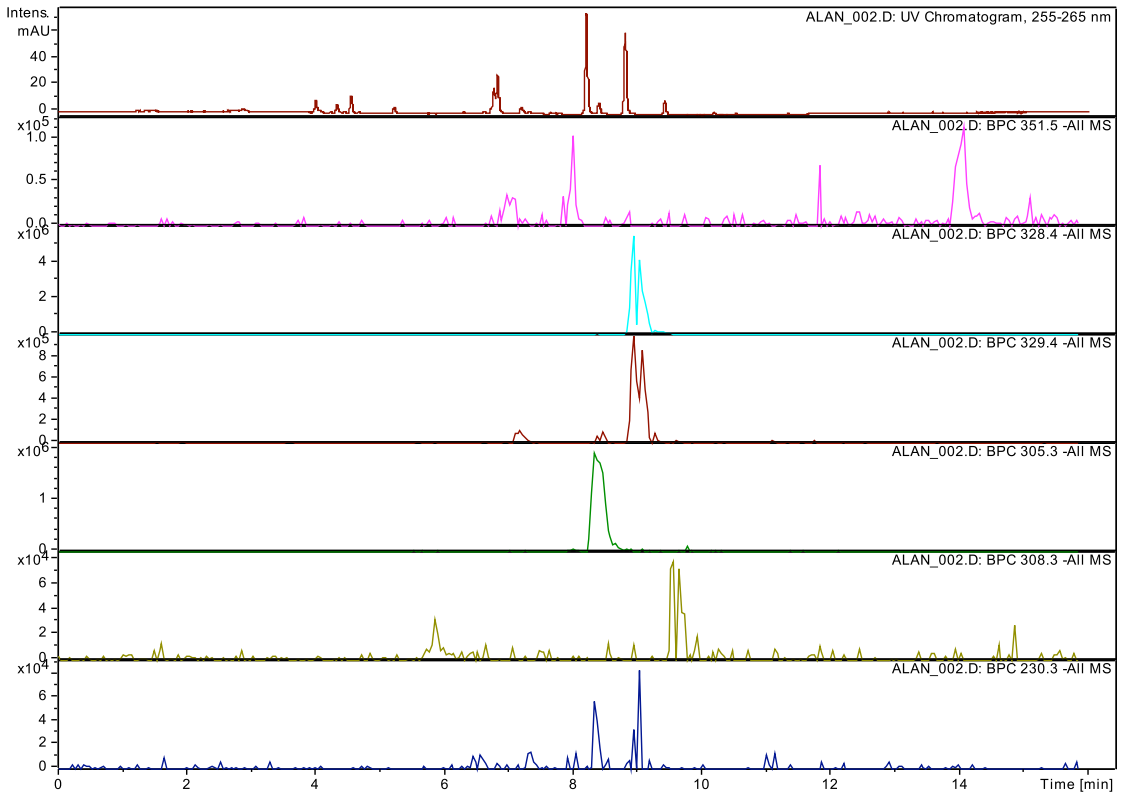
Intens.
mAU
ALAN_002.D: UV Chromatogram, 255-265 nm
ALAN_002.D: BPC 351.5 -All MS
ALAN_002.D: BPC 328.4 -All MS
ALAN_002.D: BPC 329.4 -All MS
ALAN_002.D: BPC 305.3 -All MS
ALAN_002.D: BPC 308.3 -All MS
ALAN_002.D: BPC 230.3 -All MS
Time [min]

These are the masses found under the peaks. The retention times are indicated in the picture.

Positive mass spec.

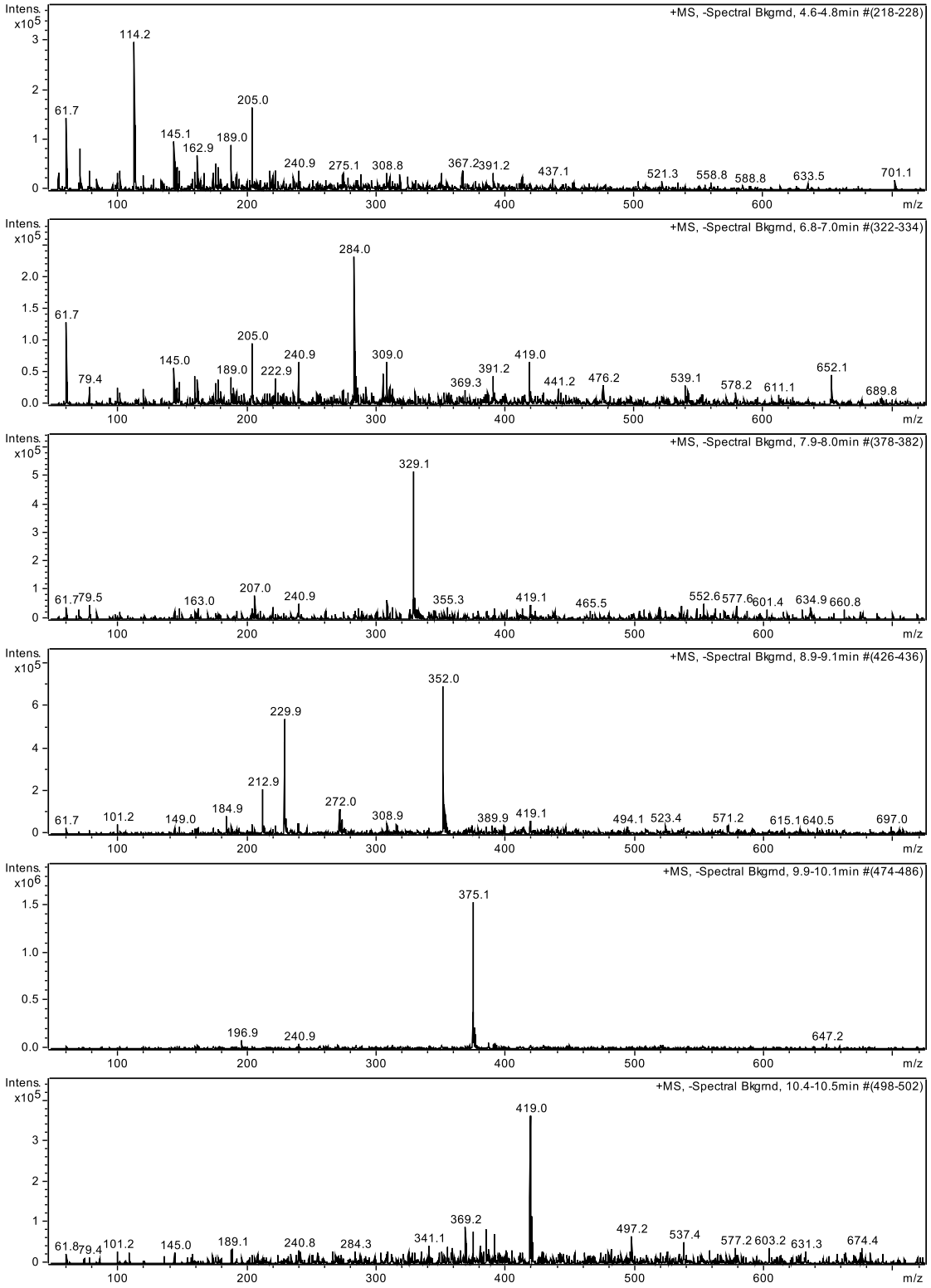

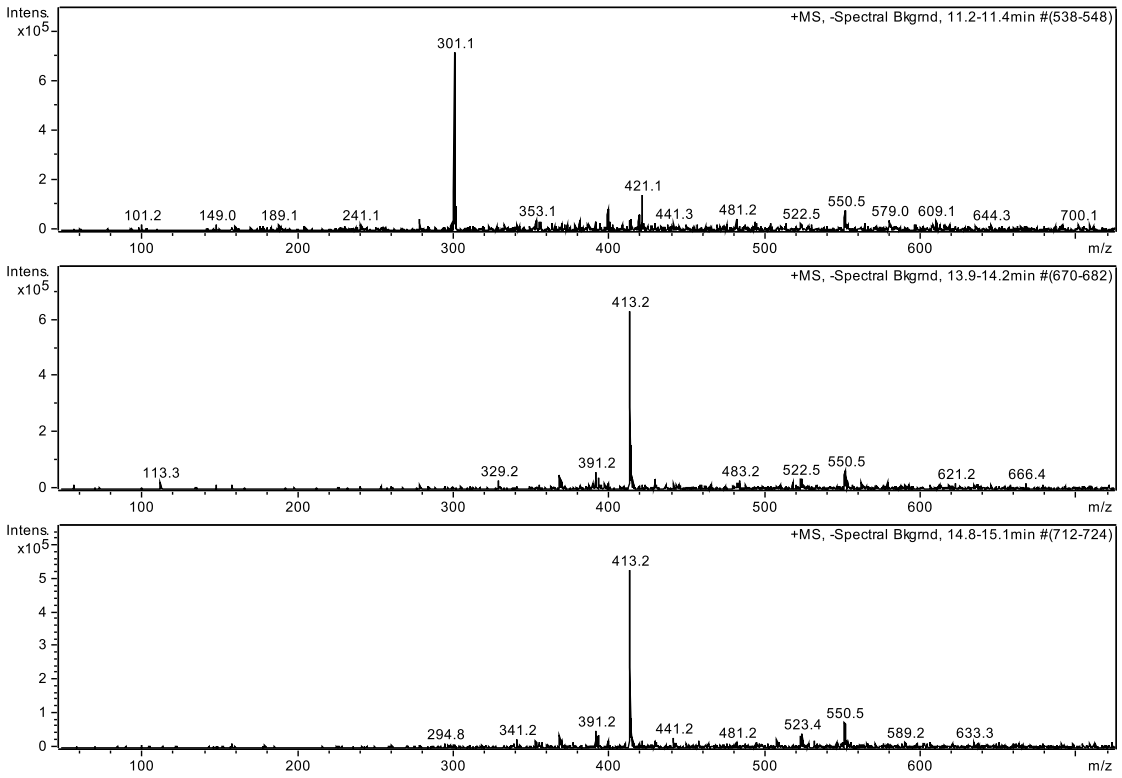
Intens.
x10^5
+MS, -Spectral Bkgrnd, 11.2-11.4min #(538-548)
301.1
421.1
101.2
149.0
189.1
241.1
353.1
441.3
481.2
522.5
550.5
579.0
609.1
644.3
700.1
m/z
+MS, -Spectral Bkgrnd, 13.9-14.2min #(670-682)
413.2
113.3
329.2
391.2
483.2
522.5
550.5
621.2
666.4
+MS, -Spectral Bkgrnd, 14.8-15.1min #(712-724)
413.2
294.8
341.2
391.2
441.2
481.2
523.4
550.5
589.2
633.3

Negative:

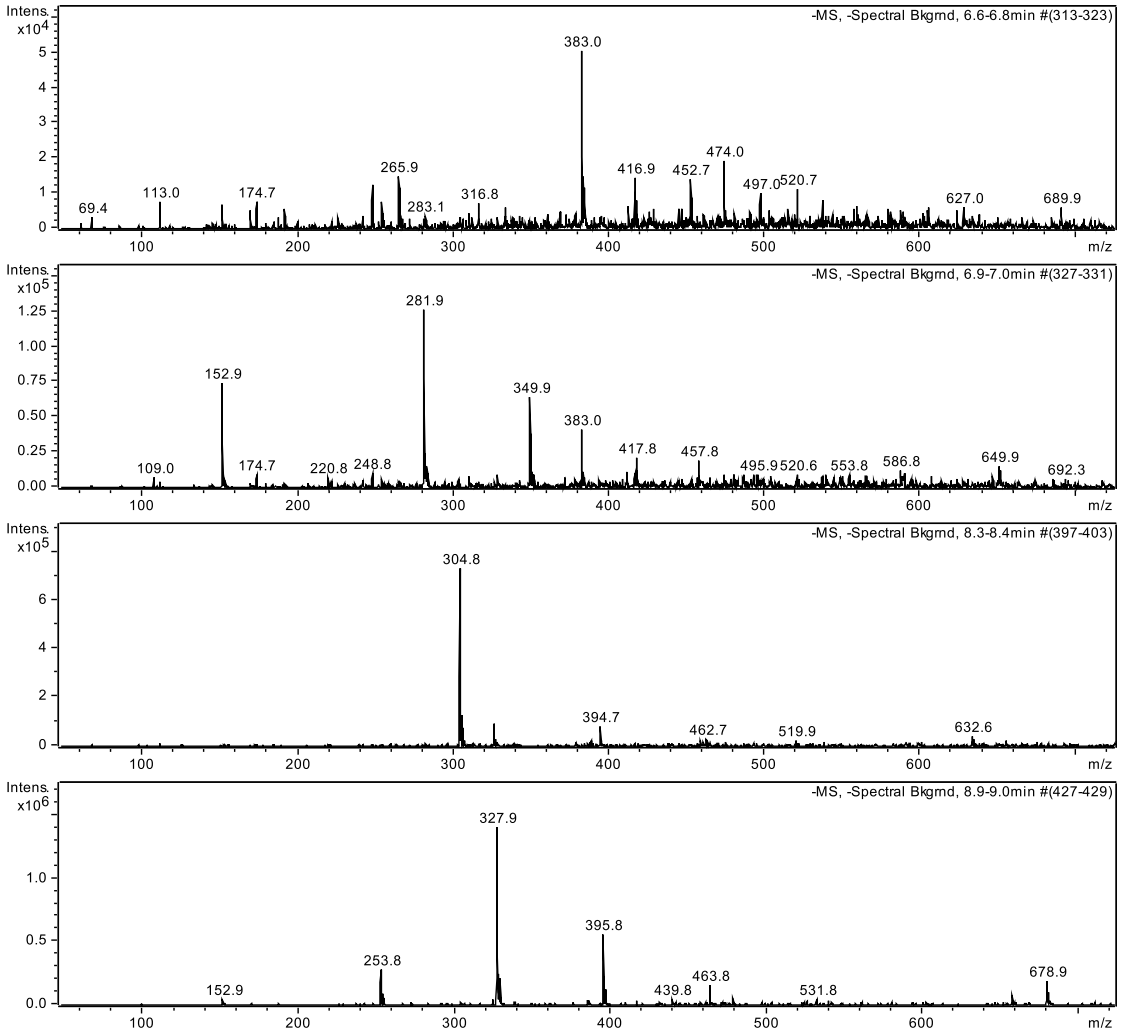
Intens.
x10^4
-MS, -Spectral Bkgrnd, 6.6-6.8min #(313-323)
383.0
69.4
113.0
174.7
265.9
283.1
316.8
416.9
452.7
474.0
497.0
520.7
627.0
689.9
m/z
Intens.
x10^5
-MS, -Spectral Bkgrnd, 6.9-7.0min #(327-331)
281.9
152.9
349.9
383.0
109.0
174.7
220.8
248.8
417.8
457.8
495.9
520.6
553.8
586.8
649.9
692.3
m/z
Intens.
x10^5
-MS, -Spectral Bkgrnd, 8.3-8.4min #(397-403)
304.8
394.7
462.7
519.9
632.6
m/z
Intens.
x10^6
-MS, -Spectral Bkgrnd, 8.9-9.0min #(427-429)
327.9
395.8
253.8
152.9
439.8
463.8
531.8
678.9
m/z

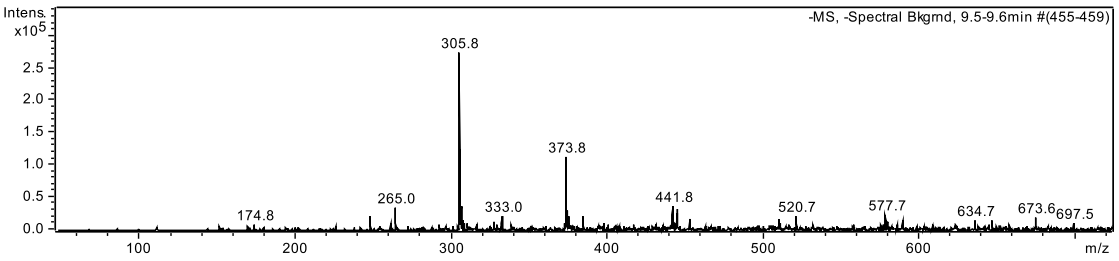
-MS, -Spectral Bkgmd, 9.5-9.6min #(455-459)
Intens.
x10^5
305.8
373.8
265.0
441.8
174.8
333.0
520.7
577.7
634.7
673.6
697.5
m/z

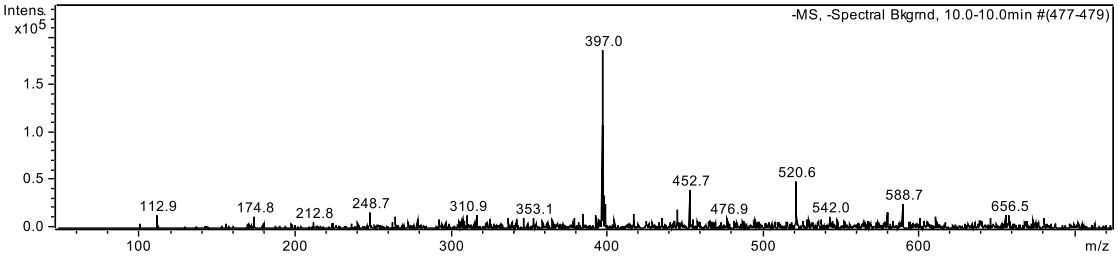
-MS, -Spectral Bkgmd, 10.0-10.0min #(477-479)
Intens.
x10^5
397.0
452.7
520.6
588.7
112.9
174.8
212.8
248.7
310.9
353.1
476.9
542.0
656.5
m/z

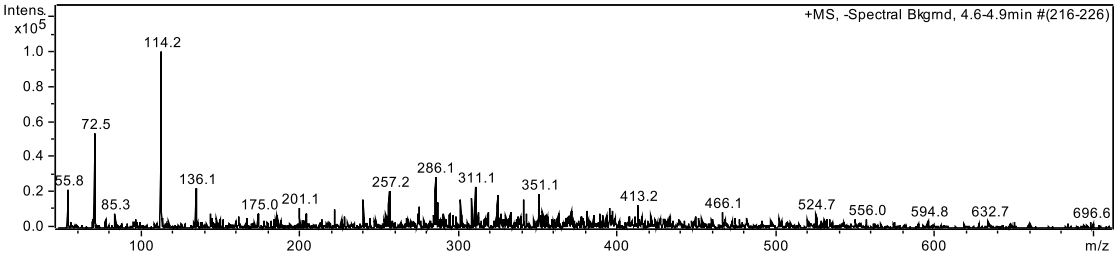
+MS, -Spectral Bkgmd, 4.6-4.9min #(216-226)
Intens.
x10^5
114.2
72.5
55.8
85.3
136.1
175.0
201.1
257.2
286.1
311.1
351.1
413.2
466.1
524.7
556.0
594.8
632.7
696.6
m/z

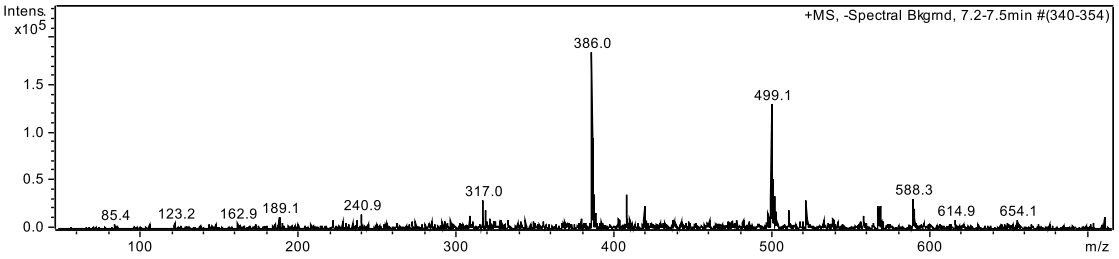
+MS, -Spectral Bkgmd, 7.2-7.5min #(340-354)
Intens.
x10^5
386.0
499.1
85.4
123.2
162.9
189.1
240.9
317.0
588.3
614.9
654.1
m/z

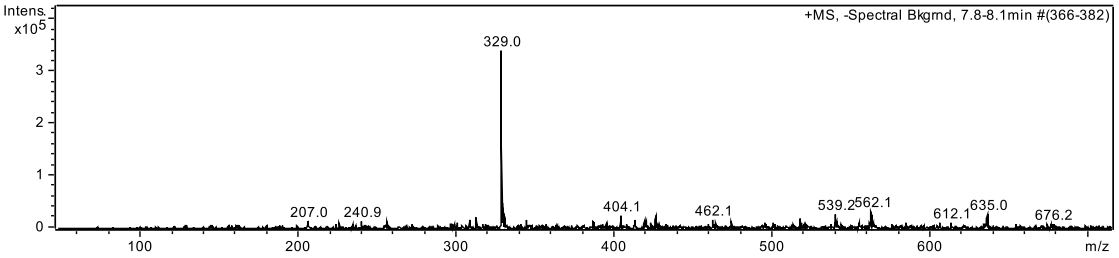
+MS, -Spectral Bkgmd, 7.8-8.1min #(366-382)
Intens.
x10^5
329.0
207.0
240.9
404.1
462.1
539.2
562.1
612.1
635.0
676.2
m/z

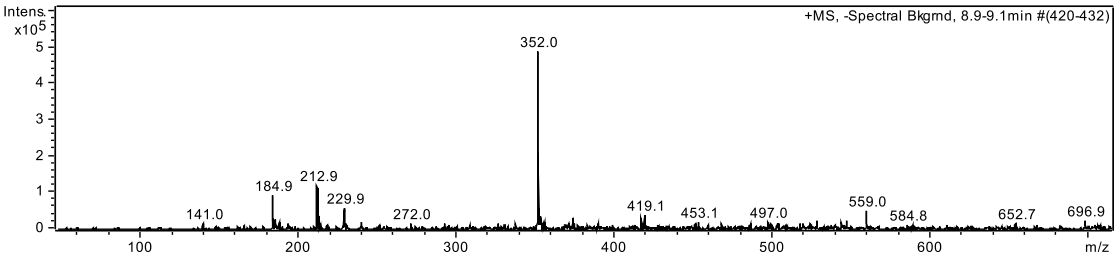
+MS, -Spectral Bkgmd, 8.9-9.1min #(420-432)
Intens.
x10^5
352.0
184.9
212.9
229.9
141.0
272.0
419.1
453.1
497.0
559.0
584.8
652.7
696.9
m/z

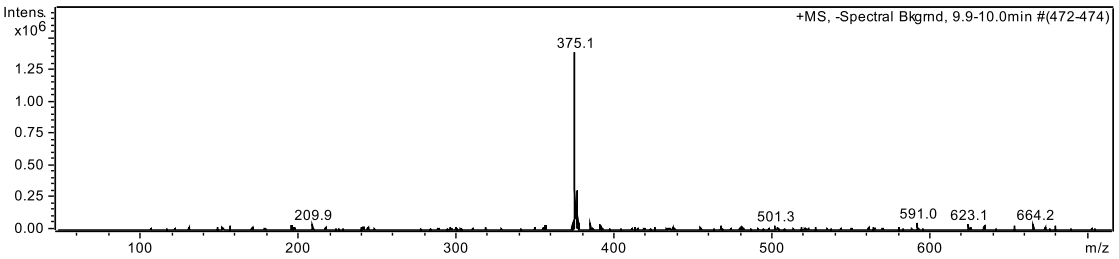
+MS, -Spectral Bkgmd, 9.9-10.0min #(472-474)
Intens.
x10^6
375.1
209.9
501.3
591.0
623.1
664.2
m/z

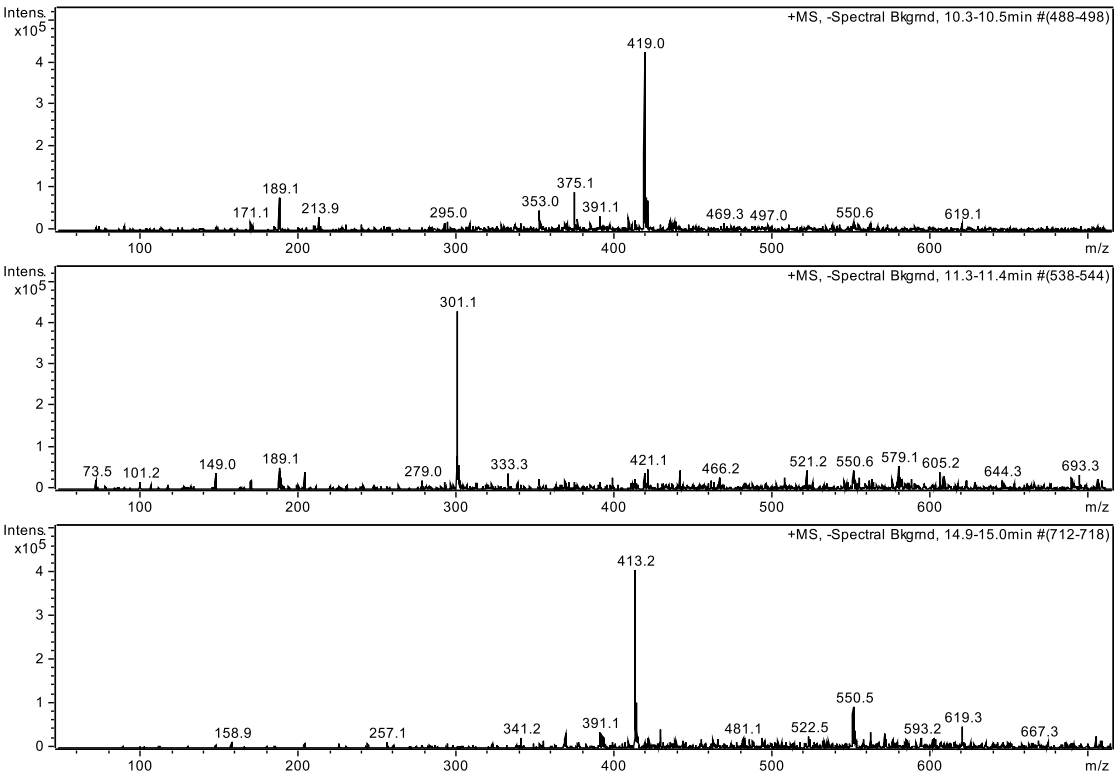
+MS, -Spectral Bkgrnd, 10.3-10.5min #(488-498)
Intens.
x10^5
419.0
189.1
171.1
213.9
295.0
375.1
353.0
391.1
469.3
497.0
550.6
619.1
m/z
+MS, -Spectral Bkgrnd, 11.3-11.4min #(538-544)
301.1
73.5
101.2
149.0
189.1
279.0
333.3
421.1
466.2
521.2
550.6
579.1
605.2
644.3
693.3
+MS, -Spectral Bkgrnd, 14.9-15.0min #(712-718)
413.2
158.9
257.1
341.2
391.1
481.1
522.5
550.5
593.2
619.3
667.3

Negative:

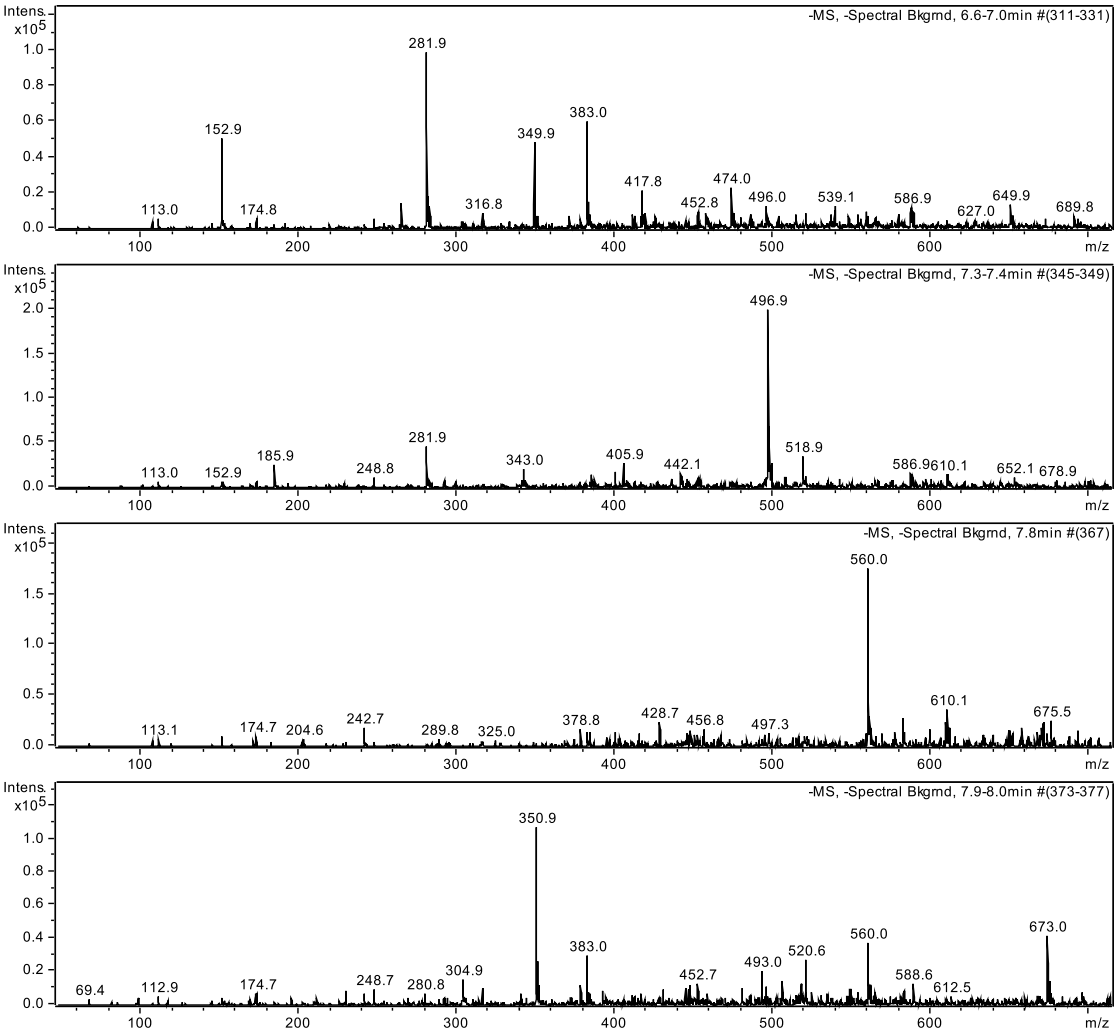
-MS, -Spectral Bkgrnd, 6.6-7.0min #(311-331)
Intens.
x10^5
281.9
152.9
349.9
383.0
113.0
174.8
316.8
417.8
452.8
474.0
496.0
539.1
586.9
627.0
649.9
689.8
m/z
-MS, -Spectral Bkgrnd, 7.3-7.4min #(345-349)
496.9
113.0
152.9
185.9
248.8
281.9
343.0
405.9
442.1
518.9
586.9
610.1
652.1
678.9
-MS, -Spectral Bkgrnd, 7.8min #(367)
560.0
113.1
174.7
204.6
242.7
289.8
325.0
378.8
428.7
456.8
497.3
610.1
675.5
-MS, -Spectral Bkgrnd, 7.9-8.0min #(373-377)
350.9
69.4
112.9
174.7
248.7
280.8
304.9
383.0
452.7
493.0
520.6
560.0
588.6
612.5
673.0

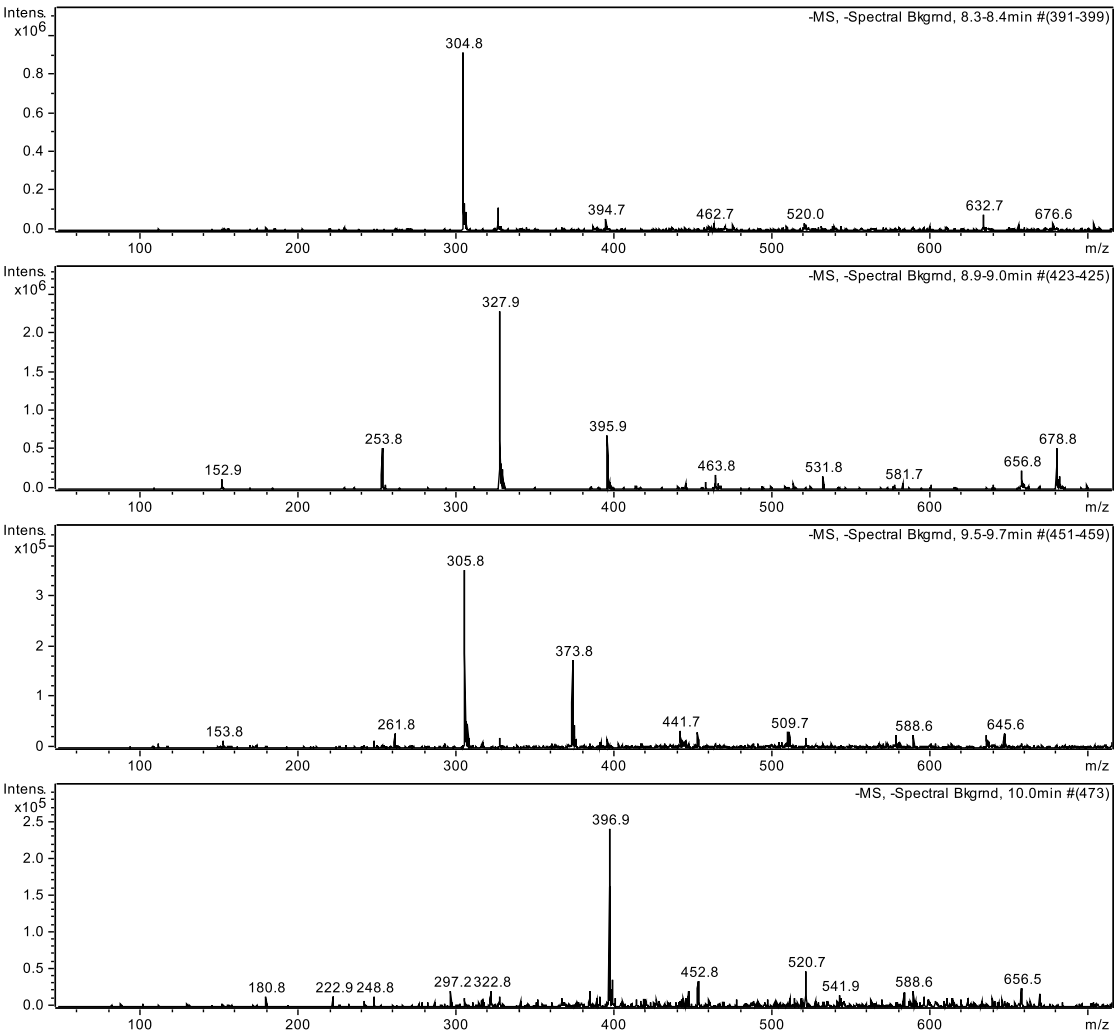
Intens.
x10^6
-MS, -Spectral Bkgmd, 8.3-8.4min #(391-399)
304.8
394.7
462.7
520.0
632.7
676.6
m/z
Intens.
x10^6
-MS, -Spectral Bkgmd, 8.9-9.0min #(423-425)
327.9
253.8
395.9
152.9
463.8
531.8
581.7
656.8
678.8
m/z
Intens.
x10^5
-MS, -Spectral Bkgmd, 9.5-9.7min #(451-459)
305.8
373.8
153.8
261.8
441.7
509.7
588.6
645.6
m/z
Intens.
x10^5
-MS, -Spectral Bkgmd, 10.0min #(473)
396.9
180.8
222.9
248.8
297.2
322.8
452.8
520.7
541.9
588.6
656.5
m/z

11 Appendix C: Published work

ORGANIC LETTERS

2006
Vol. 8, No. 7
1279−1282

Unusually Weak Binding Interactions in Tetrazole–Amidine Complexes

Alan F. Tominey, Paul H. Docherty, Georgina M. Rosair, Romain Quenardelle, and Arno Kraft*

Chemistry, School of Engineering & Physical Sciences, Heriot-Watt University, Riccarton, Edinburgh EH14 4AS, United Kingdom

a.kraft@hw.ac.uk

Received December 19, 2005

ABSTRACT

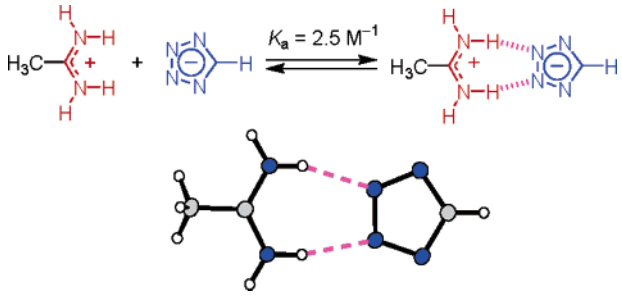

Tetrazoles frequently replace carboxylic acids in pharmaceutical drugs. However, while the binding modes of tetrazolate and carboxylate anions in amidinium complexes turns out to be similar, the association constant of the former is 2–3 orders of magnitude smaller in DMSO. Crystal structures revealed that the N···H–N hydrogen bonds in amidinium tetrazolates are bent (162° and 169°) and noticeably longer (N···N 2.96 Å) than corresponding hydrogen bonds in both amidinium carboxylates and ammonium tetrazolates.

Tetrazoles are acidic heterocycles that serve as important bioisosteric replacements for carboxylic acids in modern drug design.[1,2] The most prominent pharmaceutical application of tetrazoles is as angiotensin II receptor antagonists for the treatment of high blood pressure, and four out of six marketed drugs falling into this class contain a biphenyltetrazole pharmacophore.[3] However, no crystal structure of the membrane receptor binding site is available so far, while mutagenesis studies have led to conflicting evidence concerning the binding site of the drugs. Several reports suggest that the deprotonated tetrazole in these drugs interacts with a lysine and a histidine at the recognition site of the membrane receptor.[4,5] Others conclude that the tetrazole binds instead to a nearby arginine at the receptor binding site[6] or even that interactions involve both a lysine and an arginine.[7] What is clear, however, is that the replacement of a carboxylic acid by a tetrazole is not always beneficial in terms of pharmaceutical activity, in particular when the binding site contains an arginine.[8]

The arginine−carboxylate interaction possesses considerable importance in protein folding and a number of protein receptor−hormone (or protein receptor-drug) interactions. How does the analogous interaction between arginine and a tetrazole compare? Computational studies have indicated that a guanidinium carboxylate complex should be more stable

(1) The pK_a of the parent tetrazole is 4.6 (in 0.15 M aqueous KCl at 25 °C) and similar to that of acetic acid.

(2) Herr, R. J. *Bioorg. Med. Chem.* **2002**, *10*, 3379−3393.

(3) (a) Wexler, R. R.; Greenlee, W. J.; Irvin, J. D.; Goldberg, M. R.; Prendergast, K.; Smith, R. D.; Timmermans, P. B. M. W. M. *J. Med. Chem.* **1996**, *39*, 625−656. (b) Naka, T.; Kubo, K. *Curr. Pharm. Design* **1999**, *5*, 453−472.

(4) (a) Noda, K.; Saad, Y.; Kinoshita, A.; Boyle, T. P.; Graham, R. M.; Husain, A.; Karnik, S. S. *J. Biol. Chem.* **1995**, *270*, 2284−2289. (b) Noda, K.; Saad, Y.; Karnik, S. S. *J. Biol. Chem.* **1995**, *270*, 28511−28514.

(5) In this respect, it is interesting to note that the crystal structure of a tetrazole-containing inhibitor of HIV-1 integrase shows the tetrazolate group of the inhibitor hydrogen-bonded to two protonated lysines of the protein receptor. Goldgur, Y.; Craigie, R.; Cohen, G. H.; Fujiwara, T.; Yoshinaga, T.; Fujishita, T.; Sugimoto, H.; Endo, T.; Murai, H.; Davies, D. R. *Proc. Natl. Acad. Sci. U.S.A.* **1999**, *96*, 13040−13043.

(6) (a) Yamano, Y.; Ohyama, K.; Kikyo, M.; Sano, T.; Nakagomi, Y.; Inoue, Y.; Nakamura, N.; Morishima, I.; Guo, D.-F.; Hamakubo, T.; Inagami, T. *J. Biol. Chem.* **1995**, *270*, 14024−14030. (b) Vauquelin, G.; Fierens, F. L. P.; Gáborik, Z.; Minh, T. L.; De Backer, J.-P.; Hunyady, L.; Vanderheyden, P. M. L. *J. Renin Angiotensin Aldosteron Syst.* **2001**, *2*, S32−S36.

(7) Flower, D. R. *Biochim. Biophys. Acta* **1999**, *1422*, 207−234.

10.1021/ol053072+ CCC: $33.50 © 2006 American Chemical Society
Published on Web 03/01/2006

than a guanidinium tetrazolate.[9] To shed further light on tetrazole binding, we reinvestigated this problem using a simple amidine−tetrazole model system. Benzamidine is an obvious choice as a mimic for arginine because several para-substituted benzamidine derivatives are known to be potent, nonpeptide antagonists of the fibrinogen receptor, inhibiting platelet aggregation and preventing the coagulation of blood.[10] The benzamidine in these drugs occupies a recognition site for arginine in thrombin's Arg-Gly-Asp peptide sequence, the usual substrate for the protease.

Our previous work had already shown that tetrazoles form supramolecular complexes with imidazolines (a heterocyclic amidine) and *N*,*N*′-diethyl-substituted benzamidines, revealing distinct differences in binding modes between tetrazoles and carboxylic acids.[11,12] Tetrazolate ligands were found to display considerable flexibility in binding modes both in the crystal and in solution, although this was largely driven by the steric constraints imparted by the substituents at the nitrogens of the heterocyclic or *N*-substituted amidine. This paper describes the binding interactions between tetrazole and two *unsubstituted amidines*, benzamidine and acetamidine, which were selected as arginine mimics since they do not suffer from any such structural constraints.

Initial attempts to make the 1:1 amidine−tetrazole model complexes by ion exchange failed, and we decided to prepare the complexes by an acid−base reaction instead.[13] Treatment of the amidine hydrochlorides with a stoichiometric amount of sodium hydroxide in methanol gave the crude free amidine bases that were subsequently purified by gradient sublimation (Scheme 1). Acetamidine (**2a**) and benzamidine (**2b**) were stable in the absence of moisture. The free bases were then combined with an equimolar amount of tetrazole. A single recrystallization gave amidinium tetrazolates **3a**,**b** in high purity. Complex **4** was made analogously from acetamidine and formic acid.

Scheme 1. Synthesis of Amidine Complexes

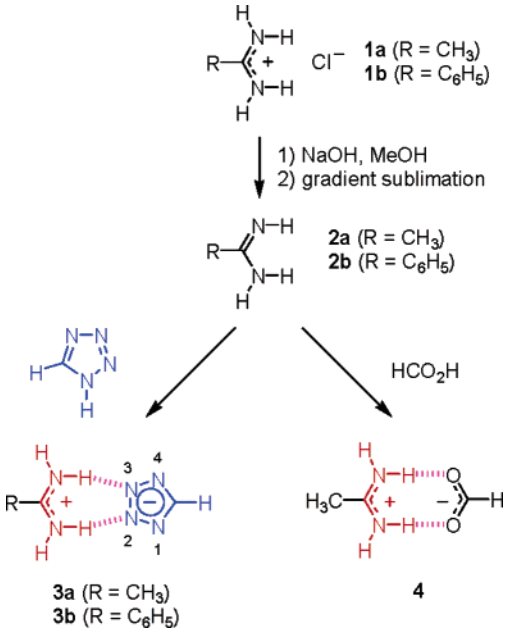

Crystals suitable for X-ray crystallography were obtained by crystallization from methanol/acetonitrile. Figures 1 and 2 display the crystal structures of tetrazolate complexes **3a** and **3b**, as well as formate complex **4**. The most striking feature is the structural similarity in the binding modes of the tetrazolate and the formate. This was somewhat unexpected as theoretical calculations predict the highest charge density to be located on N^1 and N^4 of the tetrazolate ring (for numbering of the nitrogens, see Scheme 1).[9a,14] Consequently, these two nitrogen atoms should be preferred hydrogen-bond acceptor sites, thus favoring a side-on binding arrangement of the tetrazolate ligand (through N^1 and N^2) as seen in all previous crystal structures of complexes involving tetrazolates and N-substituted amidines.[11,12] However, binding of the tetrazolate to both NH_2 groups of an amidine molecule in **3a**,**b** clearly occurs end-on, through nitrogen atoms N^2 and N^3.

The three crystal structures display an extended array of hydrogen bonds, which effectively involves every amidine NH proton and tetrazolate nitrogen (as well as formate oxygen atom). Both the formate and tetrazolate are almost coplanar to the amidinium group of the acetamidine, with torsion angles between the two binding groups being 1.11(2)° and 5.5(4)°, respectively. Only the amidine group of

(8) Examples include prostaglandin $F_{2\alpha}$ analogues: (a) Schuster, V. L.; Itoh, S.; Andrews, S. W.; Burk, R. M.; Chen, J.; Kedzie, K. M.; Gil, D. W.; Woodward, D. F. *Mol. Pharmacol.* **2000**, *58*, 1511−1516. Tyrosine phosphatase inhibitors: (b) Liljebris, C.; Larsen, S. D.; Ogg, D.; Palazuk, B. J.; Bleasdale, J. E. *J. Med. Chem.* **2002**, *45*, 1785−1798. And glutamate receptor antagonists: Frølund, B.; Greenwood, J. R.; Holm, M. M.; Egebjerg, J.; Madsen, U.; Nielsen, B.; Bräuner-Osborne, H.; Stensbøl, T. B.; Krogsgaard-Larsen, P. *Bioorg. Med. Chem.* **2005**, *13*, 5391−5398.

(9) (a) Zablocki, J. A.; Miyano, M.; Rao, S. N.; Panzer-Knodle, S.; Nicholson, N.; Feigen, L. *J. Med. Chem.* **1992**, *35*, 4914−4917. (b) Suvire, F.; Floridia, R.; Giannini, F.; Rodriguez, A.; Enriz, R.; Jauregui, E. *Molecules* **2000**, *5*, 583−584.

(10) (a) Alig, L.; Edenhofer, A.; Hadváry, P.; Hürzeler, M.; Knopp, D.; Müller, M.; Steiner, B.; Trzeciak, A.; Weller, T. *J. Med. Chem.* **1992**, *35*, 4393−4407. (b) Ewing, W. R.; Becker, M. R.; Manetta, V. E.; Davis, R. S.; Pauls, H. W.; Mason, H.; Choi-Sledeski, Y. M.; Green, D.; Cha, D.; Spada, A. P.; Cheney, D. L.; Mason, J. S.; Maignan, S.; Guilloteau, J.-P.; Brown, K.; Colussi, D.; Bentley, R.; Bostwick, J.; Kasiewski, C. J.; Morgan, S. R.; Leadley, R. J.; Dunwiddie, C. T.; Perrone, M. H.; Chu, V. *J. Med. Chem.* **1999**, *42*, 3557−3571. (c) Adler, M.; Davey, D. D.; Phillips, G. B.; Kim, S.-H.; Jancarik, J.; Rumennik, G.; Light, D. R.; Whitlow, M. *Biochemistry* **2000**, *39*, 12534−12542.

(11) (a) Peters, L.; Fröhlich, R.; Boyd, A. S. F.; Kraft, A. *J. Org. Chem.* **2001**, *66*, 3291−3298. (b) Kraft, A.; Peters, L.; Fröhlich, R. *Acta Crystallogr. Sect. C* **2002**, *58*, o272−o274.

(12) Kraft, A.; Osterod, F.; Fröhlich, R. *J. Org. Chem.* **1999**, *64*, 6425−6433.

(13) Acetamidinium hydrochloride **1a** (2.00 g, 21.2 mmol) was dissolved in methanol (20 mL). To this was added a solution of NaOH (853 mg, 21.3 mmol) in MeOH (60 mL). The mixture was then concentrated in a vacuum, and the residue was sublimed at 60 °C/0.4 mbar to yield **2a** in form of a colorless oil (150 mg, 2.59 mmol, 23%). ^{1}H NMR (200 MHz, DMSO-d_6): δ 1.75 (s, 3 H), 5.36 (br s, 3 H). A solution of tetrazole in acetonitrile (0.45 M, 5.45 mL, 2.45 mmol) was added to a solution of acetamidine **2a** (142 mg, 2.45 mmol) in MeOH (2 mL). The mixture was concentrated in a vacuum, and the residue was recrystallized from hot MeOH/MeCN to yield **3a** as a colorless solid (165 mg, 53%). DSC: 149 °C (145 J g^{-1}). ^{1}H NMR (400 MHz, DMSO-d_6, 60 mg/0.7 mL): δ 2.19 (s, 3 H), 8.23 (s, 1 H), 9.28 (br s, 4 H). ^{13}C NMR (50 MHz, DMSO-d_6, 60 mg/0.7 mL): δ 18.69 (CH_3), 149.16 (tetrazole CH), 168.42 (amidine C=N). IR (KBr, cm^{-1}): ν 3277, 1703, 1530, 1442, 1377, 1281. Anal. Calcd. for $C_3H_8N_6$ (128.14): C, 28.24; H, 6.36; N, 64.61. Found: C, 28.12; H, 6.29; N, 65.59.

(14) Biot, C.; Bauer, H.; Schirmer, R. H.; Davioud-Charvet, E. *J. Med. Chem.* **2004**, *47*, 5972−5983.

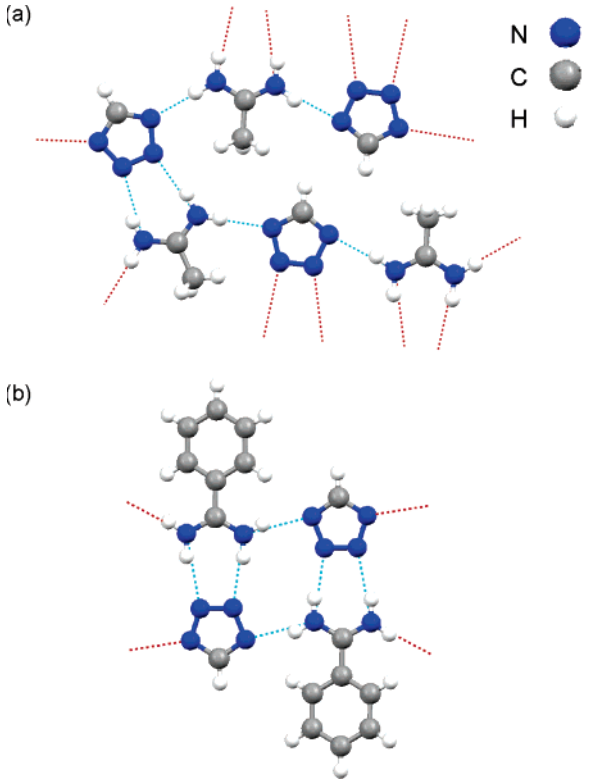

Figure 1. (a) Crystal structure and hydrogen-bonded arrangement of acetamidinium tetrazolate complex **3a**. (b) Crystal structure and hydrogen-bonded arrangement of benzamidinium tetrazolate complex **3b**.

the benzamidinium complex is tilted slightly further, by 22.8(1)°, to the plane of the tetrazolate.

Complex **4** possesses almost linear hydrogen bonds between the formate oxygen and amidinium nitrogen, with O···H−N angles of 178.6(2) and 176.6(2)° and O···N distances of 2.841(2) and 2.870(2) Å. In contrast, the hydrogen bonds in the corresponding acetamidinium tetrazolate **3a** are noticeably bent, with N···H−N angles in the range 161(2)−169(2)°. The H-bonds in **3a** are also significantly longer,

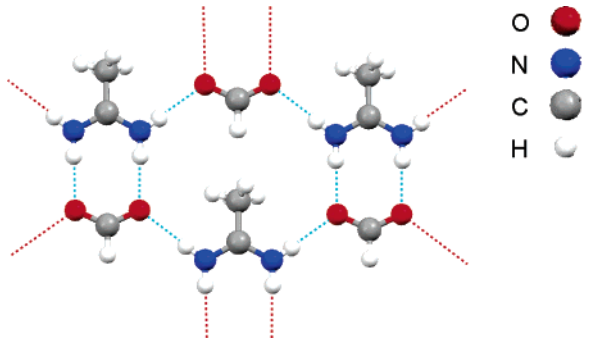

Figure 2. Crystal structure and hydrogen-bonded arrangement of complex **4** (CH_3 group disordered).

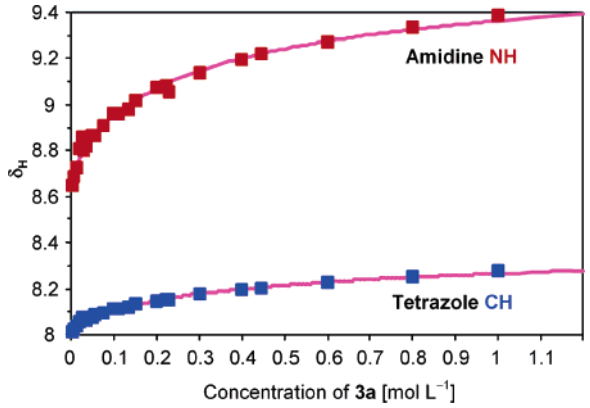

Figure 3. Concentration dependence of the tetrazolate CH and amidine NH ^{1}H NMR chemical shifts for complex **3a** in DMSO-d_6 at 25 °C. The curves represent the calculated isotherms for 1:1 binding, whereas the filled squares are experimental values. Data were obtained from two independent experiments.

with N···N distances of 2.919(3)−2.985(3) Å. Similar angles and distances are observed in complex **3b**. In both amidinium−tetrazolate complexes, the tetrazole binds in the same way as a carboxylic acid. Both the nonlinear hydrogen bond angles and the longer H-bonds serve to weaken the attraction between the tetrazolate and amidinium ions.

We note that the tetrazolate ions show shorter H-bonds when they hydrogen bond side-on through N^1 and N^4 to neighboring amidinium ions [with N···N distances of 2.919(3)−2.963(3) Å and N···H−N angles of 167(2)−177(2)° for **3a**]. This is in keeping with the theoretical calculations referred to above. Such a difference in hydrogen bond lengths was not observed for complex **4**. Its intermolecular H-bonds between neighboring complexes (O···H−N angle 176.6°, O···N distance 2.87 Å) were almost identical in length to the intracomplex hydrogen bonds between the formate and amidinium ion, forming an eight-membered ring.

Saltlike complexes **3a**,**b** and **4** were soluble in polar solvents, including water, methanol, and DMSO. Supramolecular binding was only observed in DMSO, and even in this solvent, weak binding was evident from the high concentrations that were needed before chemically induced shifts could be observed. A Job plot supported a 1:1 stoichiometry in DMSO.[15] Figure 3 depicts a typical NMR dilution curve of complex **3a** showing the concentration dependence of the tetrazolate CH and amidine NH singlets. Nonlinear regression analysis revealed a rather weak association constant, K_a, of 2.5 ± 0.5 M^{-1} for acetamidine complex **3a**, and even the analogous benzamidine complex **3b** gave rise to only a marginally higher K_a of 18 ± 3 M^{-1}.[16] In contrast, the K_a of complex **4** was found to be 1600 ± 100 M^{-1}, about 2−3 orders of magnitude larger than the binding of tetrazolates in complexes **3a**,**b**.[17]

Electrostatic arguments, as previously suggested,[9a] cannot be the sole reason for the small association constants in

(15) (a) Job, P. *Ann. Chim.* **1928**, *9*, 113−203. (b) Blanda, M. T.; Horner, J. H.; Newcomb, M. *J. Org. Chem.* **1989**, *54*, 4626−4636.

amidinium tetrazolates. While charge distribution in the tetrazolate may lead to some reduction in the anion's electrostatic attraction by an amidinium cation, the crystal structures of complexes **3a**,**b** reported in our paper provide evidence of hydrogen bonds between the amidinium ion and the two nitrogens N^2/N^3 of the tetrazolate, even though these nitrogens possess the lowest charge density. The weaker binding is more likely due to the lengthening of N···H−N hydrogen bonds in complexes **3a**,**b** by 0.1 Å to, on average, 2.96 Å compared with H-bonds between a tetrazolate and a protonated amine (average 2.85 Å), since the N···H−N angles of the hydrogen bonds in amidinium tetrazolates and ammonium tetrazolates are essentially the same.[18,19]

These findings suggest why tetrazoles are not always suitable substitutes for carboxylic acids, particularly when the crucial binding interaction requires the tetrazolate to form two strong hydrogen bonds to the guanidinium group of an arginine. Notable examples include inhibitors of the fibrinogen receptor,[9a] as well as inhibitors of the prostaglandin transporter,[8a] where replacement of a crucial carboxylic acid group by a tetrazole lowered the inhibitor efficiency by over 2 orders of magnitude and, in one case, even led to an inactive compound. However, when binding involves other cationic sites such as lysine or histidine, tetrazoles should still remain highly effective acidic pharmacophores and valuable bioisosteric replacements for carboxylic acids. In all likelyhood, tetrazole-containing angiotensin II receptor antagonists fall into this category.

Acknowledgment. We gratefully thank the School of Engineering & Physical Sciences at Heriot-Watt University for support.

Supporting Information Available: Experimental procedures, characterization details, potentiometric titration of tetrazole, NMR dilution studies, Job plot, and X-ray crystal structural information. This material is available free of charge via the Internet at http://pubs.acs.org.

OL053072+

(16) The hyperbolic shape of the dilution curve was fitted to 1:1 host−guest complexation: (a) Schneider, H. J.; Kramer, R.; Simova, S.; Schneider, U. *J. Am. Chem. Soc.* **1988**, *110*, 6442−6448. (b) Wilcox, C. S. In *Frontiers in Supramolecular Chemistry and Photochemistry*; Schneider, H.-J., Dürr, H., Eds.; VCH: Weinheim, 1991; pp 123−143. (c) Macomber, R. S. *J. Chem. Educ.* **1992**, *69*, 375−378.

(17) Carboxylates bind to amidinium ions with K_a values that are typically of the order of 1000−3500 M^{-1} in DMSO at room temperature, although K_a tends to be lower if the carboxylate is substituted with a strongly electron-withdrawing residue: (a) Deng, Y.; Roberts, J. A.; Peng, S.-M.; Chang, C. K.; Nocera, D. G. *Angew. Chem., Int. Ed. Engl.* **1997**, *36*, 2124−2127. (b) Papoutsakis, D.; Kirby, J. P.; Jackson, J. E.; Nocera, D. G. *Chem. Eur. J.* **1999**, *5*, 1474−1480. (c) Kirby, J. P.; van Dantzig, N. A.; Chang, C. K.; Nocera, D. G. *Tetrahedron Lett.* **1995**, *36*, 3477−3480. (d) Roberts, J. A.; Kirby, J. P.; Nocera, D. G. *J. Am. Chem. Soc.* **1995**, *117*, 8051−8052. (e) Krechl, J.; Smrčková, S.; Kuthan, J. *Collect. Czech. Chem. Commun.* **1990**, *50*, 460−468.

(18) For examples, see: (a) Lyakhov, A. S.; Voitekhovich, S. V.; Gaponik, P. N.; Ivashkevich, L. S. *Acta Crystallogr. Sect. C* **2003**, *59*, o22−o23. (b) Alkorta, I.; Rozas, I.; Elguero, J. *J. Chem. Soc., Perkin Trans. 2* **1998**, 2671−2675. (c) Chertanova, L. F.; Struchkov, Y. T.; Sopin, V. F.; Kovalenko, V. I.; Timokhov, V. N.; Fronchek, E. V. *Chem. Heterocycl. Compd.* **1989**, 655−657.

(19) The low dissociation constant of ammonium phenyltetrazolate of 2.87×10^{-5} M in DMSO at 25 °C (determined by electrical conductivity measurements) correlates well with the crystallographically observed short hydrogen bond in ammonium tetrazolates. Tsentovskii, V. M.; Bashkirtseva, V. E.; Evgen'ev, M. I.; Ivanova, Z. P.; Poplavskii, V. S.; Ostrovskii, V. A.; Koldobskii, G. I. *Chem. Heterocycl. Compd.* **1984**, 1238−1240.

SUPRAMOLECULAR BINDING OF PROTONATED AMINES TO FUNCTIONALIZED MICROGEL PARTICLES

Arno Kraft,[1] Alan Tominey,[1] David Andrew,[1] Juliette Dupré,[1] Andrew McIver,[1] Lewis Oliphant,[1] Georgina M. Rosair,[1] and Sijbren Otto[2]

[1] Chemistry, School of Engineering and Physical Sciences, Heriot-Watt University, Edinburgh EH14 4AS, United Kingdom.
[2] University Chemical Laboratory, University of Cambridge, Lensfield Road, Cambridge, CB2 1EW, UK

Introduction

Microgels are covalently crosslinked latex particles that form colloidal solutions and swell in the presence of a good solvent. The sponge-like, spherical particles are characterized by their small size, approximately 0.1–10 μm in diameter, which is comparable to a small virus. When composed primarily of an environmentally sensitive monomer such as *N*-isopropylacrylamide (NIPAM, **1**), microgels become susceptible to external influences, *i.e.* the extent to which they swell in a given environment can be controlled by a change in temperature or pH.[1] It is widely recognized that their structural properties and ability to quickly respond to environmental stimuli could prove to be of significant use in biomedicinal applications.

In 1998, Kiser *et al.* reported the successful loading of the anti-cancer drug doxorubicin onto an encapsulated microgel based on NIPAM, methacrylic acid and a crosslinker, and they described the subsequent controlled release of the drug following an electrical stimulus in a manner reminiscent of a secretory granule.[2] Recent work by Rotello *et al.* has explored the binding and inhibition of α-chymotrypsin by surface-modified gold nanoparticles.[3,4] Schrader and co-workers have also demonstrated that suitably designed polymers can be used to selectively bind to lysine- and arginine-rich proteins.[5] In both cases, binding resulted from the electrostatic attraction between polyanions (nanoparticles or polymers) and positively charged proteins. These recent breakthroughs have fueled interest in the area of molecular recognition and have produced promising insights into the ability of macromolecular synthetic compounds to selectively recognize other molecular species.

Developing these ideas further, we anticipated that the use of microgels should not be purely limited to the temporary physical loading of a drug within a polymer network, relying on the swelling kinetics to trap and release the confined molecule. Introducing a useful binding group by copolymerisation could then result in a supramolecular microgel receptor. The incorporation of a suitable binding site into the polymer network should provide a host–guest system where the microgel acts as the host polymer and a small molecule ligand (for example a drug or a hormone) as the guest. This idea was expected to even allow the possibility of designing a microgel with a high affinity towards specific target ligand.

Supramolecular interactions of polymeric systems with small molecules is well-known in molecular imprinting, but the systems that have been reported so far usually rely on highly hydrophobic guest molecules, with very few examples of binding in much more competitive aqueous or aqueous–organic solutions.[6] Often the low aqueous solubility of the guest molecules necessitates the use of a co-solvent which will superficially increase any observed affinity between the host polymer and the ligand in question.

The focus of this paper will be to illustrate evidence of supramolecular binding for various protonated amine-containing drugs to a supramolecular receptor microgel *in aqueous buffer at an ionic strength of 0.15 M.*

Experimental

Materials. All chemicals and reagents were purchased from commercial suppliers and were used without further purification. Monomer **2** was made as described previously.[7]

Instrumentation. ^{1}H NMR spectra in D_2O were obtained with a Bruker DPX 400 spectrometer. Ultrafiltration was carried out using a Masterflex 7518-00 peristaltic pump with a Vivaflow 50 PES filter (nominal molecular-weight cut-off, MWCO, of 100,000).

Preparation. In a typical microgel synthesis, NIPAM (1.13 g, 10 mmol), monomer **2** (0.14 g, 0.8 mmol) and *N*,*N*'-methylenebis(acrylamide) (**3**) (0.15 g, 1 mmol) were dissolved in deionized water (200 mL) along with sodium dodecylsulfate (60 mg, 0.2 mmol). The mixture was heated to 70 °C and degassed with N_2 for 15 minutes. Ammonium persulfate (60 mg, 0.5 mmol) was added and the reaction was stirred overnight at 70 °C. After cooling to room temperature, the microgel solution was purified by ultrafiltration against 2 L of deionized water, concentrated under a vacuum, and freeze-dried.

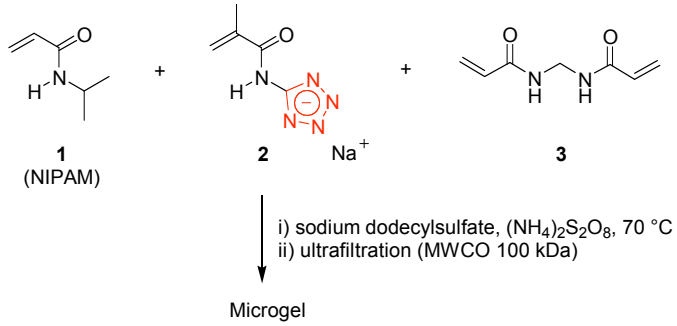

Scheme 1. Synthesis of a NIPAM-based microgel.

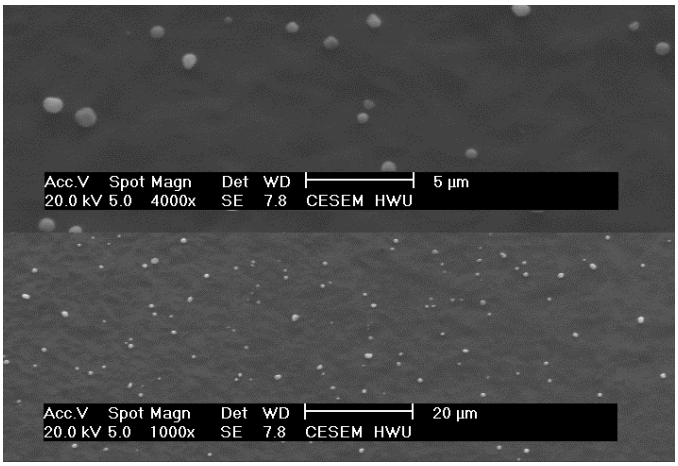

Figure 1. Scanning electron micrographs of microgel particles prepared according to Scheme 1.

Results and Discussion

Microgels were prepared by precipitation polymerisation[8] of a mixture containing about 80–84 mol% of NIPAM (**1**), 6–10 mol% of monomer (**2**), and 10 mol% of crosslinker **3** in dilute aqueous solution in the presence of a radical initiator and a detergent (Scheme 1). Tetrazole monomer **2** was chosen because it is deprotonated at neutral pH and shows improved copolymerization characteristics over methacrylic acid used hitherto in other microgel syntheses. In addition, there are strong indications that negatively charged tetrazolates have a preference to bind to protonated amines.[9] The microgel solution was purified and concentrated by ultrafiltration against deionized water, using a cross-flow membrane with a molecular weight cut-off of 100 kDa. Aggregates and macroscopic gel particles could be removed by filtration through a 0.45 μm membrane filter. The microgels were finally isolated as solids after freeze-drying.

Light scattering in solution indicated that the microgels were obtained in a narrow size distribution with a peak at 0.28 μm. This was supported by scanning electron spectroscopy (Figure 1) and by PFG-LED ^{1}H NMR spectroscopy. ^{1}H NMR spectra of the microgels confirmed the absence of low-molar-mass impurities, suggesting that ultrafiltration was an efficient way of purifying microgels. The microgels gave clear solutions in water with relatively low viscosity. In this respect, they differ considerably from polyelectrolytes which tend to form highly viscous aqueous solutions even at low concentration.

^{1}H NMR and UV titrations were used to investigate binding affinities of the microgels for various ligands (*e.g.*, spermine, spermidine, dibucaine). A series of ^{1}H NMR spectra showed clear evidence of binding in the form of signal line broadening and complexation-induced shifts at millimolar

concentrations. UV spectroscopy was chosen to probe binding behaviour at lower concentrations than those accessible by ^{1}H NMR spectroscopy.

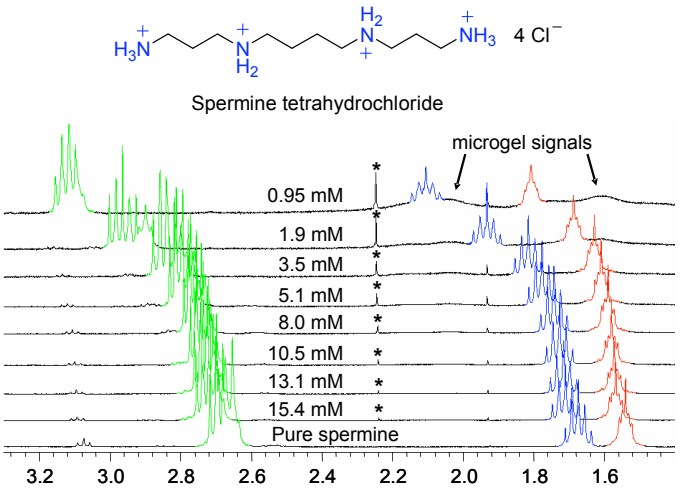

Figure 2. ^{1}H NMR titration of a spermine tetrahydrochloride stock solution into a microgel solution in aqueous phosphate buffer (pD 7.4, 0.15 M KCl). Complexation-induced shifts can be seen as evidence for binding. Concentrations refer to the spermine concentration in the spermine–microgel mixture. The ^{1}H NMR spectrum of pure spermine in pD 7.4 buffer in the absence of microgel is shown at the bottom for comparison. The asterisk marks the signal of an acetone impurity.

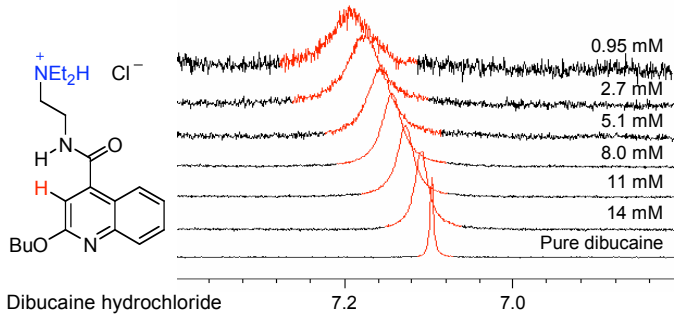

Figure 3. ^{1}H NMR titration of a dibucaine hydrochloride stock solution into a microgel solution in an aqueous phosphate buffer (pD 7.4, 0.15 M KCl). The 3-H singlet of dibucaine (labelled in red) shows a significant degree of line broadening, as well as a complexation-induced shift.

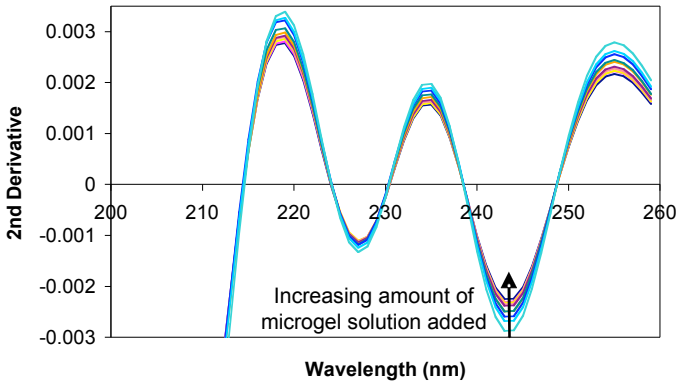

Figure 4. Second derivative UV titration of a microgel stock solution (20 mg/mL, 0–350 μL) added into an aqueous solution of dibucaine at pH 7.4 (phosphate buffer, 0.15 M KCl). The dibucaine concentration in both solutions was kept constant at 5×10^{-5} M.

Figure 2 is an example of a typical ^{1}H NMR titration of microgel and ligand. The complexation-induced shifts seen for the spermine signals is indicative of binding. Figure 3 shows the line broadening observed for dibucaine. When ^{1}H NMR measurements were repeated at pD 9.4, line-broadening of spermine and spermidine were no longer observed, indicating that protonation of the amine groups was essential for the overall binding event. It was therefore postulated that the interaction was dominated by electrostatic interactions and was occasionally helped, as in the case of dibucaine, by additional hydrophobic interactions.

Ion-exchange was ruled out as the main driving force responsible for binding, by titrating the microgel solution with a tetramethylammonium salt and a benzamidinium salt, the latter being capable of H-bonding but known to bind poorly to tetrazoles. In both cases, neither complexation-induced shifts nor line broadening was observed.

Analysis of the supramolecular interactions by UV spectroscopy was complicated by the size of the microgels that resulted in strong light scattering around 200 nm. To overcome this, second derivative spectroscopy was used to cancel out the light scattering effect and to further refine the spectrum so that the changes in the absorption could be more easily identified. Clear isosbestic points are thus revealed and indicate the presence of bound dibucaine at a typical UV concentration (Figure 4).

Binding was confirmed by microcalorimetry measurements of the spermine–microgel interaction in aqueous 0.1 M morpholine *N*-propanesulfonate buffer (pH 7.15). After correcting the titration data for dilution and fitting to an n : 1 binding model, an estimate for the binding constant of about 700 M^{-1} was obtained, and n was found to be close to the value expected for four tetrazoles per binding site.

Conclusions

Supramolecular binding of protonated amines has been observed between a tetrazole-containing microgel system and several amine ligands. ^{1}H NMR spectroscopy and microcalorimetry measurements gave evidence of binding at millimolar concentrations, with UV titrations indicating the presence of small number of binding sites with higher affinities. Work is currently underway to improve the supramolecular binding of small host molecules to suitably designed microgels and to introduce selectivity into the system.

Acknowledgement. We thank Dr Alan Boyd for NMR measurements, Dr Jim Buckman for SEM measurements, Dr Andreas Taden for light-scattering measurements, Dr Xiulan Xie (University of Marburg) for NMR diffusion measurements and the School of Engineering & Physical Sciences at Heriot-Watt University for financial support.

References

(1) Brazel, C. S.; Peppas, N. A.; *Macromolecules*, **1995**, *28*, 8016.
(2) Kiser, P.; Wilson, G.; Needham, D. *Nature* **1998**, *394*, 459.
(3) Fischer, N. O.; McIntosh, C. M.; Simard, J. M.; Rotello, V. M. *Proc. Natl. Acad. Sci. U.S.A.* **2002**, *99*, 5018.
(4) You, C.; De, M.; Rotello, V. M. *J. Am. Chem. Soc*. **2005**, *127*, 12873.
(5) Renner, C.; Piehler, J.; Schrader, T. *J. Am. Chem. Soc.* **2006**, *128*, 620.
(6) Wulff, G. *Chem. Rev.* **2002**, *102*, 1.
(7) Taden, A.; Tait, A. H.; Kraft, A. J. *Polym. Sci., Polym. Chem. Ed*. **2002**, *40*, 4333.
(8) Wu, X. Y.; Lee, P. I. *Pharm. Res*. **1993**, *10*, 1544.
(9) Tominey, A. F.; Docherty, P. H.; Rosair, G. M.; Quenardelle, R.; Kraft, A. *Org. Lett*. **2006**, *8*, 1279.

Supramolecular binding of protonated amines to a receptor microgel in aqueous medium†

Alan Tominey, David Andrew, Lewis Oliphant, Georgina M. Rosair, Juliette Dupré and Arno Kraft*

Received (in Cambridge, UK) 27th March 2006, Accepted 21st April 2006
First published as an Advance Article on the web 3rd May 2006
DOI: 10.1039/b604393c

Polyanionic microgels containing negatively charged tetrazole binding sites show supramolecular binding of various protonated amines (*e.g.* dibucaine and spermine) in a competitive aqueous medium at millimolar concentration.

Microgels are sponge-like microparticles around 0.1–10 μm in size that swell in a good solvent. Their response often takes less than a second following a change in chemical surroundings (temperature, pH, ionic strength), whereas slab gels tend to respond much more slowly, over hours or days, to reach swelling equilibrium. Although microgels are highly crosslinked polymers, they form colloidal 'solutions' in a good solvent. Intrinsic viscosities of 'water-soluble' microgels are generally low even if the gel is highly charged, and so differ considerably from ordinary polyelectrolytes. Their small size—similar to that of viruses—permits microgels to travel in the bloodstream, which makes them potentially useful in drug delivery and controlled drug release. For example, the release of doxorubicin (an anticancer drug with a single amine group that is protonated at physiological pH) from a lipid-coated polyanionic microgel can be controlled by stimulation with an electrode.[1,2] Microgels have attracted considerable interest in many areas of chemistry over recent years. It is widely recognised that their structural properties and ability to quickly respond to environmental stimuli could be applied in biomedicinal fields.[3,4].

The use of microgels is not purely limited to the temporary physical loading of a drug within a polymer network, a process that relies on the swelling kinetics to trap and release the confined molecules. We anticipated that the incorporation of a monomer with a suitable recognition group could, in fact, afford a polymeric supramolecular receptor with multiple binding sites in the polymer network. In such a host–guest system, the microgel would act as the host and small molecules as the guests, while the choice of recognition group could impart some selectivity for a target guest.

To date, a number of methods have been put forward suggesting polymers as potential supramolecular receptors. Nature already makes extensive use of antibodies and enzymes for the molecular recognition of small molecules, as well as to instigate a plethora of chemical reactions. Molecular imprinting, introduced by Wulff over 30 years ago, is a technique where a monomer is polymerised in the presence of a crosslinker, a template and a porogen.[5] The technique generates crosslinked polymer particles that, after extraction of the template, contain pores resembling an imprint of the template. Molecularly imprinted polymers mimic some of the characteristics of biological supramolecular receptors. Although highly successful for chromatographic separations, the standard molecular imprinting procedure produces insoluble polymer networks. For a polymeric supramolecular receptor, the largest hurdle which has yet to be overcome is the insolubility that imprinted polymer networks display in an aqueous medium.[6] Several reports have suggested an extension of the molecular imprinting concept to microgels.[7–9] However, re-binding of the template generally required organic (co-)solvents and did not work in water, a highly polar and competitive solvent. In almost all cases, a co-solvent such as methanol was essential, and most studies tended to focus on ligands with low intrinsic aqueous solubility.[10]

We present our initial results obtained with a 'water-soluble' polyanionic microgel that possessed the ability to bind various protonated amines (such as the local anaesthetic dibucaine, the β-blocker propranolol, and the oligoamines spermidine and spermine)—*in water at pH 7 and at an ionic strength of 0.15 M*.

N-Isopropylacrylamide, NIPAM (**1**; Scheme 1), was chosen as the major component of a supramolecular receptor microgel because of the wealth of literature available on the properties of NIPAM-based polymers. In addition, the monomer imparts amide groups along the polymer chain—reminiscent of the peptide backbone of proteins. Poly-NIPAM possesses a lower critical solution temperature (LCST) of 32 °C. Below the LCST, the polymer is water-soluble, whereas above the LCST it precipitates from an aqueous solution. Microgels based on NIPAM will precipitate likewise above their LCST.

N,*N*′-Methylenebis(acrylamide), **2**, served as crosslinker in the preparation of the microgel. It is also an acrylamide and its incorporation into a poly-NIPAM network preserves the polymer's environmentally sensitive nature.

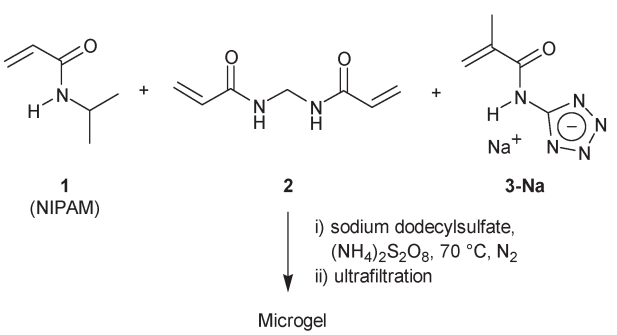

Scheme 1 Synthesis of a poly-NIPAM based microgel.

Chemistry, School of Engineering and Physical Sciences, Heriot-Watt University, Edinburgh, UK EH14 4AS. E-mail: a.kraft@hw.ac.uk; Fax: 44 131 451 3180; Tel: 44 131 449 5111

† Electronic supplementary information (ESI) available: Additional ^{1}H NMR, light-scattering, SEM, copolymerisation, microcalorimetry and crystal structure data. See DOI: 10.1039/b604393c

 This journal is © The Royal Society of Chemistry 2006

Tetrazole-containing monomer **3-Na**[11] was the third component and introduced negatively charged binding sites for cationic ligands. Tetrazoles have pK_a values similar to carboxylic acids but are generally more lipophilic. The bioisosteric replacement of a carboxylic acid functional group by a tetrazole is a well-known concept in modern drug design.[12] We chose tetrazole-containing monomer **3** (pK_a 4.5) because of its easy synthetic access and binding properties. The charge distribution of a tetrazole over a larger molecular surface area is considered to be an advantage for an H-bond donor in drug binding and supramolecular chemistry.[13,14] The crystal structure of a 4 : 1 model complex between monomer **3** and spermine (**4**) illustrates this clearly (Fig. 1) and shows each spermine NH being hydrogen-bonded to a tetrazole nitrogen.‡ In addition, the terminal spermine NH groups are involved in bifurcated H-bonds to nearby carbonyl oxygens of the methacrylamide monomer. Incorporation of a tetrazole functionality into a NIPAM-based microgel was therefore expected to create binding sites superior to those found in previously reported methacrylic acid-based microgels.[2] Moreover, whilst methacrylic acid has been the preferred comonomer for most NIPAM-based microgels reported in the literature, its copolymerisation with NIPAM is characterised by unfavourable reactivity ratios differing by three orders of magnitude. As a result, the integration of the crucial binding sites is delayed towards the late stages of the polymerisation and is difficult to control.[15] In contrast, the reactivity ratios of **3-Na** and NIPAM are close to an ideal copolymerisation (see ESI) and therefore allow a statistical distribution of key binding sites into the polymer network.

Microgels were prepared by radical polymerisation of **1** (*ca.* 80–84 mol%), **2** (10 mol%) and **3-Na** (*ca.* 6–10 mol%) at 70 °C in dilute aqueous solution, using ammonium persulfate as initiator and sodium dodecylsulfate as dispersant (Scheme 1).[16] The LCST of the microgel causes the microgel to precipitate during the polymerisation and thus helps to instill a measure of control over the final size of the polymer particles, narrowing their size distribution at the same time. The dilute microgel solution was purified and concentrated by ultrafiltration against deionised water, using cross-flow membranes with a molecular weight cut-off of 100,000 g/mol. The microgels were finally isolated as solids after freeze-drying.

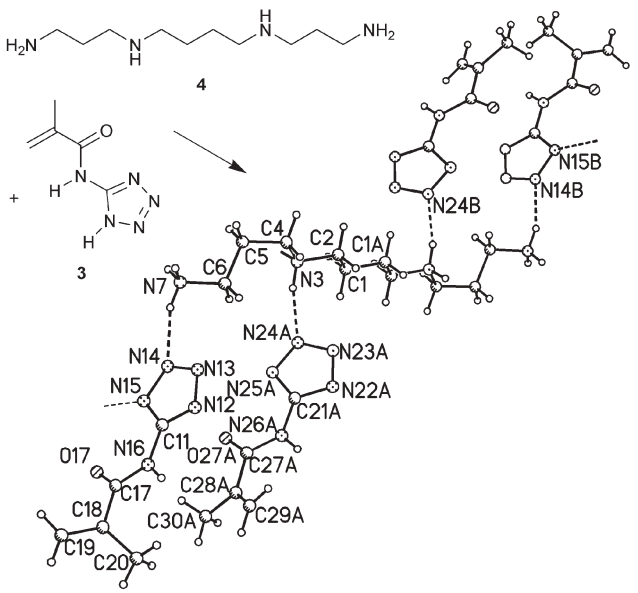

Fig. 1 Perspective view of the model compound (from spermine **4** and monomer **3**) which lies on a centre of inversion. Dotted lines indicate hydrogen bonds. Atoms labelled A are generated by the symmetry code: +x, 0.5 − y, 0.5 + z; and those labelled B: 2 − x, 1 − y, 1 − z.

The hydrodynamic radius of the microgel was determined by light scattering in solution, with the size distribution exhibiting a peak at 0.28 μm. Although additional peaks were observed at higher radii, these were thought to originate mainly from aggregation of microgel particles in solution; such large aggregates and macroscopic gel particles were readily removed by filtration of the aqueous microgel mixture through a 0.45 μm membrane filter. While this procedure was likely to eliminate the large-particle part of the size distribution, it greatly improved the solubility of the residual microgel fraction. Scanning electron microscopy (SEM) of the microgel before filtration revealed microgel particles with sizes in the 0.2–0.3 μm (Fig. 2) range in agreement with the light-scattering results. ^{1}H NMR spectra of the microgels confirmed the absence of low-molar-mass impurities, suggesting that ultrafiltration was an efficient way of purifying microgels. The microgels gave clear solutions in water.

^{1}H NMR spectroscopy was used to investigate the supramolecular binding of amines to the microgel. Evidence of binding came from complexation-induced shifts and line broadening of the ligand's NMR signals. Complexation-induced shifts refer to a change in the chemical shift of the host/guest system when binding occurs under fast exchange on the NMR time scale. The observed chemical shift is then a weighted average of the free and bound species in the system. To ensure that signal shifts during the NMR titration were not the result of changes in pD, binding studies were carried out in a pD 7.4 buffer (at 0.15 M ionic strength). Fig. 3 depicts how the signals for spermine (**4**), a tetraamine that is almost completely protonated at neutral pH (90.6% at pH 7.0), shift by over 0.3 ppm with increasing microgel-to-spermine ratio.

Line broadening of the NMR signals of the ligand is a further indication of binding—provided that contributions from other factors such as shimming errors and high viscosity can be ruled out.[17] When a low-molar-mass ligand interacts with a protein or a polymer, it takes on the macromolecule's lower tumbling rate, coinciding with a broadening of the NMR signal. While line broadening was observed for a range of compounds (*e.g.* propranolol, spermidine, see ESI), it was most noticeable for dibucaine (**5**). Fig. 4 shows the line broadening of dibucaine's aromatic 3-H signal in D_2O at pD 7.4. Like complexation-induced shifts, the extent of line broadening depends on concentration,

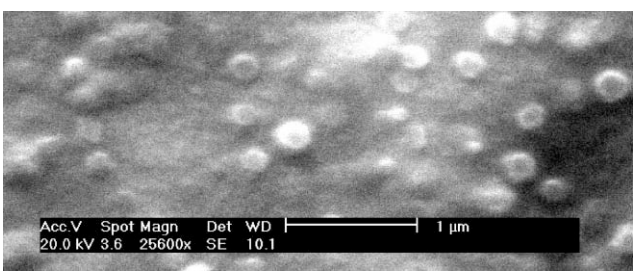

Fig. 2 SEM image showing the spherical shape of microgel particles and their narrow size distribution (typical diameter *ca.* 0.2–0.3 μm).

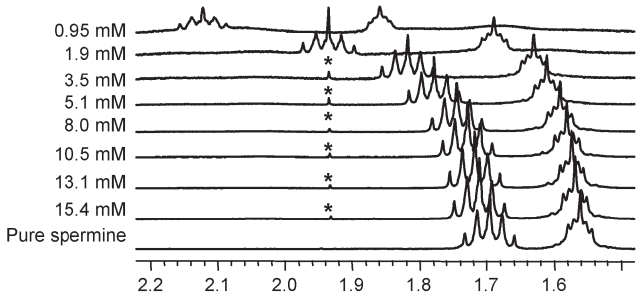

Fig. 3 ^{1}H NMR (400 MHz, D_2O, pD 7.4) spectra, obtained after adding increasing amounts of spermine (**4**) tetrahydrochloride to a microgel solution (3 mg/0.7 mL), show complexation-induced shifts of spermine signals characteristic of binding. With a content of approx. 8 mol% **3-Na** in the microgel, the concentrations correspond to spermine-to-tetrazole molar ratios of 0.4 : 1 to 7 : 1. The ^{1}H NMR spectrum of pure spermine in pD 7.4 buffer recorded in the absence of microgel is displayed for comparison. The signals of acetone impurities are marked by asterisks.

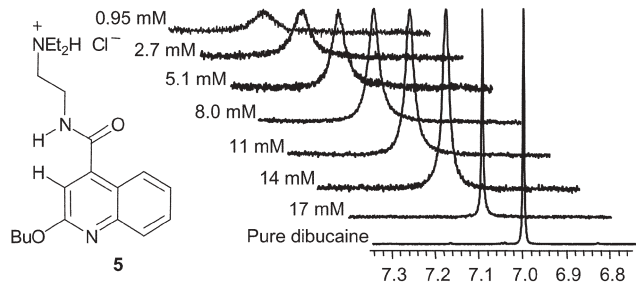

Fig. 4 Line broadening of the NMR signal of dibucaine's aromatic 3-H proton is evident in the presence of the microgel (2.2 mg/0.7 mL) at millimolar dibucaine concentrations.

with the maximum line broadening being again observed in the millimolar range.

When ^{1}H NMR measurements were repeated at pD 9.4, line-broadening of dibucaine and spermine was no longer observed. Protonation of the amine groups was thus deemed to be essential for binding. Therefore the polymer–ligand interactions were not purely hydrophobic interactions but involved a largely electrostatic component. In order to rule out a simple ion-exchange process as the main driving force responsible for binding, we repeated the NMR measurements with a tetramethylammonium salt (which is unable to hydrogen bond but capable of ion exchange) and a benzamidinium salt[14] capable of H-bonding but known to bind poorly to tetrazoles. In both cases, neither line broadening nor complexation-induced shifts were observed (see ESI).

The binding constant of the spermine–microgel interaction was determined by isothermal titration calorimetry in H_2O containing 0.1 M morpholine *N*-propanesulfonate buffer (pH 7.15). Positive values for both ΔH (3.2 kJ mol^{-1}) and $T\Delta S$ (19.2 kJ mol^{-1}) account for an endothermic, entropy-driven process. This is indicative of water being released in the binding step.[18] Similar, large endothermic binding processes are well known for protein–ligand systems when a rearrangement or closure of the binding site is necessary.[19] The flexible structure of the microgels demands some degree of rearrangement upon binding to a ligand, which helps to explain why the binding of spermine is dominated by an entropic contribution. The data were corrected for dilution and, when fitted to an n : 1 binding model, gave an estimate for the binding constant of about 700 M^{-1}, with n being close to the value expected for four tetrazoles per binding site.

In conclusion, our results demonstrated binding of various protonated amines to a tetrazole-containing anionic receptor microgel in a competitive aqueous environment. ^{1}H NMR spectra gave evidence of line broadening and complexation-induced shifts at millimolar concentrations in aqueous solution. This was backed up by microcalorimetric data. Work is currently underway to enhance the microgel's binding affinity and to introduce selectivity by using a suitable templating (molecular imprinting) technique.

We thank Andrew McIver (experimental help), Dr Alan Boyd (NMR), Dr Jim Buckman (SEM), Dr Andreas Taden (light-scattering), Dr Sijbren Otto (microcalorimetry), and the School of Engineering & Physical Sciences at Heriot-Watt University (financial support).

Notes and references

‡ *Crystal data* for model complex: Single crystal X-ray diffraction data were collected on $C_{10}H_{30}N_4{\cdot}4(C_5H_6N_5O)$ with an Oxford Diffraction Xcalibur2 diffractometer with Mo Kα radiation at 120 K. Crystal dimensions: 0.08 × 0.03 × 0.03 mm^3, M = 814.91, monoclinic, $P2_1/c$, a = 11.1364(14) Å, b = 13.482(2) Å, c = 14.299(2) Å, β = 110.275(12)°, V = 2013.8(5) Å^3, Z = 4, 10445 reflections collected; 1959 independent [R_{int} = 0.0707]. Final R indices [$I > 2\sigma(I)$, 1513 data]: $R1$ = 0.1029, w$R2$ = 0.1967; R indices (all data), $R1$ = 0.1461, w$R2$ = 0.2167. Refinement with SHELXTL. No observed intensity beyond θ = 20° because of the small weakly diffracting nature of the crystals so completeness to θ = 22.32° was only 76.1%. CCDC 603033. For crystallographic data in CIF or other electronic format see DOI: 10.1039/b604393c

1 P. Kiser, G. Wilson and D. Needham, *Nature*, 1998, **394**, 459.
2 G. M. Eichenbaum, P. Kiser, A. Dobrynin, S. Simon and D. Needham, *Macromolecules*, 1999, **32**, 4867.
3 R. H. Pelton, *Adv. Colloid Interface Sci.*, 2000, **85**, 1.
4 N. A. Peppas, *Adv. Drug Delivery Rev.*, 2005, **56**, 1529.
5 G. Wulff, *Angew. Chem., Int. Ed. Engl.*, 1995, **34**, 1812.
6 P. Pasetto, S. C. Maddock and M. Resmini, *Anal. Chim. Acta*, 2005, **542**, 66.
7 L. Ye, P. A. G. Cormack and K. Mosbach, *Anal. Chim. Acta*, 2001, **435**, 187.
8 A. Biffis, N. B. Graham, G. Siedlaczek, S. Stalberg and G. Wulff, *Macromol. Chem. Phys.*, 2001, **202**, 163.
9 D. Vaihinger, K. Landfester, I. Kräuter, H. Brunner and G. E. M. Tovar, *Macromol. Chem. Phys.*, 2002, **203**, 1965.
10 A. Weber, M. Dettling, H. Brunner and G. E. M. Tovar, *Macromol. Rapid Commun.*, 2002, **23**, 824.
11 A. Taden, A. H. Tait and A. Kraft, *J. Polym. Sci., Polym. Chem.*, 2002, **40**, 4333.
12 R. J. Herr, *Bioorg. Med. Chem.*, 2002, **10**, 3379.
13 C. Biot, H. Bauer, R. H. Schirmer and E. Davioud-Charvet, *J. Med. Chem.*, 2004, **47**, 5972.
14 L. Peters, R. Fröhlich, A. S. F. Boyd and A. Kraft, *J. Org. Chem.*, 2001, **66**, 3291.
15 W. Xue, S. Champ and M. B. Huglin, *Polymer*, 2000, **41**, 7575.
16 X. Y. Wu and P. I. Lee, *Pharm. Res.*, 1993, **10**, 1544.
17 C. Dalvit, M. Flocco, S. Knapp, M. Mostardini, R. Perego, B. J. Stockman, M. Veronesi and M. Varasi, *J. Am. Chem. Soc.*, 2002, **124**, 7702.
18 R. C. Yadav, G. S. Kumar, K. Bhadra, P. Giri, R. Sinha, S. Pal and M. Maiti, *Bioorg. Med. Chem.*, 2005, **13**, 165.
19 G. Maksay, *Neurochem. Int.*, 2005, **46**, 281.

 This journal is © The Royal Society of Chemistry 2006

Microgels and linear polymers as polymeric supramolecular receptors for proteins

Alan Tominey, Julia Liese, Douglas Ewen and Arno Kraft

Chemistry, School of Engineering and Physical Sciences, Heriot-Watt University, Edinburgh EH14 4AS, United Kingdom.

INTRODUCTION

Molecular recognition in aqueous solutions remains an important challenge in supramolecular chemistry. Recent developments have seen our understanding of the interactions of macromolecular receptors with a wide variety of ligands grow. Molecularly imprinted polymers, originally developed by Wulff in 1972, have been a key area of growth in this field; many uses have been postulated for these materials from areas as diverse as catalysis[1] and in medicinal chemistry.[2] Mosbach and co-workers have described the elegant synthesis of molecularly imprinted nanoparticles which selectively bind propranolol; the observed binding sites even distinguish between the (*S*) and (*R*) enantiomers.[3] Since Kiser et al. reported the synthesis of an artificial secretory granule, there has also been a wealth of research into the use of microgels mainly as drug delivery vectors,[4] less so for molecular imprinting and molecular recognition. In the field of protein recognition, similarly using synthetic polymers, substantial progress has been made towards the selective recognition of proteins with high affinity in an aqueous environment. Schrader et al. have reported irreversible binding of highly charged linear polymers to basic proteins like histone and ferritin in aqueous buffer using bisphosphonate monomer **4** (Figure 1).[5] Rotello et al have shown Gold and cadmium/selenium nanoparticles coated with polymer chains bind to chymotrypsin, inhibiting the enzymes catalytic behavior.[6]

Microgels are highly crosslinked discrete polymeric particles that swell in a good solvent environment and have a size in the submicrometer range (*ca* 0.1 μm to several μm). They are usually prepared by dilute aqueous radical polymerization with a high crosslinker-to-monomer ratio; this gives rise to a spongy spherical polymer with an inhomogeneous internal structure.[7] It is the similarity of this structure to the properties displayed by globular proteins such as enzymes and antibodies that has sparked a growing interest in the possibility of designing an easily synthesized and cheap alternative to these highly specific biological materials.

The combination of microgels with the new family of environmentally sensitive polymers that has been emerging over the past few decades has been showing promise for use in areas of research and development that are trying to mimic or enhance the behaviour of biological materials. [8, 9]

We have previously demonstrated that microgels have affinity to low-molecular-weight pharmaceutical drugs such as dibucaine, propranolol and chloroquine in a competitive aqueous environment.[10] So far the interactions of microgels with larger biological molecules like proteins remains largely unexplored.

It is the aim of this paper to introduce microgels that bind to proteins such as cytochrome C and haemoglobin in serum-like conditions. High affinity and selectivity are attainable by fine-tuning the composition of the polymers. In particular the choice of anionic binding sites and the inclusion of hydrophobic groups can drastically improve the binding strength of the polymers. Examples in the literature concentrate on carboxylic acid functional groups and phosphonates, being used to create non-covalent host-guest interactions.[11] Inclusion of hydrophobic groups such as *N*-alkyl and *N*-cyclohexyl acrylamide into the polymer chains serves to mimic protein receptors where Nature makes use of, not only, electrostatic interactions but also of hydrophobic attractions between nonpolar domains[12] which is indeed the driving force between many of the higher order protein structures i.e. α-helices, β-sheets and tertiary structures.

EXPERIMENTAL

Materials. All chemicals and reagents were purchased from commercial suppliers and were used without further purification. Monomer **2** and **4** were made as described previously.[13, 5]

Instrumentation. ^{1}H NMR spectra in D_2O were obtained with a Bruker DPX 400 spectrometer. Ultrafiltration was carried out using a Masterflex 7518-00 peristaltic pump with a Vivaflow 50 PES filter (nominal molecular-weight cut-off, MWCO, of 100,000) and further refinement was carried out using a Vivaflow 50 PES filter (nominal pore size 0.2 μm).

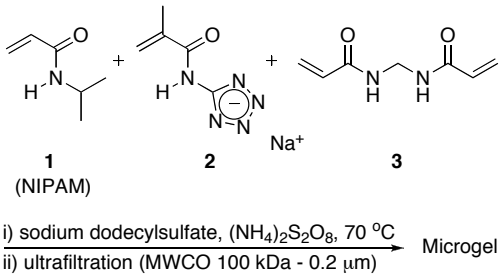

Scheme 1. Synthesis of a NIPAM-based microgel.

Preparation. In a typical microgel synthesis, NIPAM (1.13 g, 10 mmol), monomer **2** (0.14 g, 0.8 mmol) and *N*,*N*'-methylenebis(acrylamide) (**3**) (0.15 g, 1 mmol) were dissolved in deionized water (200 mL) along with sodium dodecylsulfate (60 mg, 0.2 mmol). The mixture was heated to 70 °C and degassed with N_2 for 15 minutes. Ammonium persulfate (60 mg, 0.5 mmol) was added and the reaction was stirred overnight at 70 °C. After cooling to room temperature, the microgel solution was purified by ultrafiltration against 2 L of deionized water, concentrated in a vacuum, and freeze-dried.

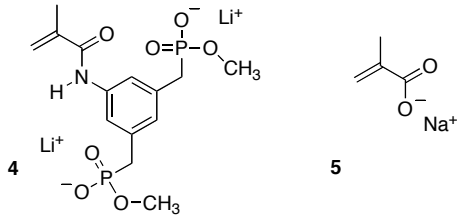

Figure 1. Alternative negatively charged functional groups can be introduced by substituting monomer **2** with either bisphosphonate (**4**) or sodium methacrylate (**5**).

RESULTS AND DISCUSSION

Microgels were prepared by precipitation polymerization[14] of a mixture containing about 80–84 mol% of NIPAM (**1**), 6–10 mol% of monomer **2**, and 10 mol% of crosslinker **3** in dilute aqueous solution in the presence of a radical initiator and a detergent (Scheme 1). Tetrazole monomer **2** was chosen because it is ionized at neutral pH. In addition, there are strong indications that negatively charged tetrazolates have a preference to bind to protonated amines.[15] The microgel solution was purified and concentrated by ultrafiltration against deionized water, using a cross-flow membrane with a molecular weight cut-off of 100 kDa. Aggregates and macroscopic gel particles were subsequently removed through further filtration across a cross-flow membrane with a nominal pore size of 0.2 μm. The microgel was finally isolated as a highly soluble white solid after freeze-drying.

UV titrations were used to probe the binding interactions of the microgels with selected proteins. The second derivative UV spectra display clear isosbestic points that provide evidence towards supramolecular binding of the proteins. Since standard UV absorption spectra showed significant light scattering effects (Figure 2) the second derivative of the absorbance was calculated using the Savitsky-Golay algorithm.[16, 17] The second derivative is a useful method of refining the spectra to a point where subtle changes in the UV absorption plot become clear (Figure 3).

By changing the anionic monomer in the reaction mixture it was found that the affinity for certain proteins increased. Methacrylate-containing polymers bind almost exclusively to cytochrome C at UV concentrations. Figure 4 shows that both the tetrazole microgel and bisphosphonate microgel display very little affinity to cytochrome C whilst the methacrylate gives a hyperbolic curve typical of supramolecular binding.

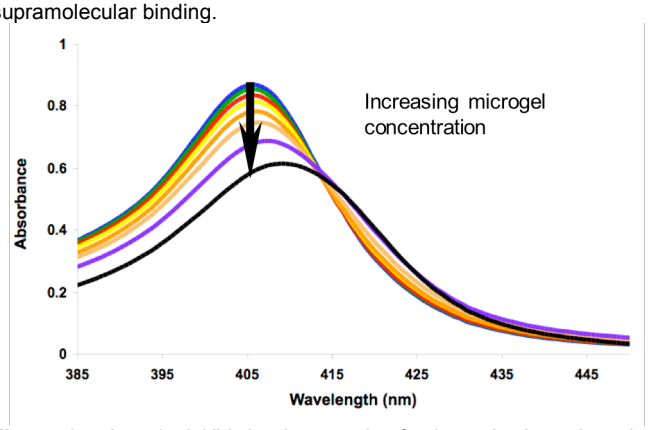

Figure 2. A typical UV titration graph of microgels titrated against haemoglobin. Light scattering effects can be clearly seen towards the smaller wavelengths as interference distorts the baseline.

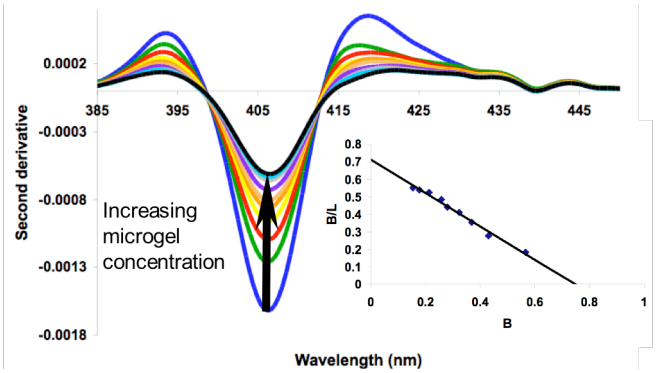

Figure 3. Second derivative spectrum of haemoglobin ($2.2*10^{-6}$ mol/L) titrated with microgel solution at pH 7 (0.15 mol/L KCl). The second derivative has been calculated using the data shown in Figure 2. Insert shows Scatchard plot indicating binding behaviour.

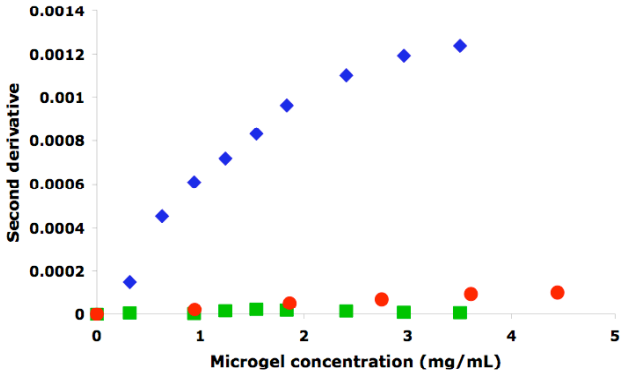

Figure 4. Normalized comparison UV titration of equine cytochrome C ($1.02*10^{-5}$ mol/L) against microgels with different anionic functional groups; methacrylate, **5**, (♦), bisphosphonate monomer, **4**, (●) and tetrazolate, **2**, (■).

The tetrazole-based microgels bind instead exclusively to haemoglobin at UV concentrations and display very little affinity to cytochrome C, ferritin or albumin. This selectivity was unexpected as both cytochrome C and haemoglobin have basic pIs and are both relatively rich in lysine residues.[18, 19] Further to this; cytochrome C has an almost even distribution of basic residues over a relatively small surface area.[5] Taking this into consideration, if the supramolecular interactions between the microgel and the proteins were purely based on electrostatic interactions, then cytochrome C would be expected to bind to both tetrazole containing microgels and methacrylate-based microgels.

Monomers **2**, **4**, and **5** were also incorporated into linear polymers using RAFT polymerization.[20] RAFT polymerization is an effective method for giving monodisperse polymers with defined molecular weight. This is beneficial in the search for accurate association constants. The selectivity observed with the microgels was maintained with the linear RAFT polymers.

CONCLUSION

Supramolecular binding of proteins to microgels was observed at UV concentrations. Selectivity is observed by inclusion of several anionic monomers. The unexpected selectivity is an indication of a more complex interaction between the macromolecules and the guest proteins.

ACKNOWLEDGEMENTS

We would like to thank Professor Thomas Schrader for the gift of a bisphosphonate monomer and the School of Engineering & Physical Sciences at Heriot-Watt University for financial support.

REFERENCES

1. Wulff, G. *Chem. Rev.* **2002**, *102*, 1.
2. Wulff, G. *Angew. Chem. Int. Ed.* **1995**, *34*, 1812.
3. Yoshimatsu, K.; Reimhult, K.; Krozer, A.; Mosbach, K.; Sode, K.; Ye, L. *Anal. Chim. Acta* **2007**, *584*, 112.
4. Kiser, P.; Wilson, G.; Needham, D. *Nature* **1998**, *394*, 459.
5. Renner, C.; Piehler, J.; Schrader, T. *J. Am. Chem. Soc.* **2006**, *128*, 620.
6. Hong, R.; Fischer, N. O.; Verma, A.; Goodman, C. M.; Emrick, T.; Rotello, V. M. *J. Am. Chem. Soc.* **2004**, *126*, 739.
7. Stieger, M. *J. Chem. Phys.* **2004**, *120*, 6197.
8. Achiha, K.; Ojima, R.; Kasuya, Y.; Fujimoto, K.; Kawaguchi. H. *Polym. Adv. Technol.* **1995**, *6*, 534.
9. Kawaguchi, H. *Front. Biomed. Biotechnol.* **1996**, *3*, 157.
10. Tominey, A.; Andrew, D.; Oliphant, L.; Dupré, J.; Kraft, A. *Chem. Commun.* **2006**, *10*, 2492.
11. Rensing, S.; Schrader, T. *Org. Lett.* **2002**, *4*, 2161.
12. Gitlin, I.; Carbeck, J.D.; Whitesides, G.M. *Angew. Chem. Int. Ed.* **2006**, *45*, 3022.
13. Taden, A.; Tait, A. H.; Kraft, A. *J. Polym. Sci., Polym. Chem. Ed.* **2002**, *40*, 4333.
14. Wu, X. Y.; Lee, P. I. *Pharm. Res.* **1993**, *10*, 1544.
15. Tominey, A. F.; Docherty, P. H.; Rosair, G. M.; Quenardelle, R.; Kraft, A. *Org. Lett.* **2006**, *8*, 1279.
16. Savitzky, A.; Golay, M. J. E. *Anal. Chem.* **1964**, *36*, 1627.
17. Steinier, J.; Termonic, Y.; Deltour, J. *Anal. Chem.* **1972**, *44*, 1906.
18. Banci, L.; Bertini, I.; Gray, H. B.; Luchinat, C.; Reddig, T.; Rosato, A.; Tarano, P. *Biochemistry* **1997**, *36*, 9867.
19. Perutz, M. F.; Fermi, G.; Pogart, C.; Paynier, J.; Krister, J. *J. Mol. Biol.* **1993**, *233*, 536.
20. Mayadunne, R. T. A.; Rizzardo, E.; Chiefari, J.; Kristina, J.; Moad, G.; Postma, A.; Thang, S. H. *Macromolecules* **2000**, *33*, 243.

12 References

[1] Koshland, D. E. *Proc. Natl. Acad. Sci. USA*. **1958**, *44*, 98–104.

[2] Stites, W. E. *Chem. Rev.* **1997**, *97*, 1233-1250.

[3] Larsen, T. A.; Olsen, A. J.; Goodsell, D. S. *Structure* **1998**, *6*, 421-427.

[4] Gitlin, I.; Carbeck, D.; Whitesides, G. M. *Angew. Chem. Int. Ed.* **2006**, *45*, 3022-3060.

[5] Janin, J.; Miller, S.; Chothia, C. *J. Mol. Biol.* **1988**, *204*, 155-164.

[6] Renner, C.; Piehler, J.; Schrader, T. *J. Am. Chem. Soc.* **2006**, *128*, 620-628.

[7] Park, H. S.; Lin, Q.; Hamilton, A. D. *J. Am. Chem. Soc.* **1999**, *121*, 8-13.

[8] Jain, R. K.; Hamilton, A. D. *Org. Lett.* **2000**, *2*, 1721-1723.

[9] Baldini, L.; Wilson, A. J.; Hong, J.; Hamilton, A.D. *J. Am. Chem. Soc.* **2004**, *126*, 5656-5657.

[10] Pasetto, P.; Maddock, S. C.; Resmini, M. *Anal. Chim. Acta* **2005**, *542*, 66-75.

[11] Wulff, G. *Angew. Chem., Int. Ed. Engl*. **1995**, *34*, 1812-1832.

[12] Wulff, G. *Chem. Rev.* **2002**, *102*, 1-27.

[13] Turner, N. W.; Jeans, C. W.; Brian, K. R.; Allender, C. J.; Hlady, V.; Britt, D. W. *Biotechnol. Prog.* **2006**, *22*, 1474-1489.

[14] Boal, A. K.; Rotello, V. M. *J. Am. Chem. Soc.* **1999**, *121*, 4914-4915.

[15] Boal, A. K.; Rotello, V. M. *J. Am. Chem. Soc.* **2000**, *122*, 734-735.

[16] Bayraktar, H.; You, C. C.; Rotello, V. M.; Knapp, M. J. *J. Am. Chem. Soc.* **2007**, *129*, 2732-2733.

[17] You, C. C.; De, M.; Rotello, V. M. *Org. Lett.* **2005**, *7*, 5685-5688.

[18] Atkins, P. W. *Physical Chemistry,* 3rd Edition, **1986**, Oxford University Press.

[19] Funke, W.; Okay, O.; Joos-Muller, B. *Adv. Polym. Sci*. **1998,** *136*, 139-234.

[20] Frank, R.; Downey, J.; Yu, K.; Stover, H. *Macromolecules* **2002**, *35*, 2728-2735.

[21] Ishikura, S.; Ishii, K.; Midzuguchi, R. *Prog. Org. Coat.* **1988**, *15*, 373-387.

[22] Kiser, P.; Wilson, G.; Needham, D. *Nature* **1998**, *394*, 459.

[23] Zhu, P.; Napper, D. *Macromolecules* **1999**, *32*, 2068-2070.

[24] Grohn, F.; Antonietti, M. *Macromolecules* **2000**, *33*, 5983-5949.

[25] Stiger, M. *J. Chem. Phys.* **2004**, *120*, 6197.

[26] Wu, X.; Pelton, R.; Hamielec, A.; Woods, D.; McPhee, W. *Colloid Polym. Sci*. **1994**, *272*, 467.

[27] Saunders, B. *Langmuir* **2004**, *20*, 3925-3932.

[28] Varga, I.; Gilanyi, T.; Meszaros, R.; Filipcsei, G.; Zrinyi, M. *J. Phys. Chem. B* **2001**, *105*, 9071-9076.

[29] Gilanyi, T.; Varga, I.; Meszaros, R.; Filipcsei, G.; Zrinyi, M. *Phys. Chem. Chem. Phys.* **2000**, *2*, 1973-1977.

[30] Quadrat, O.; Snuparek, J. *Prog. Org. Coat.* **1990**, *18*, 207.

[31] Pelton, R.; Chibante, P. *Colloids Surf.* **1986**, *20*, 247.

[32] McPhee, W.; Tam, K.; Pelton, R. *J. Colloid Interface Sci.* **1993**, *156*, 24.

[33] Peppas, N. *Adv. Drug Deliv. Rev*., **2005**, *56*, 1529.

[34] Kost, J.; Langer, R. *Adv. Drug Del. Rev.* **1991**, *6*, 19-50.

[35] Kost, J.; Langer, R. *Adv. Drug Del. Rev*. **2001**, *46*, 125-148.

[36] Missirlis, D.; Kawamura, R.; Tirelli, N.; Hubbell, J. A. *Eur. J. Pharm. Sci.* **2006**, *29*, 120-129.

[37] Bromberg, L.; Temchenko, M.; Hatton, T. *Langmuir* **2002**, *18*, 4944-4952.

[38] Lackey, C.; Press, O.; Hoffman A.; Stayton, P. *Bioconjugate Chem*. **2002**, *13*, 996.

[39] Brazel, C.; Peppas, N. *Macromolecules* **1995**, *28*, 8016-8020.

[40] Yin, X.; Hoffman, A.; Stayton, P. *Biomacromolecules* **2006**, *7*, 1381-1385.

[41] Lin, C.; Chiu, W.; Lee, C. *J. Polym. Sci., Part A: Polym. Chem*. **2006***, 44*, 356-370.

[42] Xue, W.; Champ, S.; Hughlin, M. B. *Polymer* **2000**, *41*, 7575-7581.

[43] Zhou, S. Q.; Chu, B. *J. Phys. Chem.* **1998**, *B102*, 1364-1371.

[44] Haupt, K.; Mosbach, K. *Chem. Rev.* **2000**, *14*, 163-170.

[45] Alexander, C.; Smith, C. R.; Whitcombe, M. J.; Vulfson, E. N. *J. Am. Chem. Soc.* **1999**, *121*, 6640-6651.

[46] Takeuchi, T.; Murase, N.; Maki, H.; Mukawa, T.; Shinmori, H. *Org. Biomol. Chem.* **2006**, *4*, 565-568.

[47] Pasetto, P.; Maddock, S.; Resmini, M. *Anal. Chim. Acta* **2005**, *542*, 66-75.

[48] Schiller, A.; Scopelliti, R.; Benmelouka, M.; Severin, K. *Inorg. Chem.* **2004**, *44*, 6482-6492.

[49] Benaglia, M.; Pulisi, A.; Cozzi, F. *Chem. Rev.* **2003**, *103*, 3401-3427.

[50] Helmlinger, G.; Sckell, A.; Dellian, M.; Forbes, N. S.; Rakesh, K. J. *Clin. Cancer Res.* **2002**, *8*, 1284-1291.

[51] Trevani, S.; Andonegui, G.; Giodano, M.; Lopez, D.; Gamberale, R.; Minucci, F.; Geffner, J. R. *J. Immunol.* **1999**, *162*, 4849-4857.

[52] Sassi, A. P.; Shaw, A. J.; Han, S. M.; Blanch, H. W.; Prausnitz, J. M. *Polymer*, **1996**, *11*, 2151-2164.

[53] De Geest, B. G.; Stubbe, B. G.; Jonas, A. M.; Van Thienen, T.; Hinrichs, W. L. J.; Demeester, J.; De Smedt, S. C. *Biomacromolecules*, **2006**, *7*, 373-379.

[54] Murthy, N.; Thng, Y. X.; Schuck, S.; Xu, M. C.; Frechet, J. M. J. *J. Am. Chem. Soc.* **2002**, *124*, 12398-12399.

[55] Sheihet, L.; Dubin, R. A.; Devore, D.; Kohn, J. *Biomacromolecules* **2005**, *6*, 2726-2731.

[56] Zhu, H.; McShane, M. *J. Am. Chem. Soc.* **2005**, *127*, 13448-13449.

[57] D'Oleo, R.; Alvarez-Lorenzo, C.; Sun, G. *Macromolecules* **2001**, *34*, 4965-4971.

[58] Hiratani, H.; Alvarez-Lorenzo, C.; Chuang, J.; Guney, O.; Grosberg, A.; Tanaka, T. *Langmuir* **2001**, *17*, 4431-4436.

[59] Haupt, K.; Mosbach, K. *Chem. Rev.* **2000**, *100*, 2495-2504.

[60] Kunz, W.; Belloni, L.; Bernard, O.; Ninham, B. W. *J. Phys. Chem. B* **2004**, *108*, 2398–2404.

[61] Davis, S. J.; Davies, E. A.; Tucknott, M. G.; Jones, E. Y.; van der Merwe, P. A. *Proc. Natl. Acad. Sci.* U.S.A. **1998**, *95*, 5490-5494.

[62] Larsericsdotter, H.; Oscarsson, S.; Buijs, J. *J. Colloid Interface Sci.* 2001, **237**, 98-103.

[63] Giacomelli, C. E.; Norde, W. *J. Colloid Interface Sci.* **2001**, *233*, 234-240.

[64] Kondo, A.; Fukuda, H. *J. Colloid Interface Sci.* **1998**, *198*, 34-41.

[65] Verma, A.; Simard, J. M.; Rotello, V. M. *Langmuir*, **2004**, *20*, 4178-4181.

[66] Yi-Shiun, T.; Fu-Yung, L.; Wen-Yih, C.; Chien-Cheng, L. *Colloids Surf. A: Physiochem. Eng. Aspects* **2002**, *197*, 111-118.

[67] Thompson, M. C.; Busch, D. H. *J. Am. Chem. Soc.* **1962**, *84*, 1669.

[68] Corbett, P. T.; Leclaire, J.; Vail, L.; West, K. R.; Wietor, J. -L.; Sanders, J. K. M.; Otto, S. *Chem. Rev.* **2006**, *106*, 3652-3711.

[69] Corbett, P. T.; Otto, S.; Sanders, J. K. M. *Org. Lett.* **2004**, *6*, 1825-1827.

[70] Corbett, P. T.; Sanders, J. K. M.; Otto, S. *J. Am. Chem. Soc.* **2005**, *127*, 9390-9392.

[71] Furlan, R. L. E.; Otto, S.; Sanders, J. K. M. *J. Am. Chem. Soc.* **2001**, *123*, 8876.

[72] Otto, S.; Furlan, R. L. E.; Sanders, J. K. M. *J. Am. Chem. Soc.* **2000**, *122*, 12063.

[73] Furlan, R. L. E.; Otto, S.; Sanders, J. K. M. *Proc. Natl. Acad. Sci.* U.S.A. **2002**, *99*, 4801-4804.

[74] Vial, L.; Ludlow, R. F.; Leclaire, J.; Perez-Fernandez, R.; Otto, S. *J. Am. Chem. Soc.* **2006**, *128*, 10253-10257.

[75] Hawcroft, D. M. *Electrophoresis: The Basics*, **1997**, Oxford University Press.

[76] Bushnell, G. W.; Louie, G. V.; Brayer, G. D. *J. Mol. Biol.* 1990, **214**, 585-595. Protein composition and chemical parameters were determined using *PROTPARAM*, on the ExPASy Proteomics server, http://www.expasy.ch/.

[77] Paoli, M.; Liddington, R.; Tame, J.; Wilkinson, A.; Dobson, G. *J. Mol. Biol.* **1996**, *256*, 775-792.

[78] Yin, H.; Hamilton, A. D. *Angew. Chem. Int. Ed.* **2005**, *44*, 4130-4163.

[79] Peczuh, M. W.; Hamilton, A. D. *Chem. Rev.* **2000**, *100*, 2479-2494.

[80] DeLano, W. L.; *Curr. Opin. Struct. Biol.* **2002**, *12*, 14-20.

[81] Ma, B. Y.; Elkayam, T.; Wolfson, H.; Nussinov, R. *Proc. Natl. Acad. Sci.* U.S.A. **2003**, *100*, 5772-5777.

[82] Patani, G. A.; LaVoie, E. J. *Chem. Rev.* **1996**, *96*, 3147-3176.

[83] Crenshaw, R. R.; Luke, G. M.; Bialy, G. *J. Med. Chem.* **1972**, *15*, 1179-1180.

[84] Wexler, R. R.; Greenlee, W. J.; Irvin, J. D.; Goldberg, M. R.; Prendergast, K.; Smith, R. D.; Timmermans, P. B. M. W. M. *J. Med. Chem.* **1996**, *39*, 625-656.

[85] Schuster, V. L.; Itoh, S.; Andrews, S. W.; Burk, R. M.; Chen, J.; Kedzie, K. M.; Gil, D. W.; Woodward, D. F. *Mol. Pharmacol.* **2000**, *58*, 1511-1516.

[86] Liljebris, C.; Larsen, S. D.; Ogg, D.; Palazuk, B. J.; Bleasdale, J. E. *J. Med. Chem.* **2000**, *45*, 1785-1798.

[87] Larsen, R. D.; King, A. O.; Chen, C. Y.; Corley, E. G.; Foster, B. S.; Roberts, F. E.; Yang, C.; Lieberman, D. R.; Reamer, R. A.; Tschaen, D. M.; Verhoeven, T. R.; Reider, P. J. *J. Org. Chem.* **1994**, *59*, 6391-6394.

[88] Tuccinardi, T.; Calderone, V.; Rapposelli, S.; Martinelli, A. *J. Med. Chem.* **2006**, *49*, 4305-4316.

[89] Berellini, G.; Cruciani, G.; Mannhold, R. *J. Med. Chem.* **2005**, *48*, 4389-4399.

[90] Noda, K.; Saad, Y.; Kinoshita, A.; Boyle, T. P.; Graham, R. M.; Husain, A.; Karnik, S. S. *J. Biol. Chem.* **1995**, *270*, 2284-2289.

[91] Flower, D. R. *Biochim. Biophys. Acta.* **1999**, *1422*, 207-234.

[92] Boit, C.; Bauer, H.; Schirmer, R. H.; Davioud-Charvet, E. *J. Med. Chem.* **2004**, *47*, 5972-5983.

[93] Wan, Z. K.; Follows, B.; Kirincich, S.; Wilson, D.; Binnun, E.; Xu, W.; Joseph-McCarthy, D.; Wu, J.; Smith, M.; Zhang, Y. L.; Tam, M.; Erbe, D.; Tam, S.; Saiah, E.; Lee, J. *Bioorg. Med. Chem. Lett.* **2007**, *17*, 2913-2920.

[94] Schneider, H. J.; Kramer, R.; Simova, S.; Schneider, U. *J. Am. Chem. Soc.* **1988**, *110*, 6442-6448.

[95] Wilcox, C. S. In *Frontiers in Supramolecular Chemistry and Photochemistry*; Schneider, H. -J., Dürr, H., Eds.; VCH: Weinheim, 1991; pp 123-143.

[96] Macomber, R. S. *J. Chem. Educ.* **1992**, *69*, 375-378.

[97] Job, P. *Ann. Chim.* **1928**, *9*, 113-203.

[98] Blanda, M. T.; Horner, J. H.; Newcomb, M. *J. Org. Chem.* **1989**, *54*, 4626-4636.

[99] Chierotti, M. R.; Gobetto, R. *Chem. Commun.* **2008**, *11*, 1621-1634.

[100] Zablocki, J. A.; Miyano, M.; Rao, S. N.; Panzer-Knodle, S.; Nicholson, N.; Feigen, L. *J. Med. Chem.* **1992**, *35*, 4914-4917.

[101] Lyakhov, A. S.; Voitekhovich, S. V.; Gaponik, P. N.; Ivashkevich, L. S. *Acta Crystallogr. Sect. C* **2003**, *59*, o22-o23.

[102] Deng, Y.; Roberts, J. A.; Peng, S. -M.; Chang, C. K.; Nocera, D. G. *Angew. Chem., Int. Ed. Engl.* **1997**, *36*, 2124-2127.

[103] Kirby, J. P.; van Dantzig, N. A.; Chang, C. K.; Nocera, D. G. *Tetrahedron Lett.* **1995**, *36*, 3477-3480.

[104] Roberts, J. A.; Kirby, J. P.; Nocera, D. G. *J. Am. Chem. Soc.* **1995**, *117*, 8051-8052.

[105] Mahnke, D. J.; McDonald, R.; Hof, F. *Chem. Commun.* **2007**, *36*, 3738-3740.

[106] Tsentovskii, V. M.; Bashkirtseva, V. E.; Evgen'ev, M. I.; Ivanova, Z. P.; Poplavskii, V. S.; Ostrovskii, V. A.; Koldobskii, G. I. *Chem. Hetrocycl. Compd.* **1984**, 1238-1240.

[107] Eichenbaum, G. M.; Kiser, P.; Dobrynin, A.; Simon, S.; Needham, D. *Macromolecules* **1999**, *32*, 4867-4878.

[108] Pelton, R. H. *Adv. Colloid Interface Sci.* **2000**, *85*, 1-33.

[109] Cedervall, T.; Lynch, I.; Lindman, S.; Berggard, T.; Thulin, E.; Nilsson, H.; Dawson, K. A.; Linse, S. *Proc. Natl. Acad. Sci. U.S.A* **2007**, *104*, 2050-2055.

[110] Biffis, A.; Graham, N. B.; Siedlaczek, G.; Stalberg, S.; Wulff, G. *Macromol. Chem. Phys.* **2001**, *202*, 163-171.

[111] Vaihinger, D.; Landfester, K.; Kräuter, I. Brunner, H.; Tovar, G. E. M. *Macromol. Chem. Phys.* **2002**, *203*, 1965-1973.

[112] Perez, N.; Whitcombe, M. J.; Vulfson, E. N. *Macromolecules* **2001**, *34,* 830-836.

[113] Kim, T. H.; Ki, C. D.; Chang, H. C. T.; Chang, J. Y. *Macromolecules* **2005**, *38*, 6423-6428.

[114] Hoare, T.; Pelton, R. *Langmuir* **2004**, *20*, 2123-2133.

[115] Xue, W.; Champ, S.; Huglin, M. B. *Polymer* **2000**, *41*, 7575-?

[116] Arriola, D. J.; Cutie, S. C.; Henton, D. E.; Powell, C.; Smith, P. B. *J. Appl. Polym. Sci.* **1997**, *63*, 439-451.

[117] Taden, A.; Tait, A. H.; Kraft, A. *J. Polym. Sci., Polym. Chem.* **2002**, *40*, 4333-4343.

[118] Andersson, M.; Maunu, S. L. *J. Polym. Sci., Polym. Phys.* **2006**, *44*, 3305-3314.

[119] Matsumoto, A; Kodoma, K; Aota, H.; Capek, I. *Eur. Polym. J.* **1999**, *35*, 1509-1517.

[120] Lynch, I.; Miller, I.; Gallagher, W. M.; Dawson, K. A. *J. Phys. Chem. B.* **2006**, *110*, 14581-14589.

[121] Lynch, I.; Dawson, K. A. *J. Phys. Chem. B* **2004**, *108*, 10983-10898.

[122] Theoharides, T. C. *Life* **1980**, *27*, 703-713.

[123] Beattie, J. K.; Fensom, D. J.; Freeman, H. C. *J. Am. Chem. Soc.* **1976**, *98*, 500-507.

[124] Dalvit, C.; Flocco, M.; Knapp, S.; Mostardini, M.; Perego, R.; Stockman, B. J.; Veronesi, M.; Varasi, M. *J. Am. Chem. Soc.* **2002**, *124*, 7702-7709.

[125] Maksay, G. *Neurochem. Int.* **2005**, *46*, 281-291.

[126] Götmar, G.; Ozen, C.; Serpersu, E.; Guiochon, G. *J. Chromatogr. A* **2004**, *1046*, 49-53.

[127] Yadav, R. C.; Kumar, G. S.; Bhadra, K.; Giri, P.; Sinha. R.; Pal, S.; Maiti, M. *Bioorg. Med. Chem.* **2005**, *13*, 165-174.

[128] Peters, L.; Fröhlich, R.; Boyd, A. S. F.; Kraft, A. *J. Org. Chem.* **2001**, *66*, 3291-3298.

[129] Guo, D.; Lu, Z. *J. Gen. Phys.* **2000**, *115*, 783-798.

[130] Besenius, P.; Cormack, P. A. G.; Ludlow, R. F.; Otto, S.; Sherrington, D. C.; *Chem. Commun.* **2008**, 2809-2811.

[131] Anslyn, E. V.; *J. Org. Chem.* **2007**, *72*, 687-699

[132] Wulff, G.; Sarhan, A. *Angew. Chem. Int. Ed. Engl.* **1972**, *11*, 341-347.

[133] Li, Y.; Yang. H. H.; You, Q. H.; Zhuang, Z. X.; Wang, X. *Anal. Chem.* **2006**, *78*, 317-323.

[134] Kempe, M.; Mosbach, K.I. *J. Chromatogr. A.* **1995**, *691*, 317-323.

[135] Gou, T. Y.; Xia, Y. Q.; Hao, G. J.; Song, M. D.; Zhang, B. H. *Biomaterials* **2004**, *25*, 5905-5912.

[136] Liao, J. L.; Wang, Y.; Hjertén, S. *Chromatographia* **1996**, *42*, 259-262.

[137] Shi, H.; Tsai, W. -B.; Garrison, M. D.; Ferrari, S.; Ratner, B. D. *Nature* **1999**, *398*, 593-597.

[138] Kimhi, O.; Bianco-Peled, H. *Langmuir* **2007**, *23*, 6329-6335.

[139] Schrader, T. *J. Am. Chem. Soc.* **1998**, *120*, 11816-11817.

[140] Grawe, T.; Schafer, G.; Schrader, T. *Org. Lett.* **2003**, *5*, 1641-1644.

[141] Fokkens, M.; Schrader, T.; Klarner, F. -G. *J. Am. Chem. Soc.* **2005**, *127*, 14415-14421.

[142] You, C. -C.; De, M.; Han, G.; Rotello, V. M. *J. Am. Chem. Soc.* **2005**, *127*, 12873-12881.

[143] Hong, R.; Fischer, N. O.; Verma, A.; Goodman, C. M.; Emrick, T.; Rotello, V. M. *J. Am. Chem. Soc.* **2004**, *126*, 739-743.

[144] Verma, A.; Nakade, H.; Simard, J. M.; Rotello, V. M. *J. Am. Chem. Soc.* **2004**, *126*, 10806-10807.

[145] De, M.; You, C. -C.; Srivastava, S.; Rotello, V. M. *J. Am. Chem. Soc.* **2007**, *129*, 10747-10753.

[146] Lindman, S.; Lynch, I.; Thulin, E.; Nilsson, H.; Dawson, K. A.; Linse, S. *Nano Letters* **2007**, *7,* 914-920.

[147] Ross, D.; Prenant, M.; Bessis, M. *Blood Cells* **1978**, *4*, 361-367.

[148] Savitzky, A.; Golay, M. J. E. *Anal. Chem.* **1964**, *36*, 1627-1639.

[149] Steinier, J.; Termonia, Y.; Deltour, J. *Anal. Chem*. **1972**, *44*, 1906-1909.

[150] De Levie, R. *Advanced Excel for Scientific Data Analysis*, Oxford University Press, **2003**.

[151] Lynch, I.; Miller, I.; Gallagher, W. M.; Dawson, K. A. *J. Phys. Chem. B.* **2006**, *110*, 14581-14589.

[152] Lynch, I.; Dawson, K. A. *J. Phys. Chem. B* **2004**, *108*, 10983-10898.

[153] Cytochrome C: Bushnell, G. W.; Louie, G. V.; Brayer, G. D. *J. Mol. Biol.* 1990, **214**, 585-595. Haemoglobin: Paoli, M.; Liddington, R.; Tame, J.; Wilkinson, A.; Dobson, G. *J. Mol. Biol.* **1996**, *256*, 775-792. Ferritin: Wang, Z. M.; Li, C.; Ellenburg, M. P.; Ruble, J. R.; Ho, J. X.; Carter, D. C. *Acta Crystallogr., Sect. D.* **2006**, *62*, 800-806. Albumin: Brown, J. R. *Fed. Proc.* **1975**, *34*, 591-591. Protein composition and chemical parameters were determined using *PROTPARAM*, on the ExPASy Proteomics server, http://www.expasy.ch/.

[154] Hill, H. A. O.; Röder, A.; Williams, R. J. P. *Naturwissenschaften* **1970**, *57*, 69-72.

[155] Rensing, S.; Schrader, T. *Org. Lett*. **2002**, *4*, 2161.

[156] Koch, S. J.; Renner, C.; Xie, X.; Schrader, T. Angew. Chem. 2006, 118, 6500-6503.

[157] J. Chiefari, Y. Chong, F. Ercole, J. Krstina, J. Jeffery, T. Le, R. Mayadunne, G. Meijis, C. Moad, G. Moad, E. Rizzardo, S. Thang, *Macromolecules* **1998**, *31*, 5559 – 5562

[158] Mayadunne, R. T. A.; Rizzardo, E.; Chiefari, J.; Chong, Y. -K.; Moad, G.; Thang, S. H. *Macromolecules* **1999**, *32*, 6977-6980.

[159] McCormick, C.; Lowe, A.; *Acc. Chem. Res.* **2004**, *37*, 312-325.

[160] Matyjaszewski, K.; Xia, J. *Chem. Rev.* **2001**, *101*, 2921-2990.

[161] Hawker, C. J.; Bosman, A. W.; Harth, E. *Chem. Rev.* **2001**, *101*, 3661-3688.

[162] Chong, Y. K.; Krstina, J.; Le, T. P. T.; Moad, G.; Postma, A.; Rizzardo, E.; Thang, S. H. *Macromolecules* **2003**, *36*, 2256-2272.

[163] Lowe, A. B.; McCormick, C. L. *Prog. Polym. Sci.* **2007**, *32*, 283-351.

[164] J. Lai, D. Filla, R. Shea, *Macromolecules* **2002**, *35*, 6754–6756.

[165] Barabanova, A. I.; Bune, E. V.; Gromov, A. V.; Gromov, V. F. *Eur. Polym. J.* **2000**, *36*, 479-483.

[166] Plaut, H.; Ritter, J. J. *J. Am. Chem. Soc.* **1951**, *73*, 4076-4077.

[167] Shimizu, Y. M.; Yamashita, Y.; Ishii, Y. *Makromol. Chem.* **1964**, *77*, 1.

[168] Bunyapaiboonsri, T.; Ramström, H.; Haiech, J.; Lehn, J. -M. *J. Med. Chem.* **2003**, *46*, 5803-?

[169] Goral, V.; Nelen, M. I.; Eilseev, A. V.; Lehn, J. -M. *Proc. Natl. Acad. Sci.* U.S.A. **2001**, *98*, 1347-?

[170] Billo, E. J. *Excel for Chemists: A Comprehensive Guide*, 2nd ed.; Wiley-VCH: New York, 2001; Chapter 12.